THE MOLECULAR BASIS OF THE INTERACTIONS OF COPPER METALLOCHAPERONES

Shilpa Aggarwal

Master of Biochemistry (M.Biochem)

University of Bath

Submitted for Doctor of Philosophy Degree

January 2011

Faculty of Medical Sciences

University of Newcastle upon Tyne

Declaration

I certify that this thesis contains my own work, except where acknowledged, and that no part of this material has been previously submitted for a degree or any other qualification at this or any other University.

Dedication

This thesis is dedicated to

My Mum, Dad

&

My brother, Amit

Abstract

Copper metallochaperones help prevent mis-metallation of proteins and ensure copper incorporation in specific Cu(I)-binding proteins by ligand-exchange reactions. The human copper metallochaperone (hCCS) for superoxide dismutase-1 (hSOD1) can interact via domain 1 with the carboxyl-terminal domain (CTD) of human β-secretase-1 (hBACE1). hBACE1 initiates the production of amyloid-β peptide (Aβ), the major constituent of senile plaques in Alzheimer's disease (AD). One of the aims of this thesis was to identify the residues involved in mediating the interaction between hCCS and hBACE1 CTD and to investigate the role of copper in mediating this interaction using a yeast two-hybrid system.

The data show that the Cys residues in the CXXC motifs of hCCS and hBACE1 CTD are essential for this interaction. The interaction is optimised by residues located close to the Cu(I)-binding sites. The hCCS/hBACE1 CTD interaction decreases in copper-deficient conditions. hBACE1 CTD was also shown to interact with the copper metallochaperone HAH1 involving the Cys residues in the CXXC motif of hBACE1 CTD. A model has been proposed based on the physiological implications of these data with respect to AD pathology. The interaction of hCCS with hSOD1 was also investigated using the yeast two-hybrid system. The mutation of the Cu(I)-binding residues in hCCS do not have a significant effect on the hSOD1/hCCS interaction. Interestingly, the hSOD1/hCCS interaction increases in copper-deficient conditions which can also have implications for AD pathology, as discussed in the proposed model.

The yeast two-hybrid system was also used to study the interaction of the copper metallochaperone Atx1 from *Synechocystis* PCC 6803 (ScAtx1) with the metal-binding domains (MBDs) of the Cu(I)-transporting ATPases, CtaA ($CtaA_N$) and PacS ($PacS_N$). The data show that the residues on loop 5 of the ferredoxin-like fold of ScAtx1 (His61), $CtaA_N$ (Phe87) and $PacS_N$ (Tyr65) are important for mediating protein-protein interactions. Swapping the loop 5 residue disrupted complex formation of ScAtx1 with $CtaA_N$ and $PacS_N$. The mutation of ScAtx1 His61 to a charged residue or to a neutral Ala also weakens the interactions with the MBDs, demonstrating that His61 is the best choice of amino acid in this position to enable ScAtx1 to interact optimally with both of its target proteins. The possibility that ScAtx1 may form two structurally different complexes (side-to-side or head-to-head) with $CtaA_N$ and $PacS_N$ was also investigated. The data indicate that both $CtaA_N$ and $PacS_N$ can likely form a side-to-side complex although the possibility that they can also form a head-to-head complex can not be excluded.

Acknowledgements

Thanks to my supervisor Professor Christopher Dennison and all of the lab members past (in particular Dr. Katsuko Sato) and present. A big thank you to Dr. Julian Rutherford for facilitating my understanding of yeast molecular biology, in particular. I had some very useful discussions with Dr. Kevin Waldron throughout my time at Newcastle University especially in the final stages of this degree and am particularly grateful for his help with ICP-MS. I would also like to thank Dr. Adriana Badarau for helpful discussions regarding the experiments with cyanobacterial proteins, her contribution in reading parts of this thesis, and also for her encouraging words which helped to motivate me at the time. Some of the staff members (past and present) at ICaMB also deserve my thanks, especially Professor Nigel Robinson and Dr. Nick Watkins for allowing me access to their labs whenever I required it, and Kate for her help with autoclaving and washing up!

On a more personal level, I would like to thank some of my friends who helped me throughout this degree. Juliane Klein was a wonderful companion during the many late nights we spent working in the department and during the walk home when I felt physically and mentally exhausted; her support during the latter stages of this degree is heartily appreciated. Dorota Kostrz accompanied me on numerous occasions during my "snack breaks" and helped me enjoy several pleasant evenings with deliciously cooked food. Andrew Knox gave me technical assistance, in particular for some of the computer-related problems I faced when writing this thesis and lifted my spirits with his cheerful presence. My heartfelt thanks to Mike Danson for always believing in my abilities, and for his constant encouragement and support.

Finally, my deepest thanks to the three people without whom I could not have written this thesis. My parents and my brother have always been my strength and their unwavering belief, motivation and encouragement is what spurred me on to keep going. Their unrelenting patience and love gave me courage whenever I needed it. I can not thank them enough for all that they have done for me, and this thesis is just a small token of appreciation for all of their efforts.

This work was funded by the BBSRC.

Contents Page

Index of Figures

Index of Tables

Abbreviations and Acronyms

A	Adenine (DNA)
A	Alanine (Protein)
A. fulgidus	*Archaeoglobus fulgidus*
Aβ	Amyloid-beta
AD	Alzheimer's disease
Ala	Alanine
ALS	Amyotrophic lateral sclerosis
Amp	Ampicillin
AP	Alkaline phosphatase
APP	Amyloid precursor protein
APS	Ammonium persulfate
Arg	Arginine
Asp	Aspartic acid
Asn	Asparagine
ATP	Adenosine triphosphate
ATX1	Anti-oxidant 1
B. subtilis	*Bacillus subtilis*
BACE1	β-site APP cleaving enzyme-1
BCS	Bathocuproinedisulfonic acid disodium salt
BSA	Bovine serum albumin
C	Cysteine (Protein)
C	Cytosine (DNA)
C. elegans	*Caenorhabditis elegans*
CCS	Copper metallochaperone for superoxide dismutase-1
Ci/mmol	Curies per millimole
CMD1	Calmodulin-binding protein 1
COX	Cytochrome *c* oxidase
CTD	Carboxyl-terminal domain
CTR	Copper transport proteins
C-terminal	Carboxyl-terminal
CuBD	Cu-binding domain
Cys	Cysteine
dH_2O	deionized water
ddH_2O	double deionized water
D	Aspartic Acid
D. melanogaster	*Drosophila melanogaster*

D1	Domain 1
D2	Domain 2
D3	Domain 3
DMT1	Divalent metal transporter-1
DNA	Deoxyribonucleic acid
dNTP	Deoxyribonucleotide triphosphate
DTT	Dithiothreitol
E	Glutamic Acid
E. coli	*Escherichia coli*
E. hirae	*Enterococcus hirae*
EDTA	Ethylenediaminetetraacetic acid
EtBr	Ethidium bromide
F	Phenylalanine
fALS	familial ALS
Fe-S	Iron-sulfur
G	Glycine (Protein)
G	Guanosine (DNA)
Gal	Galactose
GGA	γ-ear-containing ADP-ribosylation factor-binding
Gln	Glutamine
Glu	Glucose
Glu	Glutamic acid (Protein)
Gly	Glycine
g/L	grams per litre
GRX1	Glutaredoxin 1
H	Histidine
HA	Hemaglutinin
HADDOCK	High amibiguity driven protein-protein docking
HAH1	Human Atx1 homologue
HCl	Hydrochloric acid
HEPES	4-(2-hydroxyethyl)-1-piperazineethanesulfonic acid sodium salt
HNO_3	Nitric acid
Hrs	Hours
His	Histidine
H. sapiens	*Homo sapiens*
I	Isoleucine
ICP-MS	Inductively coupled plasma-mass spectrometry
Ile	Isoleucine

ITC	Isothermal titration calorimetry
K	Lysine
Kb	Kilobase
KCl	Potassium chloride
kDa	KiloDalton
L	Leucine (Protein)
L	Litre
LacZ	β-galactosidase
LB	Luria Bertani
Leu	Leucine
Lys	Lysine
M	Methionine
MBD	Metal-binding domain
MBS	Metal-binding site
Met	Methionine
mg	Milligram
mg/mL	Milligram per millilitre
mins	Minutes
mL	Millilitre
mM	Millimolar
MM	Minimal-medium
mmol	Millimole
MPAC	Metal-protein attenuating compound
mRNA	messenger RNA
N	Asparagine
N-terminal	Amino-terminal
NFTs	Neurofibrillary tangles
ng	nanogram
NMR	Nuclear magnetic resonance
NTD	Amino-terminal domain
NTP	Nucleoside triphosphate
OD	Optical density
ONP	*o*-nitrophenol
ONPG	*o*-nitrophenyl-β-D-galactopyranoside
P	Proline
PAGE	Polyacrylamide Gel Electrophoresis
PCR	Polymerase chain reaction
PD	Parkinson’s disease
PDB	Protein data bank

PEG	Polyethylene glycol
Pfu	*Pyrococcus furiousus*
Phe	Phenylalanine
pmol/µL	picomole per microlitre
PNK	Polynucleotide kinase
Pro	Proline
Q	Glutamine
R	Arginine
Raff	Raffinose
RNA	Ribonucleic acid
RNAP	RNA polymerase
ROS	Reactive oxygen species
Rpm	Revolutions per minute
S	Serine
S. cerevisiae	*Saccharomyces cerevisiae*
SD	Synthetic dextrose
SDS	Sodium dodecyl sulphate
Ser	Serine
SOD1	Superoxide dismutase-1
SPR	Surface plasmon resonance
T	Threonine (Protein)
T	Thymidine (DNA/RNA)
TAE	Tris-acetic acid EDTA
TBE	Tris- boric acid- EDTA
TBP	TATA binding protein
TBST	Tris buffered saline with Tween
TCA	Trichloroacetic acid
TE	Tris-HCl EDTA
TEMED	N,N,N',N'-Tetramethylethylenediamine
Tet	Tetracycline
Thr	Threonine
T_m	Melting temperature
Tris	Tris(hydroxymethyl)aminomethane
tRNA	Transfer RNA
Trp	Tryptophan
Tyr	Tyrosine
U	Uridine
U/µL	Units per microlitre
µg	Microgram

µL	Microlitre
µM	Micromolar
UV	Ultra violet
UV-Vis	Ultra violet - Visible
V	Valine (Protein)
V	Volts
v/v	Volume per volume
Val	Valine
W	Tryptophan
w/v	Weight per volume
WT	Wild-type
X-gal	5-bromo-4-chloro-3-indolyl-β-D-galactopyranoside
Y	Tyrosine
YPD	Yeast extract, peptone, dextrose

Nomenclature of the main proteins and genes discussed in this study

AfCopA	CopA copper transporter from *A. fulgidus*
AfCopZ	CopZ copper metallochaperone from *A. fulgidus*
ATP7A	ATP7A copper transporter from *H. sapiens*
ATP7B	ATP7B copper transporter from *H. sapiens*
Atx1	Atx1 copper metallochaperone from yeast
BsCopA	CopA copper transporter from *B. subtilis*
BsCopZ	CopZ copper metallochaperone from *B. subtilis*
Ccc2	Ccc2 copper transporter from yeast
CCS1	Gene coding for Ccs1 in yeast
ccs1	Genomic deletion of *CCS1* in yeast
Ccs1	Ccs1 copper metallochaperone for Sod1 from yeast
ctaA	Gene coding for CtaA in cyanobacteria
CtaA	CtaA copper transporter from cyanobacteria
$CtaA_N$	Metal-binding domain of CtaA (Residues 1-92)
CTR1	Gene coding for Ctr1 in yeast
Ctr1	Ctr1 copper import protein from yeast
EhCopA	CopA copper transporter from *E. hirae*
EhCopZ	CopZ copper metallochaperone from *E. hirae*
HAH1	HAH1 copper metallochaperone from *H. sapiens*
hBACE1 CTD	Gene coding for BACE1 C-terminal domain from *H. sapiens*
hBACE1 CTD	BACE1 C-terminal domain from *H. sapiens*
hCCS	Gene coding for CCS copper metallochaperone from *H. sapiens*
hCCS	CCS copper metallochaperone from *H. sapiens*
hCTR1	CTR1 copper import protein from *H. sapiens*
hSOD1	Gene coding for SOD1 from *H. sapiens*
hSOD1	SOD1 from *H. sapiens*
pacS	Gene coding for PacS from cyanobacteria
PacS	PacS copper transporter from cyanobacteria
$PacS_N$	Metal-binding domain of PacS (Residues 1-71)
scAtx1	Gene coding for ScAtx1 from cyanobacteria
ScAtx1	ScAtx1 copper metallochaperone from *Synechocystis* PCC 6803
Sod1	Sod1 from yeast

1. Introduction

1.1 Metals in Biology

Metals are an essential cellular requirement for all three kingdoms of life – eukarya, bacteria and archaea (Woese and Fox, 1977), although the type of metal and the quantity required vary from organism to organism based upon their habitat and lifestyle. Iron and copper in particular, play a predominant role in facilitating enzyme catalysis in living organisms. Until about 3 billion years ago ferric iron (Fe(III)) was the predominant redox-active ion utilised by living organisms. However, the oxygenation of the Earth's atmosphere rendered Fe(III) insoluble and the cupric ion (Cu(II)) soluble, thereby promoting the use of copper as one of the major redox-active protein co-factors (Frausto da Silva and Williams, 2001). Therefore, metal availability is dependent upon its solubility in water in the presence of oxygen. Metals are a vital metabolic requirement for all living organisms and their deficiency can be a major hindrance to cellular processes, as discussed below. The transport, concentration and localisation of the metal ions within the cell have to be tightly regulated because in excessive amounts these metals can be cytotoxic resulting in severe repercussions including cell death. All living cells have therefore developed mechanisms to maintain optimum metal homeostasis. Eukaryotes in particular, require additional homeostatic mechanisms to ensure the correct localisation of the required metals in the appropriate cellular organelle (see section 1.3). However, there are some common chemical and biological factors which contribute towards metal selectivity in all organisms.

1.1.1 Factors determining Metal Selectivity

While the natural habitat of an organism plays an important role in determining the variety of metals available to a cell, other chemical and biological factors determine the association of a metal ion with a specific coordination site. The first challenge posed by the cell to metal uptake is the cell membrane itself. The cell membrane not only acts as a physical barrier but the presence of membrane-associated transport proteins further regulates metal influx, albeit import proteins are not known for all types of metals (Frausto da Silva and Williams, 2001). Once inside the cell, the metal ions can associate with an assortment of proteins which can themselves regulate metal ion localisation and concentration at the level of uptake, intracellular transport and efflux. For example, the binding of copper and iron to specific transcription factors determines their uptake in the appropriate cellular compartment by controlling the transcription of copper or iron importers (De Freitas *et al.*, 2003; Frausto da Silva and Williams, 2001; Waldron *et al.*, 2009). In turn, the binding of metals to proteins is dependent upon a combination of chemical factors which can be broadly divided into thermodynamic and

kinetic considerations. The thermodynamic components include metal selectivity on the basis of size, oxidation state, preferred coordination geometry, and the shape of the coordination site (Frausto da Silva and Williams, 2001; Waldron *et al.*, 2009). The latter three factors in particular are very important from a biological perspective. For example, in the case of superoxide dismutase-1 (SOD1), coordination geometry is one of the factors that dictates the binding of copper and zinc to their respective sites. While Zn(II) is bound tetrahedrally, Cu(II) is coordinated in a tetragonal arrangement (Tainer *et al.*, 1982), discussed further in section 1.3.2.3. Metal ions are also restricted by their preference for the type of amino acid residues they bind to, as in the case of Cu(I) and Cu(II). While Cu(I) prefers to bind to sulfur donor ligands (Cys or Met), Cu(II) preferentially binds to nitrogen (His) or oxygen donors (Asp and Glu) (Frausto da Silva and Williams, 2001).

However, thermodynamic constraints alone are not sufficient to prevent mis-metallation of proteins, as exemplified by the Irving-Williams series (Mg(II), Ca(II) < Mn(II) < Fe(II) < Co(II) < Ni(II) < Cu(II) > Zn(II)). According to this series or the 'natural order of stability' Cu(II) forms the most stable complexes with ligands compared to other divalent cations (Frausto da Silva and Williams, 2001; Irving and Williams, 1948). The acquisition of the required metal ions by the cyanobacterial proteins MncA and CucA exemplifies some of the mechanisms that the cell has evolved in order to overcome the problem of mis-metallation. MncA and CucA were found to be the predominant manganese- and copper-binding proteins *in vivo* (Tottey *et al.*, 2008). However, both MncA and CucA readily and preferentially bind Cu(II) *in vitro* in comparison to manganese, as expected, based on the the Irving-Williams series. Tottey *et al.* (2008) demonstrated that the cell ensured correct metallisation of these proteins by compartmentalising MncA in the cytosol to acquire Mn(II) and CucA in the periplasm to acquire Cu(II) during protein folding. Once the proteins have acquired the appropriate metal ions, protein folding ensures that the bound-metal ions are buried and therefore protected from substitution by other metals (Tottey *et al.*, 2008). Cells also prevent mis-metallation by ensuring that there are essentially no 'free' metal ions *in vivo*. In fact, it has been estimated that there is less than one 'free' atom of copper per cell (Rae *et al.*, 1999). Proteins such as metallothionein (see section 1.3.2.1) which have a very high affinity for metals, are a major contributor in maintaining low free metal ion concentration *in vivo*. Since metalloproteins have variable metal-binding affinities, a further challenge is to ensure that all proteins acquire the required metal co-factor. Protein-protein interactions assist in overcoming some of these restraints, for example, metallochaperones (see sections 1.2.2 and 1.3.2.4) interact very specifically with their target proteins and ensure the transfer of metal to the appropriate binding site. The role of protein-protein interactions in the context of copper-homeostasis is discussed further in section 1.4, and is the main focus of this study.

1.1.2 The Biochemistry of Copper

Copper is one of the most important trace elements for all living cells. Copper-binding proteins are found in most living organisms and account for up to 1 % of the total cellular proteome (Andreini *et al.*, 2008). Copper is required as an essential co-factor in plastocyanin for transferring electrons between proteins involved in photosynthesis (Redinbo *et al.*, 1994), and in cytochrome *c* oxidase for the reduction of dioxygen to water in aerobic respiration, two of the most fundamental processes in living organisms (Bento *et al.*, 2006). Copper is also a vital co-factor for haemocyanin which mediates oxygen transport in some crustaceans, multicopper oxidases which catalyse the reduction of dioxygen to two molecules of water (Bento *et al.*, 2006; Crichton and Pierre, 2001) and several other proteins, some of which are listed in Table 1. The main chemical property of copper that makes it such an attractive protein co-factor is its ability to exist in two different biologically-relevant oxidation states – Cu(I) and Cu(II), which allows it to bind to a variety of ligands (Crichton and Pierre, 2001), as discussed in section 1.1.1. Due to the reducing environment of the cytoplasm (Ostergaard *et al.*, 2004), copper predominantly exists as Cu(I) in the eukaryotic cytosol. Most of the known cytosolic copper-binding proteins bind Cu(I) while copper-binding proteins that are compartmentalised into different organelles within the cytoplasm can alternate between the Cu(I) and Cu(II) states (Banci *et al.*, 2010c; Bertini *et al.*, 2010). In the bacterial periplasm Cu(II) can co-exist with Cu(I) since the periplasm appears to have a comparatively higher redox potential than the eukaryotic cytoplasm (Messens *et al.*, 2007).

In addition to their preference for different amino acids, Cu(I) and Cu(II) also differ in their preferred coordination number. While Cu(I) can be bound in a 2, 3 or 4 coordinate state, Cu(II) prefers a coordination number of 4, although it can also be bound by 5 or 6 coordinating ligands (Davis and O'Halloran, 2008; Frausto da Silva and Williams, 2001). Copper can readily oscillate between the Cu(I) and Cu(II) states and this redox-active property of copper is exploited by the proteins involved in photosynthesis and respiration (Crichton and Pierre, 2001; Frausto da Silva and Williams, 2001). However, the redox-active feature of copper can also result in cytotoxicity. Cu(I) can react with hydrogen peroxide and undergo Fenton-like reactions leading to the production of superoxide ($O_2^{-\bullet}$) and hydroxyl radicals ($OH^{\bullet}$) which can cause oxidative damage to nucleic acids, lipids and proteins (Equations 1-3) (Molina-Holgado *et al.*, 2007).

$$Cu(I) + H_2O_2 \rightarrow Cu(II) + OH^- + OH^{\bullet} \quad [1]$$

$$Cu(II) + O_2^{-\bullet} \rightarrow Cu(I) + O_2 \quad [2]$$

$$O_2^{-\bullet} + H_2O_2 \rightarrow O_2 + OH^- + OH^{\bullet} \quad [3]$$

Table 1: Some of the known copper-binding proteins in Humans and their Functions.

Protein	Function
Ceruloplasmin	Ferroxidase that transports iron to transferrin (see section 1.3.2.2)
Copper-transporting ATPases (ATP7A and ATP7B)	Transport copper across cellular or organelle membranes (see sections 1.3.3)
Copper metallochaperones (e.g. hCCS, HAH1)	Transport copper to their specific copper-requiring target proteins (see sections 1.3.2.4)
Copper transport protein-1 (hCTR1)	Copper uptake in eukaryotic cells (see section 1.3.1)
Cytochrome *c* oxidase	Catalyzes the conversion of molecular oxygen to water as a component of the respiratory electron transport chain in the mitochondria coupled to proton pumping
Divalent metal transporter-1 (DMT1)	Uptake of divalent metals in eukaryotic cells (see section 1.3.1)
Dopamine β-hyroxylase	Neurotransmitter synthesis, catalyses the conversion of dopamine to norepinephrine
Hephaestin	Transmembrane ferroxidase involved in iron transport from enterocytes (see section 1.3.2.2)
Human inhibitor of apoptosis	Inhibitor of apoptosis (Mufti *et al.*, 2006)
Metallothioneins	Multi-metal binding Cys-rich proteins involved in the storage of metal ions (see section 1.3.2.1)
Superoxide dismutase-1 (hSOD1)	Anti-oxidant enzyme that catalyzes the dismutation of superoxide into hydrogen peroxide and water (see section 1.3.2.3)
Tyrosinase	Catalyses oxidation of phenols, melanin synthesis

1.1.3 The Biochemistry of Iron

Similar to copper, iron is also utilised for its redox-active properties in photosynthesis and respiration. Iron can exist in three biologically relevant oxidation states – Fe(II), Fe(III) and Fe(IV) (Frausto da Silva and Williams, 2001). Iron is an extensively used co-factor for proteins involved in a wide variety of functions, and as a result the cellular requirement for iron is very high. It is estimated that an adult male contains contains ~ 3.5 grams of iron (Munoz *et al.*, 2009). Iron can be present in the cell as a heme-constituent in proteins involved in mediating redox reactions such as cytochromes and in oxygen transporting proteins like haemoglobin and myoglobin. Iron can also be

bound as a co-factor in proteins containing iron-sulphur (Fe-S) clusters such as the proteins involved in electron-transfer reactions, like the ferredoxins, proteins involved in DNA replication and transcription (Frausto da Silva and Williams, 2001; Ye and Rouault, 2010). The biological importance of iron is further highlighted by the fact that it is the most prevalent dietary deficiency amongst human beings, especially in the developed countries (Waldron *et al.*, 2009).

Similar to copper, iron can also undergo Fenton-chemistry and lead to oxidative stress (Molina-Holgado *et al.*, 2007). Apart from the similarities in their chemical nature, copper and iron are also closely-linked biologically (De Freitas *et al.*, 2003; Gambling *et al.*, 2008). Iron homeostasis is known to be strongly influenced by copper homeostasis and *vice versa*. In humans, Cu(II) and Fe(II) share a common importer – the divalent metal transporter-1 (DMT1) (see section 1.3.1), while the ferroxidase ceruloplasmin is the major copper-binding protein within the blood serum (see section 1.3.2.2). In the baker's yeast *Saccharomyces cerevisiae* (*S. cerevisiae*), copper is transported from the cytosol to the copper-transporting ATPase Ccc2 (see section 1.3.3.1) (Huffman and O'Halloran, 2000; Pufahl *et al.*, 1997) which subsequently transfers it to Fet3 – the yeast homologue of ceruloplasmin (Yuan *et al.*, 1995), to mediate the high affinity uptake of iron in the cells via association with the iron-transporter Ftr1 (Stearman *et al.*, 1996).

1.1.4 The Biochemistry of Zinc

Unlike copper and iron, zinc has a single oxidation state – Zn(II), and is therefore redox-inactive. Despite its lack of redox-activity, zinc is a widely used structural co-factor in more than 3000 proteins encoded by upto 10 % of the human genome (Maret and Li, 2009; Takeda and Tamano, 2009). Zinc poses a particular risk to copper-binding proteins due to the similarities in their chemical properties and because zinc is also more bioavailable than copper. Zinc and copper are similar in size and charge density, and in addition, share some common ligands including Cys and His (Frausto da Silva and Williams, 2001). Zinc-binding proteins are involved in cell division, cell differentiation, neurotransmission and brain function (Maret and Li, 2009; Takeda and Tamano, 2009). The disruption of zinc homeostasis is implicated in several neurological disorders, as discussed below.

1.1.5 The Role of Metals in Neurodegenerative Diseases

As mentioned above, the redox-active metals copper and iron can result in the production of reactive oxygen species (ROS) and as a consequence can lead to oxidative stress. Oxidative stress is defined as the imbalance between the production of ROS and the inability of the cellular defence mechanisms in clearing these (Molina-Holgado *et al.*, 2007). The brain, in particular, is very susceptible to oxidative stress

due to its high consumption of oxygen and the presence of relatively high concentrations of redox-active metal ions which are an integral part of synaptic transmission (Molina-Holgado *et al.*, 2007). The healthy human brain possesses remarkably efficient metal homeostatic mechanisms to maintain a delicate balance between metal utility and metal toxicity, despite containing relatively low levels of anti-oxidant agents. However, with increasing age the brain's defence mechanisms start to deteriorate and the brain becomes increasingly susceptible to oxidative stress (Molina-Holgado *et al.*, 2007). Hence, it is not surprising that with the increase in life expectancy the number of people suffering from neurodegenerative diseases is also rapidly accelerating.

Two features that many neurodegenerative diseases including Alzheimer's disease (AD), Parkinson's disease (PD), amyotrophic lateral sclerosis (ALS), and Prion diseases have in common are protein aggregation in the affected neural tissue and oxidative damage. Both of these factors are associated with the interaction between metal ions and the amyloidogenic proteins involved in these diseases (Bush, 2000; Molina-Holgado *et al.*, 2007). Although several metals including manganese, aluminium, mercury and lead have been implicated, the most common metals associated with neurodegenerative diseases are copper, iron and zinc (Bush, 2000; Molina-Holgado *et al.*, 2007). In AD, copper is found in increased quantities in senile plaques, one of the main pathological hallmarks of AD. copper has also been shown to contribute to the aggregation of the amyloid-β peptide (Aβ), the main constituent of these plaques. Aβ has also been shown to be precipitated by zinc and iron (Bush, 2003; Maynard *et al.*, 2005; Molina-Holgado *et al.*, 2007). The implications of altered copper homeostasis in AD are discussed in further in section 1.5. PD, the second most common neurodegenerative disease after AD, is characterised by the presence of Lewy bodies and protofibrils composed of aggregated α-synuclein protein (Bisaglia *et al.*, 2009). Copper has been reported to be the main metal involved in mediating α-synuclein aggregation followed by iron and zinc (Bisaglia *et al.*, 2009; Uversky *et al.*, 2001a; Uversky *et al.*, 2001b). The prion protein has been shown to be able to bind multiple copper ions which can result in conformational changes facilitating its aggregation (Brown, 2009; Molina-Holgado *et al.*, 2007). Although the cascade of events leading up to metal-associated protein aggregation and a causal link between metallotoxicity and neurodegeneration needs to be deciphered further, there is nevertheless substantial evidence to indicate that the association of metals with the amyloidogenic proteins is an integral part of neuronal pathogenesis (Brown, 2009; Bush, 2000; Molina-Holgado *et al.*, 2007).

1.2 Regulation of Copper in Prokaryotes

Copper proteins have been identified in both bacteria and archaea and comprise on average 0.3 % - 0.4 % of the proteome, respectively (Andreini *et al.*, 2008). Amongst all of the organisms studied by Andreini *et al.* (2008), *Nanoarchaeum equitans* (archaeon), *Chlamydia trachomatis* (bacterium), *Onion yellows phytoplasma* (bacterium), *Mesoplasma florum* (bacterium) and *Borrelia burgdorferi* (bacterium) were the only organisms in which a copper protein was not identified. Unlike eukaryotes, there is no cytosolic requirement for copper in prokaryotes apart from two exceptions – cyanobacteria and methanotrophic bacteria (Banci *et al.*, 2010c). In gram-negative bacteria copper-dependent proteins are typically localised in the periplasm or are attached to the plasma membrane (Tottey *et al.*, 2005). In gram-positive bacteria copper-dependent proteins are known to be bound to the plasma membrane which either protrude into the extracellular space or are secreted (Banci *et al.*, 2010c). In contrast, cyanobacteria require copper to be translocated to the membrane-bound thylakoid compartment for insertion into the photosynthetic proteins plastocyanin and cytochrome *c* oxidase (Kerfeld and Krogmann, 1998). Similarly, in methanotrophic bacteria copper is an essential cofactor for the internal membrane-bound particulate methane monooxygenase enzyme (Balasubramanian and Rosenzweig, 2007). In order to maintain tight copper homeostasis, the presence of intracellular copper is regulated at multiple levels including import, export and intracellular transport, as discussed below.

1.2.1 Import of Copper in Prokaryotes

The presence of copper inside prokaryotic cells is an enigma considering the fact that apart from a few exceptions, no copper import pathway has been elucidated in most bacterial and archaeal species. There is some evidence to suggest that copper import in gram-negative bacteria may proceed via non-specific metal ion diffusion through the outer membrane embedded proteins called porins (Nies, 2007; Nikaido and Vaara, 1985) or through methanobactins in methanotrophic bacteria (Balasubramanian and Rosenzweig, 2008; Kim *et al.*, 2004). However, conclusive evidence of a copper import pathway in most prokaryotes remains largely unavailable (Banci *et al.*, 2010c; Magnani and Solioz, 2007). The copper-transporting ATPases - CtaA from cyanobacteria and CopA from the gram-positive bacterium *Enterococcus hirae* (*E. hirae*) have also been implicated in mediating copper import into the cytosol; however, doubts have been raised regarding the direction of copper transport via these transporters, as discussed below.

1.2.1.1 Prokaryotic copper-transporting ATPases

Copper-ATPases are a part of the P_{1B}-type or CPx-type ATPases which transport heavy metal ions across membranes by coupling it with the catalytic phosphorylation of the Asp residue in the conserved DKTGT sequence (Lutsenko *et al.*, 2007b). Copper-ATPases are found in all three kingdoms of life and contain some common features including eight transmembrane domains, cytosolic N-terminal domains which contain 1-6 soluble metal-binding domains (MBDs), an actuator domain, a phosphorylation domain, a nucleotide-binding domain and a conserved CPX amino acid sequence (where X represents any amino acid) in the sixth transmembrane domain which determines the metal-binding specificity of the ATPase, as shown in Figure 1 (Arguello *et al.*, 2007). The number of MBDs varies amongst prokaryotes and eukaryotes. While prokaryotes tend to have one or two MBDs, some eukaryotic species including *Homo sapiens* (*H. sapiens*) contain upto six MBDs (Arguello *et al.*, 2007). Of particular interest to this study is the interaction between copper metallochaperones and the MBDs of the copper-ATPases. MBDs and copper metallochaperones are structurally very similar to each other as they typically possess a ferredoxin-like fold ($\beta\alpha\beta\beta\alpha\beta$) and a CXXC metal-binding motif located on loop 1 and the first α-helix (Boal and Rosenzweig, 2009a). While numerous studies have reported the interaction of copper metallochaperones with the cognate MBDs, the precise role of MBDs remains unclear.

1.2.1.1.1 The *E. hirae* copper-transporting ATPase CopA

E. hirae demonstrates one of the best understood prokaryotic copper homeostatic systems. The *E. hirae* copper homeostasis system comprises two copper-transporting ATPases – CopA (EhCopA) and CopB (EhCopB), a copper metallochaperone CopZ and a copper metallosensor CopY, which together form the *cop* operon. The *copA* gene from *E. hirae* was one of the first copper-transporting ATPases encoding gene to be identified (Odermatt *et al.*, 1992; Odermatt *et al.*, 1993). Cells lacking *copA* were reported to be phenotypically similar to the wild-type (WT) cells in terms of copper resistance under copper-replete conditions but their growth ceased in copper-deficient conditions after two to three generations (Odermatt *et al.*, 1993). *E. hirae copAΔ* mutants were also found to be significantly more sensitive to silver ions suggesting that EhCopA may function as a silver importer (Odermatt *et al.*, 1993; Odermatt *et al.*, 1994). Due to the chemical similarities between Ag(I) and Cu(I), any protein capable of transporting Ag(I) cations is a strong candidate for transporting Cu(I) cations too. Thus, the combination of data from growth studies under different copper conditions and the studies with Ag(I) led to the suggestion that EhCopA may be involved in copper uptake. However, doubts have been raised recently regarding the direction of copper transport by EhCopA (Ma *et al.*, 2009; Robinson and Winge, 2010).

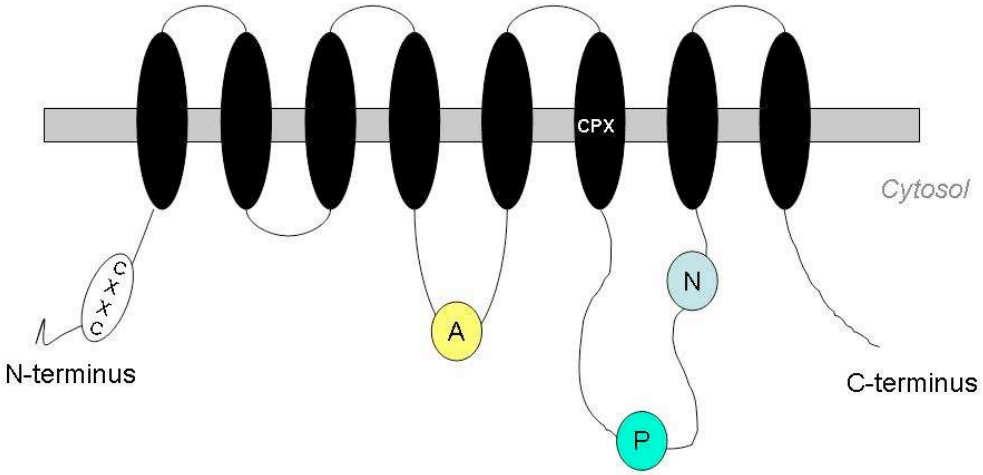

Figure 1: Generic structure of P_{1B}-type copper-ATPases. The soluble MBD containing the CXXC metal-binding motif is shown at the N-terminus, albeit the number of MBDs can vary, as discussed in section 1.2.1.1. The transmembrane domains are shown as black ovals connected by loops. The conserved CPX motif in the sixth transmembrane domain is also shown. The presence of the actuator (A), phosphorylation (P) and the nucleotide binding (N) domains are represented by yellow, green and blue circles respectively.

EhCopA possesses a single N-terminal MBD (Figure 2) which has been shown to interact with the *E. hirae* CopZ (EhCopZ) protein (Multhaup *et al.*, 2001). Surface plasmon resonance (SPR) experiments demonstrated that the presence of Cu(I) enhanced the interaction between EhCopZ and the MBD of EhCopA, and that the Cu(I)-induced enhancement was dependent upon the presence of the Cys residues in the $M_{15}XCXXC_{20}$ motif of EhCopA MBD (Multhaup *et al.*, 2001).

1.2.1.1.2 The cyanobacterial copper-transporting ATPase CtaA

Cyanobacteria are prokaryotic photosynthetic organisms and the evolution of an oxygen-rich atmosphere has mainly been attributed to their photosynthetic capabilities (Farquhar *et al.*, 2000; Kasting and Siefert, 2002). Two copper-transporting P_{1B}-type ATPases have been discovered in cyanobacteria – CtaA and PacS (Kanamaru *et al.*, 1993; Phung *et al.*, 1994; Tottey *et al.*, 2001). CtaA was first identified in *Synechococcus* PCC 7942 (Phung *et al.*, 1994). CtaA was hypothesised to be involved in mediating copper-uptake based on its sequence homology with EhCopA and from *ctaAΔ* strains which were found to be more resistant to copper than WT cells (Phung *et al.*, 1994). Of particular interest to this study is the homologue of this protein identified from *Synechocystis* PCC 6803 by Tottey *et al.* (2001). The subsequent mention of CtaA in this study will refer to the copper-transporter from *Synechocystis* PCC 6803, unless stated otherwise. In contrast to the CtaA homologue from *Synechococcus* PCC 7942, the deletion of the gene encoding CtaA in *Synechocystis PCC 6803* did not protect against copper toxicity albeit these mutants did exhibit decreased copper content compared to WT cells (Tottey *et al.*, 2001).

It has previously been shown that green algae and cyanobacteria contain two electron carrier proteins – plastocyanin and cytochrome c_6 which transfer electrons between photosystems I and II (Merchant and Bogorad, 1986; Wood, 1978). While electron transfer is mediated by plastocyanin during copper-replete conditions, the cells can switch to the heme-containing cytochrome c_6 protein under copper-deficient conditions (Merchant and Bogorad, 1986). Homologues of both plastocyanin and cytochrome c_6 have been identified in the thylakoid compartment of *Synechocystis* PCC 6803 and similar copper-dependent switching between the carriers has also been demonstrated (Zhang *et al.*, 1992). Studies by Tottey *et al.* (2001) have shown that the deletion of *ctaA* resulted in decreased transcription of the gene encoding plastocyanin and increased transcription of the gene encoding cytochrome c_6 compared to the WT cells. The *ctaAΔ* strain also exhibited increased oxidation of cytochrome c_6 when exposed to a pulse of actinic light and decreased cytochrome *c* oxidase activity compared to the WT strain. These results subsequently led to the hypothesis that CtaA may function as a plasma-membrane bound cytosolic copper importer (Tottey *et al.*, 2001).

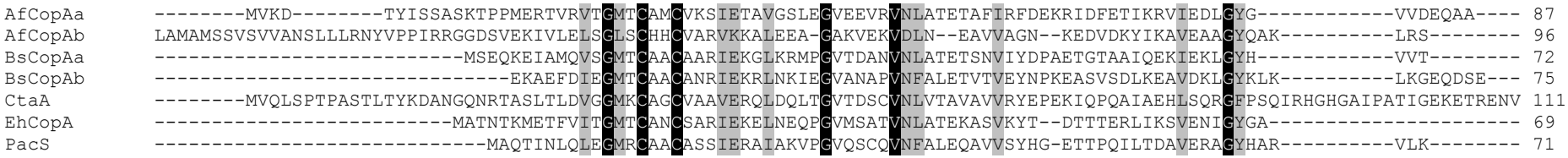

Figure 2: Sequence alignment of the soluble metal-binding domains of prokaryotic CopA-type copper-ATPases. The sequence alignment of the 2 MBDs of *Archaeoglobus fulgidus* CopA (GenBank accession code: 029777) denoted AfCopAa and AfCopAb (discussed in section 1.2.3.1), 2 MBDs of *Bacillus subtilis* CopA (GenBank accession code: 032220) denoted BsCopAa and BsCopAb (discussed in section 1.2.3.1), MBD of CtaA (GenBank accession code: NP_441938.1) (discussed in sections 1.2.1.1.2 and 1.4.3), EhCopA (GenBank accession code: AAA61835) (discussed in section 1.2.1.1.1) and PacS (GenBank accession code: NP_440588.1) (discussed in sections 1.2.3.2 and 1.4.3). Fully conserved residues are highlighted in black while semi-conserved residues are shown in grey.

However, several reports have disputed the direction of copper transport by CtaA (Ma *et al.*, 2009; Robinson and Winge, 2010). An alternative model suggests that CtaA might be located in the thylakoid membrane similar to the PacS copper-transporter and may mediate copper import into the thylakoid compartment at a different stage to PacS (Robinson and Winge, 2010).

CtaA possesses one MBD at the N-terminus with an $M_{33}XCXXC_{38}$ metal-binding motif (Figure 2) which has been shown to interact with the copper metallochaperone from *Synechocystis* PCC 6803 (ScAtx1) in a bacterial two-hybrid system (Tottey *et al.*, 2002), as discussed further in section 1.4.3. Badarau *et al.* (2010) have reported that CtaA MBD remains monomeric both in the apo- and copper-bound form. A recent study has also reported CtaA, in conjunction to PacS and ScAtx1, to be involved in copper acquisition by CucA (Waldron *et al.*, 2010).

1.2.2 Prokaryotic Copper Metallochaperones

Copper metallochaperones are typically ~8 kDa in size and ~70 amino acids in length. They contain the classic βαββαβ ferredoxin-like fold and the CXXC metal-binding motif (Markossian and Kurganov, 2003). While copper metallochaperones were initially discovered in eukaryotes (Lin and Culotta, 1995) (see section 1.3.2.4), homologues of them have been found in prokaryotes. Copper metallochaperones not only help to prevent copper toxicity by sequestering Cu(I), but also prevent aberrant copper-binding in proteins by directly delivering Cu(I) to their specific target proteins.

1.2.2.1 The *E. hirae* copper metallochaperone CopZ

The first bacterial copper metallochaperone was discovered in *E. hirae* and was termed CopZ (EhCopZ) (Figure 3 and Figure 4) (Odermatt and Solioz, 1995). EhCopZ was also the first copper metallochaperone to be structurally characterised (Wimmer *et al.*, 1999), albeit primarily in its apo-state (Figure 3). An NMR structure for the Cu(I)-bound EhCopZ was also reported but due to the relatively large structural movement in the M_9XCXXC_{14} motif the region around the metal-binding region could not be fully resolved (Wimmer *et al.*, 1999). In addition, the binding of copper was reported to lead to aggregation – most likely dimerisation of Cu(I)-EhCopZ resulting in protein precipitation. However, sufficient information was obtained from this partially resolved structure for the authors to propose that Cu(I) was likely trigonally coordinated in Cu(I)-EhCopZ, although the identity of the third ligand in addition to Cys11 and Cys14 was not deduced (Wimmer *et al.*, 1999).

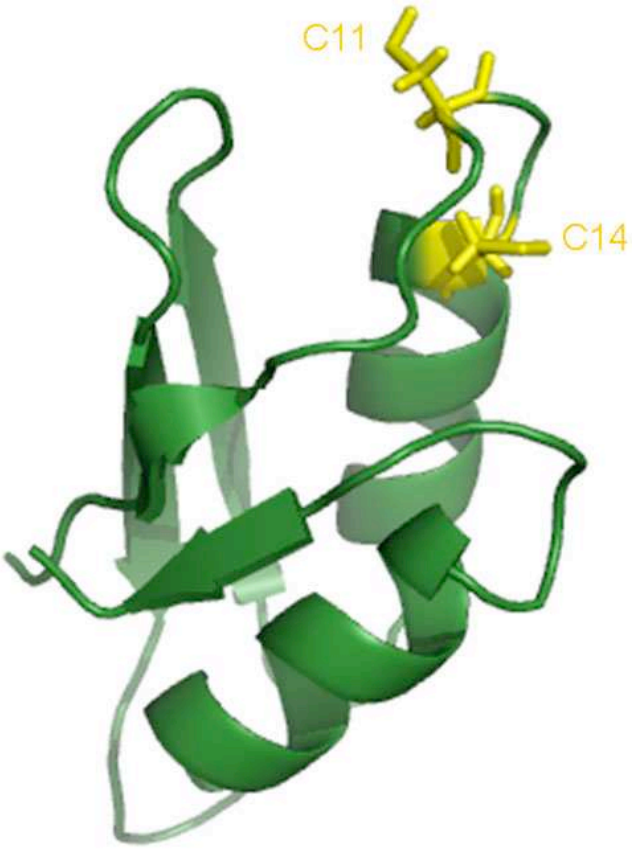

Figure 3: The NMR structure of apo-EhCopZ. The side chains of the proposed Cu(I)-binding Cys residues in the CXXC motif of apo-EhCopZ (PDB accession code: 1cpz) are shown as sticks (Wimmer *et al.*, 1999).

As mentioned above (section 1.2.1.1.1), EhCopZ has been shown to interact directly with EhCopA MBD by SPR (Multhaup *et al.*, 2001). In addition, EhCopZ can also act as the activator or de-repressor of the *E. hirae cop* operon depending upon its copper occupancy (Cobine *et al.*, 1999). In the absence of Cu(I)-bound EhCopZ, CopY binds a Zn(II) ion and represses the transcription of the downstream *cop* operon genes. In the presence of copper, the Cu(I)-bound EhCopZ transfers two Cu(I) ions to CopY which results in the removal of zinc from CopY and the release of CopY from the promoter leading to the expression of *copA* and *copB* genes (Odermatt and Solioz, 1995; Solioz and Stoyanov, 2003). In support of this model, *copZΔ* cells were reported to contain reduced levels of EhCopA and EhCopB (Odermatt and Solioz, 1995). An interaction between CopZ and EhCopB has also been reported, although further experiments are required to demonstrate this and to determine if copper is transferred from EhCopZ to EhCopB for copper efflux (Solioz *et al.*, 2010). Interestingly, EhCopZ is itself a part of a feedback loop where the expression of EhCopZ is copper-dependent. The levels of EhCopZ were reported to increase when the concentration of added copper in the growth medium was less than 0.5 mM. Further increase in copper concentration was shown to result in the proteolytic degradation of EhCopZ suggesting that excess Cu(I)-EhCopZ may be cytotoxic (Lu and Solioz, 2001). Recently, EhCopZ was also shown to interact with the stress-response regulator Gls24 by both *in vivo* and *in vitro* experiments (Stoyanov *et al.*, 2010) implicating it to be an integral member of the *E. hirae* copper homeostasis system.

1.2.2.2 The *Bacillus subtilis* copper metallochaperone CopZ

The copper metallochaperone from *Bacillus subtilis* (*B. subtilis*) was identified in 2001 and was subsequently termed BsCopZ (Figure 4 and Figure 5) (Banci *et al.*, 2001b). Similar to other copper metallochaperones, the copper source for BsCopZ is also not known (Banci *et al.*, 2010c; Radford *et al.*, 2003). To date, BsCopZ remains one of the best characterised prokaryotic copper metallochaperones as it has been studied both *in vivo* and *in vitro* and solution and crystal structures are available for this metallochaperone (Banci *et al.*, 2001b; Banci *et al.*, 2003b; Hearnshaw *et al.*, 2009; Kihlken *et al.*, 2002; Singleton *et al.*, 2009). The interaction of BsCopZ with its target protein – the CopA copper-transporter from *B. subtilis* (BsCopA) has also been studied (Banci *et al.*, 2003a; Radford *et al.*, 2003; Singleton *et al.*, 2009). The first BsCopZ structure to be reported was in its Cu(I)-bound form solved by NMR spectroscopy (Figure 5a) (Banci *et al.*, 2001b). The overall protein fold was found to be similar to apo-EhCopZ (Figure 3) although due its Cu(I)-bound state the structure of Cu(I)-BsCopZ provided additional information regarding metal-binding. As shown in Figure 5a, Cu(I) is bound directly by Cys13 and Cys16 comprising the $M_{11}XCXXC_{16}$ motif in BsCopZ. A hydrophobic interaction between Met11 and Tyr65 was also observed

which was hypothesised to protect the bound Cu(I) ion from oxidation by restricting its access by solvent (Banci *et al.*, 2001b). The structure of apo-BsCopZ provided further support for this hypothesis as in the apo-BsCopZ structure Met11 is exposed to the solvent (Banci *et al.*, 2003b) whereas in Cu(I)-BsCopZ Met11 points towards the bound Cu(I) ion (Figure 5a-b) (Banci *et al.*, 2001b). Similarly, Tyr65 was also found to be more solvent exposed in apo-BsCopZ (Figure 5a) compared to the Cu(I)-BsCopZ structure (Figure 5b) (Banci *et al.*, 2003b).

While BsCopZ was initially shown to be a monomer in solution in its apo- and Cu(I)-bound forms in the presence of dithiothreitol (DTT) (Banci *et al.*, 2001b), it was later reported that at high protein concentrations BsCopZ is a dimer in both apo- and Cu(I)-bound forms (Banci *et al.*, 2003c). Kilhken *et al.* (2002) found that in the absence of DTT and in the presence of 0.5 Cu(I) per protein, BsCopZ was primarily dimeric while in the presence of DTT and 0.5 Cu(I) per protein there was an equilibrium between the monomeric and dimeric states. Further Cu(I)-bound forms of BsCopZ have also been reported in solution (Kihlken *et al.*, 2002). The crystal structures of a Cu(I)-bound BsCopZ trimer (Singleton *et al.*, 2009) and a BsCopZ dimer containing four Cu(I) ions (Figure 5c) (Hearnshaw *et al.*, 2009) have also been determined. In the BsCopZ trimer Cu(I) was coordinated by both of the Cys residues in the MXCXXC motif and the Cys16 residue from a neighbouring subunit. Additional interactions reported in the BsCopZ trimer included interactions between Ser12 and a water molecule, between Tyr65 and two water molecules, and between His15 and Gln63 (Singleton *et al.*, 2009). In the four Cu(I)-bound BsCopZ dimer His15 from both subunits were shown to directly bind Cu(I) in addition to Cys13 and Cys16, as shown in Figure 5c (Hearnshaw *et al.*, 2009). A hydrophobic bond between Met11 and Tyr65 was also reported to contribute to the structural integrity of the protein and thus indirectly towards copper binding as well. Although the existence of the multiple copper-bound BsCopZ structures has not been reported *in vivo*, the formation of these structures highlights the flexibility in the copper-binding site of copper metallochaperones allowing it to adopt multiple copper-bound states which may exist in conditions of intracellular copper stress.

1.2.2.3 The *Archaeoglobus fulgidus* copper metallochaperone CopZ

The CopZ copper metallochaperone from the archaeon *Archaeoglobus fulgidus* (*A. fulgidus*) referred to as AfCopZ, is a relatively recent but perhaps the most unique member of the family of copper metallochaperones (Sazinsky *et al.*, 2007).

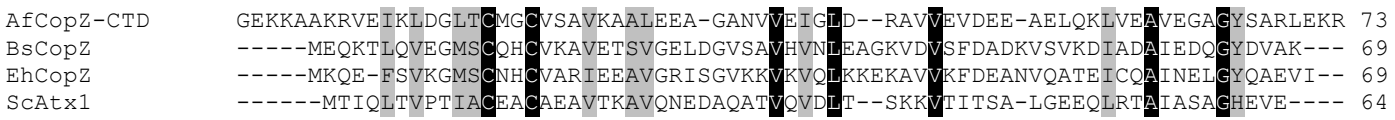

Figure 4: Sequence alignment of prokaryotic copper metallochaperones. The sequence alignments of the C-terminal copper metallochaperone domain of *A. fulgidus* CopZ denoted as AfCopZ-CTD (discussed in section 1.2.2.3) (GenBank accession code: 029901), BsCopZ (GenBank accession code: 032221) (discussed in section 1.2.2.2), EhCopZ (GenBank accession code: Q47840) (discussed in section 1.2.2.1), and ScAtx1 (GenBank accession code: NP_440560.1) (discussed in sections 1.2.2.4 and 1.4.3). Fully conserved residues are highlighted in black while semi-conserved residues are shown in grey.

Unlike the other known CopZ copper metallochaperones, AfCopZ contains an additional ~130 amino acids at the N-terminal end denoted as AfCopZ-NTD fused to the typical copper metallochaperone domain with the ferredoxin-like fold at the C-terminus denoted as AfCopZ-CTD (Figure 4) (Sazinsky *et al.*, 2007). The crystal structure of AfCopZ-NTD revealed a βααββββ-fold in addition to the presence of a 2Fe-2S cluster (Sazinsky *et al.*, 2007). AfCopZ-NTD and AfCopZ-CTD can both bind copper, while AfCopZ-NTD can also bind zinc. In addition, AfCopZ-NTD was shown to reduce Cu(II) to Cu(I) (Sazinsky *et al.*, 2007) which led to the hypothesis that perhaps Cu(II) is bound first by AfCopZ-NTD, reduced to Cu(I) and subsequently transferred to AfCopZ-CTD. It has further been proposed that the fusion of AfCopZ-NTD to AfCopZ-CTD may be a relic of evolutionary divergence between proteins containing only the ferredoxin-like fold found in the other CopZ metallochaperones (CopZ-like domain) and those containing the CopZ-like domain fused to a redox-active domain (Kim *et al.*, 2008). The transfer of Cu(I) has been demonstrated between Cu(I)-bound AfCopZ and the MBDs of AfCopA, and Cu(I)-bound AfCopZ-CTD has also been shown to deliver Cu(I) to the transmembrane metal-binding site (MBS) in AfCopA (Gonzalez-Guerrero *et al.*, 2009). In addition, Cu(I)-bound AfCopZ has also been shown to activate the Cu(I)-dependent turnover of AfCopA (Gonzalez-Guerro and Arguello, 2008).

1.2.2.4 The cyanobacterial copper metallochaperone ScAtx1

The cyanobacterial copper metallochaperone was discovered in *Synechocystis* PCC 6803 and was denoted as ScAtx1 (Tottey *et al.*, 2002). *Synechocystis* PCC 6803 cells devoid of the *scAtx1* gene exhibited decreased cytochrome *c* oxidase activity, although the effects were smaller than the cells lacking *pacS* suggesting that the effects of *scAtx1* deletion on the cytochrome *c* oxidase activity required the presence of PacS. In contrast, the deletion of both *scAtx1* and *ctaA* resulted in a greater decrease in cytochrome *c* activity compared to the cells lacking only one of these genes implying that ScAtx1 may be functional in the absence of CtaA (Tottey *et al.*, 2002). In addition, no significant difference in copper sensitivity was evident in the *scAtx1Δ* cells (Tottey *et al.*, 2002). ScAtx1 has also been shown to bind Zn(II), although the physiological importance of this has not been determined (Badarau *et al.*, 2010; Banci *et al.*, 2010b; Dainty *et al.*, 2010).

The solution structures of apo- and Cu(I)-bound ScAtx1 found it to contain a slightly shorter ferredoxin-like fold as it lacked the final β-strand in the usual βαββαβ-fold which is probably due to the fact that it is comparatively shorter (64 amino acids) than the other CopZ metallochaperones such as EhCopZ and BsCopZ (Figure 4) (Badarau *et al.*, 2010; Banci *et al.*, 2004a).

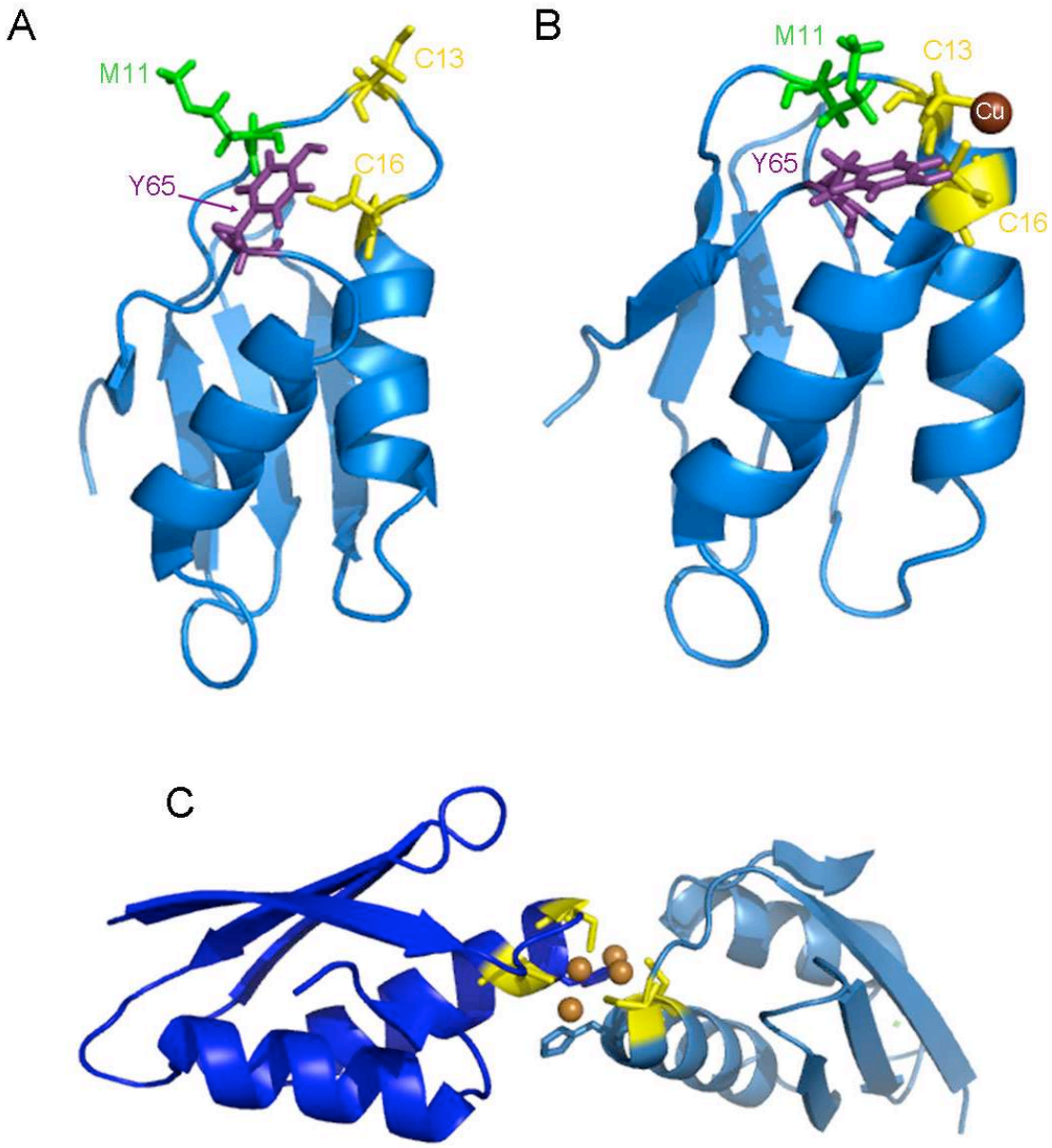

Figure 5: The structures of apo- and Cu(I)-bound BsCopZ. The solution structure of apo-BsCopZ (PDB accession code: 1p8g) (Banci *et al.*, 2003b) (A), Cu(I)-BsCopZ (PDB accession code: 1k0v) (Banci *et al.*, 2001b) (B), and the crystal structure of four Cu(I)-bound BsCopZ homodimer (PDB accession code: 2qif) (Hearnshaw *et al.*, 2009) where each subunit is shown in different shades of blue (C). In all of the figures the side chains of the metal-binding Cys residues are shown as yellow sticks. In (A) and (B) the side chains of Met11 and Tyr65 are shown as green and purple sticks, respectively. Cu(I) ions are shown as spheres in (B) and (C). The side chains of His15 are shown as sticks in (C).

Similar to BsCopZ, Cu(I) in ScAtx1 was also found to be trigonally coordinated in the solution structure (Banci *et al.*, 2004a). In addition to Cys12 and Cys15 of the $C_{12}XXC_{15}$-motif, His61 residue in loop 5 of ScAtx1 was reported as the third Cu(I)-binding ligand (Banci *et al.*, 2004a). The His61 residue in ScAtx1 is located in the analogous position to the BsCopZ Tyr65 residue, although Tyr65 was not shown to be involved in binding Cu(I) directly in the Cu(I)-bound BsCopZ structure (Banci *et al.*, 2001b). Another difference between BsCopZ and ScAtx1 involves the substitution of the Met residue in the MXCXXC motif by Ile (Ile10) in ScAtx1 which in contrast to BsCopZ Met11 residue does not change its orientation irrespective of Cu(I)-loading in ScAtx1 (Banci *et al.*, 2004a). In contrast to the solution structure of Cu(I)-ScAtx1, His61 was not shown to bind Cu(I) directly in most of the crystal structures of the Cu(I)-bound ScAtx1 dimers reported by Badarau *et al.* (2010).

The crystal structures demonstrated two Cu(I)- and four Cu(I)-bound ScAtx1 dimers in two different structural arrangements – head-to-head and side-to-side. In the head-to-head arrangement, ScAtx1 was found to dimerise either with two Cu(I) (shown in Figure 6a) or four Cu(I) ions (shown in Figure 6b). In the former structure Cu(I) atoms are directly coordinated by Cys12 and Cys15 of one subunit and Cys15 of the neighbouring subunit (Figure 6a). Whereas in the four Cu(I) per dimer, two of the Cu(I) ions are bound by Cys12 of one subunit and Cys15 and His61 of the other subunit, while the other two Cu(I) ions are coordinated by Cys12 and Cys15 of the monomer, as shown in Figure 6b (Badarau *et al.*, 2010). A crystal structure for the four Cu(I)-bound ScAtx1 homodimer in the side-to-side arrangement has also been determined in the presence of chloride (Badarau *et al.*, 2010). In this structure (Figure 6c), two of the Cu(I) ions are coordinated by Cys12 and Cys15 of each monomer while the other two Cu(I) ions are coordinated by Cys12 of each subunit and a chloride ion (Badarau *et al.*, 2010). In addition, His61 from both subunits also forms a hydrogen bond with one of the bound chloride ions (Badarau *et al.*, 2010). The importance of His61 is further highlighted by the fact that the mutation of this residue to Tyr resulted in the monomerisation of ScAtx1 at low Cu(I) concentrations (Badarau *et al.*, 2010). Further support for the physiological role for this residue was demonstrated in the studies investigating the interactions of ScAtx1 with CtaA MBD and the PacS MBD, as discussed further in section 1.4.3.

Similar to BsCopZ, the existence of multiple Cu(I)-bound structures of ScAtx1 may indicate the different structural conformations that ScAtx1 can adopt under conditions of copper stress. Badarau *et al.* (2010) also suggested that the presence of the head-to-head and the side-to-side ScAtx1 dimers may be reflective of the complexes formed between ScAtx1 and PacS MBD or CtaA MBD, as discussed further in section 1.4.3. While apo-ScAtx1 was reported to exist as a monomer in solution

(Badarau *et al.*, 2010; Banci *et al.*, 2004a), Cu(I)-bound ScAtx1 has been shown to form Cu(I)-mediated dimers (Badarau *et al.*, 2010). The dimerisation of ScAtx1 may not only help to sequester excess Cu(I) *in vivo*, but can also influence the transfer of Cu(I) from ScAtx1 to its target proteins (Badarau *et al.*, 2010), as discussed further in section 1.4.3.

1.2.2.5 The *Escherichia coli* copper metallochaperone CusF

For a long time it was thought that *Escherichia coli* (*E. coli*) did not contain a copper metallochaperone (Franke *et al.*, 2003; Gatti *et al.*, 2000). While an *E. coli* CopZ-like copper metallochaperone has not been identified to date, in 2003 the small periplasmic protein CusF (EcCusF), part of the *E. coli cusCFBA* operon was shown to interact with the periplasmic copper-binding protein CusB (EcCusB) and the copper-ATPase CusC (EcCusC) (Franke *et al.*, 2003).

The role of CusF as a copper metallochaperone was not established until 2008 when direct copper transfer was demonstrated between EcCusF and EcCusB (Bagai *et al.*, 2008). The crystal structure of apo-EcCusF demonstrated it to be a highly unusual copper metallochaperone as unlike most of the other CopZ metallochaperones it does not form a βαββαβ-fold; instead, the CusF structure comprises five β-strands that fold into a small β-barrel (Loftin *et al.*, 2005). Even more unusually, it does not contain any Cys residues, probably due to the oxidising environment of the *E. coli* periplasm which may lead to the formation of disulfide bridges between potential metal-binding Cys residues (Loftin *et al.*, 2007; Xue *et al.*, 2008). Combination of the data from Cu(I)-bound EcCusF and Ag(I)-bound EcCusF crystal structure and X-ray absorption spectroscopy on Cu(I)-bound EcCusF revealed the metal-binding site of EcCusF to trigonally coordinate one Cu(I) ion per EcCusF molecule by His36, Met47 and Met49 (Loftin *et al.*, 2005; Loftin *et al.*, 2007; Xue *et al.*, 2008). In addition, Trp44 residue was also shown to interact with the Cu(I)-binding site in CusF (Loftin *et al.*, 2005; Loftin *et al.*, 2007; Xue *et al.*, 2008). Isothermal titration calorimetry (ITC) experiments demonstrated a Cu(I)- or Ag(I)-dependent interaction between EcCusF and EcCusB where one of the two proteins was required in its apo-form (Bagai *et al.*, 2008). Both EcCusF and EcCusB were reported to have similar metal-binding affinities and in support of this, the transfer of metal between EcCusF and EcCusB was also shown to be reversible (Bagai *et al.*, 2008). This led to the suggestion that vectorial transfer of metal from EcCusF to EcCusB is likely achieved by the constant transport of Cu(I) or Ag(I) from EcCusB to the Cu(I) or Ag(I)-exporting ATPase CusC resulting in a favourable thermodynamic gradient for copper transfer (Bagai *et al.*, 2008).

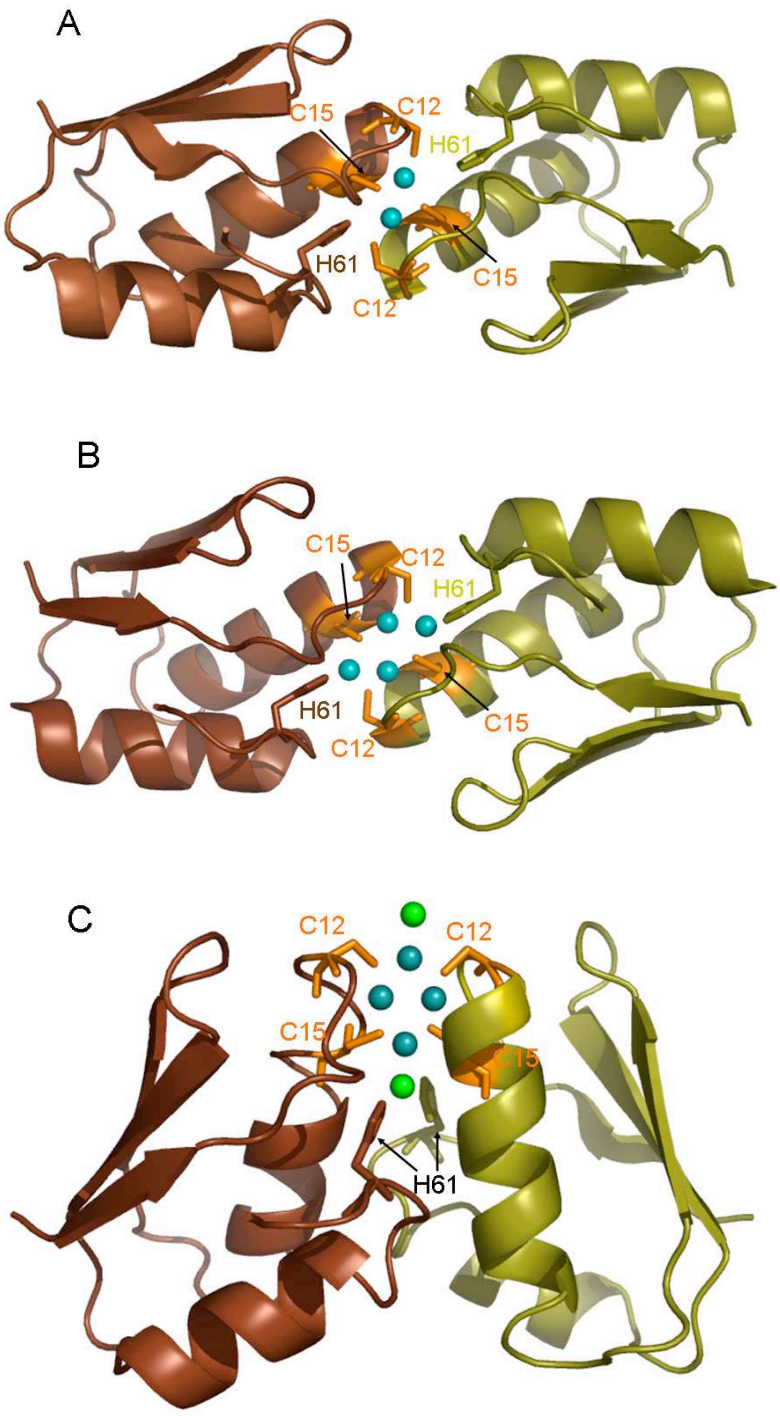

Figure 6: The crystal structures of ScAtx1 dimers. The crystal structure of ScAtx1 2 Cu(I)-bound head-to-head dimer (PDB accession code: 2xmt) (A), 4 Cu(I)-bound head-to-head dimer (PDB accession code: 2xmu) (B) and side-to-side dimer (PDB accession code: 2xmk) (C) (Badarau *et al.*, 2010). Each subunit in the dimer is represented in brown and yellow, Cu(I) ions are shown as blue spheres, chloride ions as green spheres and the side chains of the metal-binding Cys residues as orange sticks. The side chain of His61 from each subunit is shown as sticks.

1.2.3 Copper efflux in Prokaryotes

In order to minimise the concentration of free Cu(I) ions, Cu(I) is actively exported from the cells via copper-transporting ATPases. Copper-exporting ATPases from some of the prokaryotic organisms are discussed below.

1.2.3.1 CopA and CopB copper-exporting ATPases

CopA transporters have been identified in many prokaryotic organisms including *B. subtilis*, *E. coli* and *A. fulgidus*. The expression of the gene encoding CopA ATPase from *B. subtilis* (BsCopA) is induced by the presence of elevated copper levels and its deletion leads to increased copper sensitivity (Gaballa and Helmann, 2003). BsCopA contains two soluble MBDs at the N-terminus, denoted as BsCopAa and BsCopAb, which both contain the MXCXXC motif (Figure 2). Both of the BsCopA MBDs have been structurally characterised and were found to be similar to BsCopZ (Banci *et al.*, 2002; Singleton *et al.*, 2008). Although the MBDs have been shown to interact with BsCopZ and acquire copper from Cu(I)-bound BsCopZ (Banci *et al.*, 2003a; Radford *et al.*, 2003), the exact function of the MBDs is not known. A structural model between BsCopZ-Cu(I)-BsCopAb highlighted the role of the electrostatic interactions between Asp62 and Glu21 in BsCopZ and Lys23 and Arg20 of BsCopAb respectively, in mediating protein-protein interaction (Banci *et al.*, 2003a). The BsCopZ interaction with BsCopAb was proposed to progress by a ligand-transfer mechanism involving a three coordinate Cu(I)-bound intermediate, where Cu(I) was transferred from Cu(I)-BsCopZ to apo-BsCopAb (Banci *et al.*, 2003a). Formation of a multinuclear Cu(I) cluster in the presence of excess Cu(I) has also been reported to result in the dimerisation of the MBDs *in vitro* (Singleton *et al.*, 2008; Singleton and Le Brun, 2009). However, neither the presence nor the physiological relevance of these multiple Cu(I)-bound forms of BsCopA MBDs has been established. The CopA ATPase from *E. coli* (EcCopA) also contains two MBDs at the N-terminus (Rensing *et al.*, 2000). Similar to BsCopA, EcCopA is also induced by Cu(I) and confers copper resistance *in vivo* by mediating Cu(I)-efflux from the cell (Fan and Rosen, 2002; Rensing *et al.*, 2000). Determining the role of EcCopA MBDs is more challenging than in *B. subtilis* since no known CopZ-like metallochaperone has been found in *E. coli*. Studies by Fan *et al*. have shown that the deletion of EhCopA MBDs leads to perturbed copper transport and copper resistance (Fan *et al.*, 2001; Fan and Rosen, 2002).

AfCopA is unusual since unlike most of the copper-transporting P_{1B}-type ATPases, it contains a MBD at both its N- and C-termini denoted as AfCopAa and AfCopAb respectively (Mandal *et al.*, 2002). Similar to the MBDs from the other CopA proteins, both AfCopA MBDs demonstrate the βαββαβ-fold (Wu *et al.*, 2008) although recently an unusual crystal structure was reported for AfCopAb (Agarwal *et al.*, 2010). The structure of AfCopAb reveals it to be a homodimer where the N-terminal β-strand

was shown to "swap" with the analogous strand from the other monomer. However, this structure was suggested to be an artefact of crystallisation as the copper-binding Cys residues in the $C_{16}XXC_{19}$ motif were shown to form intramolecular disulfide bonds and the structure itself was shown to be stabilised by the binding of a citrate molecule, neither of which are expected to be present *in vivo* (Agarwal *et al.*, 2010). Similar to ScAtx1, AfCopAb also does not contain a MXCXXC site, as the Met residue is replaced by Leu (Leu14). Leu14 is expected to perform a similar function to Met11 in BsCopZ in stabilising the hydrophobic packing of the protein (Agarwal *et al.*, 2010). Cu(I)-transfer has been reported between Cu(I)-AfCopZ and apo-AfCopA MBDs (Gonzalez-Guerro and Arguello, 2008; Sazinsky *et al.*, 2007), although Cu(I) was shown to be transferred more efficiently from Cu(I)-AfCopZ to AfCopAb than AfCopAa (Gonzalez-Guerro and Arguello, 2008). Agarwal *et al.* (2010) proposed that the higher Cu(I) affinity of AfCopAb may be due to the presence of two His residues in the $C_{16}HHC_{19}$ motif of AfCopAb, one of which (His18) may provide a third ligand to Cu(I) in addition to Cys16 and Cys19, whereas His18 and His19 are replaced by Ala and Met respectively, in AfCopAa (Figure 2).

A low resolution electron microscopy determined structure of AfCopA revealed AfCopAa to be positioned between the N- and the A-domains of the protein (Wu *et al.*, 2008). This led the authors to propose a model where the apo-AfCopAa can interact with the N-domain of AfCopA and occlude the binding of ATP to AfCopA (Wu *et al.*, 2008). Cu(I)-bound AfCopAa may not be able to interact with the N-domain of AfCopA resulting in the binding of ATP and Cu(I)-transport across the membrane (Wu *et al.*, 2008). In support of this model, both of the AfCopA MBDs have been shown to interact with the N-domain of AfCopA, while the AfCopAb can also interact with the A-domain of AfCopA (Gonzalez-Guerrero *et al.*, 2009). However, *in vivo* studies are required to render support for the proposed model. *A. fulgidus* also contains another P_{1B}-type copper-transporting ATPase termed CopB (AfCopB) which is also involved in copper efflux (Mana-Capelli *et al.*, 2003). Unlike AfCopA, AfCopB contains a singular His-rich MBD at its N-terminus which has been implicated in mediating enzyme turnover (Mana-Capelli *et al.*, 2003). The AfCopB MBD is similar to the MBD of EhCopB which also contains several His residues. EhCopB is located in the cytoplasmic membrane of *E. hirae* and has also been shown to mediate copper efflux from the cytoplasm (Odermatt *et al.*, 1993; Odermatt *et al.*, 1994).

1.2.3.2 The cyanobacterial copper-transporting ATPase PacS

PacS was first identified in *Synechococcus* PCC 7942 located primarily at the thylakoid membrane (Kanamaru *et al.*, 1993). However, this study will focus on the PacS homologue identified in *Synechocystis* PCC 6803 (Tottey *et al.*, 2001) and unless stated otherwise, in this study PacS refers to the copper-ATPase from *Synechocystis*

PCC 6803. PacS has been shown to mediate copper transport into the thylakoid compartment where Cu(I) is required for plastocyanin and cytochrome *c* oxidase (Tottey *et al.*, 2001). Tottey *et al*. (2001) demonstrated that the deletion of *pacS* in *Synechocystis* PCC 6803 led to copper sensitivity, decreased transcription of the gene coding for plastocyanin and simultaneous increase in the transcription of the gene coding for cytochrome c_6 suggesting that Cu(I) import by PacS is essential for plastocyanin-mediated Cu(I) delivery to cytochrome *c* oxidase. PacS contains a single MBD at its N-terminus (PacS MBD) which is a monomer in solution in the apo-state (Badarau *et al.*, 2010; Banci *et al.*, 2006c) and in the presence of one equivalent of Cu(I) (Badarau *et al.*, 2010). PacS MBD has been structurally characterised in solution in its apo-state (Banci *et al.*, 2006c) and by X-ray crystallography in its Cu(I)-bound form (Badarau *et al.*, 2010). The Cu(I)-bound PacS MBD was the first native metal bound MBD from a copper-transporting ATPase to be characterised by X-ray crystallography (Badarau *et al.*, 2010). The crystal structure demonstrated a PacS MBD homotrimer where each subunit contains the βαββαβ-fold and binds one Cu(I) via Cys14 and Cys17 located in the $M_{12}XCXXC_{17}$ motif, in addition to a weak bond provided by Cys14 of the neighbouring subunit, as shown in Figure 7 (Badarau *et al.*, 2010). While there are similarities between the Cu(I)-$PacS_N$ trimer and the Cu(I)-BsCopZ trimer, there are also several differences between them including the role of the Tyr residue located in the loop 5 of these proteins. As mentioned previously (1.2.2.2), Tyr65 in the Cu(I)-BsCopZ trimer hydrogen bonds with two water molecules, whereas in the Cu(I)-PacS MBD trimer Tyr65 hydrogen bonds with the Cu(I)-coordinating Cys17 residue (Badarau *et al.*, 2010). PacS MBD has also been shown to acquire Cu(I) by direct interaction with ScAtx1, as discussed in section 1.4.3. Investigating the interaction between PacS MBD and ScAtx1 was one of the aims of this study.

1.3 Regulation of copper in Eukaryotes

Unlike prokaryotes, there is a cytosolic requirement for copper in eukaryotic cells. Copper is required to traverse the plasma membrane in order to be incorporated into copper-dependent cytosolic proteins such as SOD1 (see section 1.3.2.3) and for the function of various proteins in other cellular organelles such as the mitochondria and the golgi compartment. Another major difference between the copper homeostasis in prokaryotes compared to eukaryotes includes the multi-cellular nature of most eukaryotic organisms and the complex regulation of copper concentration and localisation in the multiple membrane-encoded organelles within the eukartyotic cells. These differences account for the considerably larger number of copper-binding proteins present in eukaryotes (31 to 160 proteins) compared to the average number of copper-binding proteins present in archaea (0 to 38 proteins) and bacteria (0 to 31 proteins) (Andreini *et al.*, 2008).

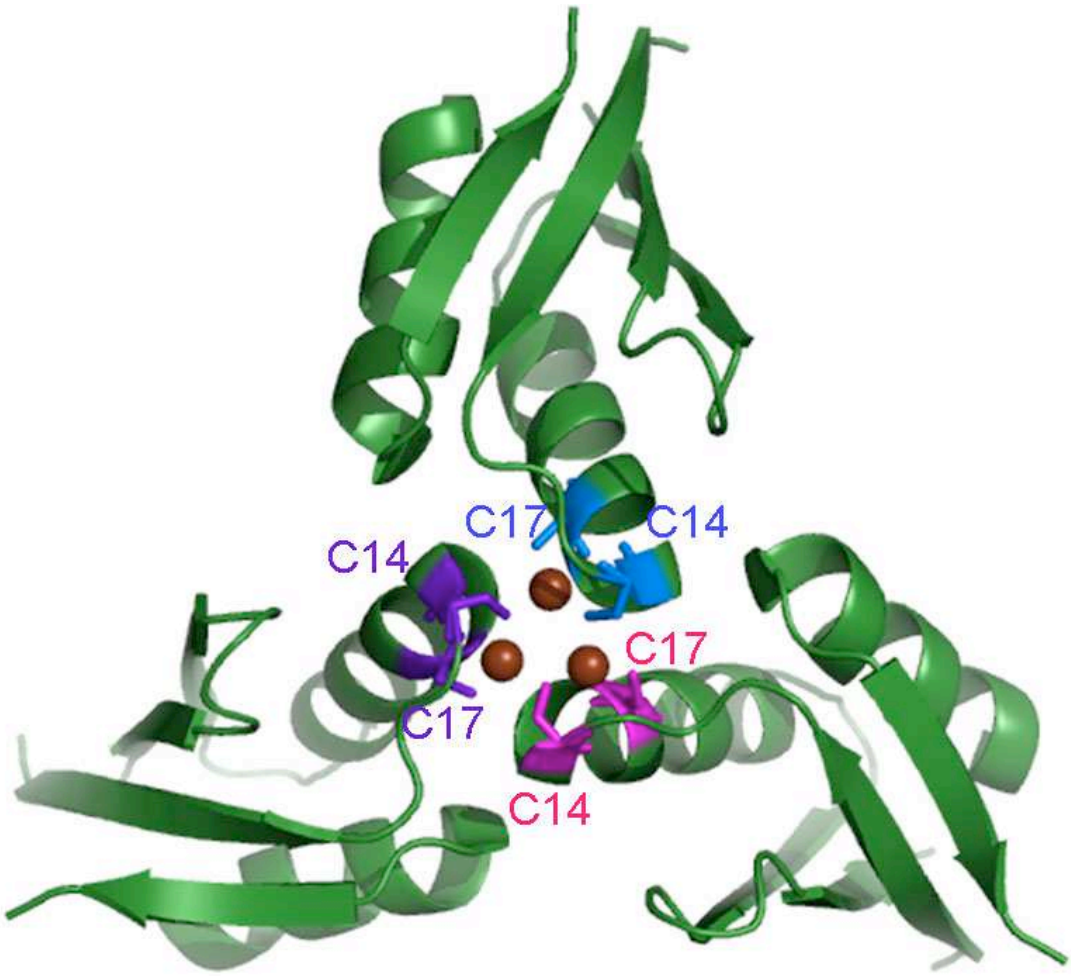

Figure 7: The crystal structure of Cu(I)-PacS MBD trimer. The structure of Cu(I)-bound PacS MBD (PDB accession code: 2xmw) trimer solved by X-ray crystallography (Badarau *et al.*, 2010). The metal-binding Cys residues are shown as sticks and Cu(I) are shown as spheres.

1.3.1 Import of copper in Eukaryotes

Copper is imported in eukaryotes by the family of copper-transport proteins (CTR) and DMT1. CTR proteins are membrane-bound copper-transporters that mediate high affinity uptake of Cu(I) into the eukaryotic cytoplasm. The number of CTR proteins varies between different eukaryotic organisms, for instance, *S. cerevisiae* and the fruit-fly *Drosophila melanogaster* (*D. melanogaster*) have three isoforms while, *H. sapiens* possess two known isoforms (Balamurugan and Schaffner, 2006).

The most ubiquitous isoform of CTR proteins in eukaryotes is the CTR1 transporter. While the size and localisation of CTR1 may vary, some conserved characteristics include the presence of an extracytoplasmic N-terminal domain (NTD), three transmembrane helices and a cytoplasmic C-terminal domain (CTD). All CTR1 proteins possess a conserved MXXXM motif in the second transmembrane helix which is known to be vital for mediating Cu(I) transport (Kaplan and Lutsenko, 2009; Molloy and Kaplan, 2009; van den Berghe and Klomp, 2010). The NTD of human CTR1 (hCTR1) and yeast Ctr1 (Ctr1) contain several Met and His residues which can potentially bind Cu(I) and mediate its uptake from currently unidentified sources (Guo *et al.*, 2004; Jiang *et al.*, 2005; Maryon *et al.*, 2007; Puig *et al.*, 2002). In addition, yeast two-hybrid experiments have implicated hCTR1 NTD in mediating oligomerisation of hCTR1 (Klomp *et al.*, 2003). It has previously been shown that the transport of Cu(I) via CTR1 is not dependent on ATP hydrolysis (Lee *et al.*, 2002a). Electron crystallography deduced structures show three monomers of hCTR1 arranged as a trimer in the lipid bilayer forming a 'cone-shaped pore' which would enable the passage of Cu(I) through it (Aller and Unger, 2006; De Feo *et al.*, 2009). De Feo *et al.* (2009) suggested that the transport of Cu(I) through hCTR1 is likely thermodynamically favourable as the 'HCH' Cu(I)-binding site in hCTR1 CTD would probably form a more stable Cu(I)-bound complex than the intramembranous Met-rich Cu(I)-binding site. The Cys residue in the hCTR1 CTD HCH-motif has also been implicated in oligomerisation of hCTR1 (Eisses and Kaplan, 2005). The import of the anti-cancer drug cisplatin via hCTR1 has further highlighted its importance in humans (Holzer *et al.*, 2004; Holzer *et al.*, 2006).

hCTR1 is primarily localised at the plasma membrane and in the membranes of endocytic vesicles (Eisses and Kaplan, 2005; Kaplan and Lutsenko, 2009; Maryon *et al.*, 2007; Prohaska, 2008). Based on the data Ctr1 and Ctr3 from *S. cerevisiae*, it has been hypothesised that hCTR1 may also be localised to the cell membrane when the extracellular copper concentration is low but gets internalised to endocytic vesicles in the presence of high extracellular copper concentration. However, there is conflicting evidence regarding this hypothesis and no consensus has been reached (Bauerly *et al.*, 2004; Eisses *et al.*, 2005; Klomp *et al.*, 2002; Molloy and

Kaplan, 2009; Petris *et al.*, 2003). CTR1 is also regulated at the transcriptional level. In yeast, the transcription of *CTR1* is regulated by the activity of Mac1 such that the transcription of *CTR1* is induced in the presence of low intracellular copper levels and inhibited at high concentrations of copper (Graden and Winge, 1997; Jensen *et al.*, 1998; Joshi *et al.*, 1999; Pena *et al.*, 1998). In humans, the transcription of *hCTR1* has recently been shown to be regulated by the zinc-finger domain of the transcription factor Sp1 in response to intracellular copper levels, similar to the regulation of *CTR1* by Mac1 (Song *et al.*, 2008). This is in contrast to the previous findings where Mac1-like regulation was not associated with hCTR1, and it was thought to be regulated primarily at the post-translational level (Kuo *et al.*, 2007; Maryon *et al.*, 2007; Prohaska, 2008; Song *et al.*, 2008; van den Berghe and Klomp, 2010). Further *in vivo* studies are therefore required to confirm the transcriptional and copper-dependent regulation of hCTR1. Unlike hCTR1, the hCTR2 transporter is predominantly localised to the lysosomal and endosomal membranes in humans. In yeast, Ctr2 has been shown to be localised in the vacuolar membrane and is hypothesised to regulate the release of Cu(I) from internal Cu(I) storage pools (Portnoy *et al.*, 2001; Rees *et al.*, 2004; van den Berghe *et al.*, 2007). While both CTR1 and CTR2 proteins are vital for high affinity copper uptake, there is some evidence to suggest the presence of CTR-independent copper uptake as well in mammalian cells (Lee *et al.*, 2002b). Although the identity of the CTR-independent copper uptake protein is not known, a possible candidate includes the DMT1 transporter.

DMT1 also known as Nramp2 or DCT1 is a membrane-bound cation transporter expressed ubiquitously in eukaryotes (Garrick *et al.*, 2003). While its main substrate is Fe(II), DMT1 is also known to transport other divalent cations including Cu(II), Zn(II), Mn(II), Co(II) and Ni(II) (Gunshin *et al.*, 1997; Knopfel *et al.*, 2000; Sacher *et al.*, 2001). There is also some evidence to suggest that copper may be transported through DMT1 in its Cu(I) oxidation state, although the bulk of the evidence indicates Cu(II) to be the preferred oxidation state for transport (Arredondo *et al.*, 2003; Garrick *et al.*, 2003; Knopfel *et al.*, 2000; Knopfel *et al.*, 2005). DMT1 may play a more important role in the brain where CTR1 is expressed in reduced levels compared to its expression in other tissues (Gunshin *et al.*, 1997; Lee *et al.*, 1998; Zhou and Gitschier, 1997). DMT1 has also been implicated in several neurodegenerative disorders including PD and AD (Xu *et al.*, 2008; Zhang *et al.*, 2009; Zheng *et al.*, 2009). In AD, DMT1 has been dectected in senile plaques, and also found to down-regulate the expression of the amyloid precursor protein (APP) resulting in decreased production of Aβ (Zheng *et al.*, 2009). Further studies are however required to establish the extent of DMT1-mediated copper uptake in eukaryotic cells and, in particular, its role in the brain.

1.3.2 Copper binding proteins in the Eukaryotic cytoplasm

Inside the cell Cu(I) remains bound to cytosolic proteins such as the copper metallochaperones and SOD1 or by small proteins like metallothionein and the tripeptide glutathione which all contribute in maintaining strict copper homeostasis.

1.3.2.1 Metallothioneins and Glutathione

Metallothioneins are small, cysteine-rich polypeptides found in all eukaryotic organisms and some prokaryotic organisms. They have a very high affinity for Cu(I), in addition to other metals including Zn(II) and Cd(II) (Blindauer and Leszczyszyn, 2010; Egli *et al.*, 2006). Multiple Cu(I) ions can be bound by metallothioneins resulting in the formation of metal-sulfur clusters (Blindauer and Leszczyszyn, 2010). In addition to metal-ion detoxification, metallothioneins have also been associated with other functions including neuroprotection, anti-inflammation and anti-oxidation in mammals (Blindauer and Leszczyszyn, 2010). The number of metallothionein proteins in eukaryotes has been shown to vary between different organisms. While *S. cerevisiae* contain only two metallothionein proteins (Cup1 and CRS5) (Butt *et al.*, 1984; Culotta *et al.*, 1994; Fogel and Welch, 1982), *D. melanogaster* (MtnA-D) (Egli *et al.*, 2006) and mammals contain four metallothionein proteins (MT1-4) (Balamurugan and Schaffner, 2006). The genes encoding metallothioneins are induced in the presence of copper toxicity, and Cu(I)-bound metallothioneins can also act as intracellular copper stores mediating copper release in the event of copper deficiency (Balamurugan and Schaffner, 2006; Miyayama *et al.*, 2009; Prohaska and Gybina, 2004; Suzuki *et al.*, 2002).

The most prominent anti-oxidant defence mechanism in eukaryotes involves the tripeptide glutathione comprised of glutamate, cysteine and glycine. It is a ubiquitously expressed non-protein thiol present in upto 10 mM concentration in both eukaryotes and prokaryotes (Dalle-Donne *et al.*, 2009; Penninckx, 2002). Glutathione is present in the cells in either its reduced state (GSH) or in an oxidised state (GSSG) and is vital for maintaining a net reducing environment in the cell (Dalle-Donne *et al.*, 2009). Under normal unstressed conditions the ratio of GSH:GSSG is more than 100 (Maher, 2005). GSH is a vital co-factor for the enzyme GSH peroxidase which catalyzes the breakdown of hydrogen peroxide into water and dioxygen, and therefore limits one of the substrates for potential Fenton reactions (see equation 1) (Chance *et al.*, 1979). Reduced GSH is in turn regenerated by the reduction of GSSG by GSH reductase (Dalle-Donne *et al.*, 2009). GSH also contributes in limiting copper-mediated cytotoxicity by sequestering Cu(I) (Equation 4) and is especially important in the brain which is particularly vulnerable to oxidative stress (Aoyama *et al.*, 2008).

$$2Cu(II) + 6GSH \rightarrow 2Cu(I)\text{-}[GSH]_2 + GSSG \qquad [4]$$

The Cu(I)-$[GSH]_2$ complex can act as a copper source for the copper-free forms of metallothionein, SOD1 and ceruloplasmin (Carroll *et al.*, 2004; Ciriolo *et al.*, 1990; Ferreira *et al.*, 1993; Musci *et al.*, 1996). However, Cu(I)-$[GSH]_2$ complex has also been implicated in facilitating the generation of superoxide anions as a consequence of its reaction with molecular oxygen (Speisky *et al.*, 2008; Speisky *et al.*, 2009). This suggests that a tight balance has to be maintained in the cell to limit the pro-oxidant capacity of GSH and enhance its role as an anti-oxidant, which requires the concerted support from other proteins involved in copper homeostasis including SOD1 and metallothionein.

1.3.2.2 Ceruloplasmin and Hephaestin

In mammals up to 95 % of copper in the serum is bound by the ferroxidase ceruloplasmin (Takahashi *et al.*, 1984). Ceruloplasmin oxidises Fe(II) to Fe(III) for the cellular distribution of iron by transferrin. Ceruloplasmin is primarily located in the liver where it receives copper from the P_{1B}-type ATPase ATP7B (section 1.3.3.3), although it is also expressed in other tissues including the brain (Fleming and Gitlin, 1990; Klomp and Gitlin, 1996). Ceruloplasmin is capable of binding upto seven Cu(II) ions per molecule (Takahashi *et al.*, 1984). Copper-binding increases the stability of ceruloplasmin and is necessary for its ferroxidase activity (Gitlin *et al.*, 1992; Holtzman and Gaumnitz, 1970) but does not affect the rate of synthesis or the secretion of ceruloplasmin (Takahashi *et al.*, 1984). Decreased concentration of ceruloplasmin is observed in patients suffering from Wilson's disease, and is one of the diagnostic tests for identifying this disease (Hellman and Gitlin, 2002; Scheinberg and Gitlin, 1952). In addition, patients suffering from the disease aceruloplasminemia contain significantly decreased levels of serum ceruloplasmin and demonstrate excessive iron accumulation in the liver and brain (Hellman and Gitlin, 2002; Morita *et al.*, 1995).

Hephaestin, a homologue of ceruloplasmin was identified in mammals in 1999 (Vulpe *et al.*, 1999). Although both ceruloplasmin and hephaestin are multi-copper ferroxidases involved in the export of iron, their different expression patterns establish a requirement for both of these proteins in mammals. While hephaestin is predominantly expressed in the small intestine and the colon, ceruloplasmin is expressed primarily in the liver with no expression detected in the small intestine (Harris *et al.*, 1999; Vulpe *et al.*, 1999). Unlike ceruloplasmin, hephaestin is a membrane-bound protein similar to Fet3p, the yeast homologue of ceruloplasmin, and has subsequently been shown to complement for the lack of ferroxidase activity in *S. cerevisiae* cells lacking the gene coding for Fet3p (Li *et al.*, 2003). Although the lack of hephaestin has not been implicated in a specific disorder, its presence explains the absence of anaemia in patients suffering from Wilson's disease (Vulpe *et al.*, 1999).

Thus, the presence of ceruloplasmin and hephaestin intricately links the homeostasis of copper and iron in eukaryotes.

1.3.2.3 Superoxide Dismutases

The superoxide dismutase (SOD) enzymes are vital for catalytically mediating the disproportionation of superoxide radicals into hydrogen peroxide and molecular oxygen (McCord and Fridovich, 1969). SOD proteins are not exclusive to eukaryotes but are also expressed in prokaryotes (Culotta *et al.*, 2006). There are three types of known SOD proteins in eukaryotes denoted SOD1, SOD2 or SOD3 on the basis of the transition metal co-factor involved in mediating the dismutation reaction, and the localisation of the expressed protein. SOD1 is a copper- and zinc-binding enzyme located primarily in the cytosol in addition to the intermembrane space of mitochondria, lysosomes, peroxisomes and the nucleus (Chang *et al.*, 1988; Keller *et al.*, 1991; Wood and Thiele, 2009). Eukaryotic SOD1 exists as a dimer where each subunit binds one copper, one zinc, and contains a conserved intra-subunit disulfide bond between two conserved cysteines – Cys57 and Cys146 in human SOD1 (hSOD1), as shown in Figure 8 (Parge *et al.*, 1992; Strange *et al.*, 2003). While copper is essential for the dismutation reaction, the binding of Zn(II) contributes to the thermal stability of SOD1 (Forman and Fridovich, 1973).

Initially it was thought that the activation of SOD1 which includes the formation of the intrasubunit disulfide bond and the acquisition of copper, was wholly dependent on the presence of the copper metallochaperone for SOD1 (CCS) (Leitch *et al.*, 2009b). However, it is now evident that the dependence on CCS for the activation of SOD1 can vary between different organisms (Leitch *et al.*, 2009a). The activation of SOD1 from *S. cerevisae* (Sod1) is completely dependent on yeast CCS (Ccs1), whereas SOD1 from *Caenorhabitis elegans* (*C. elegans*) is activated completely independently of CCS as it even lacks a CCS homologue (Jensen and Culotta, 2005; Leitch *et al.*, 2009a). In humans and other mammals, SOD1 can be activated by both CCS-dependent and independent pathways (Leitch *et al.*, 2009a; Leitch *et al.*, 2009b). Leitch *et al.* (2009b) have found that the CCS-independent activation of SOD1 is only possible with SOD1 proteins that lack a Pro residue at position 144. It has been shown that mutation of Sod1 Pro144 to Leu, Ser or Gln enables CCS-independent activation of Sod1 like hSOD1 and *C. elegans* SOD1 which lack a Pro at this position (Leitch *et al.*, 2009a).

The importance of SOD1 is highlighted in the progressive motor neurodegeneration disease familial ALS (fALS). Amongst the 10 % of the ALS cases that are known to be familial, almost one-fifth of those are caused by mutations in the *SOD1* gene (Valentine *et al.*, 2005). More than 100 fALS-causing mutations are known in SOD1 including mutations at the dimer interface and the metal-binding region

(Valentine *et al.*, 2005). Mutation in SOD1 results in the gain-of-function of toxic properties which underlie SOD1-associated fALS pathogenesis (Valentine *et al.*, 2005). The two major proposed gain-of-functions associated with fALS SOD1 mutants include the acquirement of a pro-oxidant activity and an increased propensity to aggregate. However, the precise mechanism underlying SOD1-mediated fALS pathogenesis and its link with neurodegeneration is yet to be determined conclusively (Furukawa and O'Halloran, 2006; Valentine *et al.*, 2005).

Eukaryotic SOD2 is a manganese-binding enzyme largely localised in the mitochondria where it is the chief anti-oxidant enzyme involved in the dismutation of the superoxide radicals produced as an undesired by-product of respiration (Culotta *et al.*, 2006). The deletion of the *SOD2* gene in mice and *D. melanogaster* has been shown to result in early mortality (Duttaroy *et al.*, 2003; Kirby *et al.*, 2002; Lebovitz *et al.*, 1996; Li *et al.*, 1995). Unlike SOD1, the mechanism underlying manganese incorporation in SOD2 is currently not known (Culotta *et al.*, 2006). SOD3 is a copper- and zinc-binding enzyme found in mammals, but unlike SOD1 it is produced and secreted by the vascular smooth muscle cells and is therefore localised extracellularly (Culotta *et al.*, 2006; Stralin *et al.*, 1995). In addition, SOD3 has been reported to acquire its copper co-factor not from CCS but by the ATX1 copper metallochaperones (Itoh *et al.*, 2008; Itoh *et al.*, 2009), as discussed in section 1.3.2.4.1.

1.3.2.4 Eukaryotic Copper Metallochaperones

The eukaryotic copper metallochaperones are classified into three main categories – the ATX1 proteins, CCS, and the metallochaperones involved in mediating copper delivery to cytochrome oxidase in the mitochondria.

1.3.2.4.1 The Anti-oxidant 1 (ATX1) family of copper metallochaperones

The cytosolic 73 amino acid anti-oxidant 1 protein from *S. cerevisiae* (Atx1) (Figure 9a) was first discovered in 1995 as a mediator of defence against superoxide-related cellular toxicity (Lin and Culotta, 1995). However, its role as a physiological antioxidant was later dismissed as copper-bound Atx1 was shown to dismutate superoxide in a stoichiometric and non-catalytic manner (Portnoy *et al.*, 1999). The function of Atx1 as a copper metallochaperone for the P_{1B}-type ATPase Ccc2 was established in 1997 (Lin *et al.*, 1997; Pufahl *et al.*, 1997).

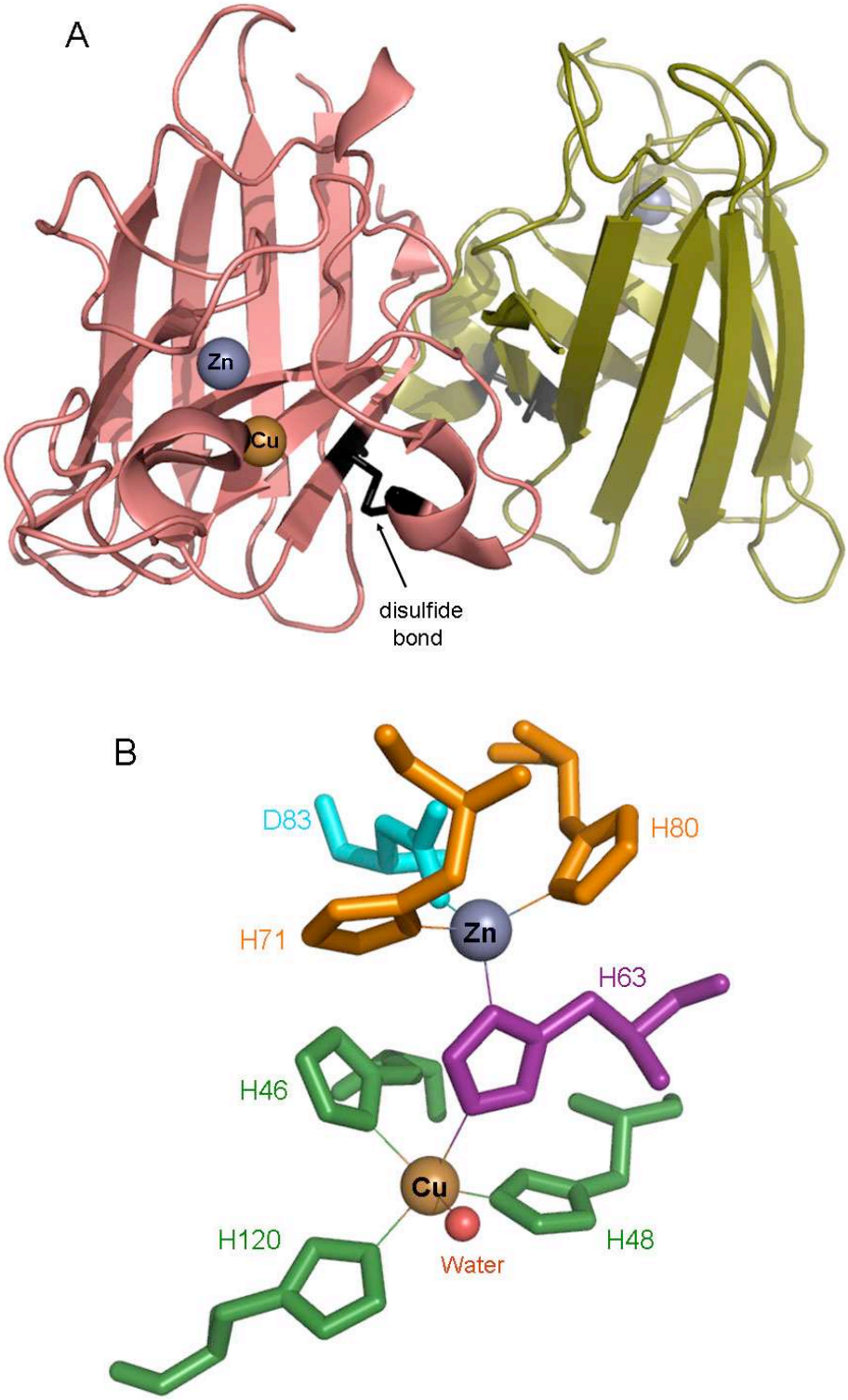

Figure 8: The crystal structure of holo-hSOD1 and the residues coordinating the binding of Cu(II) and Zn(II) in it. The crystal structure of Cu(II) (brown sphere)- and Zn(II)-bound (purple sphere) hSOD1 dimer (PDB accession code: 1hl5) is shown in (A) (Strange *et al.*, 2003). The subunits are shown in pink and yellow. The intrasubunit disulfide bonds are shown in black. The ligands coordinating the binding of Cu(II) and Zn(II) in (A) are shown in (B), as labelled.

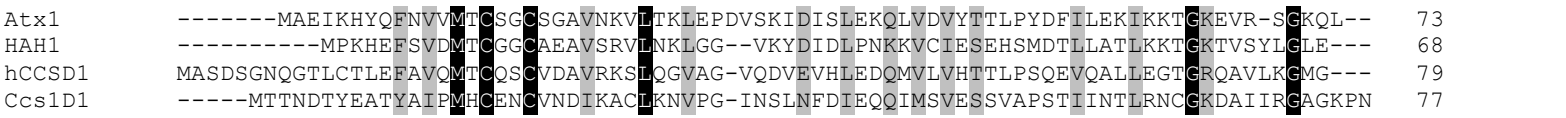

(A)

(B)

Figure 9: Sequence alignment of Eukaryotic copper metallochaperones. The sequence alignments of Atx1 (GenBank accession code: NP_014140) (discussed in section 1.3.2.4.1), HAH1 (GenBank accession code: NP_004036) (discussed in section 1.3.2.4.1), *H. sapiens* CCS domain 1 (hCCSD1; GenBank accession code: NP_005116) (discussed in sections 1.3.2.4.2 and 1.4.4) and Ccs1 domain 1 (CCSD1; GenBank accession code: NP_013752) (discussed in sections 1.3.2.4.2 and 1.4.4) are shown in (A). The sequence alignment of hCCS and Ccs1 is shown in (B). Fully conserved residues are highlighted in black while semi-conserved residues are shown in grey.

In vitro and *in vivo* studies have shown that Cu(I) transported from Atx1 to Ccc2 is subsequently required for incorporation in the copper-dependent ferroxidase Fet3 (Lin *et al.*, 1997; Stearman *et al.*, 1996; Yuan *et al.*, 1995). Yeast mutants lacking Atx1 were shown to be deficient in the high affinity uptake of iron (Lin *et al.*, 1997). *In vitro* experiments have shown Atx1 to receive Cu(I) from the Cu(I)-bound cytosolic domain of Ctr1, although this is yet to be verified *in vivo* (Xiao and Wedd, 2002; Xiao *et al.*, 2004). Solution structures of Cu(I)-bound Atx1 were shown to contain the βαββαβ-fold where Cu(I) (Arnesano *et al.*, 2001b), is coordinated by Cys15 and Cys18 of the $M_{13}XCXXC_{18}$ motif in Cu(I)-Atx1, although a higher co-ordination number has also been proposed for Cu(I)-binding (Arnesano *et al.*, 2001b; Pufahl *et al.*, 1997; Rosenzweig *et al.*, 1999). Lys65 in loop 5 of Atx1 (analogous to Tyr65 of BsCopZ), has also been proposed to be important for stabilising the metal-bound complex (Arnesano *et al.*, 2001b). The orientation of this residue towards the metal-binding site after Cu(I)-binding has been suggested to induce the movement of loop 5 such that it helps to protect the metal-bound Cys ligands from solvation (Arnesano *et al.*, 2001b). *In vivo* studies have also shown Lys65 to be important for interaction with the Ccc2 MBDs (Portnoy *et al.*, 1999), as discussed further in section 1.4.1.

The human homologue of Atx1 (HAH1) is a cytosolic 68 amino acid protein containing the $M_{10}XCXXC_{15}$ motif (Figure 9a) that binds Cu(I) and transports it to the P_{1B}-type ATPases ATP7A and ATP7B (Hamza *et al.*, 1999; Hung *et al.*, 1998; Larin *et al.*, 1999). HAH1 is a functional homologue of Atx1, as the presence of this protein was shown to reconstitute the growth defects and impaired iron homeostasis in yeast cells lacking Atx1 (Klomp *et al.*, 1997). The Cu(I)-bound crystal structure of HAH1 was the first structure to be solved by X-ray crystallography of a copper metallochaperone bound to its physiological substrate (Wernimont *et al.*, 2000). In the Cu(I)-bound HAH1 dimer, a single Cu(I) ion was shown to be tri-coordinated by Cys12 and Cys15 of one monomer and Cys15 of the other subunit, as shown in Figure 10. The HAH1 dimer was shown to be further stabilised by various intermolecular hydrogen-bonding interactions. These include the intersubunit interactions between Cys12 and Thr11 where Thr11 was also shown to hydrogen bond to a water molecule which in turn interacted with Asp9 of the same monomer (Wernimont *et al.*, 2000). Thr11 was therefore proposed to contribute to the orientation of the metal-binding loop and its stabilisation upon Cu(I)-binding (Wernimont *et al.*, 2000). The Lys60 residues in the Cu(I)-HAH1 dimer were shown to interact with the Cu(I)-binding residues via hydrogen-bonding to a bridging water molecule (Wernimont *et al.*, 2000). Unlike Lys65 in Atx1, the mutation of HAH1 Lys60 to Gly was not shown to be important for mediating the yeast two-hybrid interactions with its target proteins (Larin *et al.*, 1999), as discussed further in section 1.4.2.

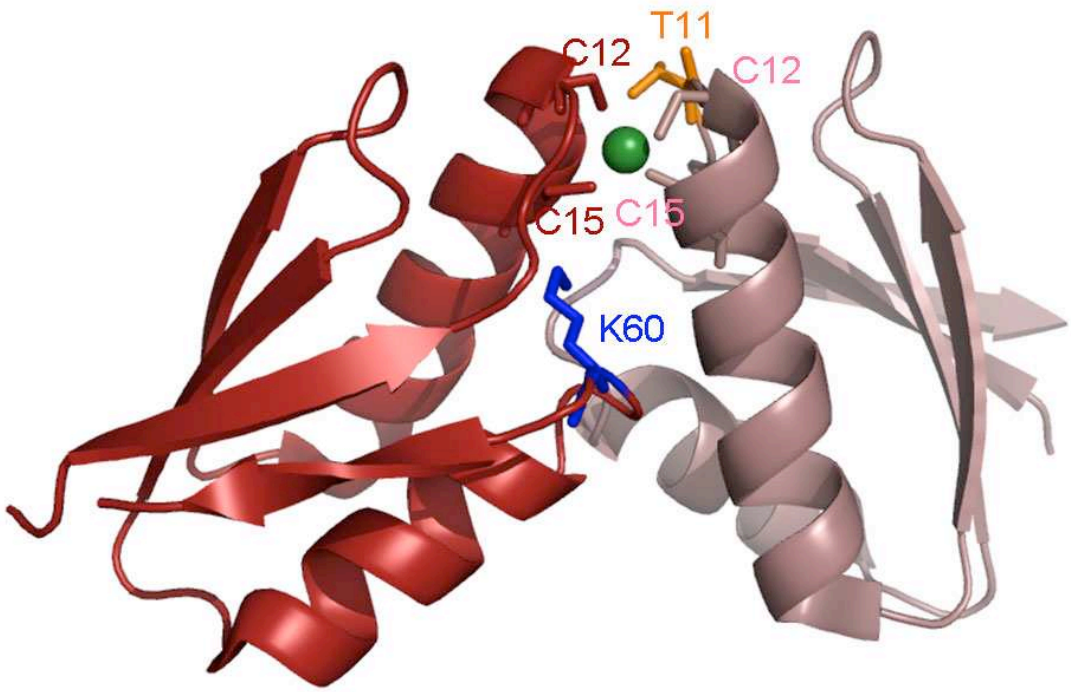

Figure 10: The crystal structure of Cu(I)-HAH1 dimer. The crystal structure of HAH1 dimer with one Cu(I) atom bound (PDB accession code: 1fee) (Wernimont *et al.*, 2000). Subunits in the dimer are represented in brown and purple, Cu(I) is shown as a sphere, and the metal-binding Cys residues are shown as sticks. The side chains of Thr11 and Lys60 from one of the subunits are also shown as orange and blue sticks, respectively.

While the Cu(I)-bound crystal structure of HAH1 was shown to be a dimer, both monomer and dimer forms of Cu(I)-bound HAH1 have been reported in solution (Anastassopoulou *et al.*, 2004; Tanchou *et al.*, 2004). HAH1 has also been shown to regulate the expression of *SOD3* in a copper-dependent manner and transport Cu(I) to SOD3 (Itoh *et al.*, 2008; Itoh *et al.*, 2009). It has been suggested that the intracellular copper concentration may be a possible factor in determining the function of HAH1 as either a metallochaperone or a transcription factor (Itoh *et al.*, 2008; Itoh *et al.*, 2009).

HAH1 has also been implicated as a possible link between cisplatin-mediated anti-cancer therapy and copper homeostasis (Safaei *et al.*, 2009). Crystal structures of monomer and homodimer cisplatin-bound HAH1 have also been reported where the platinum ion was shown to be coordinated in a square planar manner by the Cys12 and Cys15 residues in the monomer (Boal and Rosenzweig, 2009b). In the cisplatin-bound HAH1 dimer, the platinum ion is coordinated by Cys12 of each subunit with further stabilisation provided by hydrogen-bonding interactions between the amine groups of cisplatin, Thr11 and Cys12 (Boal and Rosenzweig, 2009b).

1.3.2.4.2 Copper metallochaperone for Superoxide Dismutase 1 (CCS)

The first copper metallochaperone for SOD1 was discovered in *S. cerevisiae* (Ccs1) as the protein involved in the incorporation of copper in SOD1 (Culotta *et al.*, 1997). The human homologue (hCCS) was reported simultaneously and was found to be a functional homologue of Ccs1 (Culotta *et al.*, 1997). hCCS has been found to be expressed ubiquitously in all human tissues and is largely cytosolic, although some of it was detected in the nucleus and peroxisome as well (Casareno *et al.*, 1998; Islinger *et al.*, 2009). As shown in Figure 9b, there is a high amino acid sequence homology between hCCS and Ccs1. Both hCCS and Ccs1 are modular proteins that contain three structurally and functionally distinct domains (Casareno *et al.*, 1998; Lamb *et al.*, 1999; Schmidt *et al.*, 1999a; Schmidt *et al.*, 2000). CCS Domain 1 (CCSD1) shares a high amino acid homology with Atx1 and HAH1, as shown in Figure 9a. The crystal structure of Ccs1 and the solution structure of hCCSD1 reveal them to comprise the βαββαβ-fold (Figure 11a and Figure 12) similar to Atx1, HAH1 and CopZ metallochaperones (Lamb *et al.*, 1999). Ccs1 domain 1 (Ccs1D1) has only been found to be essential for Sod1 activation under copper-limiting conditions (Schmidt *et al.*, 1999a), as opposed to the mammalian cells where CCSD1 is vital for mediating the CCS-dependent activation of SOD1 irrespective of the cellular copper concentration (Caruano-Yzermans *et al.*, 2006). CCS Domain 2 (CCSD2) is structurally and sequentially homologous to SOD1 and has been shown to be vital for the interaction with SOD1 (Lamb *et al.*, 2001; Schmidt *et al.*, 1999a). hCCS domain 2 (hCCSD2) contains all of the metal-binding residues as SOD1 apart from one of the copper-binding His (His120) at position 200, as a result of which hCCSD2 can bind Zn(II) but

not copper, whereas Ccs1 domain 2 (Ccs1D2) contains neither a zinc nor a copper-binding site (Lamb *et al.*, 2000). The mutation of Asp200 to His in hCCSD2 enables it to bind copper and the mutant protein displays SOD1-like activity (Schmidt *et al.*, 1999b). Domain 3 (D3) is the most conserved yet the most unique domain of CCS. It does not bear a particular resemblance to any other known protein domains and is the shortest and possibly the most flexible portion of CCS (Lamb *et al.*, 1999). CCSD3 contains a conserved CXC-motif which can bind Cu(I) (Eisses *et al.*, 2000; Rae *et al.*, 2001; Stasser *et al.*, 2005). CCSD3 has been shown to be essential for mediating CCS-dependent activation of SOD1, as discussed further in section 1.4.4 (Caruano-Yzermans *et al.*, 2006; Schmidt *et al.*, 1999a; Schmidt *et al.*, 2000).

The information regarding the binding of copper in CCS arises primarily from a combination of *in vitro* and *in vivo* mutation studies since there is no copper-bound structure available for either Ccs1 or hCCS. In the crystal structure of apo-Ccs1 dimer, the D1 Cys residues in the MXCXXC motif are present in an oxidised state (Lamb *et al.*, 1999). While the D1 Cys residues were reduced in the Ccs1-Sod1 crystal structure, no copper atoms were present in this complex either (Figure 11b) (Lamb *et al.*, 2001). A solution structre of apo-hCCSD1 has also been deposited in the protein data bank (code: 2crl) but there is very little information available regarding this structure (Figure 12). hCCSD1 and Ccs1D1 both contain the MXCXXC motif. The Cys residues in the MXCXXC motifs have been proposed to bind Cu(I) (Eisses *et al.*, 2000; Rae *et al.*, 2001; Stasser *et al.*, 2005). However, not all CCS homologues contain this motif such as the CCS homologue from *D. melanogaster* (Kirby *et al.*, 2008) and *Schizosaccharomyces pombe* (Laliberte *et al.*, 2004).

The structural and copper-binding information for CCSD3 is also very limited since this domain was very disordered in the Ccs1 homodimer (Lamb *et al.*, 1999). Ccs1D3 was partly folded into an α-helix in the Ccs1-Sod1 complex, as shown in Figure 11b (Lamb *et al.*, 2001). A disulfide bond between Ccs1 Cys229 and Sod1 Cys57 was also observed (Figure 11b) (Lamb *et al.*, 2001). A study by Eisses *et al.* (2000) reported an interaction between hCCSD1 and hCCSD3 via a Cys-bridged dinuclear Cu(I) cluster, which is further supported by the X-ray absorption spectroscopy data reported by Stasser *et al.* (Stasser *et al.*, 2005; Stasser *et al.*, 2007). Stasser *et al.* (2007) found that mutation of either of the hCCS Cys residues to Ala in the CXXC or the CXC motifs in D1 or D3 respectively, resulted in the binding of only one Cu(I) per hCCS molecule as opposed to the hCCS WT protein which can bind two Cu(I) ions per protein molecule. Stasser *et al.* further reported the formation of a D3-mediated hCCS dimer via the formation of a Cu(I) cluster involving Cu(I) binding by the Cys residues in hCCSD3 (Stasser *et al.*, 2005; Stasser *et al.*, 2007). The authors further proposed that the formation of a D3 mediated hCCS homodimer would promote interaction with hSOD1 as it would free hCCSD2 for interaction with hSOD1 (Stasser *et al.*, 2005;

Stasser *et al.*, 2007). However, there is no evidence to date indicating the presence of a Cu(I)-hCCS cluster *in vivo*.

As discussed previously in section 1.3.2.3, not all organisms contain homologues for CCS and SOD1 can be activated in a CCS-independent manner in some organisms (Leitch *et al.*, 2009a). SOD1-independent functions of hCCS have also been implicated (Angeletti *et al.*, 2005; Gray *et al.*, 2010; McLoughlin *et al.*, 2001). hCCSD1 has been shown to interact with the β-secretase-1 (BACE1) enzyme involved in AD pathology (Angeletti *et al.*, 2005; Gray *et al.*, 2010) as discussed further in section 1.5.6. Investigating the interaction of hCCSD1 with BACE1 was one of the main aims of this study. hCCSD3 has been reported to interact with the neuronal adaptor protein X11α (McLoughlin *et al.*, 2001). Although the implications of these interactions are not fully understood, it nevertheless highlights the potential multi-faceted involvement of hCCS in cellular biology, especially in neuronal copper homeostasis.

1.3.2.4.3 Copper metallochaperones for Cytochrome *c* Oxidase

Eukaryotic cytochrome *c* oxidase (COX) is the terminal mitochondrial-membrane-bound enzyme in the respiratory electron transfer chain. COX is composed of multiple subunits whose assembly requires several co-factors including copper and heme (Capaldi, 1990). The copper-requiring sites in COX include the binding of two Cu(I) ions in the COX2 subunit and one Cu(I) ion in the COX1 subunit (Capaldi, 1990). The incorporation of Cu(I) in COX1 and COX2 involves the transfer of Cu(I) via several copper-binding proteins including COX17, SCO1, and COX11 (Horng *et al.*, 2004). In human cells, the incorporation of Cu(I) in COX also requires the SCO2 protein (Leary *et al.*, 2004), as opposed to yeast where Sco2 is not essential for COX activation (Glerum *et al.*, 1996a).

Cox17 was first discovered in *S. cerevisiae* as a crucial cytoplasmic protein involved in the activation of COX via the delivery of copper to mitochondria (Glerum *et al.*, 1996b). COX activity was severely decreased in yeast cells lacking *COX17* but could be rescued by the addition of excess copper salts to the growth medium (Glerum *et al.*, 1996b). Human COX17 (hCOX17) is a soluble 63 amino acids protein localised in the cytoplasm and the inner membrane space (IMS) of mitochondria (Amaravadi *et al.*, 1997; Petruzzella *et al.*, 1998). COX17 proteins differ in their metal-binding site and the protein structure in comparison to the above mentioned eukaryotic metallochaperones. Instead of the ferredoxin-fold, Cox17 is folded into a helical hairpin or the coiled-coil helix CHCH structure (Arnesano *et al.*, 2005).

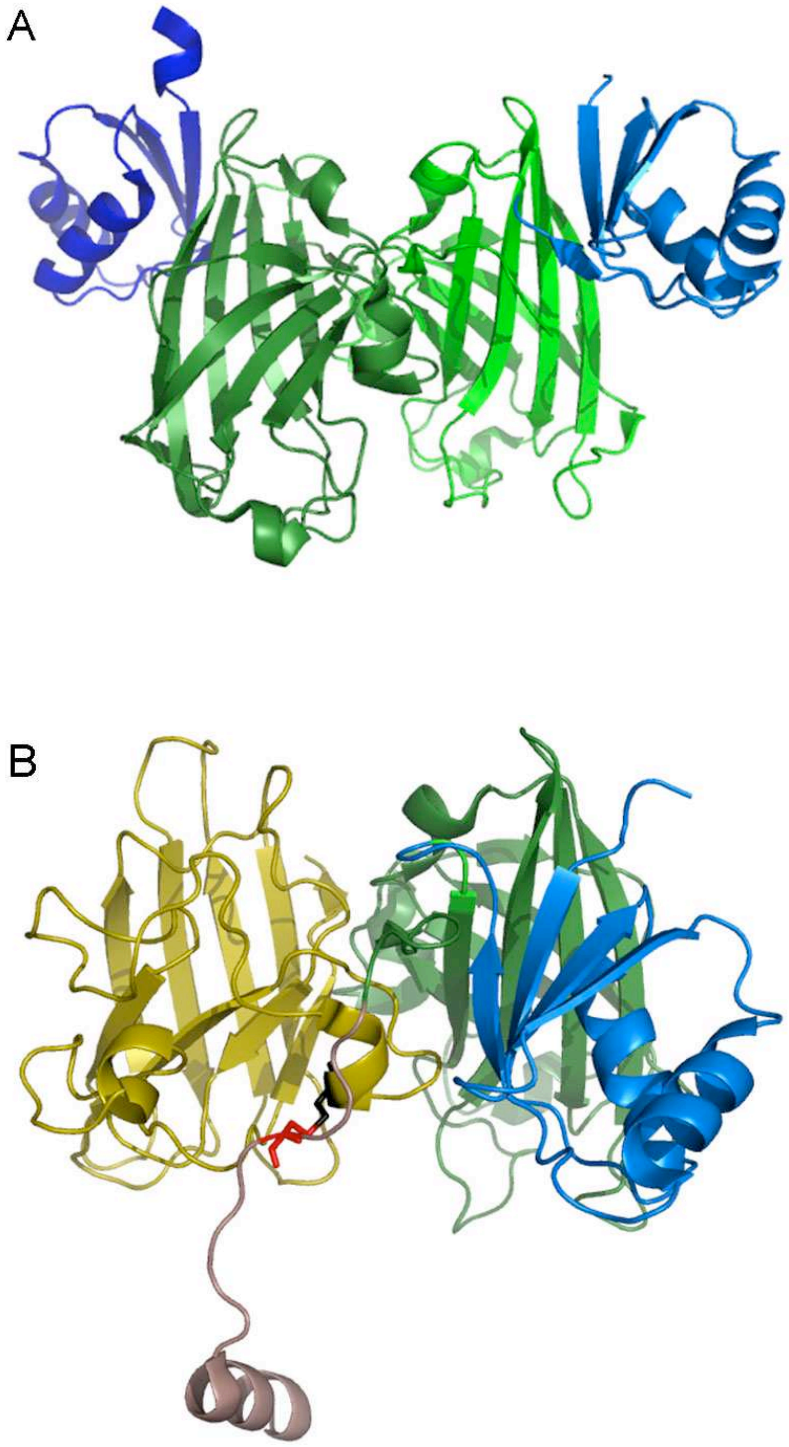

Figure 11: The crystal structures of Ccs1 and Ccs1-Sod1. The crystal structure of Ccs1 dimer with Ccs1D1 and Ccs1D2 shown in different shades of blue and green respectively (PDB accession code: 1qup) (Lamb *et al.*, 1999) (A) and Ccs1-Sod1 complex (PDB accession code: 1jk9) with Sod1 shown in yellow, Ccs1D1 in blue, Ccs1D2 in green and Ccs1D3 in black (B) (Lamb *et al.*, 2001). The disulfide bond between Sod1 Cys57 (black sticks) and Ccs1 Cys229 (red sticks) is also shown.

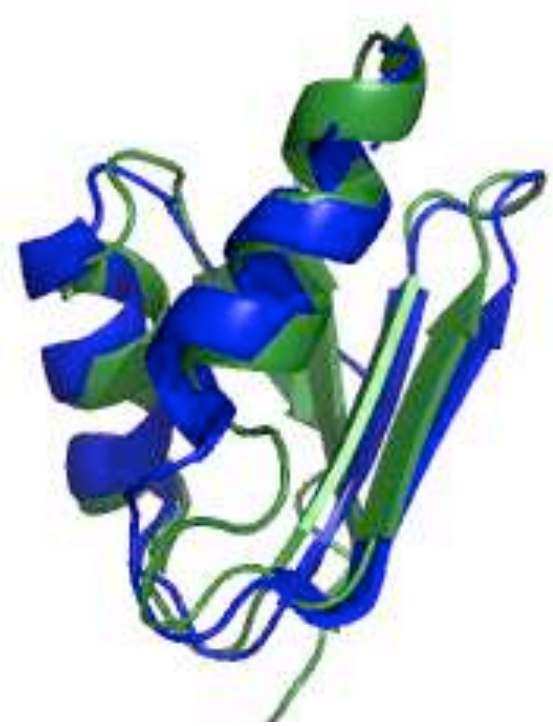

Figure 12: The superimposed structures of hCCSD1 and CcsD1. The solution structure of hCCSD1 (PDB accession code: 2crl) shown in green was superimposed on Ccs1D1 from Figure 11a, shown in blue.

Cu(I) binding in Cox17 is also unusual since it can be coordinated by two sequentially adjacent Cys residues (Cys22 and Cys23 in hCox17) (Banci *et al.*, 2008b) whereas in most of the known copper metallochaperones Cu(I) is coordinated by the Cys residues in the CXXC motif (see sections 1.2.2.1,1.2.2.2,1.2.2.3 and 1.3.2.4.1). Cox17 can also bind Cu(I) in a polycopper cluster and may act as a copper store in the mitochondria (Arnesano *et al.*, 2005). In addition, the structure of Cox17 is not similar to its partner proteins Sco1 and Cox11, unlike Atx1 and CCS which have similar structures to their target proteins (Robinson and Winge, 2010). However, like the other copper metallochaperones, direct copper transfer has been reported between Cox17, Sco1 and Cox11 by both *in vitro* and *in vivo* experiments in yeast cells (Horng *et al.*, 2004). Sco1 and Cox11 subsequently transfer Cu(I) to Cox2 and Cox1 respectively, assisting in the assembly of the COX enzyme (Carr *et al.*, 2002; Glerum *et al.*, 1996a; Khalimonchuk *et al.*, 2007; Lode *et al.*, 2000). In humans, the maturation of COX2 has been shown to require both SCO1 (hSCO1) and SCO2 (hSCO2), and it has been proposed that hSCO2 may additionally function as a thiol-disulfide oxidoreductase that oxidises the Cys residues in hSCO1 facilitating the transfer of copper from hSCO1 to COX2 (Leary *et al.*, 2009).

1.3.3 Eukaryotic copper-transporting ATPases

The Atx1 and HAH1 copper metallochaperones deliver Cu(I) the to P_{1B}-type ATPases Ccc2 or ATP7A and ATP7B respectively, located in the secretory parthway in eukaryotes, as discussed below.

1.3.3.1 The *S. cerevisiae* copper-transporting ATPase Ccc2

Ccc2 is a P_{1B}-type copper-transporting ATPase found in *S. cerevisiae* (Fu *et al.*, 1995). It is localised in the membrane of the trans-golgi compartment and is indirectly involved in the high affinity uptake of iron in yeast cells (Yuan *et al.*, 1997). Ccc2 receives Cu(I) from Atx1 via direct protein-protein interaction (section 1.4.1) and transfers it to Fet3 (Portnoy *et al.*, 1999; Pufahl *et al.*, 1997; Stearman *et al.*, 1996). Hence, Ccc2 mediates the transport of Cu(I) from the cytosol to the secretory pathway (Pufahl *et al.*, 1997; Yuan *et al.*, 1995). Ccc2 contains two soluble MBDs at the N-terminus, each ~70 amino acids long (Figure 13a) which can both interact with Atx1 (van Dongen *et al.*, 2004). While there is no structure available for the second MBD of Ccc2 (Ccc2b), there are NMR structures available for the first MBD of Ccc2 (Ccc2a) in its apo- and Cu(I)-bound forms (Banci *et al.*, 2001a). The NMR structures depict the βαββαβ-fold similar to Atx1. In the holo-Ccc2a structure, a single Cu(I) ion is bound by the Cys residues in the $M_{11}XCXXC_{16}$ motif. Thr17 in Cu(I)-Ccc2a was suggested to form a hydrogen-bonding interaction with Cys13 which may contribute in optimising the conformation of Cys13 in holo-Ccc2a (Banci *et al.*, 2001a). Met11 in Ccc2a performs an analogous

function to the Met11 and Ile10 residue in BsCopZ and ScAtx1 respectively, by acting as a hydrophobic tether in stabilising the MXCXXC site for Cu(I)-binding (Banci *et al.*, 2001a). Phe64 of Cu(I)-Ccc2a was proposed to be important for optimising the conformation of the metal-binding loop as it was shown to mediate hydrophobic interactions with Met11 and Van der Waals contact with Cys16 (Banci *et al.*, 2001a). The replacement of the basic Lys residue in Atx1 (Lys65) by the hydrophobic Phe64 residue in Ccc2a loop 5 is a conserved feature amongst these proteins and has been implicated in mediating Cu(I)-binding and protein-protein interactions with the copper metallochaperones (Banci *et al.*, 2006a; DeSilva *et al.*, 2005; Portnoy *et al.*, 1999), as discussed below.

1.3.3.2 The *H. sapiens* copper-transporting ATPase ATP7A

ATP7A, the human homologue of Ccc2, is expressed in most tissues apart from liver where ATP7B is the dominant copper-transporting ATPase (Tumer and Moller, 2010). ATP7A is important for the biosynthesis of several enzymes including peptidyl-α-monoxygenase, lysyl oxidase and tyrosinase (Lutsenko *et al.*, 2007b). In addition, ATP7A mediates the export of Cu(I) from enterocytes into the extracellular milieu for the utilisation of copper by other proteins (Lutsenko *et al.*, 2007b).

The importance of ATP7A is highlighted by the Menkes disease where genetic mutations in *ATP7A* lead to impaired copper export from enterocytes resulting in systemic copper deficiency (Chelly *et al.*, 1993; Mercer *et al.*, 1993; Vulpe *et al.*, 1993). Unlike Ccc2, ATP7A can traffic to different subcellular locations in response to copper concentration. At physiological copper concentrations ATP7A is located at the trans-golgi membrane, however, in the presence of excess copper ATP7A can relocate to vesicles which can fuse with the plasma membrane leading to the extracellular export of copper (Greenough *et al.*, 2004; Petris *et al.*, 1996). Thus the biosynthetic and homeostatic functions of ATP7A are dependent upon its subcellular location (Lutsenko *et al.*, 2007b).

The N-terminus of ATP7A comprises 6 soluble MBDs (Figure 13b) and NMR structures are available for all of them. The NMR structures display the βαββαβ-fold similar to the previously mentioned copper metallochaperones (Banci *et al.*, 2004b; Banci *et al.*, 2005a; Banci *et al.*, 2005b; Banci *et al.*, 2006a; DeSilva *et al.*, 2005; Gitschier *et al.*, 1998; Jones *et al.*, 2003). In all of the Cu(I)-containing structures, Cu(I) is bound by the Cys residues in the MXCXXC motif (Banci *et al.*, 2004b; Banci *et al.*, 2005a; Banci *et al.*, 2005b; Banci *et al.*, 2006a; DeSilva *et al.*, 2005).

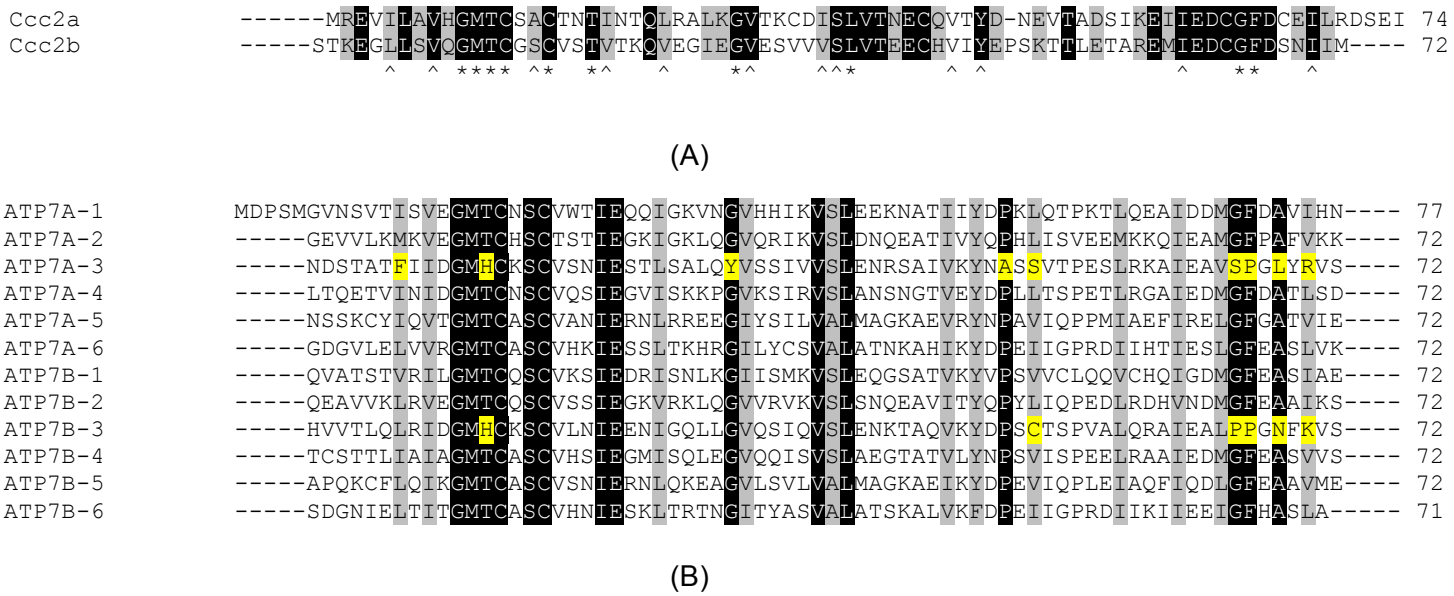

Figure 13: Sequence alignment of the soluble metal-binding domains of Eukaryotic copper-ATPases. The sequence alignment of the Ccc2 MBDs denoted as Ccc2a and Ccc2b (GenBank accession code NP_010556) (discussed in sections 1.3.3.1 and 1.4.1) is shown in (A). The sequence alignments of the six MBDs of ATP7A denoted as ATP7A-1 to 6 (GenBank accession code NP_000043) (discussed in sections 1.3.3.2 and 1.4.2) and the six MBDs of ATP7B denoted as ATP7B-1 to 6 (GenBank accession code NP_000044) (discussed in sections 1.3.3.3 and 1.4.2) is shown in (B). Fully conserved residues are highlighted in black while semi-conserved residues are shown in grey. The residues highlighted in yellow indicate the residues that are not conserved in MBD3 unlike the other MBDs of ATP7A and ATP7B. '*' denotes the residues that are fully conserved and '^' denotes the residues that are semi-conserved compared to MBDs 1, 2, 4-6 of ATP7A and ATP7B too.

Similar to Phe64 of Ccc2a, the Phe residues in loop 5 of ATP7A MBDs 1, 2 and 4 have also been shown to be important for mediating hydrophobic interactions which help maintain the hydrophobic core of the structure (Banci *et al.*, 2004b; DeSilva *et al.*, 2005; Gitschier *et al.*, 1998; Jones *et al.*, 2003). This is further supported by the results obtained by De Silva *et al.* (2005) who found that mutation of Phe71 to Ala in ATP7A MBD1 resulted in partial unfolding of the protein. However, the mutation of Phe72 to Ala in ATP7A MBD2 did not have a significant effect on the rate of Cu(I) removal from Cu(I)-bound ATP7A MBD2 (Jones *et al.*, 2003). The authors suggested that the presence of Phe72 may be important for optimising the MBS for Cu(I)-binding and may also prevent the aberrant binding of other metal ions (Jones *et al.*, 2003). The Phe residue in loop 5 is substituted Pro (Pro66) in MBD3 (Figure 13b) which has been implicated in contributing to the lowest Cu(I)-binding affinity of MBD3 compared to the other ATP7A MBDs (Banci *et al.*, 2006a; Banci *et al.*, 2010a) and the lack of formation of an adduct with HAH1 (Banci *et al.*, 2006a).

While the exact function of MBDs is not known, mutation of the copper-binding Cys residues in the MXCXXC motifs of the MBDs has been shown to disrupt the copper-dependent trafficking of ATP7A to the plasma membrane in the presence of excess copper (Voskoboinik *et al.*, 1999). The MBDs have also been shown to interact with the oxidoreductase glutaredoxin 1 (GRX1) in a yeast two-hybrid system in a copper-dependent manner (Lim *et al.*, 2006a). The interaction of ATP7A MBDs with GRX1 was shown to be mediated by the copper-binding Cys residues in the MXCXXC motifs of the MBDs. The authors proposed that the interaction of MBDs with GRX1 may promote Cu(I)-binding to the Cys residues by either de-glutathionylation of the Cys residues or by reducing the formation of potential intramolecular disulfide bonds in the MBDs (Lim *et al.*, 2006a). Of particular interest to this study is the interaction of the ATP7A MBDs with its copper metallochaperone HAH1 (section 1.4.2). Although all of the MBDs are capable of binding Cu(I) *in vitro* and *in vivo* (Lutsenko *et al.*, 1997), the Cu(I)-binding affinities of the MBDs are not equivalent (Banci *et al.*, 2010a). The Cu(I)-binding affinities of ATP7A MBDs 1 and 6 were shown to be higher than the Cu(I)-affinity of MBDs 2, 3 and 5 (Banci *et al.*, 2010a). In addition, the Cu(I)-affinities of MBDs 1, 2 and 6 were significantly higher than the Cu(I)-binding affinity of HAH1 which may have implications for the Cu(I)-dependent interactions of ATP7A MBDs with HAH1, discussed in section 1.4.2.

1.3.3.3 The *H. sapiens* copper-transporting ATPase ATP7B

ATP7B, the second copper-transporting ATPase in humans, is predominantly expressed in the liver, in addition to brain, kidney and other tissues (Lutsenko *et al.*, 2007b). Similar to ATP7A, ATP7B also resides in the trans-golgi membrane and receives Cu(I) from HAH1 via direct protein-protein interaction (see section 1.4.2).

ATP7B is responsible for the incorporation of copper into ceruloplasmin under physiological copper concentrations (Terada *et al.*, 1998). In the presence of excess copper, ATP7B has been shown to relocate near the apical surface in hepatocytes resulting in the export of Cu(I) via bile (Hung *et al.*, 1997; Schaefer *et al.*, 1999). Genetic mutations in *ATP7B* can lead to the Wilson's disease due to the disruption of copper export from hepatocytes resulting in the accumulation of copper leading to liver cirrhosis and neurodegeneration (Das and Ray, 2006; Lutsenko *et al.*, 2007b). Like ATP7A, ATP7B also contains six soluble MBDs in its NTD which all contain the MXCXXC motif (Figure 13a) and can bind Cu(I) ions via the Cys residues of this motif (Lutsenko *et al.*, 1997; Yatsunyk and Rosenzweig, 2007). The mutation of the Cu(I)-binding Cys residues in the MBDs to Ser has been shown to disrupt the Cu(I)-translocating activity of ATP7B and its trafficking (Mercer *et al.*, 2003). MBDs 5 and 6 in particular have been shown to be important for the Cu(I)-dependent trafficking of ATP7B (Mercer *et al.*, 2003; Strausak *et al.*, 1999).

The ATP7B MBDs have also been shown to interact with GRX1 (Lim *et al.*, 2006a) and with the p62 subunit of dynactin (Lim *et al.*, 2006b). Both of these interactions were reported to be Cu(I)-dependent and mediated by the copper-binding Cys residues in the MBDs. The ATP7B MBDs have also been shown to interact with the Murr1 protein which may be important for facilitating the ATP7B-mediated Cu(I) excretion into bile (Tao *et al.*, 2003). A recent study also reported intercommunication between the MBDs via hydrogen-bonding interactions to influence the redox status and the conformation of the N-terminus of ATP7B (LeShane *et al.*, 2010). However, this study will focus primarily on the molecular basis of the interaction of HAH1 with the MBDs of ATP7B, as discussed further in section 1.4.2.

1.4 The Molecular Basis of the Interaction of Copper metallochaperones with their partner proteins

The major goal of this study was to further investigate the molecular basis of the complex formation of copper metallochaperones with their interacting partner proteins. Most of the copper metallochaperones and their target proteins share two common features namely the ferredoxin-like fold and the CXXC metal-binding motif. However, not all of the copper metallochaperones and their target proteins contain these two factors. For example, COX17, SCO1, SCO2 and the CusF copper metallochaperones do not contain either of these two factors. Similarly, the presence of these two factors is not sufficient to enable Cu(I) transfer from a copper metallochaperone to a Cu(I)-binding protein. For example, Atx1 and Ccs1D1 both contain the CXXC motif and the ferredoxin-fold yet Atx1 is unable to substitute for Ccs1D1 *in vivo* (Schmidt *et al.*, 1999a). Thus, in order to understand the specificity with which copper metallochaperones associate with and deliver Cu(I) to their target proteins it is vital to

study the molecular basis of these protein-protein interactions. As highlighted by some of the examples discussed below, the interactions are governed by several factors including the surface charge of the proteins, hydrogen bonding and hydrophobic interactions between the proteins.

1.4.1 Interaction of Atx1 with Ccc2

Several studies have reported the complex formation between Atx1 and the MBDs of Ccc2 to be mediated by Cu(I)-binding (Arnesano *et al.*, 2001a; Portnoy *et al.*, 1999; Pufahl *et al.*, 1997). Atx1 interacts with Ccc2a and Ccc2b by a combination of electrostatic, hydrophobic and hydrogen-bonding interactions (Arnesano *et al.*, 2001b; Banci *et al.*, 2006b). Atx1 contains several surface-exposed Lys residues that provide an overall positively charged surface. In similar positions Ccc2 MBDs contain several residues that provide it with a negatively charged surface, and thus assist in complex formation with Atx1 on the basis of electrostatic interactions (Arnesano *et al.*, 2001b; Banci *et al.*, 2006b). This is further supported by the results reported by Portnoy *et al.* (1999) who found that the mutation of Lys24 and Lys28 to Ala or Glu in Atx1 decreased the uptake of ^{55}Fe in yeast cells lacking *ATX1*. While the mutation of Atx1 Lys65 to Glu also resulted in reduced uptake of ^{55}Fe in *atx1Δ* cells, the Atx1 Lys65Ala, Lys65Phe did not have a significant effect on ^{55}Fe uptake (Portnoy *et al.*, 1999). Similar results were also reported for the yeast two-hybrid interaction between Atx1 and Ccc2 MBDs, where the Atx1 Lys24Glu,Lys28Glu; Lys61Glu,Lys62Glu; and Lys65Glu mutations also abolished the interactions (Portnoy *et al.*, 1999). The high ambiguity driven protein-protein docking (HADDOCK) model of Atx1-Cu(I)-Ccc2a provided further evidence for the role of Atx1 Lys65 in mediating protein-protein interactions. While in apo-Atx1, Lys65 appears to be further away from the metal site (Arnesano *et al.*, 2001b), in the complex of Cu(I)-Atx1 with Ccc2a, the side chain of Atx1 Lys65 forms intermolecular hydrogen bonds with either Ala15 or Asn18 of Ccc2a (Arnesano *et al.*, 2004).

An NMR derived Cu(I)-mediated complex between Atx1 and Ccc2 (Figure 14) has also been reported (Banci *et al.*, 2006b). This complex depicted Cu(I) to be tri-coordinated by Cys15 of Atx1 and Cys13 and Cys16 of Ccc2a. Cu(I) transfer was shown to be mediated by ligand transfer reactions via the formation of this complex (Banci *et al.*, 2006b), as proposed previously by Pufahl *et al.* (1997). In addition, the Atx1-Ccc2 MBD interactions were shown to be dependent on the copper concentration. Both high and low copper concentrations resulted in significantly weaker yeast two-hybrid interactions between Atx1 and Ccc2 MBDs (Pufahl *et al.*, 1997; van Dongen *et al.*, 2004). The dependence of the interaction between Atx1 and Ccc2 MBDs on copper is further highlighted by the evidence that mutation of the Cu(I)-binding Cys residues in the CXXC motif of Atx1 to Ala abolished the yeast two-hybrid interactions between them (Portnoy *et al.*, 1999).

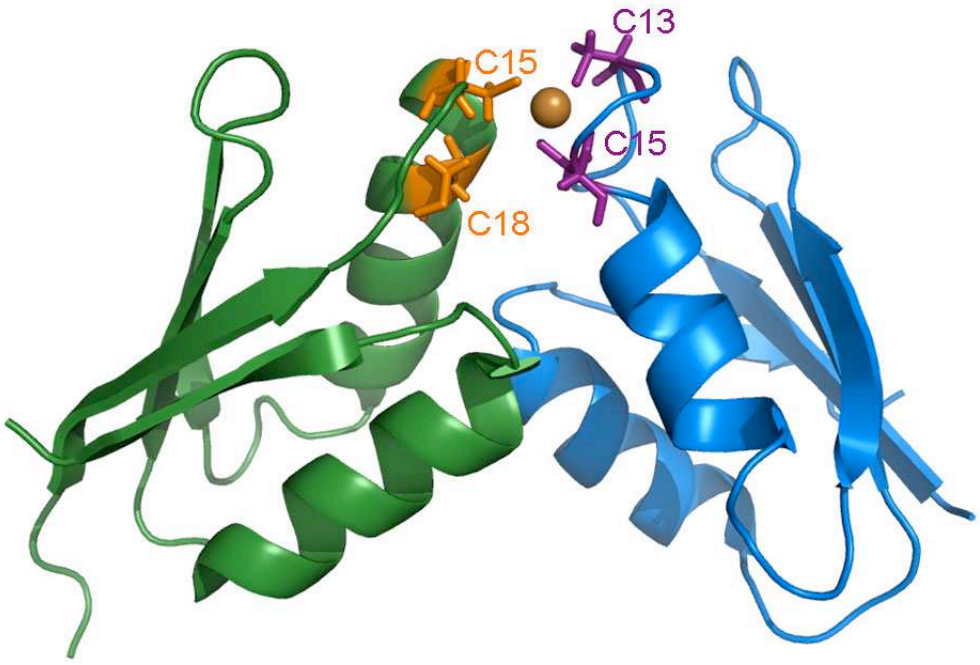

Figure 14: The solution structure of Cu(I)-bound Atx1-Ccc2a complex. The solution structure of Atx1-Cu(I)-Ccc2a (PDB accession code: 2ggp) where Atx1 is shown in green and Ccc2a is shown in blue (Banci *et al.*, 2006b). The Cu(I)-binding Cys residues are shown as sticks and Cu(I) is shown as a sphere.

1.4.2 Interaction of HAH1 with ATP7A and ATP7B

HAH1 has been shown to interact with the MBDs of ATP7A and ATP7B both *in vitro* and *in vivo* in a Cu(I)-dependent manner which requires the Cu(I)-binding Cys residues of the CXXC motif (Hamza *et al.*, 1999; Larin *et al.*, 1999; Strausak *et al.*, 2003). However, there is some discrepancy regarding which MBDs can interact with and acquire Cu(I) from Cu(I)-bound HAH1. Yeast two-hybrid studies have revealed HAH1 to interact with constructs containing ATP7A MBDs 2-6 (Larin *et al.*, 1999), MBDs 1 and 2, and MBDs 3 and 4 (Strausak *et al.*, 2003). No yeast two-hybrid interaction was reported between HAH1 and a construct containing ATP7A MBDs 5 and 6 (Strausak *et al.*, 2003). In contrast, experiments using SPR found HAH1 to interact with all of the individual MBDs in ATP7A (Strausak *et al.*, 2003). Initially, Cu(I) transfer was reported between HAH1 and ATP7A MBD2 or 5 (Banci *et al.*, 2005b). However, studies using NMR spectroscopy revealed the formation of Cu(I)-mediated protein complexes between Cu(I)-HAH1 and ATP7A MBD1, between Cu(I)-HAH1 and ATP7A MBD4, but not between Cu(I)-HAH1 and ATP7A MBDs 2 or 3 (Banci *et al.*, 2007). In addition, Cu(I)-HAH1 was shown to transfer Cu(I) to ATP7A MBD1, MBD4, MBD6 and possibly MBD5 (Banci *et al.*, 2007). It is possible that this discrepancy may be due to the fact that the previous study was conducted using the isolated domain of ATP7A MBD5 (Banci *et al.*, 2005b) whereas the latter study used a construct containing all of the MBDs of ATP7A which is likely more physiologically relevant (Banci *et al.*, 2007).

The results are in partial agreement with the Cu(I)-binding affinity data where the Cu(I)-binding affinity of HAH1 was reported to be significantly weaker than the Cu(I)-affinity of ATP7A MBDs 1, 2 and 6 (Banci *et al.*, 2010a). Whereas, the Cu(I)-affinity of ATP7A MBDs 5 was found to be only slightly higher than the Cu(I)-affinity of HAH1 (Banci *et al.*, 2010a). A solution structure has also been reported for the Cu(I)-containing HAH1-ATP7A MBD1 complex (Banci *et al.*, 2009). The HAH1-Cu(I)-ATP7A MBD1 complex was shown to be bridged by a Cu(I) ion and the interaction was also reported to be electrostatically favourable as HAH1 has a positively charged surface compared to ATP7A MBD1 (Banci *et al.*, 2009). Site-directed mutagenesis studies indicated that the HAH1-Cu(I)-ATP7A MBD1 adduct formation required only three of the four Cu(I)-binding Cys where HAH1 Cys12 and ATP7A MBD1 Cys15 were found to be essential (Banci *et al.*, 2009), similar to the Atx1-Cu(I)-Ccc2a complex formation (Banci *et al.*, 2006b).

Discrepancies have also been reported between the interactions of Cu(I)-HAH1 with ATP7B MBDs. Larin *et al.* (1999) found that HAH1 can interact with a construct comprising ATP7B MBDs 1-6 and various other combinations including MBDs 1-4 but not with a construct containing only MBDs 5 and 6 in a yeast two-hybrid system. In support of these experiments, no complex formation or Cu(I) transfer was evident between Cu(I)-HAH1 and ATP7B MBDs 5 and 6 *in vitro* (Achila *et al.*, 2006). However,

titration of apo-ATP7B MBDs 5 and 6 with Cu(I)-ATP7A MBD4 demonstrated partial Cu(I) transfer, suggesting that ATP7B MBDs 5 and 6 may be able to acquire Cu(I) from other Cu(I)-bound MBDs *in vivo* (Achila *et al.*, 2006). Cys-labelling and ITC studies have also reported that Cu(I) may preferentially be transferred first from Cu(I)-HAH1 to the ATP7A MBD2 (Walker *et al.*, 2004; Wernimont *et al.*, 2004), whether a similar preference is reflected *in vivo* is not known. Cu(I)-dependent complex formation and Cu(I) transfer has also been reported between Cu(I)-HAH1 and ATP7B MBD4 (Achila *et al.*, 2006; Banci *et al.*, 2008a; Bunce *et al.*, 2006; Hussain *et al.*, 2009). Hussain *et al.* (2009) found that the HAH1-Cu(I)-ATP7B MBD4 interaction was disrupted by the mutation of Lys60 to Ala or Tyr in HAH1, in addition to decreased Cu(I)-transfer between these HAH1 mutants and ATP7B MBD4. Met10 and Thr11 of HAH1 were also shown to be important for mediating Cu(I) transfer to ATP7B MBD4, as the mutation of these residues resulted in decreased Cu(I) transfer (Hussain *et al.*, 2009). Molecular mechanics studies further suggested that the transfer of Cu(I) from Cu(I)-HAH1 to apo-ATP7B MBD4 likely involves a 3 coordinate intermediate species where the N-terminal Cys residues in the MXCXXC sites of both proteins are vital for Cu(I) transfer (Rodriguez-Granillo *et al.*, 2010). Cu(I)-transfer has also been shown between HAH1 and ATP7B MBD1, although whether this can also occur *in vivo* is not known (Bunce *et al.*, 2006).

1.4.3 Interaction of ScAtx1 with the metal-binding domains of PacS and CtaA

Synechocystis PCC 6803 provides a rare example where a P_{1B}-type copper transporter (CtaA) has been proposed to mediate Cu(I)-import into the prokaryotic cytosol. In addition, the copper metallochaperone ScAtx1 has been shown to interact with the MBDs of both CtaA and PacS (Tottey *et al.*, 2001). Compared to the interaction of ScAtx1 with PacS MBD there is relatively little information available regarding the interaction of ScAtx1 with CtaA MBD. Bacterial two-hybrid assays have demonstrated that the interaction of ScAtx1 with PacS MBD and CtaA MBD require the Cys12 and Cys15 residues of the CXXC motif in ScAtx1 (Tottey *et al.*, 2002). The presence of His61 in loop 5 of ScAtx1 in place of Tyr or Lys – the usual amino acids in prokaryotic and eukaryotic copper metallochaperones respectively, is unusual and has been proposed to be one of the main driving forces in mediating the transfer of Cu(I) from CtaA MBD to ScAtx1 and the subsequent transfer of Cu(I) from ScAtx1 to PacS MBD (Banci *et al.*, 2004a; Tottey *et al.*, 2002). In the proposed model, the movement of ScAtx1 His61 towards the Cu(I)-binding site is suggested to promote the acquisition of Cu(I) from CtaA MBD while its outward movement results in the release of Cu(I) from ScAtx1 to PacS MBD (Banci *et al.*, 2004a). In addition, the mutation of ScAtx1 His61 to Arg was shown to enhance the bacterial two-hybrid interaction between ScAtx1 and

PacS MBD but did not have a significant effect on the interaction with CtaA MBD (Borrelly *et al.*, 2004). The authors therefore suggested that this residue can interact differently with both domains (Borrelly *et al.*, 2004). Previously, based on the solution structure of Cu(I)-ScAtx1, the His61 residue was also proposed to bind Cu(I) in addition to Cys12 and Cys15 (Banci *et al.*, 2004a). However, the recent crystal structures of ScAtx1 dimers clearly depict that His61 does not act as a direct Cu(I)-binding ligand (Figure 6) (Badarau *et al.*, 2010). Mutation of this residue was however shown to result in major conformational changes (Badarau *et al.*, 2010), as discussed previously in section 1.2.2.4. One of the aims of this study was to further investigate the precise role of this residue in mediating the interactions of ScAtx1 with CtaA MBD and PacS MBD.

Badarau *et al.* (2010) have recently shown that while the transfer of Cu(I) from CtaA MBD to ScAtx1 is favourable *in vitro*, the subsequent transfer of Cu(I) from one Cu(I)-bound ScAtx1 dimer to PacS MBD is unfavourable. Cu(I) was shown to transfer more readily from ScAtx1 to PacS MBD if the Cu(I) source was two Cu(I)-bound ScAtx1 dimer instead of one Cu(I)-bound ScAtx1 dimer (Badarau *et al.*, 2010). The dimerisation state of ScAtx1 can therefore be an important factor in determining Cu(I) transfer between these proteins (Badarau *et al.*, 2010). Further information regarding the interaction of ScAtx1 with PacS MBD can be gained from the HADDOCK model of the ScAtx1-Cu(I)-PacS MBD complex where the proteins were bridged by a single Cu(I) ion (Banci *et al.*, 2006c). The complex was proposed to be further stabilised by a network of electrostatic and hydrophobic interactions between the two interacting surfaces, although the surface charges of ScAtx1 and PacS MBD are not as pronounced as in the case of Atx1-Ccc2a or BsCopA-BsCopAb (Banci *et al.*, 2006c). Unlike ScAtx1-PacS MBD there is no structural information available regarding the ScAtx1-CtaA MBD interaction. The isolation of two different structural arrangements of Cu(I)-ScAtx1 homodimers (Figure 6) led the authors to suggest that these may represent different structural complexes regarding the interaction of ScAtx1 with each of its target MBDs (Badarau *et al.*, 2010). Since the HADDOCK model of ScAtx1-PacS MBD depicted it to be a side-to-side complex (Banci *et al.*, 2006c) it is possible that the head-to-head conformation may be favoured for the ScAtx1-CtaA MBD complex formation (Badarau *et al.*, 2010). This hypothesis was further investigated in this study, as discussed in section 1.6.

1.4.4 Interaction of CCS with SOD1

Despite several studies, the exact mechanism underlying the CCS-dependent activation of SOD1 is not fully resolved. The most popular model regarding CCS-mediated SOD1 activation involves the “pivot, insert, release” pathway (Furukawa *et al.*, 2004; Rae *et al.*, 2001). Based on this model the first step involves the interaction of CCS with the

disulfide reduced, zinc-bound form of SOD1. However, there is some discrepancy regarding the identity of the oligomeric species between CCS and SOD1. The Ccs1-Sod1 crystal structure was found to be a dimer involving one monomer of SOD1 and one monomer of Ccs1 (Lamb *et al.*, 2001). An alternative theory regarding the CCS-dependent activation of SOD1 proposes the formation of a hetero-tetramer between a dimer of CCS and a dimer of SOD1 (Hall *et al.*, 2000). Irrespective of the oligomeric species formed, the CCS-SOD1 interaction is mediated by a combination of electrostatic, hydrophobic and hydrogen-bonding mediated interactions between CCSD2 and SOD1 (Hall *et al.*, 2000; Lamb *et al.*, 2001). The CCS-dependent activation of SOD1 requires the formation of the essential disulfide bond in SOD1 between Cys57 and Cys146 and the incorporation of copper in the SOD1 copper-binding site in the presence of oxygen, followed by the dissociation of the CCS-SOD1 heterooligomer (Brown *et al.*, 2004; Furukawa *et al.*, 2004; Rae *et al.*, 2001). The transfer of Cu(I) from CCS to SOD1 has been shown to involve the formation of an intermolecular disulfide bond between the CXC motif in CCSD3 and SOD1 (Hall *et al.*, 2000; Lamb *et al.*, 2001; Schmidt *et al.*, 1999a). An intermolecular disulfide bond is also evident between Sod1 Cys57 and Ccs1 Cys229 in the Ccs1-Sod1 crystal structure (Figure 11b). It has further been proposed that the incorporation of copper in SOD1 involves the transfer of Cu(I) from CCSD3 to SOD1 since Ccs1D1 was shown to be located too far away from the Sod1 active site in the Ccs1-Sod1 complex (Lamb *et al.*, 2001). CCSD3 is likely the most flexible part of CCS and is located closer to the Sod1 active site in the Ccs1-Sod1 complex than Ccs1D1. It was therefore suggested that Cu(I) may be transferred from CCSD3 to SOD1 (Lamb *et al.*, 2001).

The role of CCSD1 in SOD1 activation is less clear and has been subsequently described as the most “enigmatic” region of CCS (Leitch *et al.*, 2009b). There is evidence to indicate that the role of D1 may be species specific. Studies in yeast documented Ccs1D1 to be important for SOD1 activation only when copper is limiting suggesting that under these conditions copper is initially bound by D1 and then transferred to D3 for incorporation into Sod1 (Schmidt *et al.*, 1999a; Schmidt *et al.*, 2000). Studies in mammalian cells have shown that CCSD1 is essential for the activation of SOD1 in both copper-limiting and copper-replete conditions (Caruano-Yzermans *et al.*, 2006). In contrast, GST-purification assays have shown that the D1 of hCCS is not required for mediating the interaction with SOD1 (Casareno *et al.*, 1998). Furthermore, the mutation of the Cu(I)-binding Cys residues in hCCSD1 did not abrogate the CCS-mediated activation of hSOD1 *in vitro* (Stasser *et al.*, 2005; Stasser *et al.*, 2007). Hence, there is discrepancy regarding the role of hCCSD1 with respect to the interaction with and Cu(I) transfer to SOD1. Stasser *et al.* also reported the formation of a Cu(I)-cluster involving Cu(I)-binding by the Cys244 and Cys246 residues of two hCCS monomers (Stasser *et al.*, 2005; Stasser *et al.*, 2007). The authors

proposed that while apo-hCCS dimerises via interactions involving D2, upon the formation of the Cu(I)-cluster, hCCS can instead dimerise via D3 (Stasser *et al.*, 2005; Stasser *et al.*, 2007). The D3-mediated dimerisation of hCCS would subsequently allow hCCS to interact with SOD1 via D2 (Stasser *et al.*, 2005; Stasser *et al.*, 2007). However, whether this cluster can form *in vivo* is currently not known. One of the aims of this study was to elucidate the role of hCCS Cu(I)-binding residues in mediating the interaction with hSOD1 *in vivo*.

1.5 The Role of Copper in Alzheimer's disease

AD is the most common form of dementia and is known to affect more than 29 million people in the world. The major risk factor for AD remains age and it is usually diagnosed in over 65 year olds (van Es and van den Berg, 2009). Irreversible neurodegeneration leads to memory loss and cognitive decline in the affected individuals. Although AD was discovered more than 100 years ago, the cause of the disease in the majority of cases still remains unknown. Approximately 1 % of AD cases are known to be familial and the mutations are traced to the genes involved in the production of Aβ peptide including the genes encoding for presenilin 1, presenilin 2 – components of the γ-secretase complex, and the gene coding for APP (Goate *et al.*, 1991; Levy-Lahad *et al.*, 1995; Sherrington *et al.*, 1995; van Es and van den Berg, 2009). Another challenge in controlling AD is its late diagnosis. To date, the most conclusive evidence for AD involves post-mortem analysis of the brain tissue (van Es and van den Berg, 2009). Two distinct pathological hallmarks of AD are the presence of intracellular neurofibrillary tangles (NFTs) and extracellular senile plaques (Morrissette *et al.*, 2009).

1.5.1 Neuropathology of Alzheimer's disease

In the 1980s it was discovered that NFTs were composed of aggregated microtubule-associated tau protein as a result of excessive and abnormal phosphorylation (Grundke-Iqbal *et al.*, 1986; Kosik *et al.*, 1986), whereas the major component of the senile plaques was identified as the Aβ peptide (Glenner and Wong, 1984; Masters *et al.*, 1985). Other pathological factors associated with AD include oxidative damage, synaptic injury and metal mis-homeostasis (Bush, 2003; Molina-Holgado *et al.*, 2007). The major focus of AD research remains the aggregation of Aβ as described by the 'amyloid cascade hypothesis' of AD (Hardy and Higgins, 1992). Aβ is produced as a result of the endoproteolytic cleavage of APP (Kang *et al.*, 1987) by a combination of secretases, shown in Figure 15. The major component of senile plaques is the 42 amino acid Aβ peptide ($A\beta_{42}$) which is produced by the amyloidogenic processing of APP (Younkin, 1998). The amyloidogenic pathway involves the cleavage of APP by BACE1 to generate the N-terminal end of Aβ followed by the intramembranous

cleavage of APP by the γ-secretase complex at the C-terminus leading to the release of Aβ (Figure 15). In the non-amyloidogenic pathway, a truncated Aβ peptide is produced due to the cleavage of Aβ by the α-secretases instead of BACE1 (LaFerla *et al.*, 2007), as shown in Figure 15. The formation of the longer $A\beta_{42}$ peptide and its subsequent aggregation is thought to be one of the major pathological causes of AD as described by the 'amyloid cascade hypothesis' (Hardy and Higgins, 1992).

1.5.2 The 'amyloid cascade hypothesis' of Alzheimer's disease

The 'amyloid cascade hypothesis' was first proprosed by Hardy and Higgins in 1992. According to this hypothesis, the deposition of Aβ into senile plaques is the primary event leading to AD as a consequence of synaptic injury and neuronal loss (Hardy and Higgins, 1992). Although the role of Aβ as a major contributor in AD pathogenesis is indisputable, the neurotoxicity of extracellular Aβ aggregates and their role as the main causative agent has been questioned due to the studies showing a lack of correlation between the deposition of senile plaques and the extent of the observed cognitive decline (Bush, 2003; Cuajungco *et al.*, 2000; Hardy and Selkoe, 2002; Terry *et al.*, 1991). In addition, Aβ was also found to be a component of the healthy human brain, although its exact function remains unknown (Haass *et al.*, 1992). However, in the healthy brain, Aβ is present in a soluble, monomeric form which is non-toxic, whereas the main constituent of senile plaques is the aggregated oligomeric form of Aβ (Piccini *et al.*, 2005). A more consistent biomarker appears to be the presence of soluble oligomers of Aβ (Hardy and Selkoe, 2002). Several studies have shown a correlation between the presence of the soluble oligomeric form of Aβ and cognitive decline (Knobloch *et al.*, 2007; Naslund *et al.*, 2000; Oddo *et al.*, 2003). It has been postulated that the intracellular deposition of Aβ is an upstream event in AD pathogenesis as opposed to the presence of senile plaques which perhaps occurs at a relatively late stage of AD pathogenesis (LaFerla *et al.*, 2007). The aggregation of Aβ has been closely associated with the mis-homeostasis of metals in AD, in particular copper, as discussed below.

1.5.3 Copper mis-homeostasis in Alzheimer's disease

AD brains can contain up to 400 % more copper than the healthy human brain, and a high concentration of copper has also been detected in association with senile plaques (Lovell *et al.*, 1998). Copper mis-homeostasis in AD has an added complexity, as it appears to involve an imbalance between the extracellular and the intracellular concentration of copper (Filiz *et al.*, 2008). While excess extracellular copper is thought to be a strong contributor to oxidative stress, decreased intracellular copper concentration in AD is associated with reduced activity of cuproenzymes including

SOD1 and COX (Bayer *et al.*, 2003; Maurer *et al.*, 2000). As mentioned previously (section 1.1.5), the brain is particularly vulnerable to metal-mediated toxicity which gets further aggravated by the age-dependent decline of the activity of the brain's antioxidant enzymes. In addition, Aβ, APP and BACE1, the main protein components involved in AD pathogenesis, have all been implicated in copper mis-homeostasis in AD.

1.5.4 Amyloid-β and copper mis-homeostasis

The Aβ peptide readily binds metals, in particular, copper and zinc (Faller, 2009). Copper-binding in Aβ has been shown to be coordinated by three His residues (His6, His13 and His14) and the carboxyl group of the N-terminus (Karr *et al.*, 2005; Syme *et al.*, 2004). *In vitro* experiments have reported Aβ to reduce Cu(II) to Cu(I) and the copper-bound Aβ complex has been shown to be more toxic than apo-Aβ as it can react with molecular oxygen to form hydrogen peroxide and further contribute to oxidative stress (Atwood *et al.*, 2004; Huang *et al.*, 1999). In contrast, Aβ has also been shown to act as an anti-oxidant (Atwood *et al.*, 2003; Kontush *et al.*, 2001). A study by Nakamura *et al.* (2007) reported decreased production of hydroxyl radicals in the presence of Aβ by free Cu(II). Conflicting results have also been reported regarding copper-mediated aggregation of Aβ. While some studies have shown copper to promote Aβ aggregation, other studies have reported Aβ oligomers to adopt a distorted structure in the presence of copper that is less prone to aggregation (Atwood *et al.*, 2004; Jiao and Yang, 2007).

It has been proposed that metal-bound Aβ can act both as a pro-oxidant and as an anti-oxidant depending upon the oligomeric state of Aβ (Zou *et al.*, 2002). In its monomeric state, Aβ protects the neurons against metal-mediated oxidative damage, whereas in its aggregated state the presence of metals including copper, promotes oxidative damage. Further studies are however required to determine the precise effect of copper-binding on Aβ conformation and the subsequent effects of copper-bound Aβ peptide in the pathogenesis of AD.

1.5.5 The Role of Amyloid Precursor Protein in Copper homeostasis

Amyloid precursor protein is a single-membrane spanning glycoprotein found in higher eukaryotic organisms including humans, rodents and worms (Coulson *et al.*, 2000; Kang *et al.*, 1987; Suazo *et al.*, 2009). There are several splice variants known for APP, but the most common form in the brain is the protein containing residues 1-695 (Haass *et al.*, 1991; Kong *et al.*, 2008). APP consists of a large extracellular domain, a transmembrane domain and a short intracellular domain, as shown in Figure 15. The precise function of APP is not known although it has been implicated as a cell surface receptor involved in signal transduction and neurite growth (Jin *et al.*, 1994; Kong *et al.*, 2008; Schubert *et al.*, 1991).

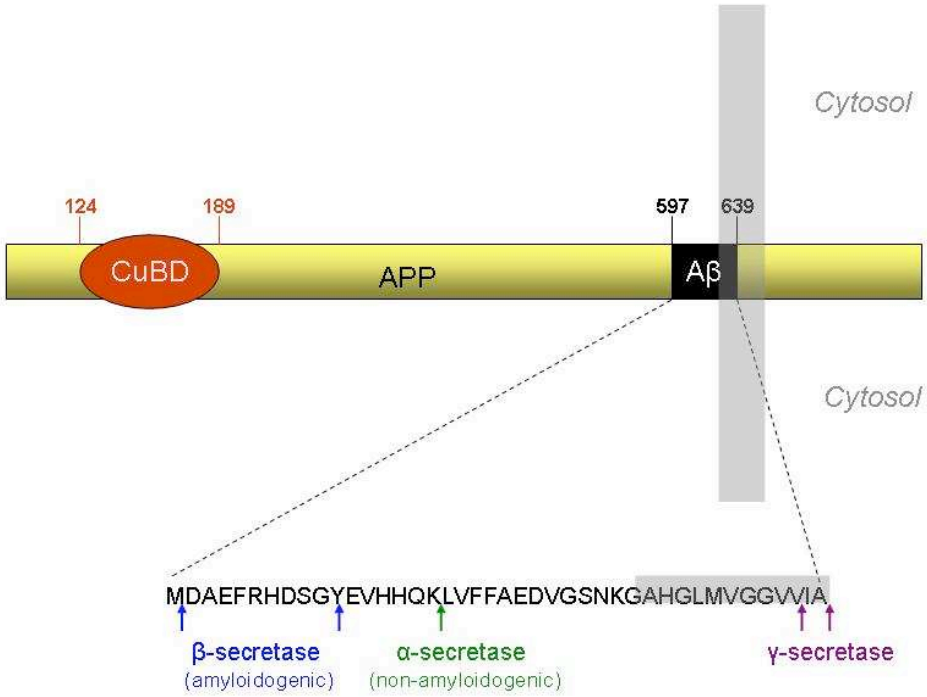

Figure 15: Model depicting the proteolytic processing of the amyloid precursor protein (APP). APP can be cleaved in the Aβ region by α-secretase (green arrow) and γ-secretase (purple arrow) resulting in the release of a truncated Aβ peptide which is non-amyloidogenic (Venugopal *et al.*, 2008). Alternatively, APP can be cleaved in either one of the two locations (blue arrows) by the β-secretase (BACE1) followed by γ-secretase leading to the release of longer Aβ fragments which are amyloidogenic (Gouras *et al.*, 1998; Sinha and Lieberburg, 1999). The extracellular copper-binding domain (CuBD) in APP is depicted as a red oval. The numbers indicate the position of amino acids within APP (Faller and Hureau, 2009; Kong *et al.*, 2008).

APP has also been implicated in the maintenance of neuronal copper homeostasis (Bellingham *et al.*, 2004; Maynard *et al.*, 2002; Suazo *et al.*, 2009; Treiber *et al.*, 2004; White *et al.*, 1999). APP contains two copper-binding sites with one of them located in the Aβ region and another in the extracellular portion (Atwood *et al.*, 2000; Hesse *et al.*, 1994). The extracellular copper-binding domain of APP (APP CuBD) has been shown to readily bind Cu(II) via two His residues (His147 and His151), a Tyr residue (Tyr168) and two water ligands (Kong *et al.*, 2007a). *In vitro* experiments have also highlighted the role of Cys144 and Met170 in the APP-mediated reduction of Cu(II) to Cu(I) (Ruiz *et al.*, 1999). Structural characterisation of APP CuBD by NMR spectroscopy (Barnham *et al.*, 2003) and X-ray crystallography (Kong *et al.*, 2007a; Kong *et al.*, 2007b) revealed the copper-binding site to be relatively solvent-exposed in a similar way to the metal-binding site of the copper metallochaperones Atx1 and CCS, leading to the hypothesis that APP may act as a neuronal copper metallochaperone (Barnham *et al.*, 2003).

The role of APP in copper homeostasis is further highlighted by several studies reporting changes in intracellular copper concentration with respect to APP expression levels, although these studies have provided contrasting results. While some studies have highlighted the role of APP in copper export due to increased intracellular copper concentration when it is overexpressed and decreased intracellular copper concentration in mice lacking APP, others have shown an opposite effect (Bellingham *et al.*, 2004; Maynard *et al.*, 2002; White *et al.*, 1999). Overexpression of APP was also reported to result in increased intracellular copper concentration in human embryonic kidney (HEK) cells due to increased reduction of extracellular Cu(II) followed by greater uptake of Cu(I) (Suazo *et al.*, 2009). This was further supported by the subsequent increase in metallothionein levels, implicating APP in promoting the storage of excess copper. Copper has also been shown to modulate APP processing and can result in decreased production of Aβ (Bayer *et al.*, 2003; Borchardt *et al.*, 1999). Further studies are required to conclusively determine the effect of copper-binding to APP on Aβ production (Miller *et al.*, 2006).

1.5.6 β-secretase Amyloid Precursor Protein Cleaving Enzyme 1 and its Role in Copper homeostasis

BACE1 is the rate-limiting enzyme involved in the production of Aβ by the proteolytic cleavage of APP at either the beginning of Aβ sequence (Asp1) or at Glu11 to liberate either $A\beta_{42}$ or a truncated Aβ peptide following cleavage by γ-secretase, as shown in Figure 15 (Gouras *et al.*, 1998; Sinha and Lieberburg, 1999). The open reading frame of BACE1 constitutes a 501 amino acid membrane-bound protein comprising a proprotein domain, a large luminal domain, a transmembrane domain and a short cytosolic domain (CTD), as shown in Figure 16 (Hussain *et al.*, 1999; Lin *et al.*, 2000;

Sinha *et al.*, 1999; Sinha and Lieberburg, 1999; Vassar *et al.*, 1999; Yan *et al.*, 1999). In the brain BACE1 has been implicated in myelination, neurotransmission, and in the maintenance of synaptic function (Cole and Vassar, 2007; Harrison *et al.*, 2003; Willem *et al.*, 2006). BACE1 is also highly expressed in the pancreas albeit this isoform is devoid of β-secretase activity (Bodendorf *et al.*, 2001; Ehehalt *et al.*, 2002; Vassar *et al.*, 1999). The physiological function of pancreatic BACE1 is not known. While the active site of BACE1 resides in the luminal portion, the cytosolic C-terminal domain (CTD) mediates the trafficking and intracellular localisation of BACE1 (Benjannet *et al.*, 2001; Capell *et al.*, 2000; Huse *et al.*, 2000; Walter *et al.*, 2000).

Human BACE1 CTD (hBACE1 CTD) contains a $C_{482}XXC_{485}$ motif which has been shown to bind Cu(I) *in vitro* (Angeletti *et al.*, 2005). In addition to Cys482 and Cys485, hBACE1 CTD also contains a third Cys residue at position 478. Angeletti *et al.* (2005) reported that the binding of Cu(I) to hBACE1 CTD was mediated via Cys482 in association with either Cys478 or Cys485 and a third unidentified ligand. In addition, Angeletti *et al.* (2005) also reported an interaction between hCCS and hBACE1 CTD ina yeast two-hybrid system which is mediated by D1 of hCCS. This interaction was further confirmed by co-immunoprecipitation and glutathione-*S*-transferase (GST) pull-down assays and co-localisation experiments. The overexpression of BACE1 was shown to result in decreased SOD1 activity which could be rescued by increased expression of CCS, suggesting that BACE1 might play a role in neuronal copper homeostasis as a potential partner of CCS (Angeletti *et al.*, 2005). This is further supported by the studies in neuronal cells, where the deletion or depletion of *CCS* was shown to result in increased production of Aβ due to increased processing of APP via BACE1 (Gray *et al.*, 2010). However, the mechanism underlying the observed effects was not determined. One of the aims of this study was to further characterise the hCCS-hBACE1 CTD interaction by determining the molecular basis of this interaction, as discussed further in section 0.

1.5.7 Current Therapeutics Targeting Copper mis-homeostasis in Alzheimer's disease

Copper mis-homeostasis appears to be an integral part of AD pathology and may be one of the upstream factors in AD pathogenesis. Although the exact role of Aβ, APP and BACE1 with respect to copper homeostasis is not yet established, there is sufficient evidence to suggest that targeting copper imbalance in AD is an attractive therapeutic strategy. A key requirement for a copper-based therapeutic includes targeting the copper imbalance in the brain, that is, increased extracellular concentration of copper and decreased concentration of copper intracellularly, as discussed in section 1.5.3. This led to the use of 5-chloro-7-iodo-8-hydroxyquinoline commonly known as clioquinol as a metal-protein attenuating compound (MPAC) which can interact with the MBS of

the target protein (Bush, 2003; Cuajungco *et al.*, 2000). Clioquinol is a lipophilic compound that has relatively moderate (nanomolar) affinity for Cu(II) and Zn(II) (Bush, 2003). Studies with clioquinol in transgenic mouse models and clinical trials reported increased cognitive improvement and decreased deposition of Aβ in the brain (Cherny *et al.*, 2001; White *et al.*, 2006). It was proposed that clioquinol was able to extract copper and zinc from the extracellular plaques resulting in disaggregation of Aβ. Copper-bound clioquinol was also reported to be able to traverse the cell membrane and due to its weak binding affinity for Cu(II), it was able to release Cu(II) inside the cells resulting in its redistribution inside the cell. Increased intracellular concentration of copper also led to increased activation of matrix metalloproteinases which mediate the degradation of Aβ (Cherny *et al.*, 2001; White *et al.*, 2006). However, this compound was withdrawn from clinical trials due to iodine-based contamination during its synthesis (Bush and Tanzi, 2008; Opazo *et al.*, 2006). A second 8-hydroxyquinoline derivate – PBT2 was synthesised which is not only more soluble than clioquinol but also lacks the iodine component and hence overcomes the iodine-mediated contamination problems (Adlard *et al.*, 2008). Studies in mice and phase II clinical trials have reported decreased Aβ load and improved cognition, however, larger scale studies are required to determine the full efficacy of this compound (Faux *et al.*, 2010; Lannfelt *et al.*, 2008).

1.6 Copper homeostasis in *S. cerevisiae*

This study used the yeast two-hybrid system to investigate the protein-protein interactions between metallochaperones and various binding partners. Homologues of most of the copper-binding proteins investigated in this study are also present in *S. cerevisiae*. Therefore, it is important to identify the proteins and pathways that can potentially be affected by the two-hybrid experiments carried out in this study. While the individual components have been discussed previously, Figure 17 illustrates the main proteins that can be affected by the two-hybrid experiments.

Similar to human cells, copper is present in the yeast cytoplasm in its reduced form as Cu(I) (as discussed in section 1.1.2). In order to enter the cell, Cu(II) is reduced at the cell surface by the metalloreductases Fre1 and Fre2, as shown in Figure 17. The Fre1/Fre2 reductases are responsible for reducing Cu(II) and Fe(III) to Cu(I) and Fe(II) respectively (Dancis *et al.*, 1992; Georgatsou *et al.*, 1997; Hassett and Kosman, 1995). Cu(I) is then transported through to the cytoplasm via the high-affinity copper transport proteins Ctr1 and Ctr3 (discussed in section 1.3.1). A third Ctr protein, Ctr2, is located at the vacuolar membrane and is responsible for mobilising copper from the vacuole into the cytosol under conditions of copper deficiency (section 1.3.1).

1 MAQALPWLLLWMGAGVLPAHGTQHGIRLPLRSGLGGAPLGLRLPRETDEE

51 PEEPGRRGSFVEMVDNLRGKSGQGYYVEMTVGSPPQTLNILVDTGSSNFA

101 VGAAPHPFLHRYYQRQLSSTYRDLRKGVYVPYTQGKWEGELGTDLVSIPH

151 GPNVTVRANIAAITESDKFFINGSNWEGILGLAYAEIARPDDSLEPFFDS

201 LVKQTHVPNLFSLQLCGAGFPLNQSEVLASVGGSMIIGGIDHSLYTGSLW

251 YTPIRREWYYEVIIVRVEINGQDLKMDCKEYNYDKSIVDSGTTNLRLPKK

301 VFEAAVKSIKAASSTEKFPDGFWLGEQLVCWQAGTTPWNIFPVISLYLMG

351 EVTNQSFRITILPQQYLRPVEDVATSQDDCYKFAISQSSTGTVMGAVIME

401 GFYVVFDRARKRIGFAVSACHVHDEFRTAAVEGPFVTLDMEDCGYNIPQT

451 DESTLMTIAYVMAAICALFMLPLCLMVCQWRCLRCLRQQHDDFADDISLL

501 K

Figure 16: The amino acid sequence of human BACE1. The signal peptide is shown in purple, propeptide domain in green, protease domain in black, transmembrane domain in grey and the cytosolic C-terminal domain in blue. The two catalytic motifs are highlighted in yellow and the predicted Cu(I)-binding residues are shown in red. The numbers indicate the position of amino acids within human BACE1. The sequence was obtained from GenBank accession number AF190725 (Vassar *et al.*, 1999).

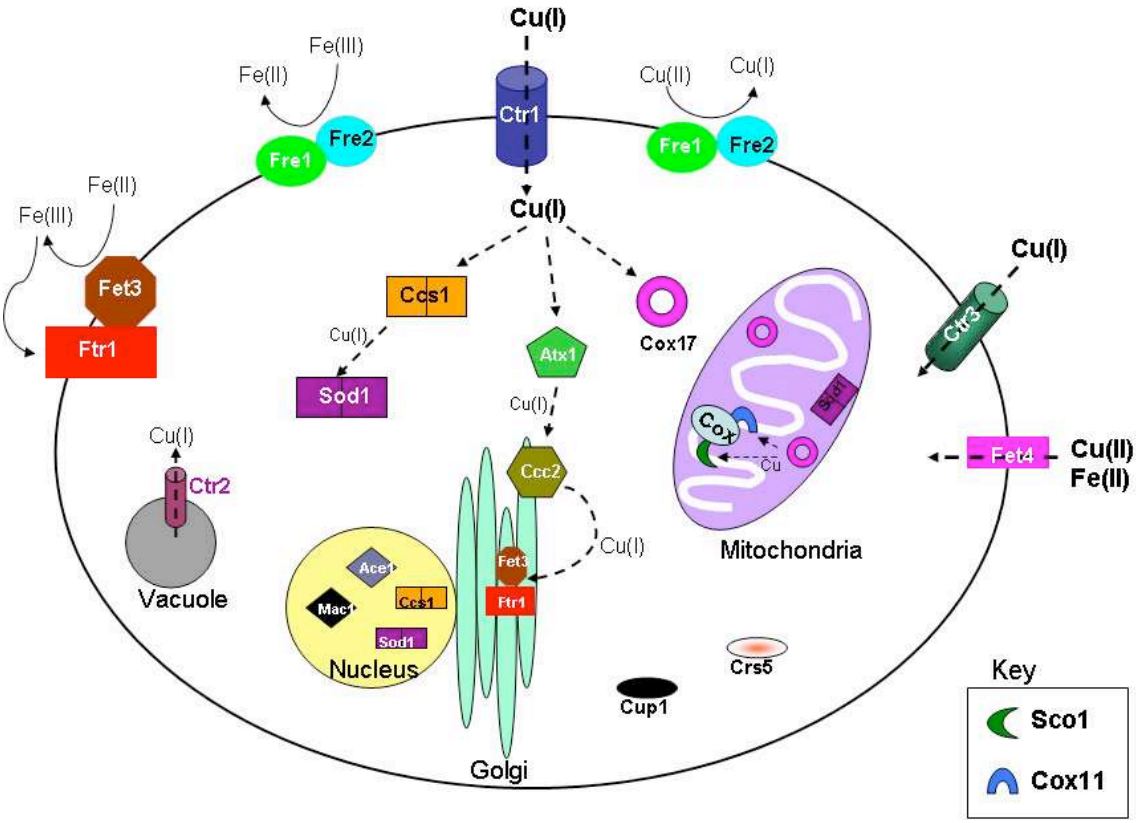

Figure 17: Copper homeostasis in *S. cerevisiae*. The model depicts the proteins and pathways involved in copper homeostasis. Cu(II) is reduced at the cell surface by the Fre1/Fre2 reductases and is transported into the cell by Ctr1 and the Ctr3 transporters. Once inside the cell, Cu(I) can be bound by the metallochaperones Ccs1, Atx1 and Cox17. Ccs1 delivers Cu(I) to Sod1 which is localised in the cytosol, nucleus and the mitochondria. Atx1 incorporates Cu(I) into Ccc2 which transports it to the Fet3/Ftr1 complex in the golgi. Cu-bound Fet3/Ftr1 complex translocates to the plasma membrane to enable high-affinity iron uptake. Cox17 binds Cu(I) in the cytosol and delivers it to the Sco1 and Cox11 proteins in the mitochondria which further transport Cu(I) to cytochrome *c* oxidase. The copper-dependent transcription factors Mac1 and Ace1 regulate the induction of proteins involved in copper homeostasis, as discussed in section 1.6. Excess copper can be bound by the metallothionein proteins Cup1 and Crs5 or stored in the vacuole. In conditions of copper deficiency, Ctr2 can mobilise copper from the vacuole into the cytoplasm. Copper can also enter the cell via the divalent cation transporter Fet4.

Inside the cell, Cu(I) can bind to the copper metallochaperones Atx1 (section 1.3.2.4.1), Ccs1 (section 1.3.2.4.2) and Cox17 (section 1.3.2.4.3) which deliver Cu(I) to their respective target proteins. Copper can also leak through the plasma membrane-bound low-affinity Fet4 transporter which is not specific for Fe(II) and can also transport other divalent cations including Cu(II) (Hassett *et al.*, 2000).

As discussed previously, copper homeostasis can also be regulated at the level of gene transcription. While the copper-dependent transcription factor Mac1 induces the transcription of proteins involved in copper uptake such as *CTR1* and *CTR3* (section 1.3.1), the Ace1 transcription factor induces the transcription of proteins involved in preventing copper toxicity such as Sod1 and the metallothioneins Cup1 and Crs5 (Jensen *et al.*, 1996; Pena *et al.*, 1998; Strain and Culotta, 1996). Figure 17, also illustrates the overlap between copper and iron homeostasis. Both Cu(II) and Fe(III) are reduced by the Fre1/Fre2 reductases for high-affinity uptake into the cytosol. The Fet3/Ftr1 complex requires the transport of Cu(I) from Ccc2 to the multicopper oxidase Fet3 in the golgi prior to its translocation to the cell surface for high-affinity iron uptake. In addition, the transcription of *FRE1* is regulated by not only the iron-responsive transcription factor Aft1 but also Mac1 (Georgatsou *et al.*, 1997; Labbe *et al.*, 1997; Yamaguchi-Iwai *et al.*, 1995; Yamaguchi-Iwai *et al.*, 1996).

1.7 Research Aims

The goal of this study is to further the understanding of the molecular basis of the interaction of copper metallochaperones with their partner proteins. The first aim of this study was to determine the molecular basis of the interaction between hCCS and hBACE1 CTD. The recent evidence showing that CCS deficiency can result in enhanced Aβ production due to increased cleavage of APP by BACE1 (Gray *et al.*, 2010) demonstrates that the interaction of hCCS with hBACE1 CTD may be of relevance to AD pathology. Moreover the increase in interaction between hCCS and hBACE1 CTD can also lead to decreased interaction of hCCS with hSOD1 (Angeletti *et al.*, 2005). Since hCCS and hBACE1 CTD can both bind Cu(I), one of the aims of this study was to determine the role of copper-binding in mediating the formation of a complex between them. The complex formation was studied using a two-hybrid system. To demonstrate a role for copper in complex formation, the interactions were tested in conditions of copper deficiency and copper excess. This study also aimed to identify the amino acids involved in mediating the interaction of hCCS with hBACE1 CTD.

The complex formation of hCCS with hSOD1 was also studied using a yeast two-hybrid system. As discussed in section 1.4.4, there is conflicting evidence regarding the role of D1 and D3 in the CCS-dependent activation of SOD1. A lot of the information is based on the interaction of Ccs1 with Sod1. However, it is now evident

that the CCS-dependent activation of SOD1 may vary depending upon the homologues studied (Leitch *et al.*, 2009a; Leitch *et al.*, 2009b). This study aimed to investigate the effect of copper concentration and the role of Cu(I)-binding residues in hCCS in mediating the interaction with hSOD1. As mentioned above, the interplay between the interactions of hCCS with hBACE1 CTD and hSOD1 may also be of relevance to AD pathology.

The interaction of ScAtx1 with the MBDs of PacS and CtaA was also studied using a yeast two-hybrid system. As discussed in section 1.4.3, cyanobacteria provide a rare example where the copper metallochaperone (ScAtx1) has been shown to interact with a proposed copper donor (CtaA) and copper acceptor (PacS) (Tottey *et al.*, 2001; Tottey *et al.*, 2002). It has been shown that the complex formation of ScAtx1 with its partner MBDs requires the Cu(I)-binding Cys ligands in ScAtx1. This study aimed to investigate the effect of copper concentration on the interaction of ScAtx1 with the MBDs from PacS and CtaA. Since there is comparatively little information available regarding the interaction of ScAtx1 with the CtaA MBD both *in vitro* and *in vivo*, this study aimed to provide vital information regarding the amino acids involved in mediating the complex formation between them. Additionally, the role of these amino acids on the complex formation of ScAtx1 and PacS MBD was also demonstrated. In light of the two different structural arrangements obtained by X-ray crystallography for the ScAtx1 dimer (head-to-head and side-to-side), this study investigated the proposed idea that these arrangements may reflect the formation of structurally different complexes of ScAtx1 with PacS MBD and CtaA MBD (Badarau *et al.*, 2010).

2. Materials and Methods

2.1 Chemicals, Reagents and Equipment

All chemicals were purchased from Sigma-Aldrich (Dorset, UK) except for growth medium components which were purchased from Formedium (Norfolk, UK), unless stated otherwise. All restriction endonucleases were purchased from New England BioLabs (Herts, UK) while the *Pfu* DNA polymerase enzyme was purchased from Stratagene (Leicestershire, UK). DNA oligomers were synthesised by Sigma-Genosys (Suffolk, UK). The pGEMt_hCCS vector was received as a kind gift from Professor Colin Dingwall, King's College London, UK. The pCIneo_hSOD1 construct was generously provided by Professor Christopher Miller, King's College London, UK. The DNA oligomers used for S1 nuclease assays were kindly provided by Dr. Julian Rutherford, Newcastle University, UK. Deionized (dH_2O) or double-dH_2O (ddH_2O) water purified using the Millipore Simplicity system (Millipore, UK) was used throughout. For molecular biology purposes, ddH_2O was sterilised by autoclaving at 121 ^oC for 30 mins. All optical density (OD) readings were measured using a Perkin-Elmer lambda 35 UV-Vis spectrophotometer.

2.2 Strains

2.2.1 *E. coli*

All *E. coli* strains (Table 2) were maintained either on solid medium containing Luria-Bertani (LB) medium (10 g/L tryptone, 10 g/L NaCl, 5 g/L yeast extract) (Sambrook and Russell, 2001) supplemented with 1.7 % (w/v) agar and the appropriate antibiotic at 4 ^oC or as a cryo-stock containing 1.5 mL of pelleted bacterial culture resuspended in 250 µL of 1 % (w/v) peptone and 250 µL of 50 % (v/v) glycerol, stored at -80 ^oC.

2.2.2 *S. cerevisiae*

All *S. cerevisiae* strains (Table 3) were maintained either on solid medium containing 1 % (w/v) yeast extract, 2 % (w/v) peptone, 2 % (w/v) glucose or dextrose (YPD medium) supplemented with 2 % (w/v) agar at 4 ^oC or as a cryo-stock containing 1 mL of overnight cell culture with 1 mL of 30 % (v/v) glycerol and 80 µL dimethyl sulfoxide at -80 ^oC.

2.3 Molecular Biology in *E. coli*

2.3.1 Preparation of competent *E. coli* cells

An isolated colony of *E. coli* was inoculated in 5 mL LB medium overnight at 37 ^oC with shaking at 250 rpm in an orbital shaker (New Brunswick Scientific Co. Inc., USA). The

culture was diluted 1:100 in LB medium (10 mL) the following day and grown for a further 2-3 hrs with shaking at 37 ^{o}C. The cells were pelleted by centrifugation at 1600 x *g* at 4 ^{o}C. The pellet was resuspended in 1 mL ice-cold sterile TSS (85 % (v/v) LB, 10 % (w/v) polyethylene glycol 8000 (PEG), 5 % (v/v) dimethyl sulfoxide, 50 mM magnesium chloride pH 6.5) and stored at 4 ^{o}C (Chung *et al*., 1989).

Table 2: *E. coli* strains used in this study.

Strain	Genotype	Purpose	Source
JM101	F^{-} *traD36 proA^{+}B^{+} lacI^{q} Δ(lacZ)M15/ Δ(lac-proAB) glnV thi*	Cloning	Lab stock
XL-1 Blue	*recA1 endA1 gyrA96 thi-1 hsdR17 supE44 relA1 lac* [F´ *proAB^{+} lacIqZΔM15 Tn10 (Tet^{r})]*	Site-directed mutagenesis	Lab stock
XL-1 Blue MRF'	*Δ(mcrA)183 Δ(mcrCB-hsdSMR-mrr)173 endA1 supE44 thi-1 recA1 gyrA96 relA1 lac* [F´ *proAB lacIqZΔM15. Tn10 (Tet^{r})*]	BacterioMatch® Bacterial 2-Hybrid	Agilent Biotechnologies, UK
BTH101	F^{-}, *cya-99*, *araD139, galE15, galK16, rpsL1 (Str^{r}), hsdR2, mcrA1, mcrB1*	BACTH (Bacterial two-hybrid) system	Euromedex, France

Table 3: *S. cerevisiae* strains used in this study.

Strain	Genotype	Purpose	Source
EGY48	*MATα his3 trp1 ura3-52 leu2: : pleu2-LexAop6*	Yeast two-hybrid	K. Freeman, GSK, UK
BY4741-*ccs1Δ*	*MATα his3Δ1 leu2Δ0 met15Δ0 ura3Δ0 ccs1Δ: : KAN^{R}*	Deleting *CCS1* from the genome of EGY48	Yeast genome collection, Research Genetics, USA
SAY1	*MAT, his3, trp. 1, ura3-52, leu2: : pleu2-LexAop6, ccs1Δ: : KAN^{R}*	Yeast two-hybrid	This study

2.3.2 Transformation in *E. coli*

50 µL of competent *E. coli* cells were incubated with 1 µL of plasmid DNA and stored on ice for 20 mins. The cells were heat-shocked by incubating them at 42 ^{o}C for 1 min, followed by 2 mins incubation on ice. 0.5 mL of LB medium was added to the cells and incubated at 37 ^{o}C with shaking for 1 hr. 100 µL of the transformed culture was spread on LB-agar plates with the appropriate antibiotics and incubated overnight at 37 ^{o}C (Sambrook and Russell, 2001).

2.3.3 DNA manipulation

All the vectors and DNA oligomers used in this study are listed in Table 4 and Table 5 respectively.

2.3.3.1 Extraction of DNA from *E. coli* cells

Plasmid DNA was isolated from bacterial cultures using the Sigma GenElute Plasmid Miniprep kit according to the manufacturer's instructions.

2.3.3.2 Digestion of DNA using restriction endonucleases

Plasmid DNA was digested by incubating the DNA at 37 ^{o}C with the appropriate restriction endonucleases for 1-2 hrs according to the manufacturer's instructions and analysed by agarose gel electrophoresis.

2.3.3.3 DNA analysis using agarose gels

1 % (w/v) agarose was dissolved in 60 mL 1x TAE buffer (40 mM Tris-acetate, 1 mM EDTA pH 8.0) by boiling in a microwave, cooled to ~60 ^{o}C, poured into a gel cast (Bio-Rad, UK) with 0.1 % (v/v) of 1 µg/mL ethidium bromide and left to set at room temperature. Once set, the gel was placed inside a gel tank containing 1x TAE buffer, loaded with DNA samples containing 1x DNA-loading dye (0.4 % (w/v) bromophenol blue, 5 % (v/v) glycerol) and electrophoresed at 100 V for 30-60 mins. Lambda DNA (Promega, UK) digested with *PstI* endonuclease was used as molecular weight markers. Gels were photographed under UV irradiation (Bio-Rad Gel Doc 1000).

2.3.3.4 Isolation of DNA from agarose gels

The target band was excised using a scalpel from the agarose gel by visualising it under ultraviolet light using a transilluminator (UV Tec, UK). The DNA was isolated from the gel slice using the Sigma GenElute Gel Extraction kit according to the manufacturer's instructions.

Table 4: List of all the vectors used in this study. The details regarding the genes ligated into the multi-cloning site of the vectors are also provided including the amino acid residue numbers corresponding to the protein sequence. (-) indicates empty vector.

Name of the Vector	Gene 'Insert'	Source
Vectors used for cloning PCR products		
pGEMt	-	Promega, UK
pJET	-	Fermentas, UK
Source of *hSOD1* gene		
pCIneo_hSOD1	Full-length *hSOD1*	Christopher Miller
Source of *hCCS* gene		
pGEMt_hCCS	Full-length *hCCS*	Colin Dingwall
BacterioMatch® Two-Hybrid system constructs		
pBT	-	Nigel Robinson
pBT_ScAtx1	Full-length *scAtx1*	Nigel Robinson
pTRG	-	Nigel Robinson
pTRG_PacS95	PacS NTD (Res 1-95)	Nigel Robinson
pBT_hBACE1 CTD	hBACE1 CTD[a]	This study
pBT_hSOD1	Full-length *hSOD1*	This study
pTRG_hCCS	Full-length *hCCS*	This study
BACTH system constructs		
pUT18C	-	Richard Daniel
pKT25	-	Richard Daniel
pUT18C_Zip	Leucine zipper of GCN4	Richard Daniel
pKT25_Zip	Leucine zipper of GCN4	Richard Daniel
pUT18C_hCCS	Full-length *hCCS*	This study
pUT18C_hCCSD1	hCCS Domain 1[b]	This study
pKT25_hBACE1 CTD	hBACE1 CTD[a]	This study
Yeast 2-Hybrid system constructs		
pMW112	-	Katie Freeman
pJG4.5	-	Katie Freeman
p423lexAkan	-	Katie Freeman
pJG4.5_hCCS	Full-length *hCCS*	This study
pJG4.5_hCCSD1	hCCS D1[b]	Katie Freeman
pJG4.5_hCCSD2	hCCS D2[c]	Katie Freeman
pJG4.5_hCCSD3	hCCS D3[d]	Katie Freeman
pJG4.5_hCCS C22S	Full-length *hCCS*	This study
pJG4.5_hCCS C25S	Full-length *hCCS*	This study
pJG4.5_hCCS C22S,C25S	Full-length *hCCS*	This study
pJG4.5_hCCS C224S	Full-length *hCCS*	This study
pJG4.5_hCCS C224S,C226S	Full-length *hCCS*	This study
pJG4.5_hCCSD1 C22S	hCCS D1[b]	This study
pJG4.5_hCCSD1 C25S	hCCS D1[b]	This study
pJG4.5_hCCSD1 C22S,C25S	hCCS D1[b]	This study
pJG4.5_hCCS R71A	Full-length *hCCS*	This study
pJG4.5_hCCS R71E	Full-length *hCCS*	This study
pJG4.5_hCCS R71K	Full-length *hCCS*	This study
pJG4.5_hCCSD1 R71A	hCCS D1[b]	This study
pJG4.5_hCCSD1 R71E	hCCS D1[b]	This study
pJG4.5_hCCSD1 R71K	hCCS D1[b]	This study
pJG4.5_hSOD1	Full-length *hSOD1*	This study
pJG4.5_HAH1	Full-length *HAH1*	Katie Freeman
pJG4.5_Ccs1	Full-length *CCS1*	Katie Freeman
pJG4.5_Ccs1 K66R	Full-length *CCS1*	This study
pJG4.5_ScAtx1	Full-length *scAtx1*	This study

pJG4.5_ScAtx1 A11K	Full-length *scAtx1*	This study
pJG4.5_ScAtx1 A11R	Full-length *scAtx1*	This study
pJG4.5_ScAtx1 E13A	Full-length *scAtx1*	This study
pJG4.5_ScAtx1 E13Q	Full-length *scAtx1*	This study
pJG4.5_ScAtx1 K21D	Full-length *scAtx1*	This study
pJG4.5_ScAtx1 N25R	Full-length *scAtx1*	This study
pJG4.5_ScAtx1 S58A	Full-length *scAtx1*	This study
pJG4.5_ScAtx1 H61A	Full-length *scAtx1*	This study
pJG4.5_ScAtx1 H61E	Full-length *scAtx1*	This study
pJG4.5_ScAtx1 H61F	Full-length *scAtx1*	This study
pJG4.5_ScAtx1 H61K	Full-length *scAtx1*	This study
pJG4.5_ScAtx1 H61Y	Full-length *scAtx1*	This study
p423lexAkan_hBACE1 CTD	hBACE1 CTD[a]	This study
p423lexAkan_hBACE1 CTD C478S	hBACE1 CTD[a]	This study
p423lexAkan_hBACE1 CTD W480M	hBACE1 CTD[a]	This study
p423lexAkan_hBACE1 CTD R481A	hBACE1 CTD[a]	This study
p423lexAkan_hBACE1 CTD R481E	hBACE1 CTD[a]	This study
p423lexAkan_hBACE1 CTD R481K	hBACE1 CTD[a]	This study
p423lexAkan_hBACE1 CTD C482S	hBACE1 CTD[a]	This study
p423lexAkan_hBACE1 CTD R484A	hBACE1 CTD[a]	This study
p423lexAkan_hBACE1 CTD C485S	hBACE1 CTD[a]	This study
p423lexAkan_hBACE1 CTD R487A	hBACE1 CTD[a]	This study
p423lexAkan_hBACE1 CTD D491A,D492A	hBACE1 CTD[a]	This study
p423lexAkan_hCCS	Full-length *hCCS*	This study
p423lexAkan_hCCS C22S	Full-length *hCCS*	This study
p423lexAkan_hCCS C25S	Full-length *hCCS*	This study
p423lexAkan_hCCS C22S,C25S	Full-length *hCCS*	This study
p423lexAkan_hCCS C244S	Full-length *hCCS*	This study
p423lexAkan_hCCS C244S,C246S	Full-length *hCCS*	This study
p423lexAkan_hCCSD3	hCCS D3[d]	This study
p423lexAkan_hCCS R71A	Full-length *hCCS*	This study
p423lexAkan_hCCS R71E	Full-length *hCCS*	This study
p423lexAkan_hCCS R71K	Full-length *hCCS*	This study
p423lexAkan_Ccs1	Full-length *yCCS*	This study
p423lexAkan_Ccs1 K66R	Full-length *yCCS*	This study
p423lexAkan_$PacS_N$	PacS NTD[e]	This study
p423lexAkan_$PacS_N$ R13A	PacS NTD[e]	This study
p423lexAkan_$PacS_N$ Y65H	PacS NTD[e]	This study
p423lexAkan_$CtaA_N$	CtaA NTD[f]	This study
p423lexAkan_$CtaA_N$ K34A	CtaA NTD[f]	This study
p423lexAkan_$CtaA_N$ F87H	CtaA NTD[f]	This study
p423lexAkan_$CtaA_N$ F87Y	CtaA NTD[f]	This study
p423lexAkan_CtaA111	CtaA NTD (Res 1-111)	This study

[a] hBACE1 CTD residues 478-501.

[b] hCCS D1 residues 1-79.

[c] hCCS D2 residues 79-231.

[d] hCCSD3 residues 235-274.

[e] PacS NTD residues 1-71.

[f] CtaA NTD residues 1-92.

Table 5: List of all the DNA oligomers used in this study.

No.	Sequence (5'→3')	Purpose
1	GCACTAGTGATTTTTGGATCCGCTTCGGATTCGGGG	Cloning hCCS into pTRG
2	GGCCGCGGGATTTTTGAATTCTCAAAGGTGGGCAGGGGG	
3	GGCCGCATGCCAGTGGCGTTGCCTGCGTTGCCTGCGTCAGCAGCATGATGATTTTGCGGATGATATCAGCCTGCTGAAATAAG	hBACE1 CTD for pBT
4	AATTCTTATTTCAGCAGGCTGATATCATCCGCAAAATCATCATGCTGCTGACGCAGGCAACGCAGGCAACGCCACTGGCATGC	
5	GAAGCGGCCGCGCGACGAAGGCCGTGTGCG	Cloning hSOD1 into pBT
6	GAAGAATTCTTATTGGGCGATCCCAATTACACC	
7	CTGCCCCCAGATTCTGCAAGAATTCTTAGCCCATGCCCTTGAGTACC	Cloning hCCSD1 into pTRG/pUT18C
8	GGGATTCCACTAGTGATTTTGGATCCCGCTTCGGATTCGGGG	Cloning hCCS into pUT18C
9	CCCCGAATCCGAAGCGGGATCCAAAATCACTAGTGGAATCCC	
10	GCGTGCCAGTGGCGTTGCCTGCGTTGCCTGCGTCAGCAGCATGATGATTTTGCGGATGATATCAGCCTGCTGAAATAAGAG	hBACE1 CTD for pKT25
11	GATCCTCTTATTTCAGCAGGCTGATATCATCCGCAAAATCATCATGCTGCTGACGCAGGCAACGCAGGCAACGCCACTGGCACGCTGCA	
12	GAAGAATTCATGGCTTCGGATTCGGGGAACCAGGGG	Cloning hCCS into pJG4.5
13	GAACTCGAGTCAAAGGTGGGCAGGGGGCTGCGC	
14	GGTGCAGATGACCTCTCAGAGCTGTGTGG	Creating hCCS C22S mutation
15	CCACACAGCTCTGAGAGGTCATCTGCACC	
16	CCTGTCAGAGCTCTGTGGACGCGGTGC	Creating hCCS C25S mutation
17	GCACCGCGTCCACAGAGCTCTGACAGG	
18	GCAGATGACCTCTCAGAGCTCTGTGGACGCG	Creating hCCS C22S,C25S mutation
19	CGCGTCCACAGAGCTCTGAGAGGTCATCTGC	
20	GGCACGGGGGCGCAGGCGGTACTCAAGGGC	Creating hCCS R71A mutation
21	GCCCTTGAGTACCGCCTGCGCCCCCGTGCC	
22	CCTTGAGTACCGCCTGTTCCCCCGTGCCTTCC	Creating hCCS R71E mutation
23	GGAAGGCACGGGGGAACAGGCGGTACTCAAGG	
24	GGAAGGCACGGGGAAACAGGCGGTACTCAAGG	Creating hCCS R71K mutation
25	CCTTGAGTACCGCCTGTTTCCCCGTGCCTTCC	
26	CCCAAGCAGATCTCCTCTTGCGATGGCC	Creating hCCS C244S mutation
27	GGCCATCGCAAGAGGAGATCTGCTTGGG	
28	GGTGAGGCCATCGGAAGAGGAGATCTGCTTGG	Creating hCCS C244S,C246S mutation
29	CCAAGCAGATCTCCTCTTCCGATGGCCTCACC	
30	AATTCTGCCAATGGCGCTGCCTCCGCTGCCTGCGCCAGCAGCATGATGACTTTGCTGATGACATCTCCCTGCTGAAGTGAC	hBACE1 CTD for p423lexAkan
31	TCGAGTCACTTCAGCAGGGAGATGTCATCAGCAAAGTCATCATGCTGCTGGCGCAGGCAGCGGAGGCAGCGCCATTGGCAG	
32	AATTCTCCCAATGGCGCTGCCTCCGCTGCCTGCGCCAGCAGCATGATGACTTTGCTGATGACATCTCCCTGCTGAAGTGAC	hBACE1 CTD C478S for p423lexAkan
33	TCGAGTCACTTCAGCAGGGAGATGTCATCAGCAAAGTCATCATGCTGCTGGCGCAGGCAGCGGAGGCAGCGCCATTGGGAG	

34	AATTCTGCCAAATGCGCTGCCTCCGCTGCCTGCGCCAGC AGCATGATGACTTTGCTGATGACATCTCCCTGCTGAAGTG AC	hBACE1 CTD W480M for p423lexAkan
35	TCGAGTCACTTCAGCAGGGAGATGTCATCAGCAAAGTCA TCATGCTGCTGGCGCAGGCAGCGGAGGCAGCGCATTTG GCA	
36	AATTCTGCCAATGGGCTTGCCTCCGCTGCCTGCGCCAGC AGCATGATGACTTTGCTGATGACATCTCCCTGCTGAAGTG AC	hBACE1 CTD R481A for p423lexAkan
37	TCGAGTCACTTCAGCAGGGAGATGTCATCAGCAAAGTCA TCATGCTGCTGGCGCAGGCAGCGGAGGCAAGCCCATTG GCAG	
38	AATTCTGCCAATGGGAATGCCTCCGCTGCCTGCGCCAGC AGCATGATGACTTTGCTGATGACATCTCCCTGCTGAAGTG AC	hBACE1 CTD R481E for p423lexAkan
39	TCGAGTCACTTCAGCAGGGAGATGTCATCAGCAAAGTCA TCATGCTGCTGGCGCAGGCAGCGGAGGCATTCCCATTG GCAG	
40	AATTCTGCCAATGGAAATGCCTCCGCTGCCTGCGCCAGC AGCATGATGACTTTGCTGATGACATCTCCCTGCTGAAGTG AC	hBACE1 CTD R481K for p423lexAkan
41	TCGAGTCACTTCAGCAGGGAGATGTCATCAGCAAAGTCA TCATGCTGCTGGCGCAGGCAGCGGAGGCATTTCCATTGG CAG	
42	AATTCTGCCAATGGCGCTCCCTCCGCTGCCTGCGCCAGC AGCATGATGACTTTGCTGATGACATCTCCCTGCTGAAGTG AC	hBACE1 CTD C482S for p423lexAkan
43	TCGAGTCACTTCAGCAGGGAGATGTCATCAGCAAAGTCA TCATGCTGCTGGCGCAGGCAGCGGAGGGAGCGCCATTG GCAG	
44	AATTCTGCCAATGGCGCTGCCTCGCTTGCCTGCGCCAGC AGCATGATGACTTTGCTGATGACATCTCCCTGCTGAAGTG AC	hBACE1 CTD R484A for p423lexAkan
45	TCGAGTCACTTCAGCAGGGAGATGTCATCAGCAAAGTCA TCATGCTGCTGGCGCAGGCAAGCGAGGCAGCGCCATTG GCAG	
46	AATTCTGCCAATGGCGCTGCCTCCGCTCCCTGCGCCAGC AGCATGATGACTTTGCTGATGACATCTCCCTGCTGAAGTG AC	hBACE1 CTD C485S for p423lexAkan
47	TCGAGTCACTTCAGCAGGGAGATGTCATCAGCAAAGTCA TCATGCTGCTGGCGCAGGGAGCGGAGGCAGCGCCATTG GCAG	
48	AATTCTGCCAATGGCGCTGCCTCCGCTGCCTGGCTCAGC AGCATGATGACTTTGCTGATGACATCTCCCTGCTGAAGTG AC	hBACE1 CTD R487A for p423lexAkan
49	TCGAGTCACTTCAGCAGGGAGATGTCATCAGCAAAGTCA TCATGCTGCTGAGCCAGGCAGCGGAGGCAGCGCCATTG GCAG	
50	AATTCTGCCAATGGCGCTGCCTCCGCTGCCTGCGCCAGC AGCATGCTGCTTTTGCTGATGACATCTCCCTGCTGAAGTG AC	hBACE1 CTD D491A,D492A for p423lexAkan
51	TCGAGTCACTTCAGCAGGGAGATGTCATCAGCAAAAGCA GCATGCTGCTGGCGCAGGCAGCGGAGGCAGCGCCATTG GCAG	
52	CCGCGGGATTAAGCGAATTCGCGACGAAGGCCGTGTG	Cloning hSOD1 into p423lexAkan
53	GCCGCACTAGTGATTGAACTCGAGTTATTGGGCGATCCC	
54	GCGAAACTGTGGTAGAGACGCCATCATAAGAGG	Creating Ccs1 K66R mutation
55	CCTCTTATGATGGCGTCTCTACCACAGTTTCGC	
56	GGAAGAGGGTAAAAATTCATTGTTCGG	PCR of *KAN*^{R} (from BY4741-*ccs1Δ*)
57	ATTGCCACATGCGTATGTACATGTCCG	

58	GTTCCTGCGCCGGTTGCATTCGATTCC	Verifying *ccs1Δ* genomic deletion
59	GATGGTGTCAAGAACCGGCTTGGCTGC	
60	GAAGAATTCATGACTATTCAACTAACTGTACC	Cloning ScAtx1 into pJG4.5
61	GAACTCGAGTCACTCAACTTCATGGCCCGCCG	
62	CTGTACCCACCATTAAATGTGAAGCCTGTGC	Creating ScAtx1 A11K mutation
63	GCACAGGCTTCACATTTAATGGTGGGTACAG	
64	CTGTACCCACCATTAGATGTGAAGCCTGTGC	Creating ScAtx1 A11R mutation
65	GCACAGGCTTCACATCTAATGGTGGGTACAG	
66	CCACCATTGCCTGTGCTGCCTGTGCCGAAGC	Creating ScAtx1 E13A mutation
67	GCTTCGGCACAGGCAGCACAGGCAATGGTGG	
68	CCACCATTGCCTGTCAAGCCTGTGCCGAAGC	Creating ScAtx1 E13Q mutation
69	GCTTCGGCACAGGCTTGACAGGCAATGGTGG	
70	CGAAGCTGTGACCGATGCCGTGCAAAATGAGG	Creating ScAtx1 K21D mutation
71	CCTCATTTTGCACGGCATCGGTCACAGCTTCG	
72	CCAAAGCCGTGCAAAGAGAGGATGCCCAAGC	Creating ScAtx1 N25R mutation
73	GCTTGGGCATCCTCTCTTTGCACGGCTTTGG	
74	CGAACGGCGATCGCCGCTGCGGGCCATGAAGTTG	Creating ScAtx1 S58A mutation
75	CAACTTCATGGCCCGCAGCGGCGATCGCCGTTCG	
76	CTCACTCAACTTCAGCGCCCGCCGAGGCG	Creating ScAtx1 H61A mutation
77	CGCCTCGGCGGGCGCTGAAGTTGAGTGAG	
78	GCCTCGGCGGGCGAAGAAGTTGAGTG	Creating ScAtx1 H61E mutation
79	CACTCAACTTCTTCGCCCGCCGAGGC	
80	GCCTCGGCGGGCTTTGAAGTTGAGTG	Creating ScAtx1 H61F mutation
81	CACTCAACTTCAAAGCCCGCCGAGGC	
82	GCCTCGGCGGGCAAAGAAGTTGAGTG	Creating ScAtx1 H61K mutation
83	CACTCAACTTCTTTGCCCGCCGAGGC	
84	CGCCTCGGCGGGCTATGAAGTTGAGTGAG	Creating ScAtx1 H61Y mutation
85	CTCACTCAACTTCATAGCCCGCCGAGGCG	
86	GAAGAATTCATGGCCCAAACCATCAATCTGC	Cloning $PacS_N$ into p423lexAkan
87	GAACTCGAGTCATTTAAGCACCCTAGCGTGG	
88	GCAACTAGAGGGAATGGCTTGTGCGGCCTGTGC	Creating $PacS_N$ R13A mutation
89	GCACAGGCCGCACAAGCCATTCCCTCTAGTTGC	
90	GGAGCGAGCGGGTCACCACGCTAGGGTGC	Creating $PacS_N$ Y65H mutation
91	GCACCCTAGCGTGGTGACCCGCTCGCTCC	
92	GAAGAATTCATGGTTCAACTTTCCCCGACCCC	Cloning $CtaA_N$ into p423lexAkan
93	GAACTCGAGTCAACGAATCTGACTGGGAAATCCC	
94	CGTGGGGGGCATGGCTTGTGCCGGTTGTGTGG	Creating $CtaA_N$ K34A mutation
95	CCACACAACCGGCACAAGCCATGCCCCCCACG	
96	GAGTCAGCGGGGACATCCCAGTCAGATTCG	Creating $CtaA_N$ F87H mutation
97	CGAATCTGACTGGGATGTCCCCGCTGACTC	
98	GAGTCAGCGGGGATATCCCAGTCAGATTCG	Creating $CtaA_N$ F87Y mutation
99	CGAATCTGACTGGGATATCCCCGCTGACTC	
100[a]	GGGCAAAGGCTTCTTTGAATTCAGCAATTTGTTCTTCGGT GGTGCC	*CMD1* primer for S1 nuclease assay
101[a]	CCCCGTTGGGCAGCTACATGATTTTTGGCATTGTTCATTA TTTTTGCAGCTACCACATTGATGCCA	*CUP1* primer for S1 nuclease assay
102[a]	CGCCATACTCGATGCTACTGTCTTGGATGCACTAGACATG GCGTCCATATTCATGCTGTTTGC	*CTR1* primer for S1 nuclease assay

[a] These oligomers were received as a kind gift from Dr. Julian Rutherford, University of Newcastle, UK.

2.3.3.5 DNA Ligation

50 ng of the desired vector was digested with the appropriate restriction endonucleases and electrophoresed on an agarose gel. The desired DNA band was purified from the gel as discussed in section 2.3.3.4. The purified digested vector was subsequently ligated with the insert DNA using the T4 DNA ligase (Fermentas, UK) according to the manufacturer's instructions. An exceptional strategy was used for the ligation of the DNA oligomers coding for hBACE1 CTD into the desired vector. The double-stranded hBACE1 CTD DNA oligomers comprised two individual complementary single-stranded DNA oligomers coding for hBACE1 CTD (Table 5). The single-stranded DNA oligomers underwent an 'annealing' step prior to ligation into the desired vector, involving the incubation of a mixture containing 0.75 % (v/v) of 2 ng/µL of each single-stranded DNA oligomer, 0.125 % (v/v) TE buffer (10 mM Tris-HCl pH 8.0, 1 mM EDTA pH 8.0) and 0.125 % of 25 mM $MgCl_2$, at 94 ^{o}C for 90 secs in a PCR machine, followed by 15 mins incubation at room temperature. Successful ligation was verified by the digestion of the ligated vector with the appropriate restriction endonucleases followed by agarose gel electrophoresis and by obtaining the DNA sequence of the ligated vector using the DNA sequencing silver service, Beckman-Coulter Genomics, UK.

2.3.3.6 Polymerase chain reaction

Polymerase chain reactions (PCR) were prepared in 0.5 mL eppendorf tubes containing 2 ng template DNA, 0.4 mM deoxyribonucleotide triphosphates (dNTPs) mix (Promega, UK), 50 pmol/µL of each primer, 1 µL of 2.5 U/µL *Pfu* polymerase (Stratagene, UK), 5 µL 10x *Pfu* buffer and sterile dH_2O. The PCR conditions were modified according to the manufacturer's instructions.

2.3.3.7 Site-directed mutagenesis

Mutations in DNA were created by preparing a 50 µL reaction mixture consisting of 15-20 ng template DNA, 125 ng of each DNA oligomer, 0.5 mM dNTPs mix, 5 µL 10x *Pfu* polymerase buffer, 1 µL of 2.5U/µL *Pfu* polymerase and sterile dH_2O. The reaction mixture was incubated in a PCR machine according to the conditions specified in the protocol for Stratagene's QuikChange® Site-directed mutagenesis kit (Stratagene, UK).

2.4 Bacterial 2-Hybrid

2.4.1 BacterioMatch® Two-Hybrid System (Stratagene, UK)

An overview of the principles underlying the BacterioMatch® two-hybrid system is provided in Figure 18. Some of the vectors used in this system (Table 4) were received as a kind gift from Professor Nigel Robinson (Newcastle University, UK).

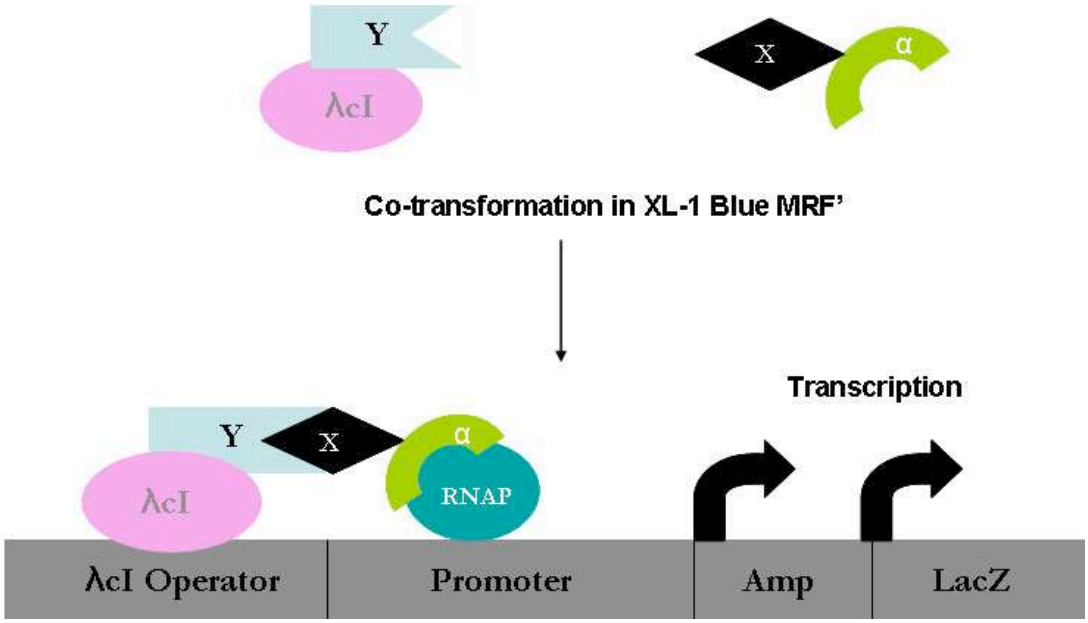

Figure 18: Overview of the BacterioMatch® Bacterial Two-Hybrid System. Ligation of any genes – *X* and *Y* into the multi-cloning site of the vectors pTRG and pBT results in the expression of the fusion proteins α-X (α domain of RNA polymerase (RNAP)-X) and λcI-Y respectively, when co-expressed in the reporter strain XL-1 Blue MRF'. When λcI binds to the λcI operator, an interaction between X and Y promotes the binding of α to RNAP resulting in the stable recruitment of RNAP to the promoter leading to the transcription of the reporter genes – *amp*^{r} and *lacZ*.

2.4.1.1 Cloning & Co-transformation

All constructs were cloned into the BacteroMatch® vectors – pTRG and pBT. The constructs created in this study were cloned into the *BamHI* and *EcoRI* sites of pTRG and into the *NotI* and *EcoRI* sites of pBT. 10 ng of each vector was co-transformed into the XL-Blue MRF' cells based on the procedure discussed in section 2.3.2.

2.4.1.2 Spreading co-transformed cells onto LB-agar plates

XL-1 Blue MRF' cells co-transformed with pTRG_X and pBT_Y (where X and Y represent the presence of a fusion gene) were plated onto LB-agar plates containing tetracycline, chloramphenicol and kanamycin (LB-TCK) and incubated at 30 ^{o}C for 3 days.

2.4.1.3 β-galactosidase Assay

The protocol used for β-galactosidase assay was based on the method detailed in Bowness (2004). A colony of XL-1 Blue MRF' cells co-transformed with pTRG_X and pBT_Y was grown in 5 mL LB-TCK medium at 30 ^{o}C overnight with shaking at 250 rpm. The following day, 0.5 mL of exponentially growing cells (OD_{595} ~0.15-0.3) were pelleted by centrifugation at 16000 x *g* for 1 min. The pellet was resuspended in 0.5 mL ice-cold Z-buffer (60 mM $K_2HPO_4.3H_2O$, 40 mM KH_2PO_4, 10 mM KCl, 1 mM $MgSO_4.7H_2O$) with 0.3 % (v/v) β-mercaptoethanol. 50 µL of 1 % (w/v) SDS and 100 µL chloroform was added to the resuspended cells and vortexed at maximum speed for 30 secs to ensure lysis. The tubes were incubated at room temperature for ~20 mins to allow for the chloroform to settle. 176 µL of the aqueous layer was added to a 96-well microtitre plate containing 35 µL of 4 mg/mL (in 0.1 M potassium phosphate buffer, pH 7.0) *o*-nitrophenyl-β-D-galactopyranoside (ONPG) and incubated at room temperature for ~70 mins or until a yellow colour developed. The reaction was stopped by the addition of 88 µL of 1 M sodium carbonate. The time between the addition of cell lysate and sodium carbonate was recorded as the reaction time (t). As a control (t_0) a well containing 35 µL ONPG and 176 µL dH_2O was also incubated and stopped with all the other reaction samples by the addition of 88 µL of 1 M sodium carbonate. The OD_{414} of the reaction samples was measured using a microtitre plate reader, and the β-galactosidase activity was calculated using Equation 5 (Bowness, 2004).

$$\text{nmoles ONP min}^{-1}\text{ mg}^{-1}\text{ protein} = 300\,(OD_{414}(t) - OD_{414}(t_0))/\,1.83\,(t \times V \times OD_{595}) \quad [5]$$

where, $OD_{414}(t)$ = absorbance measured at 414 nm in the sample well, $OD_{414}(t_0)$ = absorbance measured at 414 nm in the control well, OD_{595} = absorbance measured at 595 nm of initial cell culture (cell density), t = reaction time (mins), V = volume of cells used (mL); since, OD_{414} of 300 nmoles ONP solution = 1, ~1 mg/mL of total

protein is obtained from OD_{595} of cell culture = 1/1.83 (Bowness, 2004).

2.4.2 Bacterial Adenylate Cyclase Two-Hybrid System (EuroMedex, France)

An overview of the principles underlying the bacterial adenylate cyclase two-hybrid (BACTH) system is provided in Figure 19. The BACTH system strain, BTH101 and the vectors (Table 2 and Table 4) were received as a kind gift from Dr. Richard Daniel (Newcastle University, UK).

2.4.2.1 Cloning & Co-transformation

All constructs were cloned into the BACTH vectors – pKT25 and pUT18C (Table 4), and co-transformed into the BTH101 cells, according to the manufacturer's instructions.

2.4.2.2 Spreading co-transformed cells onto Minimal Medium-agar plates

BTH101 cells co-transformed with pKT25_X and pUT18C_Y (where X and Y represent the presence of a fusion gene) were washed twice with minimal medium (MM) before spreading them onto MM-agar plates. MM-agar plates were prepared by autoclaving a solution containing 3.6 µM $FeCl_3.6H_2O$, 40 µM $MgCl_2.6H_2O$, 100 µM $MnCl_2.4H_2O$, 10 mM NH_4Cl, 0.7 mM Na_2SO_4, 0.5 mM KH_2PO_4, 1.2 mM NH_4NO_3 and 1 % (w/v) agar at 121 ^oC for 30 mins followed by the addition of 0.8 % (w/v) filter-sterile glucose, 0.4 % (w/v) casamino acids, 0.004 % (w/v) 5-bromo-4-chloro-3-indolyl-β-D-galactopyranoside (X-Gal), 25 µg/mL kanamycin, 100 µg/mL ampicillin, 3 µM thiamine and 0.1 mM isopropyl-β-D-1-thiogalactopyranoside (IPTG) after the medium had cooled to ~40 ^oC. The plates were incubated at 30 ^oC for 3 days.

2.4.2.3 β-galactosidase Assay

A colony of BTH101 cells co-transformed with pKT25_X and pUT18C_Y was grown in 5 mL LB-medium with the appropriate amino acids at 30 ^oC overnight with shaking at 250 rpm. The following day, 0.5 mL of exponentially growing cells (OD_{595} ~0.15-0.3) was pelleted and assayed for β-galactosidase activity as detailed in section 2.4.1.3.

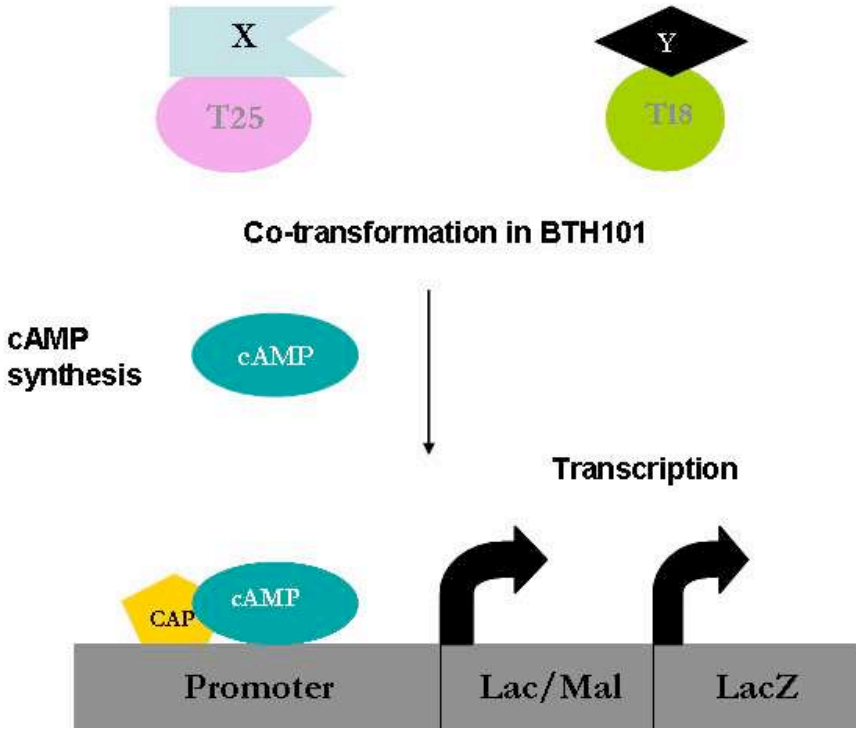

Figure 19: Overview of the BACTH system. Ligation of any genes – *X* and *Y* into the multi-cloning site of the vectors pKT25 and pUT18C results in the expression of the fusion proteins T25-X and T18-Y when co-expressed in the reporter strain BTH101. Interaction between X and Y brings T25 and T18, components of the catalytic domain of adenylate cyclase, into close proximity. Functional complementation of T25 and T18 results in the synthesis of cyclic AMP (cAMP) by adenylate cyclase which forms a complex with the catabolite activator protein, CAP and binds to the promoter resulting in the transcription of the reporter genes for *lac/mal* allowing for growth on medium lacking lactose/maltose and *lacZ*.

2.5 Manipulation of *S. cerevisiae*

2.5.1 Preparation of competent *S. cerevisiae* cells

A few isolated colonies of either untransformed *S. cerevisiae* cells were inoculated in 5 mL YPD or a few isolated colonies of transformed *S. cerevisiae* cells were inoculated in 5 mL synthetic-dextrose (SD)-glucose medium (0.17 % (w/v) yeast nitrogen base, 0.5 % (w/v) ammonium sulphate, 2 % (w/v) glucose and the appropriate amino acids) overnight and incubated at 30 ^{o}C with shaking at 250 rpm in an orbital shaker. The following day the cells were diluted 1:50 in fresh 50 mL YPD or SD medium respectively, and incubated at 30 ^{o}C with shaking at 300 rpm until absorbance at 600 nm was ~0.8. Cells were pelleted by centrifugation at 1000 x *g* at 4 ^{o}C. The supernatant was discarded and the pellet was washed three times with 1mL sterile ddH_2O with centrifugation at 3000 x *g*. The pellet was resuspended in 300 µL of filter-sterilised 100 mM lithium acetate and stored at 4 ^{o}C (Ausubel *et al.*, 2002).

2.5.2 DNA transformation in *S. cerevisiae*

50 µL of competent *S. cerevisiae* cells were added to a 1.5 mL eppendorf tube containing 240 µL of filter-sterilised 50 % (w/v) PEG 4000 and 10 µL of 10 mg/mL salmon-sperm DNA followed by the addition of ~800 ng of plasmid DNA and mixed by gently vortexing the tube. 32 µL of filter-sterilised 1 M lithium acetate was added to the tube and incubated at 30 ^{o}C for 20 mins followed by heat-shock at 42 ^{o}C for 15 mins. The cells were pelleted and washed with 1 mL sterile ddH_2O by centrifugation at 1000 x *g*. The pellet was resuspended in 300 µL of sterile ddH_2O and stored at 4 ^{o}C (Ausubel *et al.*, 2002). 150 µL of the resuspended pellet was spread on YPD- or SD-agar plates, as appropriate.

2.5.3 Isolation of genomic DNA from *S. cerevisiae*

A few isolated colonies of the strain were grown in 10 mL YPD medium overnight at 30 ^{o}C with shaking at 250 rpm. 5 mL of the cell culture was centrifuged at 1200 x *g* and the pellet was washed with sterile ddH_2O. The cells were briefly vortexed at 1800 rpm to remove any residual medium. The pellet was resuspended in 200 µL breaking buffer (1 % (w/v) SDS, 2 % (v/v) Triton X-100, 100 mM NaCl, 10 mM Tris-HCl pH 8.0, 1 mM EDTA pH 8.0) followed by the addition of 0.3 g glass beads and 200 µL of phenol/chloroform/isoamyl alcohol mixture and vortexed at 2400 rpm for 3 mins. 200 µL of TE buffer was added to the lysed cells and vortexed briefly. The cell lysate (aqueous layer) was separated from the cell debris by centrifugation at 16000 x *g* for 5 mins and transferred to a 1.5 mL tube. 1 mL of 100 % ethanol was added to the cell lysate and mixed by inversion. The tube was centrifuged at 16000 x *g* for 3 mins and the pellet was resuspended in 0.4 mL TE buffer. The lysate was incubated with 0.075

% (v/v) TE buffer containing 0.7 µg/µL RNase A at 37 °C for 15 mins, followed by the addition of 0.025 % (v/v) of 4 M ammonium acetate and 1 mL of 100 % ethanol. The genomic DNA was pelleted by centrifugation at 16000 x *g* for 3 mins. The supernatant was discarded and any remaining ethanol was removed by drying the pellet at 60 °C for 10 mins. The genomic DNA pellet was resuspended in 100 µL TE buffer and stored at -20 °C (Ausubel *et al.*, 2002).

2.5.4 Isolation of RNA from *S. cerevisiae*

S. cerevisiae cells were grown in the appropriate medium as required and pelleted by centrifugation at 1000 x *g* at 4 °C. The pellet was resuspended in 400 µL TES buffer (10 mM Tris-HCl pH 7.5, 10 mM EDTA, 0.5 % (w/v) SDS) followed by the addition of 400 µL acid phenol. The mixture was vortexed briefly at 2400 rpm and incubated at 65 °C for 60 mins with intermittent vortexing. The mixture was cooled to 4 °C and centrifuged at 16000 x *g* for 5 mins at 4 °C. The aqueous layer was isolated in a 1.5 mL tube and equivalent volume of acid-phenol was added to it followed by vortexing at 2400 rpm for ~30 secs and centrifugation at 16000 x *g* for 5 mins at 4 °C. The aqueous layer was isolated in a 1.5 mL tube and the RNA was precipitated by the addition of 0.07 % (v/v) of 3 M sodium acetate pH 5.3 and 1 mL of ice-cold 100 % ethanol by incubation at -20 °C for ~60 mins. RNA was pelleted by centrifugation at 16000 x *g* for 5 mins at 4 °C. The pellet was washed with ice-cold 70 % ethanol and centrifuged at 16000 x *g* for 5 mins at 4 °C. The RNA pellet was resuspended in 100 µL sterile ddH_2O and stored at -20 °C (Ausubel *et al.*, 2002).

2.5.5 Whole cell protein extraction

S. cerevisiae cells were grown in the appropriate medium and pelleted by centrifugation at 1000 x *g* at 4 °C. The pellet was resuspended in 500 µL ice-cold resuspension buffer containing 20 mM Tris-HCl pH 8.0, 50 mM ammonium acetate, 2 mM EDTA and added to a 1.5 mL tube containing ~0.3 g 0.5 mM glass beads and 500 µL of ice-cold 20 % trichloroacetic acid (TCA). The cells were lysed by five cycles of ribolysation for 30 secs followed by 1 min incubation on ice. The liquid phase was isolated into a fresh 1.5 mL tube and stored on ice. 500 µL of a mixture containing 50 % (v/v) resuspension buffer and 50 % (v/v) 20 % TCA was added to the tube containing the glass beads, and was ribolysed for an additional 30 secs followed by 1 min incubation on ice. The aqueous phase was isolated and added to the previously extracted supernatant and centrifuged at 16000 x *g* for 10 mins at 4 °C. The pellet was resuspended in 300 µL loading buffer (120 mM Tris base 3.5 % (w/v) SDS, 14 % (v/v) glycerol, 80 mM EDTA, 0.02 % (w/v) bromophenol blue and 12 % (v/v) 1M DTT). The cell lysate was incubated at 100 °C for 10 mins followed by centrifugation at 16000 x *g* for 10 mins. The supernatant was isolated and stored at -20 °C.

2.6 Yeast two-hybrid

An overview of the principles underlying the yeast two-hybrid system is provided in Figure 20. The yeast two-hybrid strain EGY48, the vectors pJG4.5 and p423lexAkan, and some of the constructs used in this study (Table 4) were generously provided by Dr. Katie Freeman, GlaxoSmithKline (GSK), UK.

2.6.1 Transformation of EGY48 with reporter plasmid pMW112

Competent EGY48 cells were prepared and transformed with the reporter plasmid pMW112 containing the reporter genes for leucine (leu) and β-galactosidase, as detailed in sections 2.5.1 and 2.5.2 respectively.

2.6.2 Cloning into Yeast two-hybrid vectors

All genes were cloned into the unique *EcoRI* and *XhoI* sites of the pJG4.5 and p423lexAkan vectors, according to the standard procedures discussed above.

2.6.3 Co-transformation in EGY48

EGY48 cells transformed with pMW112 vector (EGY48_pMW112) were further co-transformed with the yeast two-hybrid vectors pJG4.5_X and p423lexAkan_Y (where X and Y represent the presence of a fusion gene) as discussed in section 2.5.2.

2.6.4 β-galactosidase assays

A few isolated colonies containing EGY48_pMW112 cells co-transformed with pJG4.5_X and p423lexAkan_Y vectors were inoculated in 5mL SD-gluclose-leu medium (0.84 % (v/v) 7.2 mg/mL leu) and incubated overnight at 30 ^{o}C with shaking at 250 rpm. The following day the cells were diluted into fresh 5 mL SD-galactose (gal; 2 %, w/v)-raffinose (raff; 1 %, w/v)-leu medium such that the initial absorbance at 600 nm was ~0.4, and grown at 30 ^{o}C with shaking at 300 rpm for 3-5 hrs until absorbance at 600 nm was ~0.5-0.8 (exact OD_{600} was recorded). 1.5 mL of the cells were pelleted by centrifugation at 16000 x *g* and washed twice with 1.5 mL ice-cold Z-buffer (section 2.4.1.3). The pelleted cells were finally resuspended in 0.5 mL ice-cold Z-buffer. 100µL of the resuspended cells were lysed by three freeze-thaw cycles constituting flash-freezing in liquid nitrogen followed by thawing at 37 ^{o}C for 2 mins. 0.7 mL of ice-cold Z-buffer containing 0.3 % (v/v) β-mercaptoethanol was added to the lysed cells followed by 0.16 mL of ONPG (section 2.4.1.3). The tubes were incubated inside a 30 ^{o}C incubator (dark environment) for ~60 mins or until yellow colour developed. The reaction was stopped by the addition of 0.4 mL of 1 M sodium carbonate. The time between the addition of ONPG and sodium carbonate was recorded as the reaction time (t). The cell debris was pelleted by centrifugation at 16000 x *g* and the OD_{420} of

the supernatant was recorded. The β-galactosidase activity of the reaction mixture was measured using Equation 6 adapted from Miller (1972).

$$\beta\text{-galactosidase Activity (Miller Units)} = 1000 \times OD_{420} / (t \times V \times OD_{600}) \quad [6]$$

where, t = reaction time (mins), V = volume of cells (mL) x concentration factor (3), OD_{600} = absorbance measured at 600 nm of initial cell culture (cell density), OD_{420} = absorbance at 420 nm.

2.6.5 Studying the role of copper using the yeast two-hybrid system

The effect of Cu concentration on interactions was studied by growing the desired EGY48_pMW112 with pJG4.5_X and p423lexAkan_Y co-transformants in SD growth medium containing 0.17 % (w/v) Cu-depleted yeast nitrogen base without amino acids and ammonium sulfate, 0.5 % (w/v) ammonium sulphate, 2 % (w/v) glucose, 0.84 % (v/v) 7.2 mg/mL leu and other amino acids, as appropriate with varying amounts of filter-sterilised copper sulfate ($CuSO_4$) and/or filter-sterilised bathocuproinedisulfonic acid disodium salt (BCS) solution, as required and assayed for β-galactosidase activity according to 2.6.4.

2.6.5.1 Growth Curves

EGY48_pMW112 cells $\pm$ pJG4.5 and p423lexAkan were grown in SD-Gal-Raff-leu medium with and without $CuSO_4$ and BCS. The OD_{600} was recorded at various time intervals and the data points were plotted on a line graph.

2.6.5.2 Determination of intracellular copper content using inductively coupled plasma - mass spectrometry

The Cu content of the EGY48_pMW112 cells $\pm$ pJG4.5 and p423lexAkan was determined by measuring the Cu concentration of the whole cell lysate using inductively coupled plasma-mass spectrometry (ICP-MS). Exponentially growing cells (OD_{600} 0.5-0.8), such that the final OD at 600 nm was ~30 in SD-gal-raff-leu medium with and without $CuSO_4$ and BCS, were harvested by centrifugation at 1000 x *g* at 4 ^{o}C. The pellet was washed with sterile ddH_2O and flash-frozen in liquid nitrogen. After thawing the pellet at room temperature, the cells were lysed by the addition of 1 mL of 65 % (v/v) Suprapur® HNO_3 (Merck, UK) and incubated at 30 ^{o}C for 3 nights. 1 mL of ddH_2O was added to the lysed cells and the cell debris was pelleted by centrifugation at 1000 x *g* for 10 mins at 4 ^{o}C. Samples for ICP-MS were prepared by adding 0.3 mL of the supernatant to 1.2 mL of ddH_2O. Cu standard solutions in the range of 0-400 µg/L were prepared by the dilution of stock Cu solution (987 µg/mL in 1.2 % HNO_3; Sigma, UK) in 3 % (v/v) Suprapur® HNO_3.

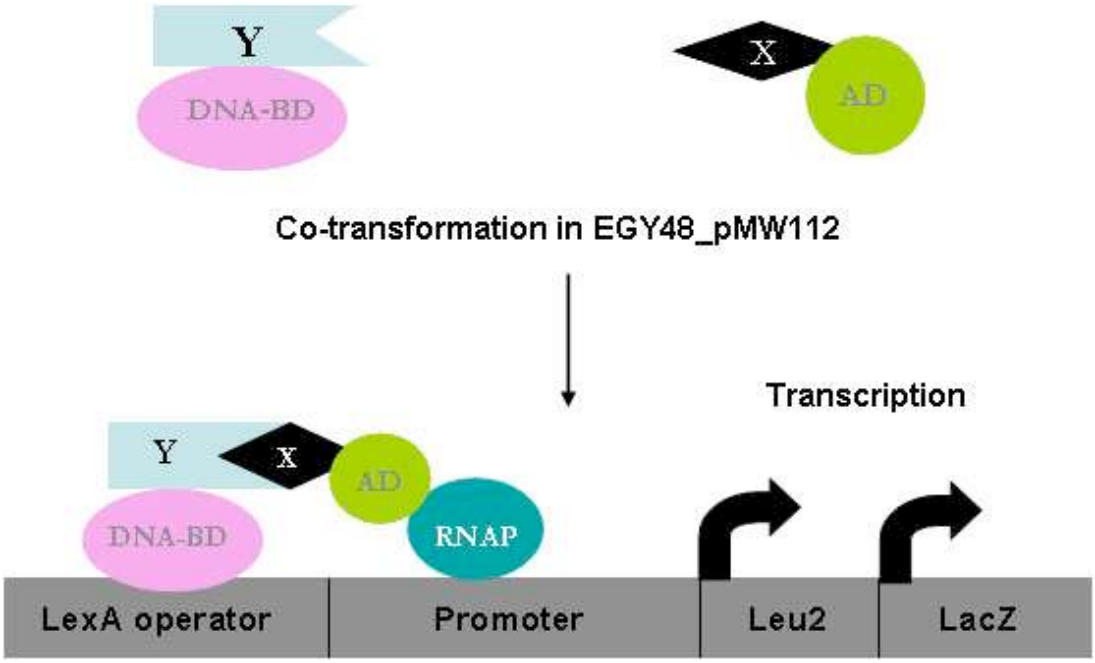

Figure 20: Overview of the Yeast two-hybrid system. Ligation of any genes X and Y into the multi-cloning site of the vectors pJG4.5 and p423lexAkan results in the expression of the fusion proteins AD_X (Activation Domain of B42_X) and DNA-BD_Y (DNA binding domain of LexA_Y) respectively when co-expressed in the reporter strain EGY48 transformed with the reporter vector pMW112. When DNA-BD binds to the LexA operator, an interaction between X and Y can stabilize the binding of RNAP to the promoter via its interaction with AD resulting in the transcription of the reporter genes – *LEU2* and *LACZ*.

All samples and standards were analysed by the peak jump method, averaged over 100 reads per sample in triplicate using an auto-tuned Thermo X-series ICP-MS. The copper content was defined as the amount of copper atoms per cell, calculated on the basis that OD_{600} of 1 is equivalent to ~3 x 10^7 cells/mL (Treco and Lundblad, 1993).

2.6.5.3 Studying the expression of nuclear proteins by S1 nuclease assays

The effect of copper concentration on the expression of nuclear proteins was studied by monitoring the expression levels of the *CTR1* and *CUP1* genes in EGY48_pMW112 with pJG4.5_X and p423lexAkan_Y co-transformants. RNA was extracted from a pellet constituting exponentially growing cells (OD_{600} 0.5-0.8), such that the final absorbance at 600 nm was ~40 in SD-gal-raff-leu medium with and without $CuSO_4$ and BCS as discussed in section 2.5.4.

2.6.5.3.1 Labeling S1 probes with ATP-[γ- ^{32}P]

The S1 probes were prepared by labeling the *CTR1* and *CUP1* DNA oligomers (Table 5) with ATP-[γ-^{32}P] (6000 Ci/mmol; Perkin-Elmer, UK). This involved the incubation of a 25 µL reaction mixture containing 20 % (v/v) of 1 pmol/µL of *CTR1* (or *CUP1*) oligomer, 20 % (v/v) of 1 pmol/µL of a *calmodulin*-binding DNA oligomer (*CMD1*) with 10 % (v/v) 10x T4 polynucleotide kinase (PNK) buffer (Promega, UK), 0.04 % (v/v) T4 PNK enzyme (Promega, UK) and 0.04 % (v/v) ATP-[γ^{-32}P] at 37 ^{o}C for 30 mins. The reaction was stopped by the addition of 50 % (v/v) TE buffer. The labeled probe was isolated and purified using the Illustra^{TM} ProbeQuant G-50 Micro Columns Radiolabeled Probe Purification kit (GE Healthcare, UK) according to the manufacturer's instructions.

2.6.5.3.2 Hybridization and purification of labeled S1 probes with RNA

A 50 µL reaction mixture containing 0.02 % (v/v) of the labeled S1 probe, 0.8 % (v/v) of 700 ng/µL RNA (from the desired co-transformants), 0.15 % (v/v) of hybridization buffer (257 mM 4-(2-hydroxyethyl)-1-piperazineethanesulfonic acid sodium salt (HEPES) pH 7.0, 6.8 mM EDTA pH 7.5, 2 mM NaCl and 0.7 % (v/v) Triton X-100) was incubated at 55 ^{o}C overnight. The following day, samples were cooled to room temperature and incubated with 0.45 mL of S1 reaction mixture containing (0.0001 % (v/v) S1 nuclease (Promega, UK), 333 mM NaCl, 2.2 mM $ZnCl_2$, 66 mM sodium acetate pH 4.6) at 37 ^{o}C for 30 mins. 3 µL of 10 µg/mL tRNA was added to the side of the tubes, vortexed and centrifuged at 16000 x *g* for 30 secs. 0.9 mL of ice-cold 100 % ethanol was added to the tubes and incubated at -20 ^{o}C for 90 mins to precipitate the DNA-RNA hybrid. The hybrid was pelleted by centrifuging the tubes at 16000 x *g* for 10 mins and washed with 70 % ethanol. The supernatant was discarded and any remaining ethanol was removed by incubating the pellet at 65 ^{o}C for 20 mins. The pellet was resuspended in 10 µL S1 loading buffer containing 90 % (v/v) formamide, 0.5x TBE buffer (44.5 mM

Tris-base, 44.5 mM Boric acid, 2 mM EDTA pH 8.0) and 0.5 µL of 6x loading dye (0.25 % (w/v) bromophenol blue, 30 % (v/v) glycerol) and incubated at 65 ^{o}C for 10 mins. The tubes were centrifuged at 16000 x *g* for 15 secs and stored on ice. Subsequently the samples were electrophoresed on a polyacrylamide-urea based gel.

2.6.5.3.3 Analysis of the S1 samples by polyacrylamide-urea gel electrophoresis

The polyacrylamide-urea gel constituted 50 % (w/v) urea, 20 % (v/v) of 40 % acrylamide/bis-acrylamide solution (19:1) in 1x TBE buffer polymerized by the addition of 0.07 % ammonium persulfate (APS) and 0.03 % N,N,N',N'-Tetramethylethylenediamine (TEMED). The gel mixture was poured into a gel cast (Bio-Rad, UK) followed by the insertion of a plastic comb to create individual lanes and left to polymerise at room temperature for 90 mins. Prior to loading the samples, the polyacrylamide-urea gel was pre-run by loading 10 µL of 6x loading dye (mentioned above) and electrophoresed in 1x TBE buffer at 200 V for 60 mins. After loading the samples, the gel was electrophoresed at 200 V for 2.5-3 hrs. Following electrophoresis, the gel was incubated in fixing solution (10 % (v/v) methanol, 10 % (v/v) acetic acid) for 1 hr with rocking and lifted onto a piece of 3MM Whatman® paper (Fisher, UK). The gels were dried using a gel drier (Drygel Sr. Slab Gel Dryer Model SE 1160) at 80 ^{o}C for 2 hrs. The dried gels were incubated with a standard X-ray film overnight at room temperature or at -80 ^{o}C (for higher intensity), and developed using an auto-developer (Konica Minolta SRX-101A).

2.6.5.4 Phosphorimaging

The expression of messenger RNA (mRNA) was quantified by incubating the X-ray film pre-exposed to the S1 gel (section 2.6.5.3.3) with a phophorimaging screen at room temperature for 30-60 mins. The screen was scanned using the rolling ball method of the Typhoon TRIO Variable Mode Imager (GE Healthcare, UK).

2.6.6 Sodium dodecyl sulfate-Polyacrylamide gel electrophoresis

The expression of proteins was studied using sodium dodecyl sulfate-polyacrylamide gel electrophoresis (SDS-PAGE). The gels consisted of a 5 % acrylamide/bis-acrylamide stacking gel poured above a layer of 10 % or 15 % acrylamide/bis-acrylamide separation gel with a plastic comb to produce the ridges in the gel. The stacking gel was prepared by adding 0.05 % (w/v) APS and 0.1 % (v/v) TEMED to a solution containing 125 mM Tris-HCl pH 6.8 and 0.1 % (w/v) SDS. The running gel was prepared by adding 0.05 % (w/v) APS, 0.05 % (v/v) TEMED) to a solution containing 375 mM Tris-HCl pH 8.8, 0.1 % (w/v) SDS and 10 % (v/v) glycerol. Once the gels had polymerized 20 µL of the protein samples (section 2.5.5) were loaded on to the gel, along with a broad range (2.3 kDa – 200 kDa) molecular weight markers or pre-stained

markers (20 kDa – 6.5 kDa; Bio-Rad, UK). All electrophoresis experiments were carried out using a Mini-Protein II Cell (Bio-Rad, UK) containing 1x SDS-PAGE buffer (25 mM Tris-HCl pH 8.8, 200 mM glycine, 0.1% (w/v) SDS) at a constant voltage of 200 V for 60-90 mins until the dye front reached the bottom of the separation gel.

2.6.7 Western Blotting

The expression of fusion proteins in EGY48_pMW112 cells ± pJG4.5_X and p423lexAkan_Y was verified by immunoblotting. Whole cell extract from exponentially growing cells (OD_{600} 0.5-0.8), such that the final absorbance at 600 nm was ~2.5 in SD-gal-raff-leu medium was prepared as detailed in section 2.5.5. 20 µL of the cell extract was loaded on to 15 % SDS-PAGE gels (see section 2.6.6) along with 5 µL of pre-stained protein molecular weight markers and electrophoresed at 200 V until the dye-front reached the bottom of the gel. The gel was subsequently placed on a piece of blotting card (Sigma, UK) with a foam pad underneath inside a plastic cast. A piece of Hybond™ ECL™ nitrocellulose membrane (GE Healthcare, UK) was placed on top of the gel followed by another piece of blotting card and a foam pad. The blotting cards, foam pads and the nitrocellulose membrane were all pre-soaked in the transfer buffer (0.5x SDS-PAGE buffer without SDS (see section 2.6.6), 20 % (v/v) methanol) and after assembly were firmly pressed from the centre towards the sides to remove trapped air bubbles before the cast was sealed and placed inside a Mini-Protean II Cell (Bio-Rad, UK) containing 1x transfer buffer. Transfer was achieved by applying a constant current at 270 mA for 90 mins. The membrane was subsequently removed and rinsed with TBST buffer (10 mM Tris-HCl pH 7.4, 150 mM NaCl, 0.05 % Tween 20) followed by 30 mins incubation in Ponceau S staining solution (0.25 % (w/v) Ponceau S, 5 % (v/v) acetic acid). The membrane was rinsed several times with water until the background was clear. The membrane was photographed and rinsed with TBST buffer before blocking it in 1x TBST buffer containing 25 % (w/v) blot-qualified bovine serum albumin (BSA; Promega, UK) for 60 mins with gentle rocking. The blocking solution was discarded and the membrane was incubated overnight in 1x TBST buffer containing 25 % (w/v) blot-qualified BSA and either 1 in 1000 dilution of rabbit anti-HA primary antibody (Sigma-Aldrich, UK) or 1 in 25000 dilution of rabbit anti-LexA primary antibody (Abcam, UK) at 4 ^{o}C with gentle rocking.

The following day the membrane was washed three times with TBST buffer and incubated for 1 hr with 1x TBST buffer containing 7 % (v/v) of goat anti-rabbit alkaline phosphatase (AP) secondary antibody (Promega, UK) at room temperature with gentle rocking. Subsequently the membrane was washed with AP buffer (100 mM Tris-HCl pH 9.5, 100 mM NaCl, 5 mM $MgCl_2$) and incubated with 20 mL AP buffer containing 0.44 % (v/v) nitro blue tetrazolium (Promega, UK) and 0.32 % (v/v) 5-bromo-4-chloro-3-indolyl phosphate (Promega, UK) for 3-20 mins in a dark environment until

protein bands were visible on the membrane. The reaction was stopped by washing the membrane with dH_2O and photographed.

2.6.8 Creation of the *ccs1Δ*-knockout mutant of EGY48

Genomic DNA (section 2.5.3) was isolated from the BY4741-*ccs1Δ* strain (Table 3) and used as a template for amplifying the *KAN*^{R} gene which is present in place of *CCS1* in this strain. The *S. cerevisiae* genome sequence was obtained from the online Sachharomyces Genome Database resource (SGD) in order to design DNA oligomers homologous to the region ~100 bp before the start and end of the *CCS1* gene (Table 5). A 50 µL PCR reaction was prepared in a 0.5 mL eppendorf tube comprising 100 ng BY4741- *ccs1Δ* genomic DNA template, 0.4 mM dNTPs mix, 50 pmol/µL of each primer, 1 µL of 2.5 U/µL *Pfu* polymerase, 5 µL 10x *Pfu* buffer and sterile ddH_2O and incubated in a PCR machine according to the conditions stated in Table 6. The PCR product was subsequently electrophoresed on a 1.5 % agarose gel and the desired band was isolated according to sections 2.3.3.3 and 2.3.3.4.

The purified PCR product consisting of the *Kan*^{R} gene from the BY4741-*ccs1Δ* strain was transformed into EGY48 (section 2.5.2) to enable the removal or 'knocking-out' of *CCS1* from the EGY48 genome and the insertion of the *KAN*^{R} gene in place of it. This strain would subsequently be denoted as SAY1. 200 µL of the transformation mixture was inoculated in 5 mL YPD and incubated overnight at 30 ^oC with shaking at 250 rpm. The following day, the transformants were spread on to YPD-agar plates containing 400 µg/mL of the G-418 antibiotic (Formedium, UK) and incubated for 1-2 days at 30 ^oC. Since only the cells containing *KAN*^{R} should grow on YPD-agar plates containing G-418, all of the colonies evident on these plates should contain the desired SAY1 strain. A diagnostic PCR was also performed to verify the success of homologous recombination resulting in the replacement of *CCS1* with *KAN*^{R}.

Two DNA primers were designed where one primer was homologous to *KAN*^{R} while the other primer was homologous to a portion of the *S. cerevisiae* genome ~150 bp downstream of the *CCS1* gene (that is, ~50 bp upstream of DNA oligomer no. 57, Table 5). Two PCR reactions, similar to the reactions mentioned above, were prepared with either EGY48 or SAY1 genomic DNA as the template, and incubated according to the conditions stated in Table 6. The PCR samples were loaded on to 1.5 % agarose gels and the presence of a band at the appropriate size in the lane containing the PCR product from the SAY1 strain only confirmed the successful knockout of *CCS1* from EGY48.

Table 6: PCR conditions used for amplifying the *Kan^R* gene from BY4741-*ccs1Δ*.

Purpose	Incubation Temperature (°C)	Incubation Time	Number of cycles
DNA denaturation	99	5 mins	1
DNA denaturation	95	40 sec	35
Annealing of DNA primer to the template	T_m – 5 °C[a]	30 sec	
Primer extension	68	2 mins	
Completion	68	5 mins	1

[a] The melting temperature (T_m) of the DNA oligomer.

2.7 Bioinformatics

The ClustalW2 software was used to align amino acid sequences of proteins using the default settings (http://www.ebi.ac.uk/Tools/clustalw/). The figures depicting crystal structures of proteins were created using PyMol (PyMol molecular graphics system, Version 1.3, Schrodinger, LLC). The models of ScAtx1-PacS_N and ScAtx1-CtaA_N were created in PyMol by superimposing and aligning a monomer of PacS_N or CtaA_N on the appropriate ScAtx1 dimer. While the PacS_N monomer was selected from the 2xmw structure in the PDB database, the CtaA_N monomer was obtained by using the Swiss PDB modelling software. The sequence of CtaA_N was submitted into the Swiss PDB modelling software and the automated mode was used to obtain a model of it (http://swissmodel.expasy.org). The structural alignment of hCCSD1 and CcsD1 shown in Figure 12, was performed in PyMol by selecting the CcsD1 sequence from the 1qup structure in the PDB database and superimposing it on the hCCSD1 structure (PDB accession code: 2crl) using the default settings.

2.8 Statistical Analysis

The significance of difference between the β-galactosidase activity of the WT and mutant proteins was determined by analyzing the data by one-way analysis of variance and the Bonferroni post hoc test. Significance level of 0.05 was used, such that $P < 0.05$ implied a significant difference whereas $P > 0.05$ implied the lack of significant difference in β-galactosidase activities.

3. Results

3.1 Investigating the molecular basis of the interaction between copper metallochaperones and hBACE1 CTD

Initially the bacterial two-hybrid systems were utilised to study the interaction between hBACE1 CTD and hCCS. Bacterial two-hybrid systems provide the advantage of minimising the potential interference by endogenous copper-binding proteins on the interaction of hBACE1 CTD with hCCS since there are no known Cu(I)-binding proteins in the cytosol of *E. coli* (Tottey *et al.*, 2005), the site of bacterial two-hybrid interactions. The interaction of hBACE1 CTD with hCCS was first studied using the BacterioMatch® bacterial two-hybrid system, which is a well-established system for investigating the interaction of copper metallochaperones with their target proteins. Some of the previously explored interactions using this system include the interaction of BsCopZ with the MBDs of BsCopA (Radford *et al.*, 2003) and the interaction of ScAtx1 with the MBDs of PacS and CtaA (Banci *et al.*, 2006c; Banci *et al.*, 2010b; Borrelly *et al.*, 2004; Tottey *et al.*, 2002). The interaction of ScAtx1 with the MBD of PacS comprising residues 1-95 (PacS95) was used as the positive control for this system. Empty pBT and pTRG, that is vectors lacking the proteins under investigation (for example ScAtx1, PacS95 or hCCS) as the translational fusions, were used as the negative controls. As shown in Figure 21, a significant interaction (P<0.05) was detected between ScAtx1 and PacS95, consistent with previous reports (Borrelly *et al.*, 2004; Tottey *et al.*, 2002). However, a significant interaction was not observed between hBACE1 CTD and hCCS (P>0.05) (Figure 22a). Since, the interaction of hCCS with hBACE1 CTD has previously been shown to be mediated by D1 of hCCS (Angeletti *et al.*, 2005), the interaction of hBACE1 CTD with isolated D1 of hCCS was also tested. However, no significant interaction was evident between hBACE1 CTD and hCCSD1 either (Figure 22b). It was hypothesised that the lack of interactions may be because the tertiary protein structure of hCCS and hCCSD1 may not be optimal for interacting with hBACE1 CTD due to their expression as fusion proteins with the components of the BacterioMatch® two-hybrid system. In order to address this issue, the BACTH two-hybrid system was used to study the interaction of hBACE1 CTD with hCCS and hCCSD1. Significant interactions were not detected between hBACE1 CTD and full-length hCCS (Figure 23) or hCCSD1 (Figure 24) in this system either. Since neither of the two bacterial two-hybrid systems yield a significant interaction between hBACE1 CTD and hCCS or hCCSD1, it was proposed that these proteins may not be able to fold properly in the bacterial cytoplasm due to their eukaryotic origins. Hence the interactions were investigated using the yeast two-hybrid system instead.

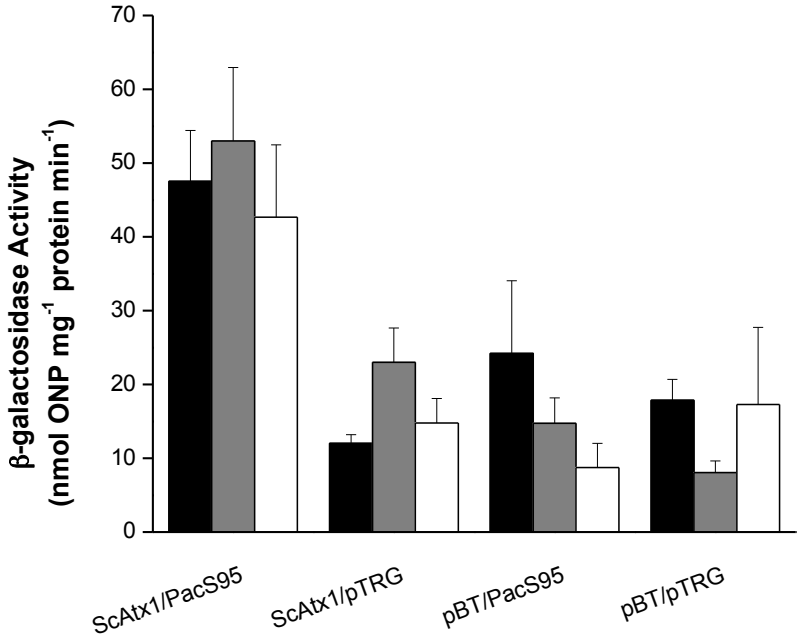

Figure 21: β-galactosidase activity assays of ScAtx1 with PacS95 using the BacterioMatch® two-hybrid system. XL-1 Blue MRF' cells were co-transformed with pBT and pTRG with or without *scAtx1* and *pacS95* respectively, as the translational fusions. Data from three independent co-transformants are presented in black, grey or white. Each data bar represents the average of a co-transformant assayed in triplicate + SD.

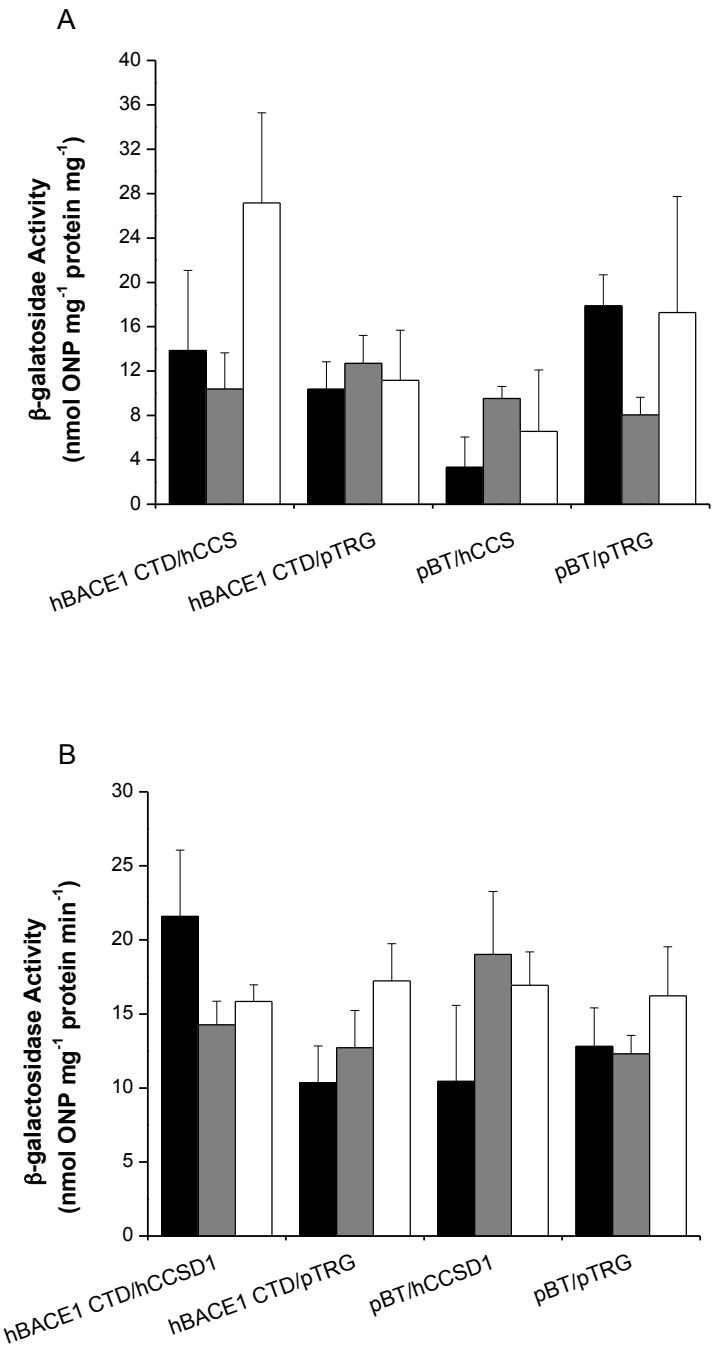

Figure 22: β-galactosidase activity assays of hBACE1 CTD with hCCS and hCCSD1 using the BacterioMatch® two-hybrid system. XL-1 Blue MRF' cells were co-transformed with pBT and pTRG with or without *hBACE1 CTD* and *hCCS* (A) or *hCCSD1* (B) respectively, as the translational fusions. Data from three independent co-transformants are presented in black, grey or white. Each data bar represents the average of a co-transformant assayed in triplicate + SD.

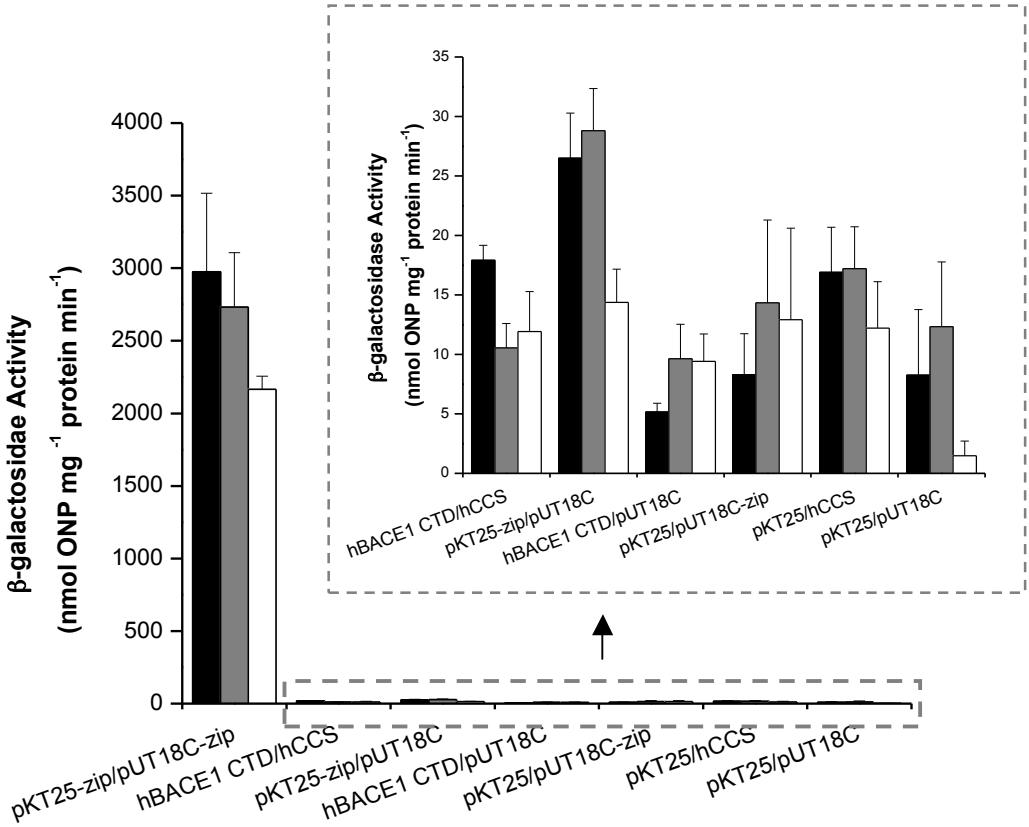

Figure 23: β-galactosidase activity assays of hBACE1 CTD with hCCS using the BACTH two-hybrid system. BTH101 cells were co-transformed with pKT25 and pUT18C with or without the constructs mentioned above as the translational fusions. Data from three independent co-transformants are presented in black, grey or white. Each data bar represents the average of a co-transformant assayed in triplicate + SD.

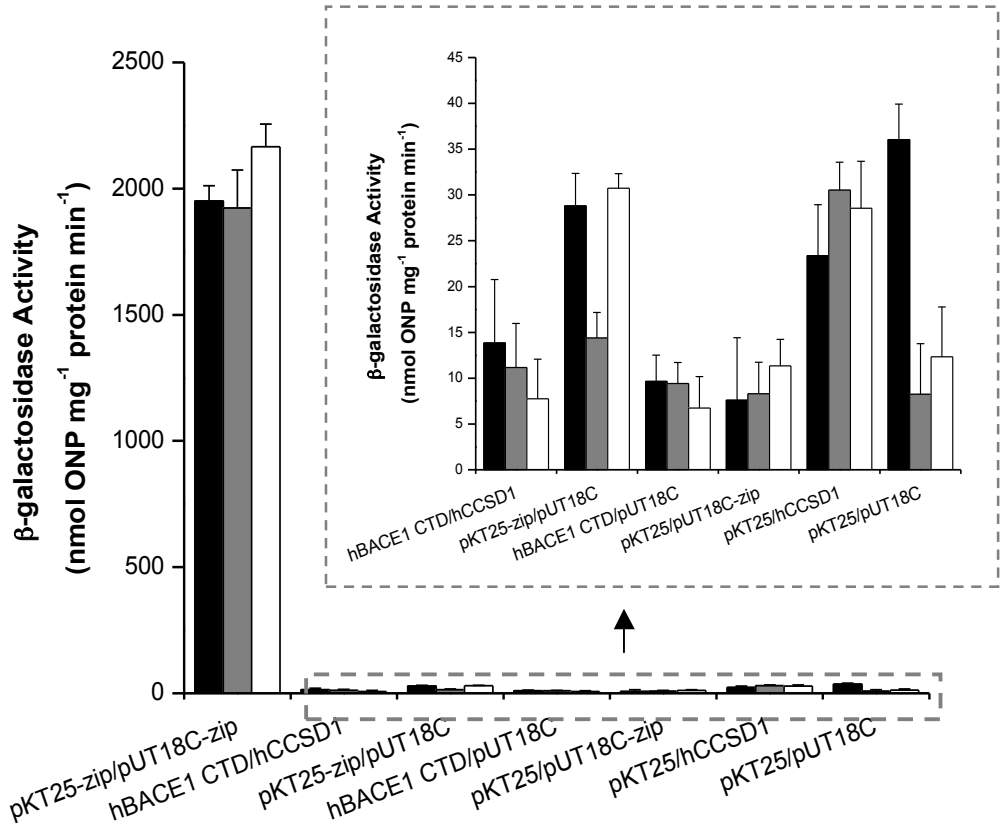

Figure 24: β-galactosidase activity assays of hBACE1 CTD with hCCSD1 using the BACTH two-hybrid system. BTH101 cells were co-transformed with pKT25 and pUT18C with or without the constructs mentioned above as the translational fusions. Data from three independent co-transformants are presented in black, grey or white. Each data bar represents the average of a co-transformant assayed in triplicate + SD.

A significant interaction was detected between hCCS and hBACE1 CTD (Figure 25) using the yeast two-hybrid system, consistent with the results reported previously by Angeletti *et al.* (2005). Also in agreement with previous reports (Angeletti *et al.*, 2005), a significant interaction was only detected between hCCSD1 and hBACE1 CTD but not between hCCSD2 and hBACE1 CTD or between hCCSD3 and hBACE1 CTD (Figure 26). However, the interaction of hCCSD1 with hBACE1 CTD was ~ 5-fold weaker in comparison to the interaction of full-length hCCS with hBACE1 CTD (Figure 26). While a significant interaction was not detected between Ccs1 and hBACE1 CTD, a significant interaction was consistently observed between HAH1 and hBACE1 CTD (Figure 27).

3.1.1 Effect of copper concentration on the interactions of copper metallochaperones with hBACE1 CTD

Since hCCS, HAH1, and hBACE1 CTD can all bind Cu(I) (Angeletti *et al.*, 2005; Eisses *et al.*, 2000; Wernimont *et al.*, 2000), it was hypothesised that the interactions of hCCS and HAH1 with hBACE1 CTD may be dependent upon the formation of a Cu(I)-bridged complex. This hypothesis is supported by previous studies where interactions between copper metallochaperones and their target proteins were shown to be dependent upon the presence of copper. These include the interactions of Atx1 with Ccc2 MBDs (Banci *et al.*, 2006b; Portnoy *et al.*, 1999; Pufahl *et al.*, 1997), HAH1 with the MBDs of ATP7A or ATP7B (Hamza *et al.*, 1999; Larin *et al.*, 1999; van Dongen *et al.*, 2004) and the interaction of BsCopZ with BsCopAb (Banci *et al.*, 2003a). To demonstrate a role for copper in mediating the interaction of hCCS with hBACE1 CTD, the co-transformants were cultured in minimal yeast medium containing copper-depleted yeast nitrogen base with BCS or $CuSO_4$ added to it. To verify that the presence of $CuSO_4$ or BCS in the growth medium results in altered copper content in the nucleus of the co-transformed cells, the site of yeast two-hybrid interactions, the transcription of *CTR1* and *CUP1* mRNAs were studied by S1 nuclease assays. The mRNA level of *CMD1*, the gene coding for the calmodulin protein, was also measured to ensure equivalent sample loading, based on the methods used previously by Keller *et al.* (2000). To ensure that the changes in nuclear copper content were not due to the presence of the hCCS and hBACE1 CTD fusions, co-transformants containing empty pJG4.5 and p423lexAkan vectors, that is, vectors lacking the hCCS and hBACE1 CTD proteins were also assayed for *CTR1*, *CUP1* and *CMD1* mRNA levels.

Previous studies have established that the transcription of *CTR1* is dependent upon the activity of the transcription factor Mac1 which induces the transcription of its target genes, including *CTR1*, under copper-limiting conditions (Labbe *et al.*, 1997; Yamaguchi-Iwai *et al.*, 1997; Zhu *et al.*, 1998). S1 nuclease assays indicate that the addition of 500 µM BCS to the growth medium induce the transcription of *CTR1* while no *CTR1* transcription was detected in the samples obtained from the co-

transformants cultured in basal medium (medium lacking BCS or $CuSO_4$) or in the presence of 10 μM $CuSO_4$ (Figure 28a). Similarly, the addition of 10 μM $CuSO_4$ was shown to induce the transcription of *CUP1*, the gene coding for the metallothionein protein CUP1 (Figure 28b). The transcription of *CUP1* has been shown to be regulated by the Ace1 transcription factor under copper-replete conditions (Thiele, 1988). Interestingly, residual *CUP1* expression was also evident in the samples obtained from the co-transformants cultured in 500 μM BCS (Figure 28b). Since the addition of 500 μM BCS results in increased transcription of *CTR1* (Figure 28a), this may subsequently lead to a rapid copper influx in the cell. In order to ensure that this influx does not result in free copper atoms in the cell, *CUP1* may be constitutively expressed at low levels even in the presence of BCS.

The mRNA levels of *CTR1* and *CMD1* were quantified using phosphorimaging analysis, as shown in Figure 28c. Approximately 2-fold higher levels of *CTR1* mRNA levels are evident in the co-transformants containing empty vectors in comparison to the co-transformants containing vectors with hCCS and hBACE1 CTD as the translational fusions cultured in the presence of 500 μM BCS (Figure 28c). Unlike the data obtained with the addition of 500 μM BCS (Figure 28c), similar *CUP1* mRNA levels are evident for the co-transformants cultured in the presence of 10 μM $CuSO_4$ containing either empty vectors or hCCS and hBACE1 CTD (Figure 28d). The latter results are in agreement with the copper content data determined by ICP-MS which reveal an ~ 20-fold increase in the copper content of all of the co-transformants cultured in 10 μM $CuSO_4$ compared to the co-transformants incubated in the basal medium (Figure 28e-f). Similar copper content is also evident for all of the co-transformants cultured in the presence of 500 μM BCS (Figure 28e-f). However, the copper content of the co-transformants containing hCCS and hBACE1 CTD was ~ 2-fold higher than the co-transformants containing the empty vectors when grown in basal medium (Figure 28e-f). Therefore, the presence of 500 μM BCS results in ~ 4-fold or ~2-fold decrease in the copper content of the co-transformants containing hCCS and hBACE1 CTD or empty vectors, respectively, compared to the co-transformants cultured in basal medium.

β-galactosidase activity assays indicate that the addition of 500 μM BCS significantly decreases the interaction of hCCS with hBACE1 CTD compared to the co-transformants cultured in the basal medium (Figure 28e). However, the addition of 10 μM $CuSO_4$ to the basal medium does not have a significant effect on the β-galactosidase activity of the hCCS/hBACE1 CTD co-transformants (Figure 28e). No significant effect of 500 μM BCS or 10 μM $CuSO_4$ is evident on the β-galactosidase activitiy of the co-transformants containing empty vectors (Figure 28f).

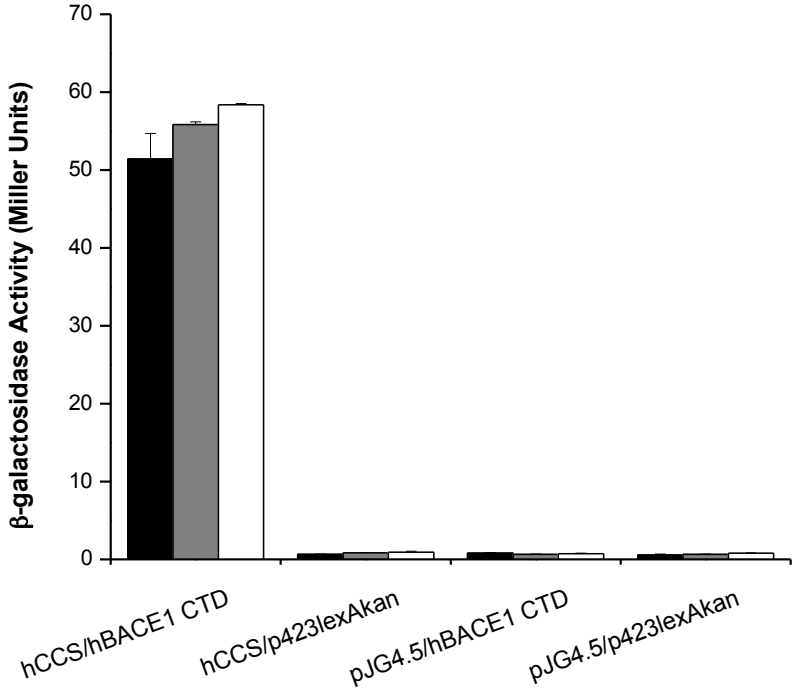

Figure 25: β-galactosidase activity assays of hCCS with hBACE1 CTD using the yeast two-hybrid system. EGY48 cells were co-transformed with pJG4.5 and p423lexAkan vectors with or without *hCCS* and *hBACE1 CTD* respectively, as the translational fusions. Data from three independent co-transformants are presented in black, grey or white. Each data bar represents the average of a co-transformant assayed in triplicate + SD.

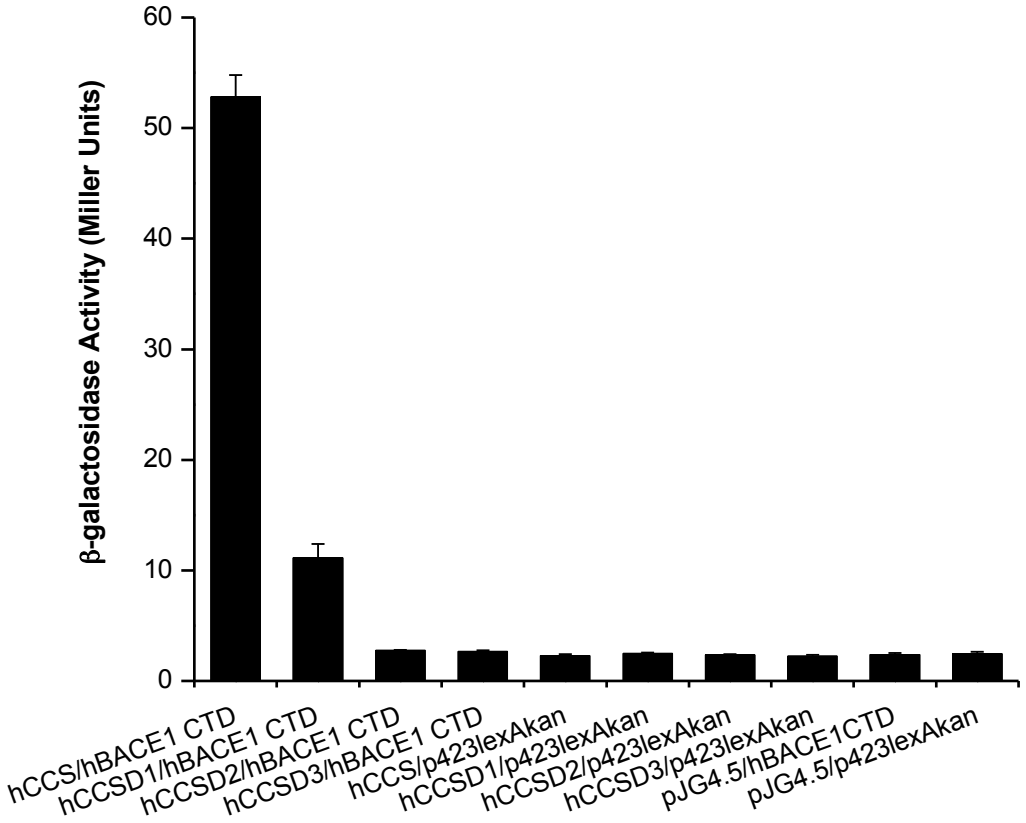

Figure 26: β-galactosidase activity assays of the individual domains of hCCS with hBACE1 CTD using the yeast two-hybrid system. EGY48 cells were co-transformed with pJG4.5 and p423lexAkan with or without the constructs mentioned above as the translational fusions. Each data bar represents the average of three co-transformants assayed in triplicate + SD.

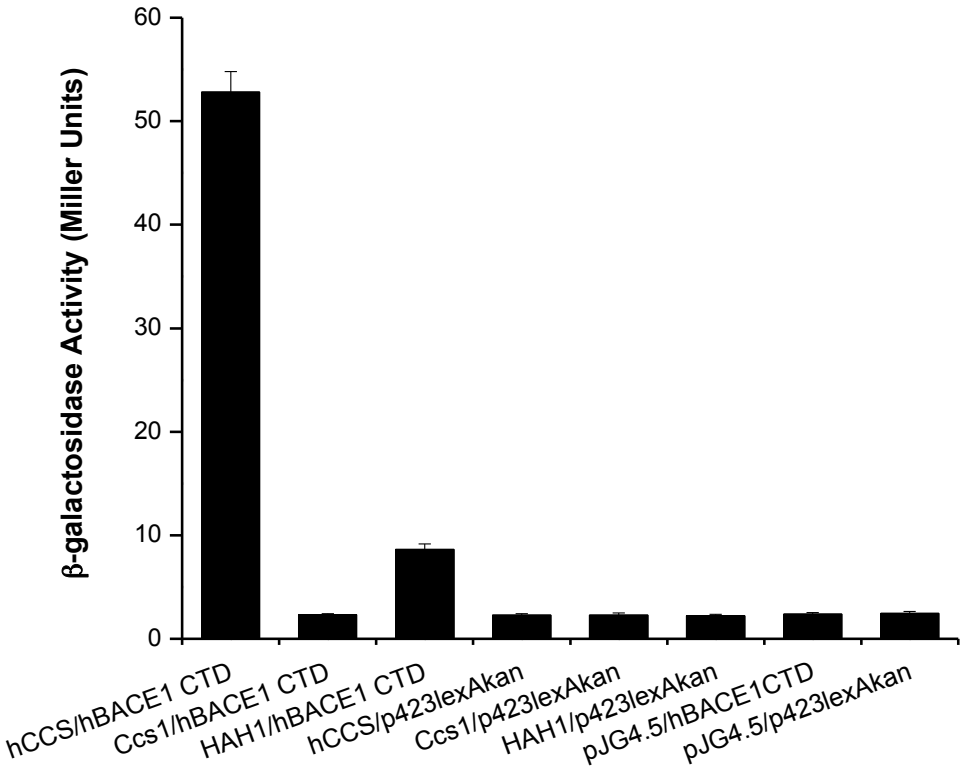

Figure 27: β-galactosidase activity assays of hCCS, Ccs1 and HAH1 with hBACE1 CTD using the yeast two-hybrid system. EGY48 cells were co-transformed with pJG4.5 and p423lexAkan with or without the constructs mentioned above as the translational fusions. Each data bar represents the average of three co-transformants assayed in triplicate + SD.

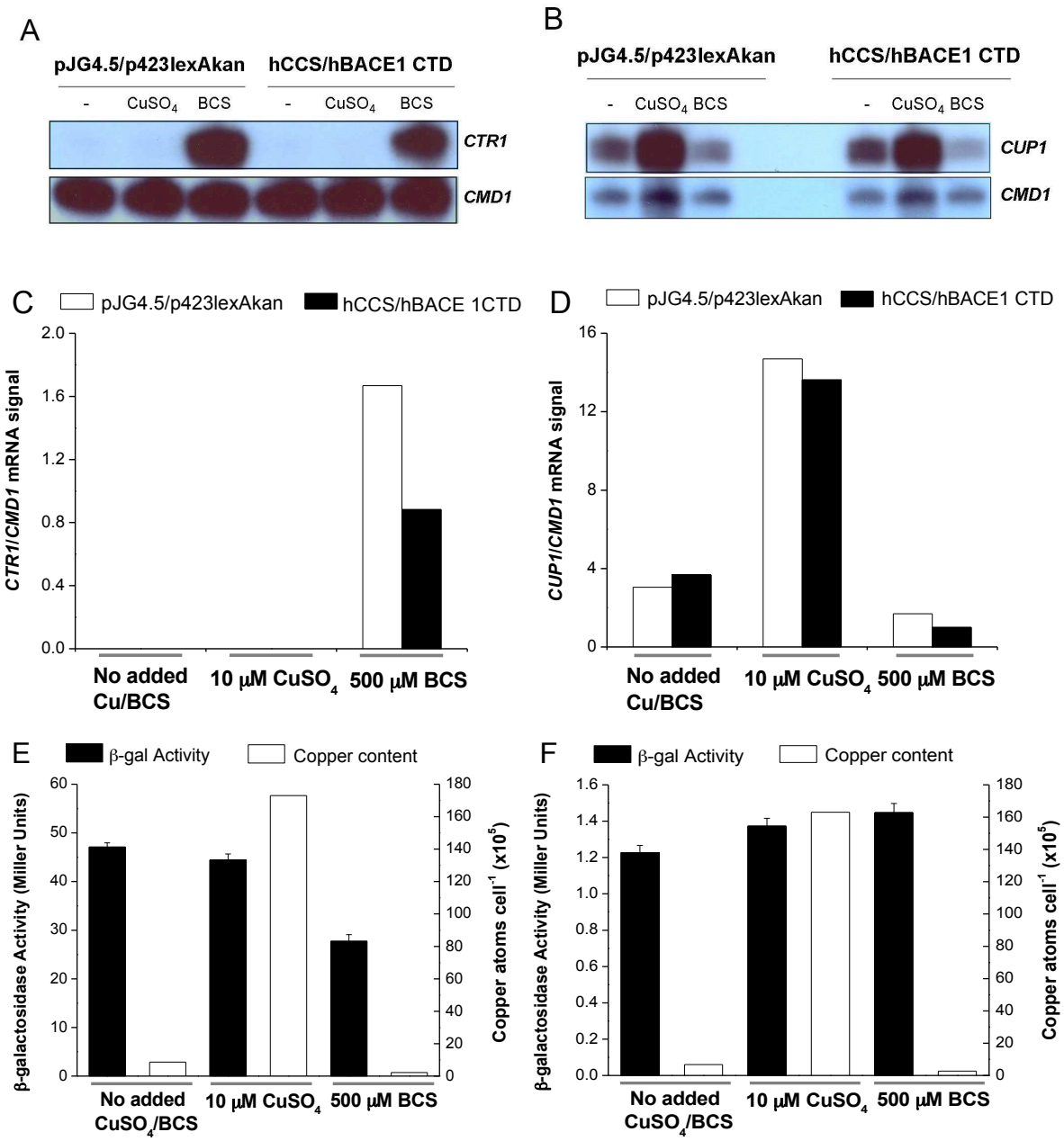

Figure 28: S1 nuclease protection assays, β-galactosidase activity assays and copper content analyses of the pJG4.5/p423lexAkan and hCCS/hBACE1 CTD co-transformants cultured in different copper conditions. EGY48 cells co-transformed with pJG4.5 and p423lexAkan with or without *hCCS* and *hBACE1 CTD* respectively, as the translational fusions were grown in basal medium with or without 10 µM CuSO4 and 500 µM BCS. The expression levels of *CMD1* in addition to *CTR1* (A) and *CUP1* (B) were determined by S1 nuclease protection assays. The mRNA level of *CMD1*, quantified by phophorimaging analysis, was compared with the mRNA level of *CTR1* or *CUP1* as shown in (C) and (D) respectively. β-galactosidase activity assays of the co-transformants containing pJG4.5_hCCS and p423lexAkan_hBACE1 CTD (E) or pJG4.5 and p423lexAkan (F) using the yeast two-hybrid system are also shown. In (E) and (F) the black bar represents the average β-galactosidase activity of the co-transformants assayed in triplicate + SD, whereas the white bar represents the copper content determined by ICP-MS.

To determine if higher concentrations of BCS or $CuSO_4$ can have a greater effect on the hCCS/hBACE1 CTD interaction, the co-transformants were incubated in the presence of 30 μM – 3 mM BCS or 0.3 – 300 μM $CuSO_4$. The growth rates of the co-transformants cultured in the highest concentrations of BCS and $CuSO_4$ were compared to the growth rates of the co-transformants cultured in the basal medium. As shown in Figure 29, the growth rates for all of the co-transformants were very similar up to 6 hours of incubation confirming that the presence of 3 mM BCS or 300 μM $CuSO_4$ do not impair the growth of the co-transformants during the exponential phase of the growth curve. Western blot analysis was used to ensure that the change in copper concentration due to the presence of $CuSO_4$ or BCS did not affect the protein expression levels compared to the co-transformants grown in the basal medium. Cell lysates from hCCS/hBACE1 CTD co-transformants grown in the presence of $CuSO_4$ or BCS were immunoblotted with the anti-HA (for the pJG4.5 constructs) and the anti-LexA (for the p423lexAkan constructs) antibodies. The protein expression levels from these co-transformants were compared with the cell lysates from the co-transformants grown in the basal medium. Prior to immunoblotting, the nitrocellulose membranes were stained with Ponceau S to determine equivalent protein loading in all lanes. The expression levels of endogenous proteins were used as loading controls, since due to the relatively low expression levels of the desired fusion proteins they could not be detected by the Ponceau S stain. As shown in Figure 30 and Figure 31, the addition of BCS or $CuSO_4$ does not result in aberrant changes in protein expression as equivalent protein expression levels were detected for all of the co-transformants. While the addition of 30 μM or 100 μM BCS does not result in a significant change in the copper content compared to the co-transformants cultured in basal medium, the addition of 500 μM and 1 mM BCS results in ~ 2-fold and ~ 5-fold reduction in cellular copper content, respectively (Figure 32). The presence of 3 mM BCS results in greater than 200-fold decrease in the cellular copper content compared to the co-transformants incubated in the basal medium (Figure 32).

Consistent with the copper content data, the addition of 30 μM or 100 μM BCS does not have a significant effect on the interaction of hCCS with hBACE1 CTD, as determined by β-galactosidase activity assays (Figure 32). The addition of 500 μM BCS significantly decreases the interaction between hCCS and hBACE1 CTD compared to the β-galactosidase activity of the co-transformants cultured in basal medium (Figure 32). Despite the difference in copper content between the co-transformants incubated in 500 μM, 1 mM and 3 mM BCS, the addition of 1 mM or 3 mM BCS does not decrease the interaction further compared to the results obtained with the addition of 500 μM BCS (Figure 32). The data therefore indicate that although the hCCS and hBACE1 CTD interaction decreases in a copper-deficient environment, it is nevertheless not abolished completely. Unlike the results obtained with copper

depletion, the β-galactosidase activity assays do not indicate a significant effect of increased copper content on the interaction of hCCS with hBACE1 CTD (Figure 33). Despite an ~ 50-fold increase in cellular copper content with the addition of 300 μM $CuSO_4$, the interaction between hCCS and hBACE1 CTD remains similar to the co-transformants cultured in the basal medium (Figure 33). The effect of copper concentration on the interaction of hCCSD1 and HAH1 with hBACE1 CTD was also studied. As shown in Figure 34 and Figure 35, neither the addition of BCS nor the presence of $CuSO_4$ had a significant effect on the hCCSD1/hBACE1 CTD or HAH1/hBACE1 CTD interactions. Surprisingly, the addition of 100 μM BCS to the growth medium results in ~ 2-fold increase in the HAH1/hBACE1 CTD interaction compared to the co-transformants cultured in basal medium (Figure 35).

3.1.2 The role of Cu(I)-binding residues in hCCS in mediating the interaction with hBACE1 CTD

Since copper depletion decreases the interaction of hCCS with hBACE1 CTD (Figure 28e and Figure 32), it was hypothesised that this interaction may require the copper-binding Cys residues in hCCS. As the interaction between these proteins is associated with D1 of hCCS (Figure 26), the copper-binding Cys residues (Cys22 and Cys25) in this domain, present in a CXXC-motif, were mutated to Ser. Mutation of either Cys22 or Cys25 to Ser in hCCS results in ~ 8-9-fold weaker interaction with hBACE1 CTD compared to the interaction of hCCS wild-type (WT) protein with hBACE1 CTD (Figure 36). Mutation of both of the D1 Cys residues in hCCS completely abolishes the interaction with hBACE1 CTD (Figure 36). Similarly, the mutation of both Cys22 and Cys25 in hCCSD1 also abolishes the interaction with hBACE1 CTD (Figure 37). While the mutation of either Cys22 or Cys25 in hCCSD1 significantly decreases the interaction with hBACE1 CTD, the difference compared with the interaction of hCCSD1 WT protein with hBACE1 CTD is only ~ 2-fold (Figure 37) unlike the single mutations in full-length hCCS where the difference is ~ 9-fold (Figure 36). The data therefore indicate that both Cys22 and Cys25 are important for the hCCS/hBACE1 CTD and hCCSD1/hBACE1 CTD interactions. Western blot and Ponceau S analyses (Figure 38) indicate similar protein expression levels for the hCCS and hCCSD1 WT and mutant proteins suggesting that the effects of Cys mutations observed on the interaction with hBACE1 CTD are not due to aberrant changes in protein expression levels.

Rae *et al.* (2001) proposed that Cu(I)-binding in hCCSD1 may induce structural changes in Arg71 resulting in the orientation of this residue towards the metal-binding site. Analogous residues in Atx1 and HAH1 have been shown to be important for mediating the interactions with their respective target proteins (Arnesano *et al.*, 2001a; Arnesano *et al.*, 2004; Hussain *et al.*, 2008; Portnoy *et al.*, 1999; Wernimont *et al.*, 2000). To investigate the role of this residue in mediating the

interaction of hCCS with hBACE1 CTD, Arg71 was mutated to Ala, Glu or Lys. While all three mutations in full-length hCCS result in a significant decrease in the interaction with hBACE1 CTD, the most dramatic effects were obtained with the hCCS Arg71Glu and Arg71Lys mutations (Figure 39). The hCCS Arg71Glu and Arg71Lys mutations both result in an ~ 10-fold decrease in the interaction with hBACE1 CTD compared with the interaction of hCCS WT protein with hBACE1 CTD (Figure 39). The mutation of Arg71 in hCCSD1 also results in a significant decrease in the interaction with hBACE1 CTD (Figure 40). Unlike the results obtained with the full-length hCCS Arg mutations where Arg71Glu and Arg71Lys mutations had a greater effect than the Arg71Ala mutation, all three Arg71 mutations in hCCSD1 result in very similar interactions with hBACE1 CTD (~3-fold lower than hCCSD1 WT/hBACE1 CTD). No aberrant effect of the Arg71 mutations in hCCS and hCCSD1 was observed on protein expression levels (Figure 41).

Similar to hCCSD1, Ccs1D1 also contains a positively charged residue in loop 5 in the analogous location to Arg71 in hCCSD1, although this residue is substituted by Lys in Ccs1 (Lys65) (Figure 9b). In light of the evidence that the mutation of hCCS Arg71 to Lys significantly decreases the interaction with hBACE1 CTD, it was hypothesised that the incorporation of an Arg residue in the analogous position in Ccs1 may enhance its interaction with hBACE1 CTD. While the data indicate a slight increase in interaction between Ccs1 Lys66Arg and hBACE1 CTD compared to the Ccs1 WT/hBACE1 CTD interaction, this increase was not found to be significant (Figure 42). Western blot and Ponceau S analyses indicate similar protein expression levels for both Ccs1 Lys66Arg and Ccs1 WT proteins (Figure 43).

In addition to Cys22 and Cys25, hCCS can also bind Cu(I) via the Cys244 and Cys246 residues in D3 (Caruano-Yzermans *et al.*, 2006; Eisses *et al.*, 2000; Rae *et al.*, 2001). To investigate the role of Cys244 and Cys246 residues in mediating the interaction of hCCS with hBACE1 CTD, these residues were mutated to Ser. However, neither the mutation of Cys244 nor the mutation of both Cys244 and Cys246 had a significant effect on the interaction with hBACE1 CTD compared to the interaction of hBACE1 CTD with hCCS WT protein (Figure 44). The data therefore suggest that the Cu(I)-binding Cys residues in hCCSD3 are not required for the interaction between hCCS and hBACE1 CTD. Western blot and Ponceau S analyses indicate equivalent expression levels for hCCS WT, hCCS Cys244Ser and hCCS Cys244Ser,Cys246Ser proteins (Figure 45).

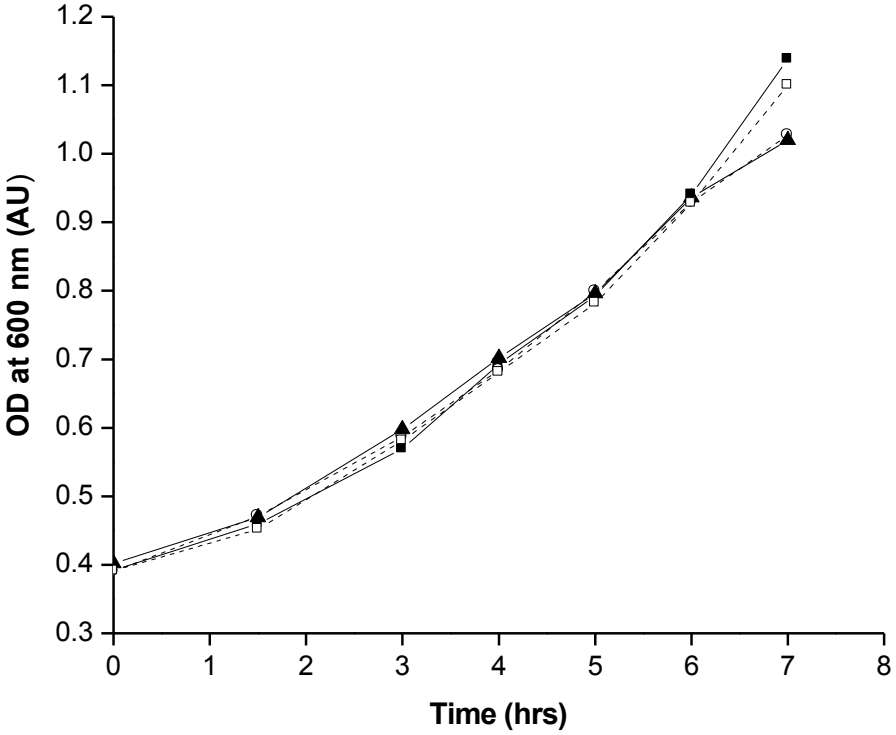

Figure 29: Growth curves for the co-transformants containing hCCS and hBACE1 CTD cultured in basal medium and in medium containing 300 µM $CuSO_4$, 500 µM BCS or 3 mM BCS. EGY48 cells co-transformed with pJG4.5_hCCS and p423lexAkan_hBACE1 CTD were grown in basal medium (■) or in medium containing 300 µM CuSO4 (○), 500 µM BCS (▲) or 3 mM BCS (□) over a course of 7 hrs.

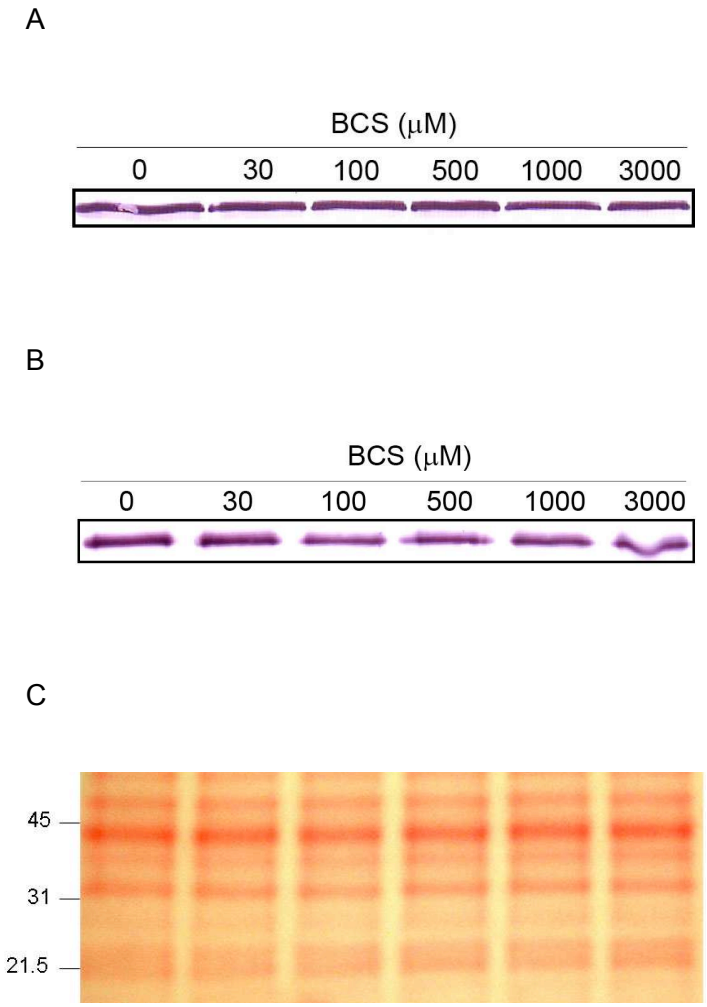

Figure 30: Western blot and Ponceau S analyses of the co-transformants containing hCCS and hBACE1 CTD cultured in varying concentrations of BCS. Whole cell extracts from EGY48 cells co-transformed with pJG4.5_hCCS and p423lexAkan_hBACE1 CTD grown in different concentrations of BCS were analysed with the anti-HA antibody by western blot analysis and show intense bands at ~42 kDa for the hCCS translational fusions (A). The co-transformants were also analysed with the anti-LexA antibody and show intense bands at ~27 kDa for the hBACE1 CTD translational fusions (B). The nitrocellulose membranes were stained with Ponceau S to determine equivalent protein loading in each lane (C). The position of the protein molecular weight markers in (C) are shown on the left in kDa.

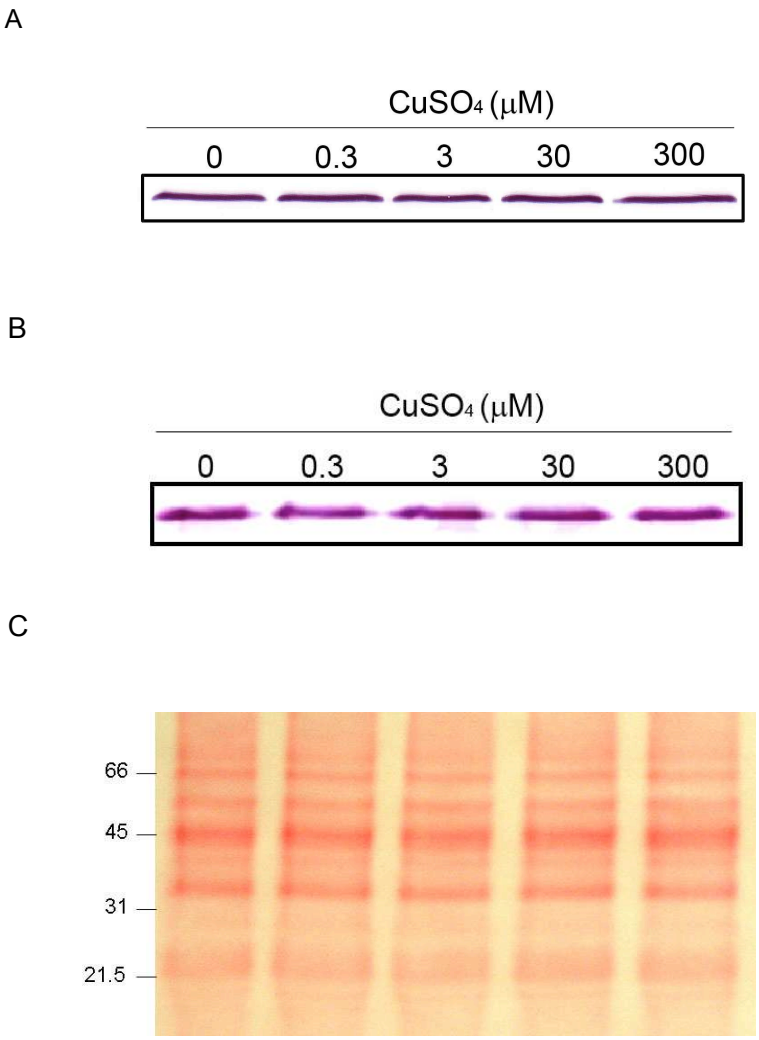

Figure 31: Western blot and Ponceau S analyses of the co-transformants containing hCCS and hBACE1 CTD cultured in varying concentrations of $CuSO_4$. Whole cell extracts from EGY48 cells co-transformed with pJG4.5_hCCS and p423lexAkan_hBACE1 CTD grown in different concentrations of CuSO4 were analysed with the anti-HA antibody and show intense bands at ~42 kDa for the hCCS translational fusions (A). The co-transformants were also analysed with the anti-LexA antibody and show intense bands at ~27 kDa for the hBACE1 CTD translational fusions (B). The nitrocellulose membranes were stained with Ponceau S to determine equivalent protein loading in each lane (C). The position of the protein molecular weight markers in (C) are shown on the left in kDa.

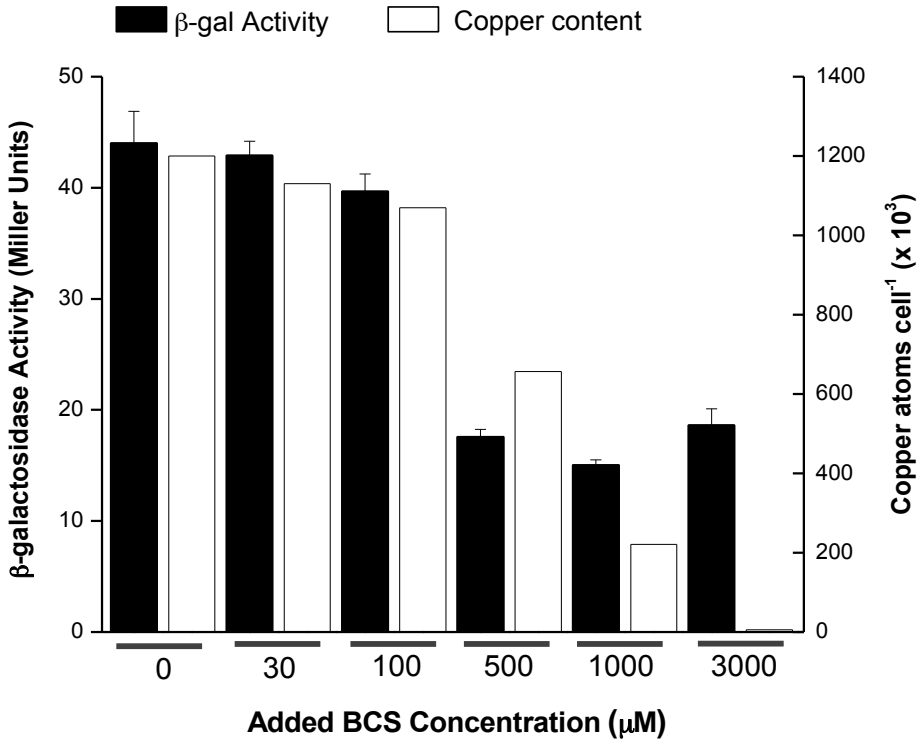

Figure 32: β-galactosidase activity assays using the yeast two-hybrid system and the copper content of the co-transformants containing hCCS and hBACE1 CTD cultured in basal medium or in varying concentration of BCS. EGY48 cells co-transformed with pJG4.5_hCCS and p423lexAkan_hBACE1 CTD were grown in various concentrations of BCS and assayed for β-galactosidase activity. The black bar represents the average β-galactosidase activity for the co-transformants assayed in triplicate + SD. The white bar represents the cellular copper content determined using ICP-MS.

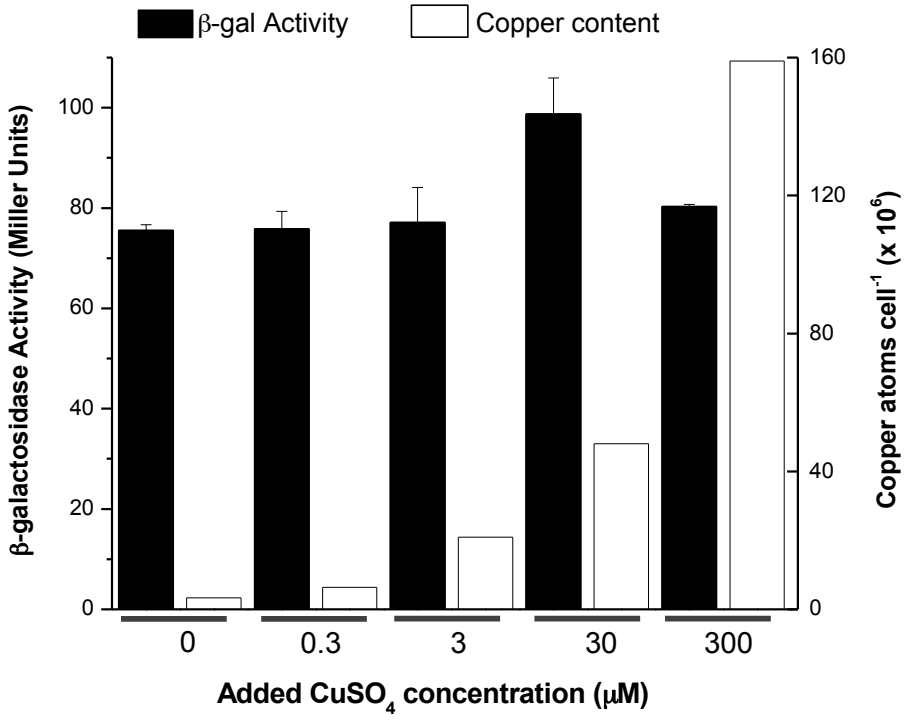

Figure 33: β-galactosidase activity assays using the yeast two-hybrid system and the copper content of the co-transformants containing hCCS and hBACE1 CTD cultured in basal medium or in varying concentration of $CuSO_4$. EGY48 cells co-transformed with pJG4.5_hCCS and p423lexAkan_hBACE1 CTD were grown in various concentrations of CuSO4 and assayed for β-galactosidase activity. The black bar represents the average β-galactosidase activity for the co-transformants assayed in triplicate + SD. The white bar represents the cellular copper content determined using ICP-MS.

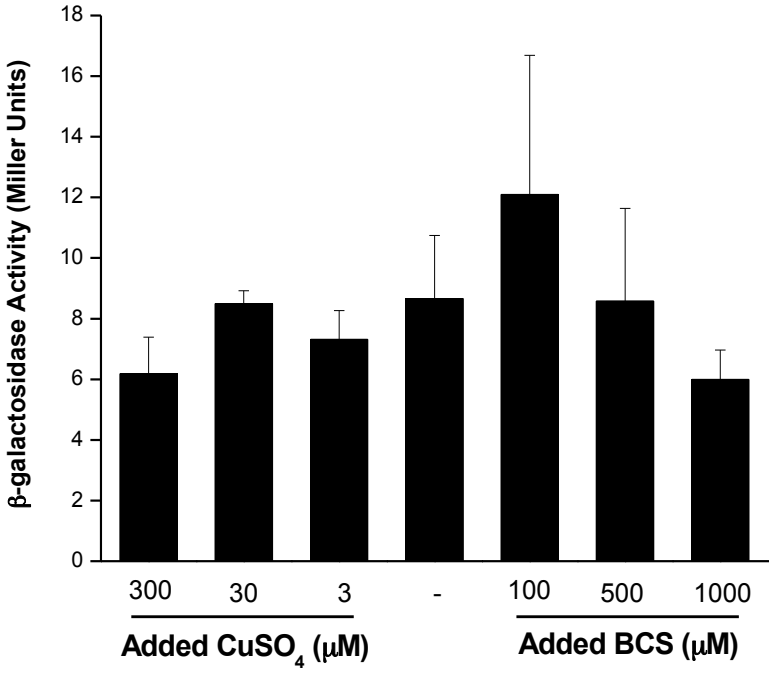

Figure 34: β-galactosidase activity assays using the yeast two-hybrid system for the co-transformants containing hCCSD1 and hBACE1 CTD cultured in basal medium or in medium containing BCS or $CuSO_4$. EGY48 cells co-transformed with pJG4.5_hCCSD1 and p423lexAkan_hBACE1 CTD were grown with or without (-) added CuSO4 or BCS at the concentrations shown above and assayed for β-galactosidase activity. Each data bar represents the average of three co-transformants assayed in triplicate + SD.

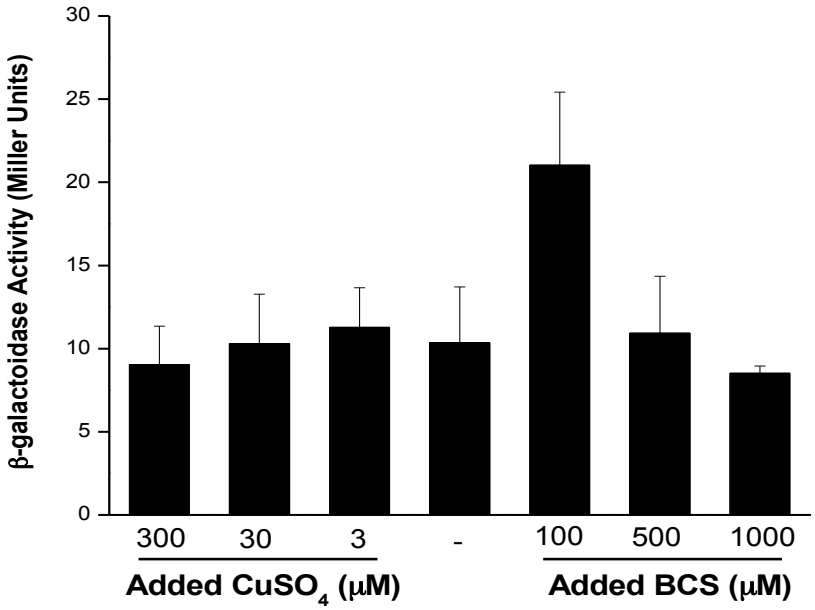

Figure 35: β-galactosidase activity assays using the yeast two-hybrid system for the co-transformants containing HAH1 and hBACE1 CTD cultured in basal medium or in medium containing BCS or $CuSO_4$. EGY48 cells co-transformed with pJG4.5_HAH1 and p423lexAkan_hBACE1 CTD were grown with or without (-) added CuSO4 or BCS at the concentrations shown above and assayed for β-galactosidase activity. Each data bar represents the average of three co-transformants assayed in triplicate + SD.

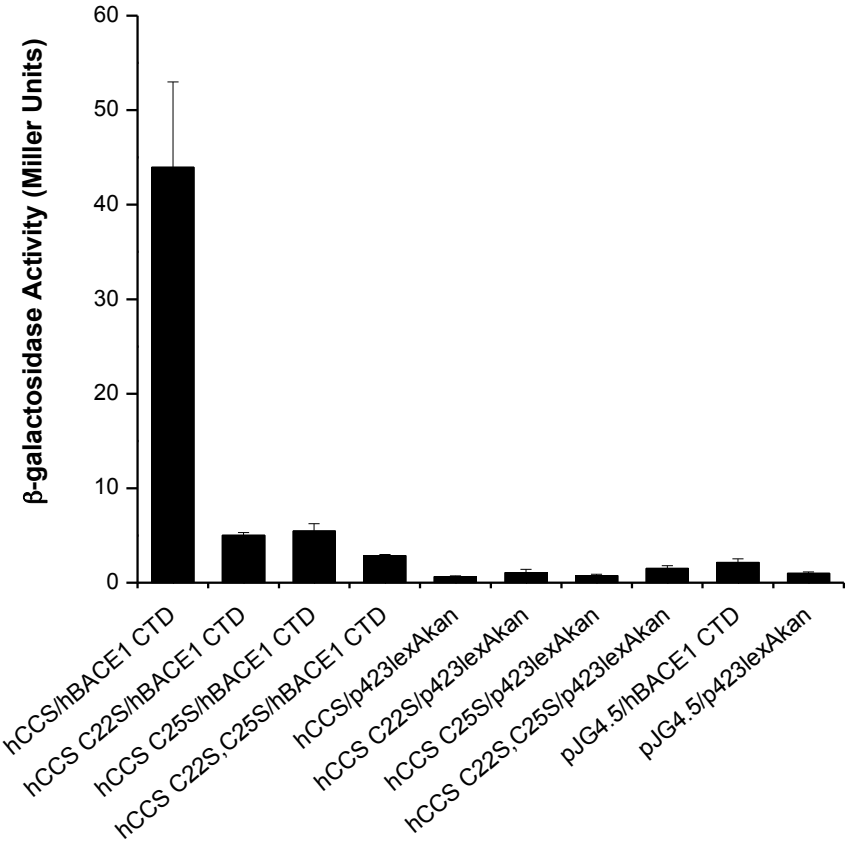

Figure 36: β-galactosidase activity assays showing the effects of hCCS Cys22 and Cys25 mutations on the interaction with hBACE1 CTD using the yeast two-hybrid system. EGY48 cells were co-transformed with pJG4.5 and p423lexAkan with or without the constructs mentioned above as the translational fusions. Each data bar represents the average of three co-transformants assayed in triplicate + SD.

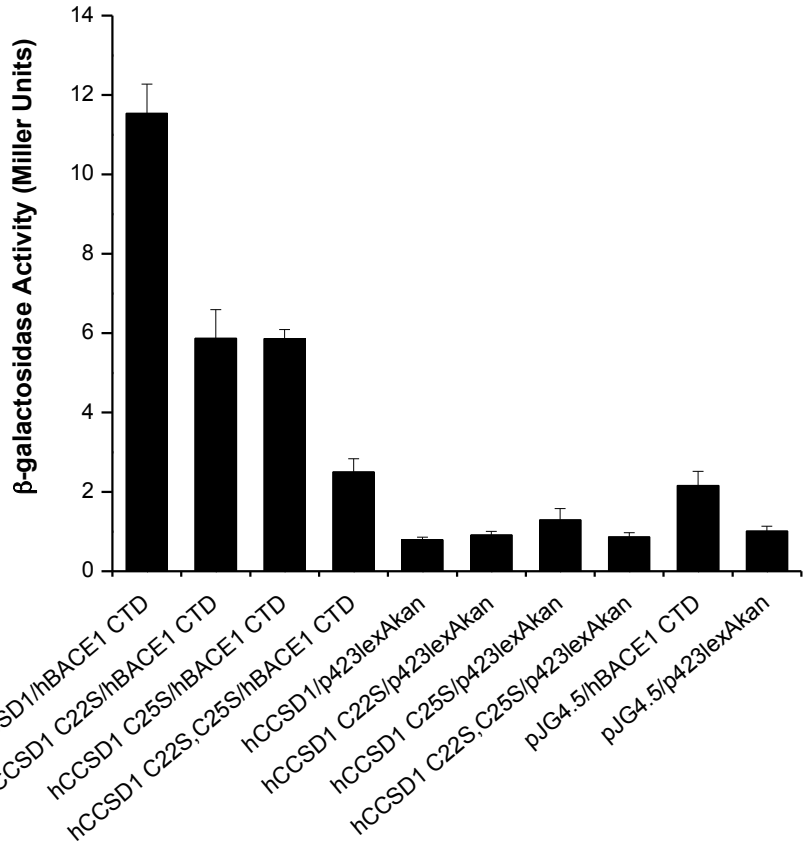

Figure 37: β-galactosidase activity assays showing the effect of hCCSD1 Cys22 and Cys25 mutations on the interaction with hBACE1 CTD using the yeast two-hybrid system. EGY48 cells were co-transformed with pJG4.5 and p423lexAkan with or without the constructs mentioned above as the translational fusions. Each data bar represents the average of three co-transformants assayed in triplicate + SD.

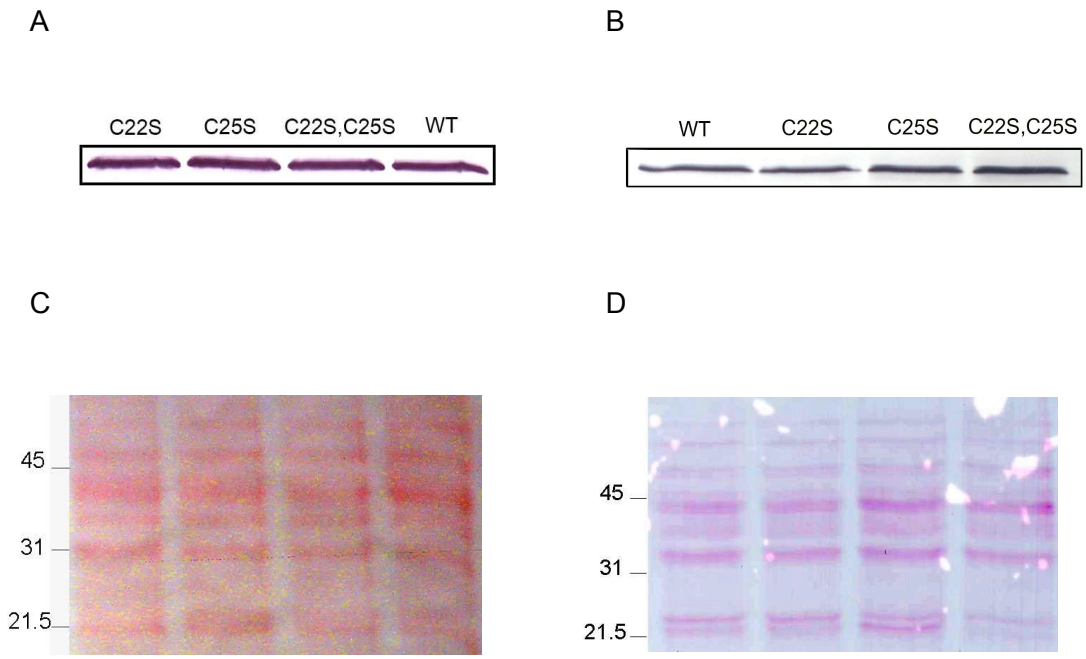

Figure 38: Western blot and Ponceau S analyses of hCCS and hCCSD1 WT, Cys22Ser, Cys25Ser and Cys22Ser,Cys25Ser proteins with the anti-HA antibody. Whole cell extracts from EGY48 cells co-transformed with p423lexAkan_hBACE1 CTD and pJG4.5 with the *hCCS* (A) or *hCCSD1* (B) constructs as the translational fusions were analysed with the anti-HA antibody by western blot analysis. The intense bands shown in (A) at ~42 kDa represent the hCCS translational fusion, while the intense bands at ~ 20 kDa in (B) represent the hCCSD1 translational fusions. The nitrocellulose membranes shown in (A) and (B) were stained with Ponceau S prior to immunoblotting to determine equivalent protein loading in each lane, as shown in (C) and (D) respectively. The position of the protein molecular weight markers in (C) and (D) are shown on the left in kDa.

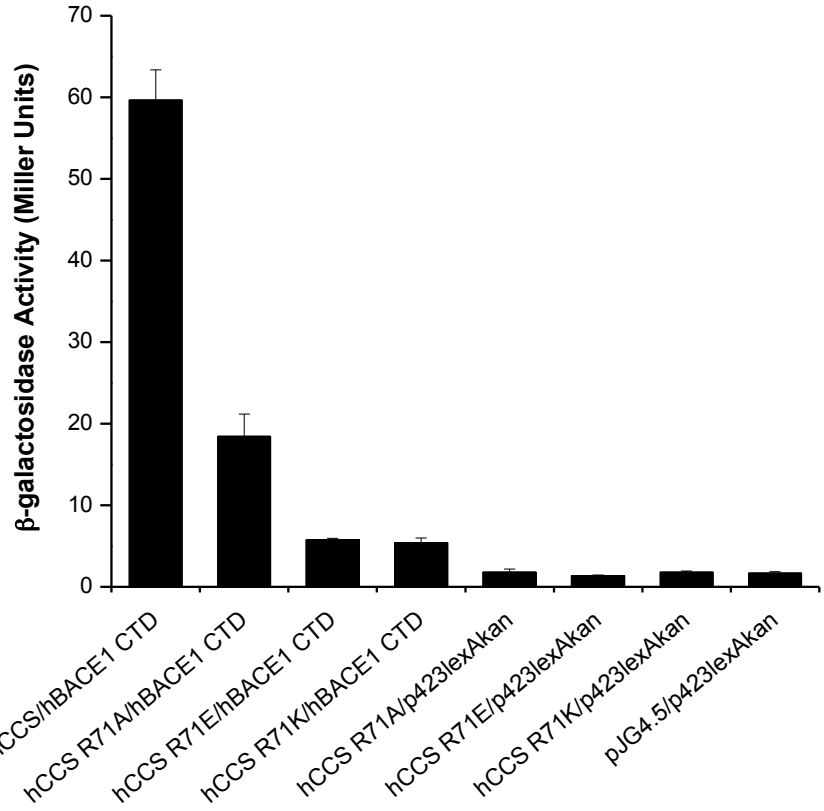

Figure 39: β-galactosidase activity assays showing the effect of hCCS Arg71 mutations on the interaction with hBACE1 CTD using the yeast two-hybrid system. EGY48 cells were co-transformed with pJG4.5 and p423lexAkan with or without the constructs mentioned above as the translational fusions. Each data bar represents the average of three co-transformants assayed in triplicate + SD.

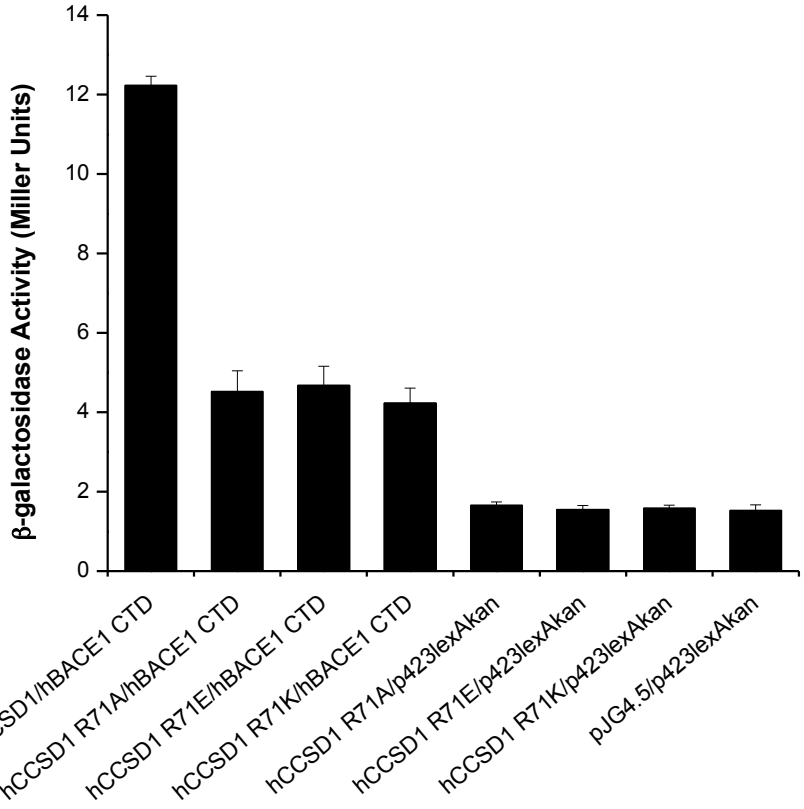

Figure 40: β-galactosidase activity assays showing the effect of hCCSD1 Arg71 mutations on the interaction with hBACE1 CTD using the yeast two-hybrid system. EGY48 cells were co-transformed with pJG4.5 and p423lexAkan with or without the constructs mentioned above as the translational fusions. Each data bar represents the average of three co-transformants assayed in triplicate + S.D.

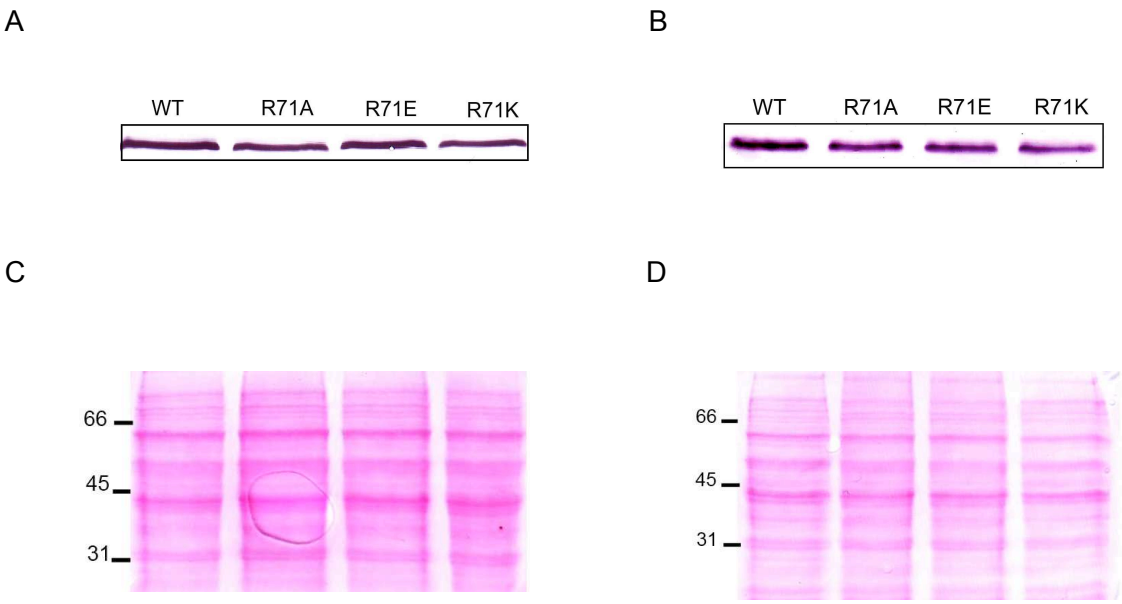

Figure 41: Western blot and Ponceau S analyses of hCCS and hCCSD1 WT, Arg71Ala, Arg71Glu and Arg71Lys proteins with the anti-HA antibody. Whole cell extracts from EGY48 cells co-transformed with p423lexAkan_hBACE1 CTD and pJG4.5 with *hCCS* (A) or *hCCSD1* (B) constructs as the translational fusions were analysed with the anti-HA antibody by western blot analysis. The intense bands in (A) at ~42 kDa represent the hCCS translational fusion, while the intense bands at ~ 20 kDa in (B) represent the hCCSD1 translational fusions. The nitrocellulose membranes shown in (A) and (B) were stained with Ponceau S prior to immunoblotting to determine equivalent protein loading in each lane, as shown in (C) and (D) respectively. The position of the protein molecular weight markers in (C) and (D) are shown on the left in kDa.

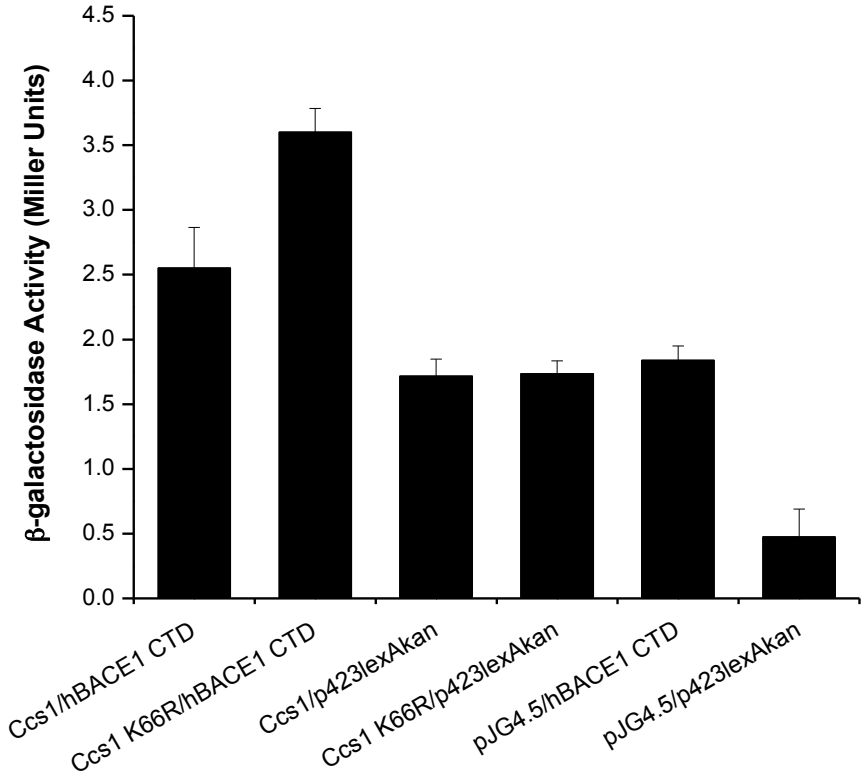

Figure 42: β-galactosidase activity assays showing the effect of Ccs1 Lys66Arg mutation on the interaction with hBACE1 CTD using the yeast two-hybrid system. EGY48 cells were co-transformed with pJG4.5 and p423lexAkan with or without the constructs mentioned above as the translational fusions. Each data bar represents the average of three co-transformants assayed in triplicate + SD.

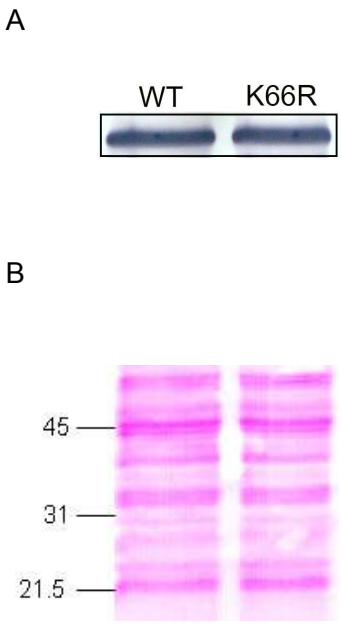

Figure 43: Western blot and Ponceau S analyses of Ccs1 WT and Lys66Arg proteins with the anti-HA antibody. Whole cell extracts from EGY48 cells co-transformed with p423lexAkan_hBACE1 CTD and pJG4.5 with *CCS1 WT* or *CCS1 lys66arg* as the translational fusions were analysed with the anti-HA antibody by western blot analysis and show intense bands at ~ 39 kDa for the Ccs1 translational fusions (A). The nitrocellulose membrane was stained with Ponceau S to determine equivalent protein loading in each lane (B). The position of the protein molecular weight markers in (B) are shown on the left in kDa.

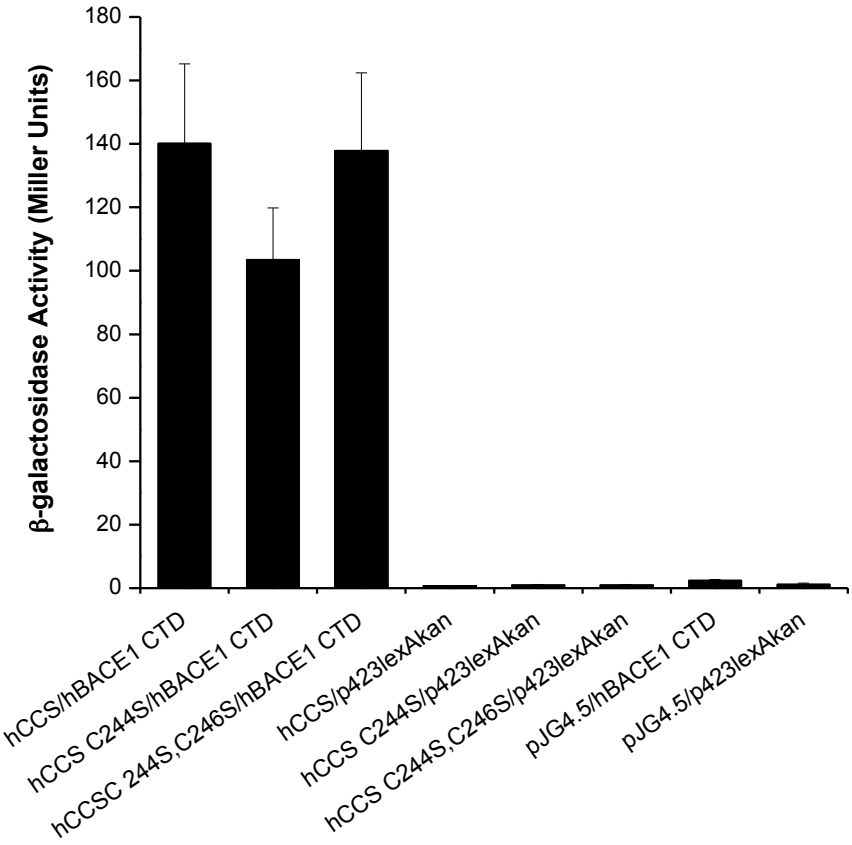

Figure 44: β-galactosidase activity assays showing the effect of hCCS Cys244Ser and Cys244Ser,Cys246Ser mutations on the interaction with hBACE1 CTD using the yeast two-hybrid system. EGY48 cells were co-transformed with pJG4.5 and p423lexAkan with or without the constructs mentioned above as the translational fusions. Each data bar represents the average of three co-transformants assayed in triplicate + SD.

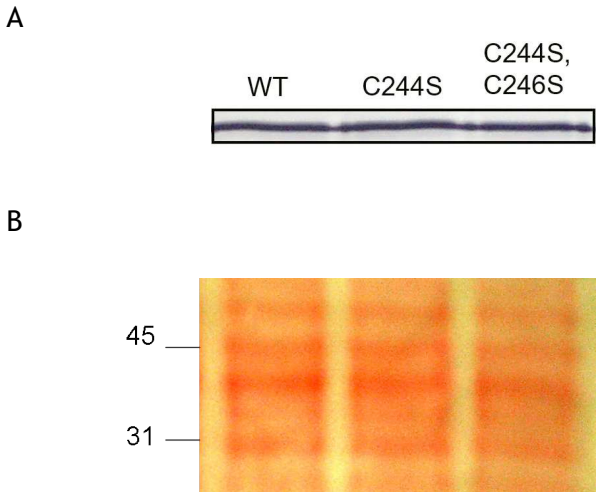

Figure 45: Western blot and Ponceau S analyses of hCCS WT, Cys244Ser and Cys244Ser,Cys246Ser proteins with the anti-HA antibody. Whole cell extracts from EGY48 cells co-transformed with p423lexAkan_hBACE1 CTD and pJG4.5 with the *hCCS* constructs shown above as the translational fusions were analysed with the anti-HA antibody by western blot analysis and show intense bands at ~42 kDa for the hCCS translational fusions (A). The nitrocellulose membrane was stained with Ponceau S to determine equivalent protein loading in each lane (B). The position of the protein molecular weight markers in (B) are shown on the left in kDa.

3.1.3 The role of Cu(I)-binding Cys residues in hBACE1 CTD in mediating the interaction with copper metallochaperones

Since the mutation of the Cu(I)-binding Cys residues in D1 of hCCS abolishes the interaction with hBACE1 CTD (Figure 36 and Figure 37), the Cu(I)-binding residues Cys478, Cys482 and Cys485 in hBACE1 CTD (Angeletti *et al.*, 2005) were also mutated to Ser to determine their roles in the interactions with hCCS and HAH1. As shown in Figure 46, the mutation of Cys478 to Ser results in significantly increased interactions of hBACE1 CTD with hCCS, hCCSD1 and HAH1. In contrast, the mutation of either Cys482 (Figure 47) or Cys485 (Figure 48) abolishes the interaction of hBACE1 CTD with hCCS, hCCSD1 and HAH1. The data therefore indicate that the Cys residues in the CXXC motif of both hBACE1 CTD and hCCS are vital for their interaction. Western blot and Ponceau S analyses indicate that the hBACE1 CTD Cys mutations do not have an aberrant effect on protein expression levels as equivalent protein levels were observed for all of the mutation proteins compared to the hBACE1 CTD WT protein (Figure 49).

3.1.4 Identifying additional residues in hBACE1 CTD involved in mediating the interactions with hCCS and HAH1

The data shown in Figure 47 and Figure 48 clearly demonstrate that the Cys residues in the CXXC motif of hBACE1 CTD are essential for the interactions with hCCS and HAH1. It was subsequently hypothesised that the residues surrounding the CXXC motif in hBACE1 CTD may also be involved in the interaction of hBACE1 CTD with copper metallochaperones. To investigate this further, some of the residues located close to the CXXC-motif were mutated to study the effects of those mutations on the interactions of hBACE1 CTD with hCCS and HAH1.

The Trp480 residue is located two residues upstream of Cys482 in hBACE1 CTD. In the analogous position, most of the copper metallochaperones and the cognate MBDs possess a Met residue (Arnesano *et al.*, 2002). This Met residue has been shown to be important for maintaining the hydrophobic core of the ferredoxin-fold (Banci *et al.*, 2001b; Hearnshaw *et al.*, 2009; Poger *et al.*, 2005; Wernimont *et al.*, 2000). While hBACE1 CTD is too short to form a ferredoxin-fold, it is possible that Trp480 may also play a structural role in the organisation of the CXXC motif for Cu(I)-binding in hBACE1 CTD. Therefore, the Trp480 residue was mutated to Met to determine its effect on the interaction of hBACE1 CTD with hCCS and HAH1. As shown in Figure 50, the Trp480Met mutation significantly decreases the interaction of hBACE1 CTD with hCCS and almost abolishes the interactions with hCCSD1 and HAH1, suggesting that this residue is important for mediating the interactions with copper metallochaperones.

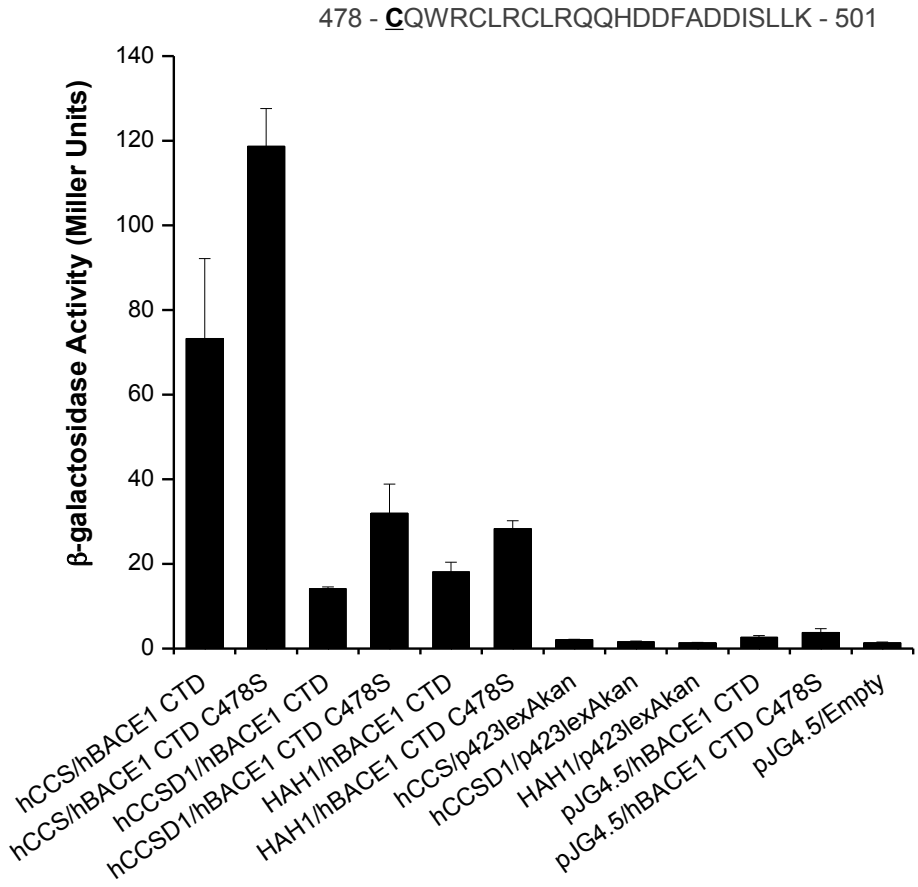

Figure 46: β-galactosidase activity assays showing the effect of hBACE1 CTD Cys478Ser mutation on the interactions with hCCS, hCCSD1 and HAH1 using the yeast two-hybrid system. EGY48 cells were co-transformed with pJG4.5 and p423lexAkan with or without the constructs mentioned above as the translational fusions. Each data bar represents the average of three co-transformants assayed in triplicate + SD. The amino acid sequence of hBACE1 CTD is shown and the residue mutated is underlined.

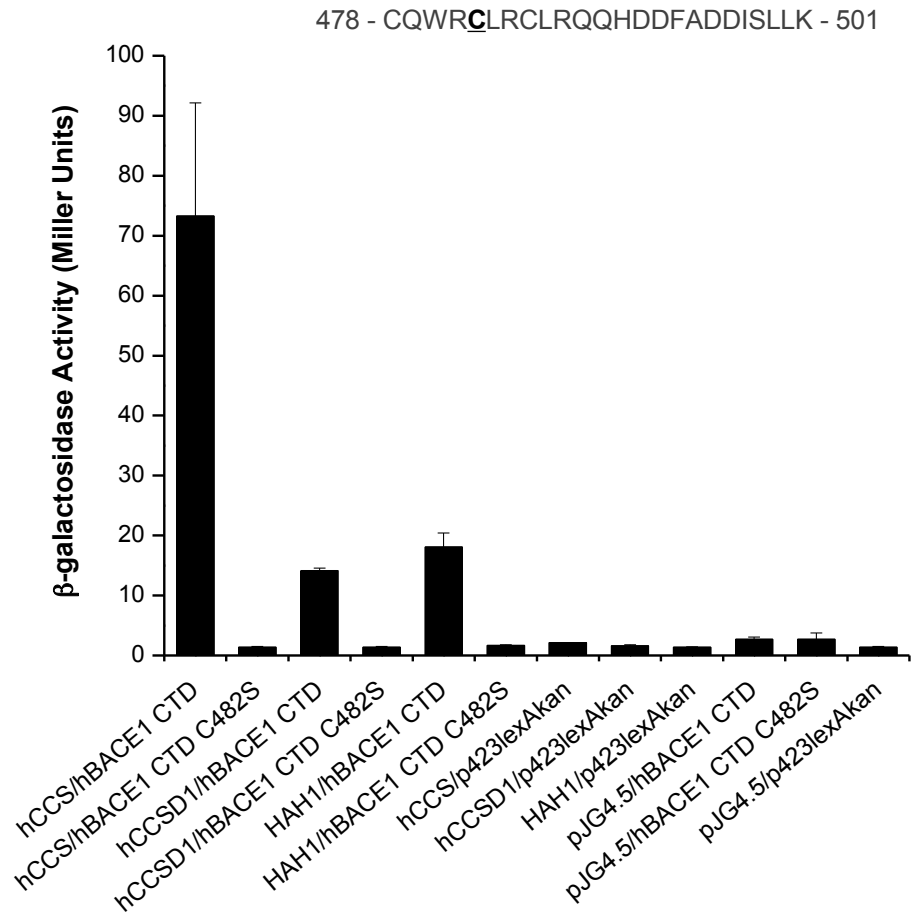

Figure 47: β-galactosidase activity assays showing the effect of hBACE1 CTD Cys482Ser mutation on the interactions with hCCS, hCCSD1 and HAH1 using the yeast two-hybrid system. EGY48 cells were co-transformed with pJG4.5 and p423lexAkan with or without the constructs mentioned above as the translational fusions. Each data bar represents the average of three co-transformants assayed in triplicate + SD. The amino acid sequence of hBACE1 CTD is shown and the residue mutated is underlined.

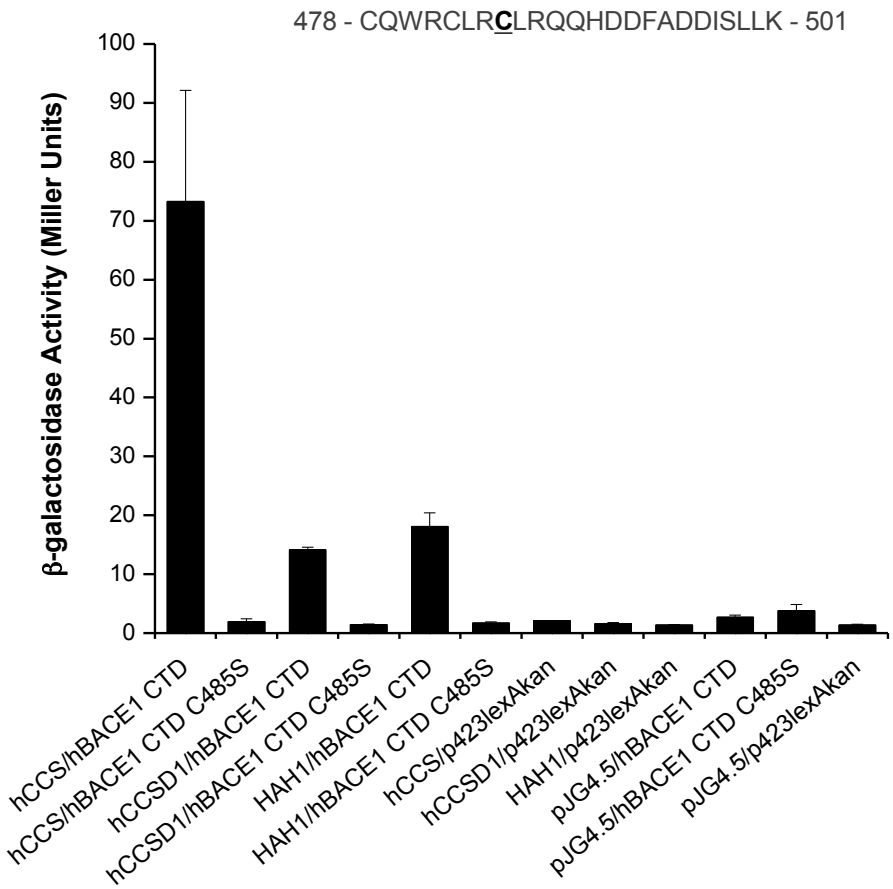

Figure 48: β-galactosidase activity assays showing the effect of hBACE1 CTD Cys485Ser mutation on the interactions with hCCS, hCCSD1 and HAH1 using the yeast two-hybrid system. EGY48 cells were co-transformed with pJG4.5 and p423lexAkan with or without the constructs mentioned above as the translational fusions. Each data bar represents the average of three co-transformants assayed in triplicate + SD. The amino acid sequence of hBACE1 CTD is shown and the residue mutated is underlined.

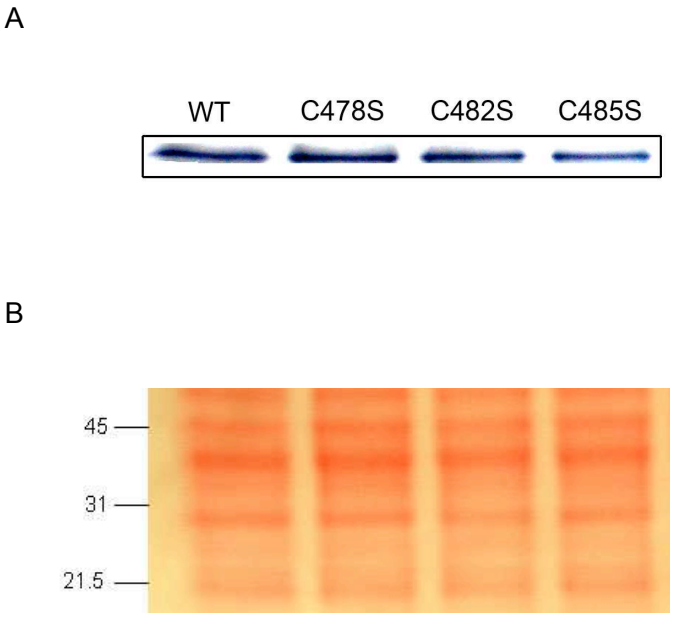

Figure 49: Western blot and Ponceau S analyses of hBACE1 CTD WT, Cys478Ser, Cys482Ser and Cys485Ser proteins with the anti-LexA antibody. Whole cell extracts from EGY48 cells co-transformed with pJG4.5_hCCS and p423lexAkan with the *hBACE1 CTD* constructs shown above as the translational fusions were analysed with the anti-LexA antibody by western blot analysis and show intense bands at ~27 kDa for the hBACE1 CTD translational fusions (A). The nitrocellulose membrane was stained with Ponceau S to determine equivalent protein loading in each lane (B). The position of the protein molecular weight markers in (B) are shown on the left in kDa.

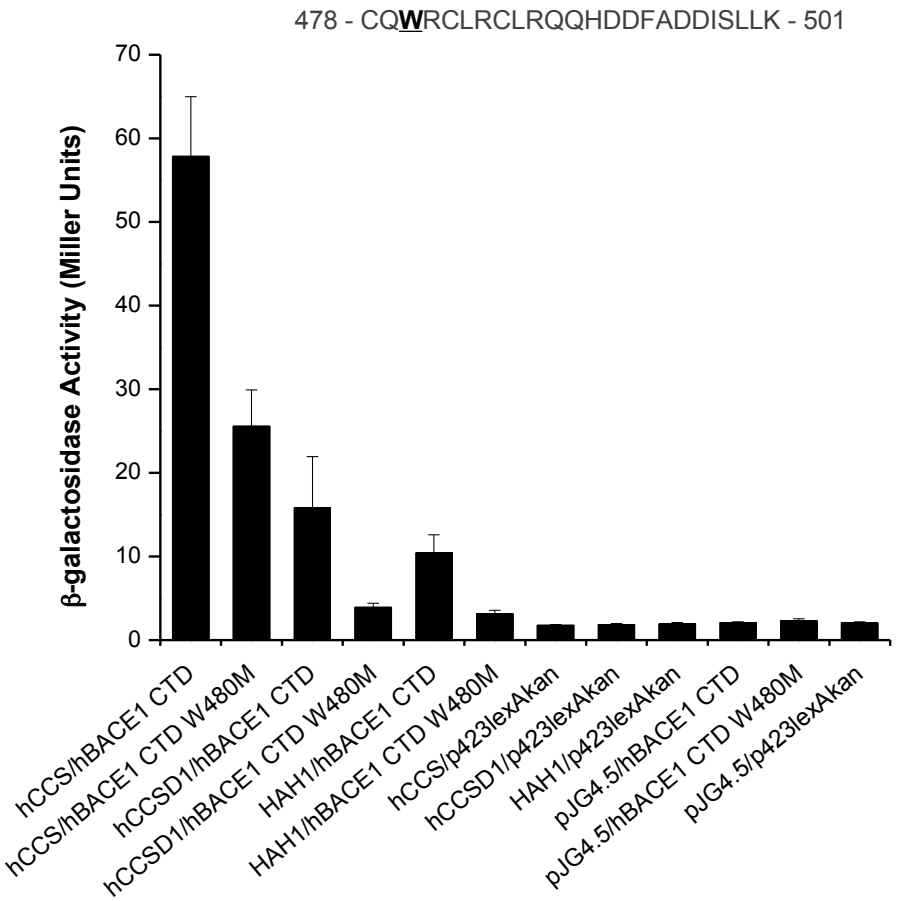

Figure 50: β-galactosidase activity assays showing the effect of hBACE1 CTD Trp480Met mutation on the interactions with hCCS, hCCSD1 and HAH1 using the yeast two-hybrid system. EGY48 cells were co-transformed with pJG4.5 and p423lexAkan with or without the constructs mentioned above as the translational fusions. Each data bar represents the average of three co-transformants assayed in triplicate + SD. The amino acid sequence of hBACE1 CTD is shown and the residue mutated is underlined.

Arg481 is one of the three Arg residues surrounding the CXXC motif in hBACE1 CTD. Arg481 was mutated to Ala to determine its influence on the interactions of hBACE1 CTD with hCCS, hCCSD1 and HAH1. As shown in Figure 51, the Arg481Ala mutation significantly decreases the interaction of hBACE1 CTD with hCCS and HAH1, and abolishes the interaction with hCCSD1. To determine if the decrease in interactions is due to the loss of positive charge in this position, the Arg481 residue was also mutated to Glu and Lys. The results obtained with the Arg481Glu mutation are similar to the Arg481Ala data, where the interactions of hBACE1 CTD with hCCS and HAH1 are significantly lower while the interaction with hCCSD1 is completely abolished (Figure 52). However, the Arg481Lys mutation leads to an ~ 2-fold increase in the interactions of hBACE1 CTD with hCCS and hCCSD1 and abolishes the interaction of hBACE1 CTD with HAH1 (Figure 51). In contrast to the results obtained with the Arg481Ala mutation, the mutation of Arg484 or Arg487 to Ala in hBACE1 CTD results in significantly increased interactions with hCCS and HAH1 (Figure 53 and Figure 54). While the Arg484Ala mutation significantly increases the interaction of hBACE1 CTD with hCCSD1 (Figure 53), the increase in β-galactosidase activity with the Arg487Ala mutant with hCCSD1 was not found to be significant (Figure 54).

All of the residues studied in hBACE1 CTD were located around the N-terminal region of the hBACE1 CTD due to their proximity to the CXXC motif. Furthermore, it has been proposed that the interaction of hCCS with hBACE1 CTD is likely mediated by the residues located in the N-terminal region of hBACE1 CTD (Rentmeister *et al.*, 2006). The C-terminal region of hBACE1 CTD – in particular the residues between Asp495 and Lys501 have been implicated in regulating the intracellular localisation of hBACE1 by undergoing post-translational modifications and interactions with other proteins (Benjannet *et al.*, 2001; Huse *et al.*, 2000; Walter *et al.*, 2001). However, there are two consecutive Asp residues in hBACE1 CTD, Asp491 and 492, which are located between the CXXC motif and the Asp495-Lys501 residues. To investigate whether the negative charge of these residues is important for the interactions of hBACE1 CTD with copper metallochaperones, both of these residues were mutated to Ala. As shown in Figure 55, mutation of Asp491 and 492 to Ala does not have a significant effect on the interactions with hCCS or hCCSD1. In contrast, the Asp491Ala,Asp492Ala mutation abolishes the interaction of hBACE1 CTD with HAH1 suggesting that these residues may be required for the interaction with HAH1 but not with hCCS (or hCCSD1). Equivalent protein expression levels are observed for all of the hBACE1 CTD mutant proteins compared to the hBACE1 CTD WT protein (Figure 56).

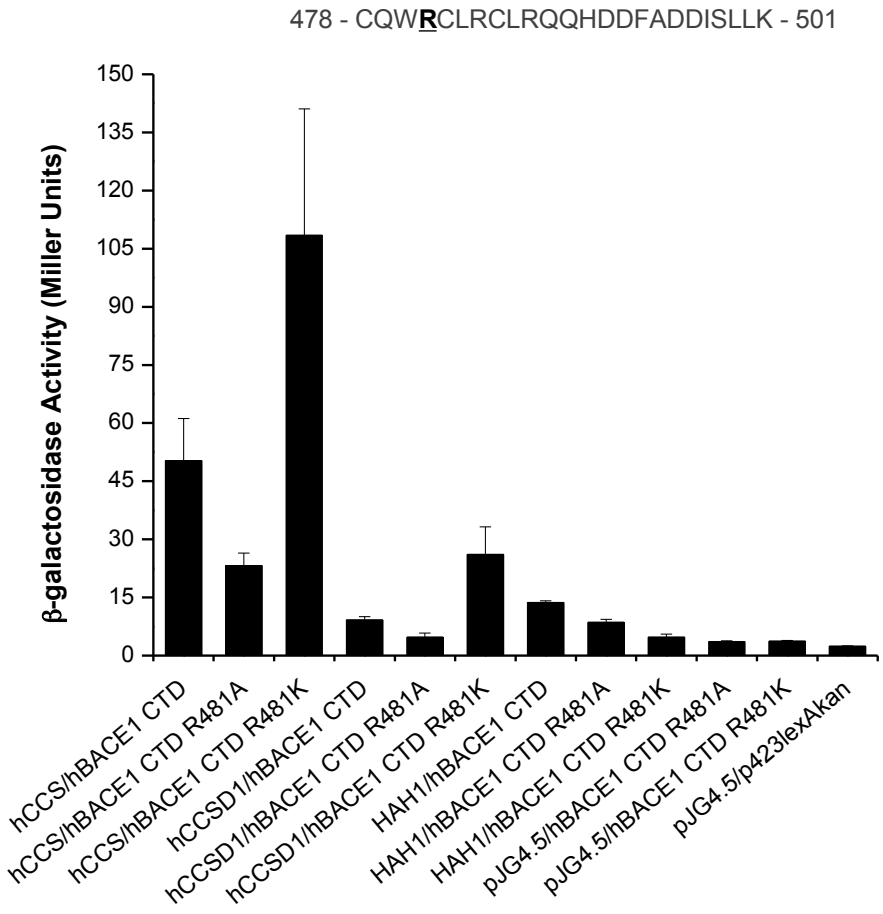

Figure 51: β-galactosidase activity assays showing the effect of hBACE1 CTD Arg481Ala and Arg481Lys mutations on the interactions with hCCS, hCCSD1 and HAH1 using the yeast two-hybrid system. EGY48 cells were co-transformed with pJG4.5 and p423lexAkan with or without the constructs mentioned above as the translational fusions. Each data bar represents the average of three co-transformants assayed in triplicate + SD. The amino acid sequence of hBACE1 CTD is shown and the residue mutated is underlined.

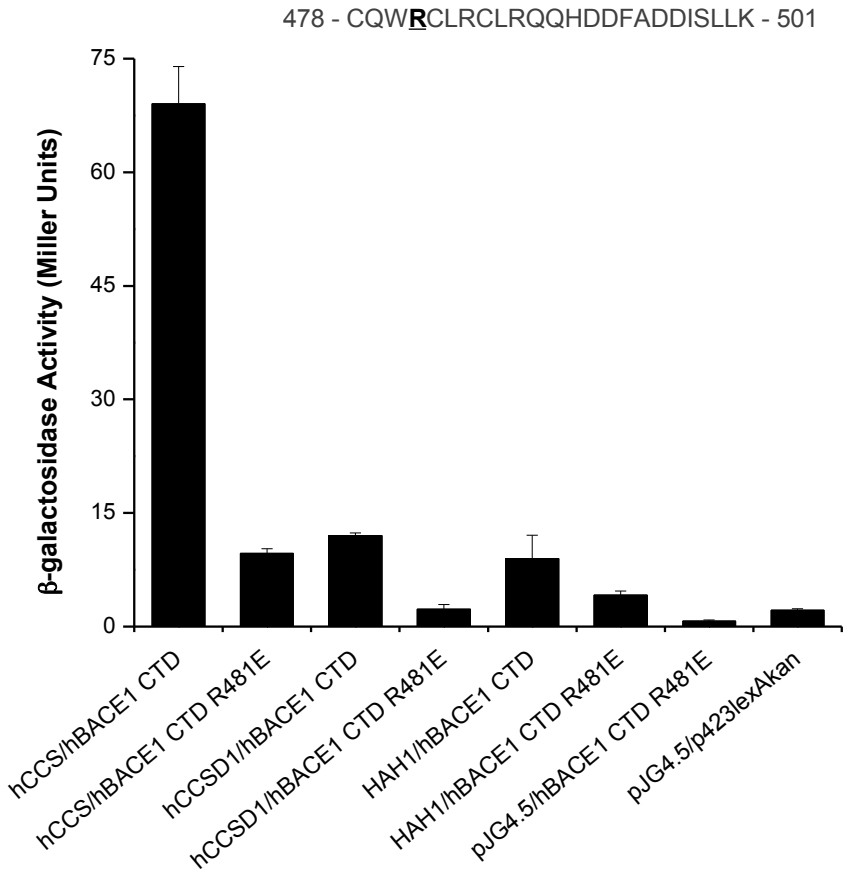

Figure 52: β-galactosidase activity assays showing the effect of hBACE1 CTD Arg481Glu mutation on the interactions with hCCS, hCCSD1 and HAH1 using the yeast two-hybrid system. EGY48 cells were co-transformed with pJG4.5 and p423lexAkan with or without the constructs mentioned above as the translational fusions. Each data bar represents the average of three co-transformants assayed in triplicate + SD. The amino acid sequence of hBACE1 CTD is shown and the residue mutated is underlined.

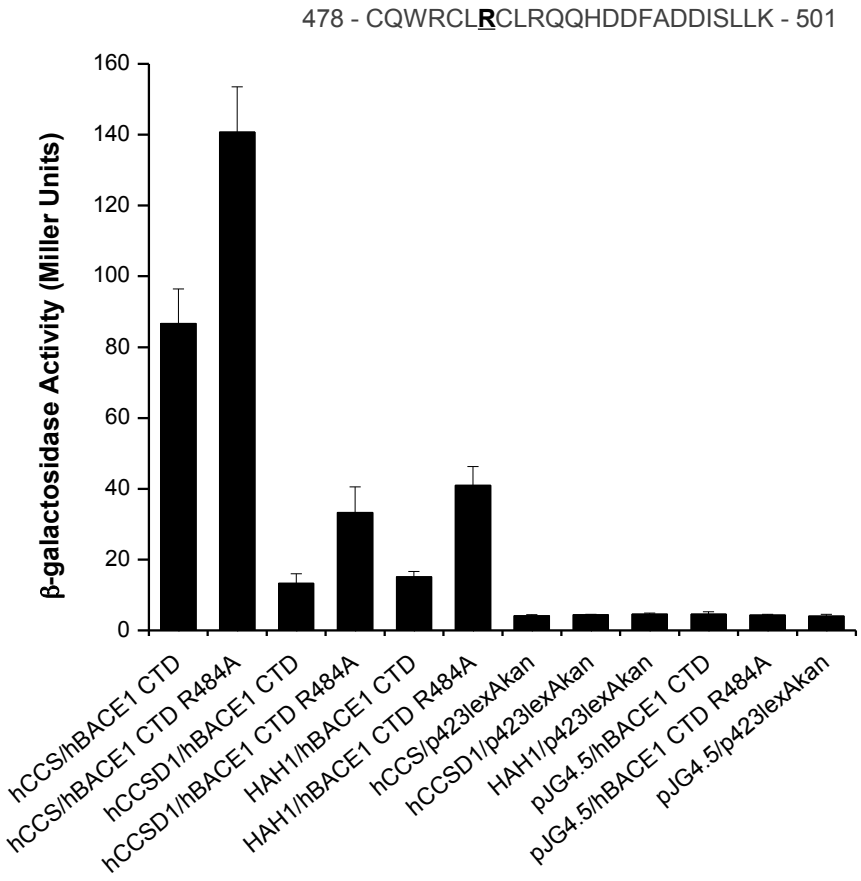

Figure 53: β-galactosidase activity assays showing the effect of hBACE1 CTD Arg484Ala mutation on the interactions with hCCS, hCCSD1 and HAH1 using the yeast two-hybrid system. EGY48 cells were co-transformed with pJG4.5 and p423lexAkan with or without the constructs mentioned above as the translational fusions. Each data bar represents the average of three co-transformants assayed in triplicate + SD. The amino acid sequence of hBACE1 CTD is shown and the residue mutated is underlined.

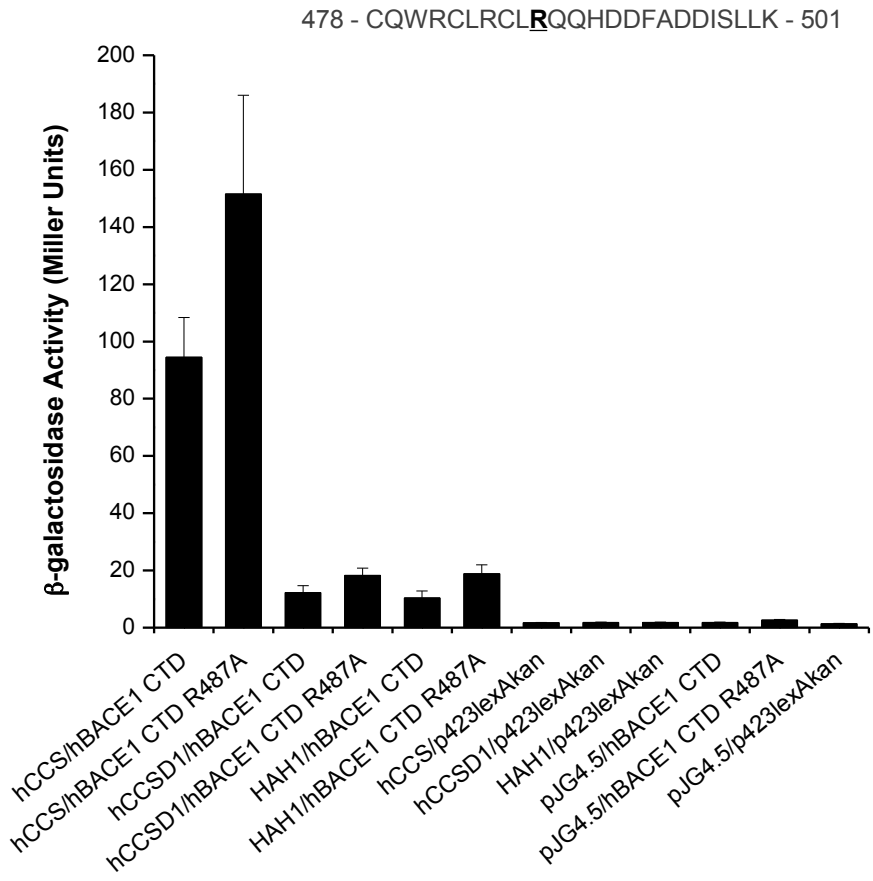

Figure 54: β-galactosidase activity assays showing the effect of hBACE1 CTD Arg487Ala mutation on the interactions with hCCS, hCCSD1 and HAH1 using the yeast two-hybrid system. EGY48 cells were co-transformed with pJG4.5 and p423lexAkan with or without the constructs mentioned above as the translational fusions. Each data bar represents the average of three co-transformants assayed in triplicate + SD. The amino acid sequence of hBACE1 CTD is shown and the residue mutated is underlined.

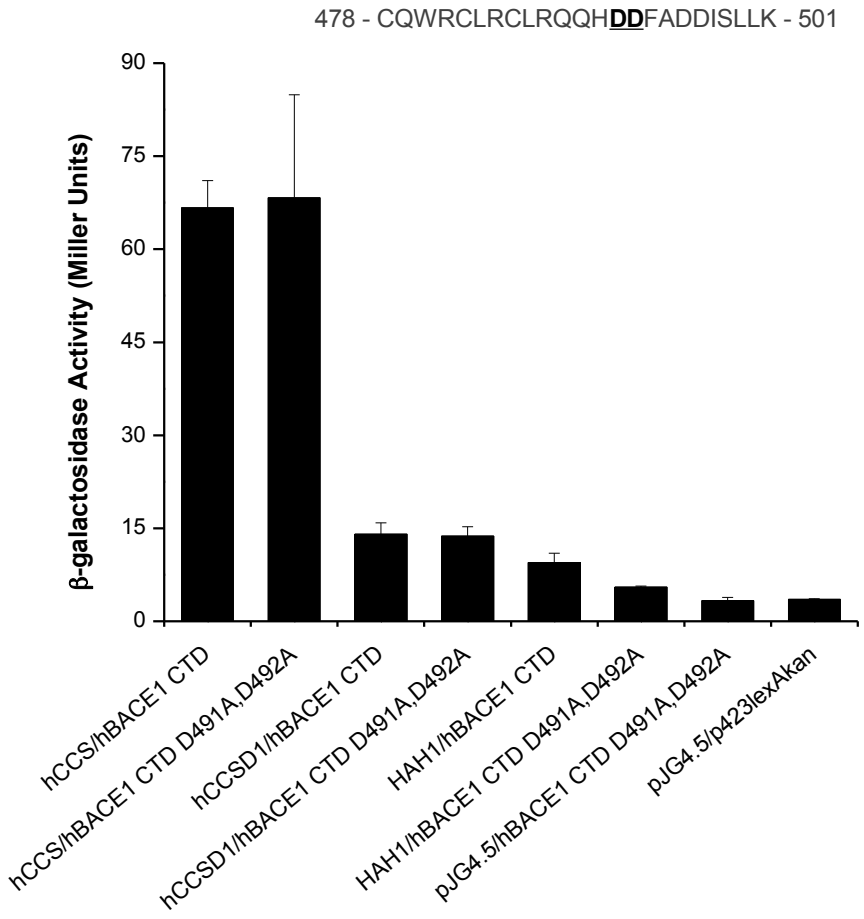

Figure 55: β-galactosidase activity assays showing the effect of hBACE1 CTD Asp491Ala,Asp492Ala mutation on the interactions with hCCS, hCCSD1 and HAH1 using the yeast two-hybrid system. EGY48 cells were co-transformed with pJG4.5 and p423lexAkan with or without the constructs mentioned above as the translational fusions. Each data bar represents the average of three co-transformants assayed in triplicate + SD. The amino acid sequence of hBACE1 CTD is shown and the residues mutated are underlined.

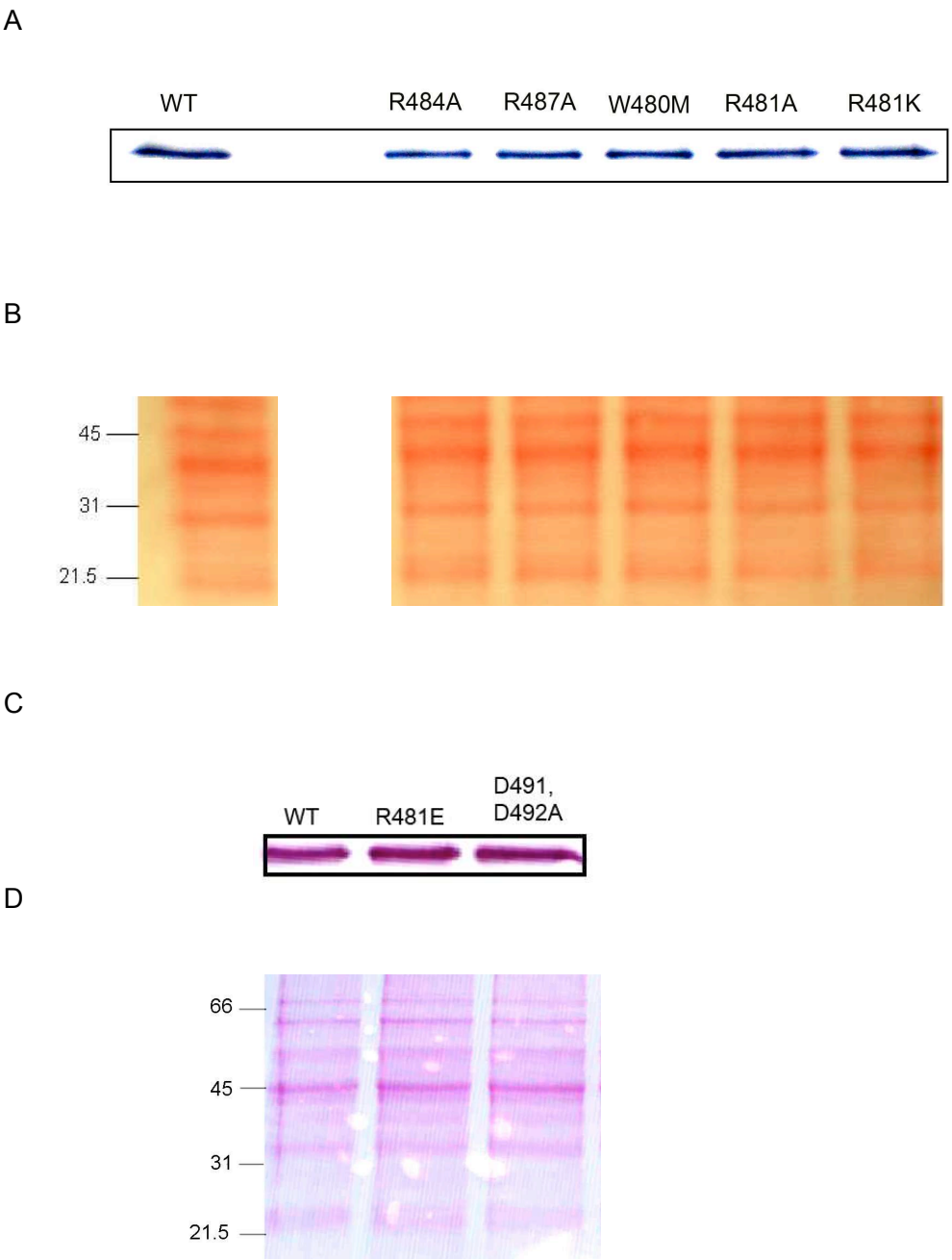

Figure 56: Western blot and Ponceau S analyses of hBACE1 CTD WT, Arg484Ala, Arg487Lys, Trp480Met, Arg481Ala, Arg481Lys, Arg481Glu and Asp491Ala,Asp492Ala proteins with the anti-LexA antibody. Whole cell extracts from EGY48 cells co-transformed with pJG4.5_hCCS and p423lexAkan with the *hBACE1 CTD* constructs shown above as the translational fusions were analysed with the anti-LexA antibody by western blot analysis. (A) and (C) show intense bands at ~27 kDa for the hBACE1 CTD translational fusions. The nitrocellulose membranes shown in (A) and (C) were stained with Ponceau S prior to immunoblotting to determine equivalent protein loading in each lane, as shown in (B) and (D) respectively. The position of the protein molecular weight markers in (B) and (D) are shown on the left in kDa.

3.2 Investigating the interaction of hSOD1 with hCCS

The yeast two-hybrid system was also used to further the understanding of the interaction of hSOD1 with hCCS. Unexpectedly, no significant interaction was observed between hSOD1 and hCCS as shown in Figure 57. Since hCCS has been shown to interact with Ccs1 and Sod1 in *S. cerevisiae* (Schmidt *et al.*, 2000), it was hypothesised that the lack of interaction between hSOD1 and hCCS may be due to interference by endogenous Ccs1 or Sod1. Hence, an EGY48 *ccs1Δ* strain, denoted as SAY1, was created where the *CCS1* gene was substituted with the KAN^R gene by homologous recombination. PCR analysis confirmed the successful substitution of *CCS1* with KAN^R in the SAY1 strain (Figure 58). pJG4.5_hSOD1 and p423lexAkan_hCCS were subsequently co-transformed in the SAY1 strain. As shown in Figure 59, a significant interaction was detected between hSOD1 and hCCS in this strain, consistent with the hypothesis that endogenous Ccs1 can interfere with the yeast two-hybrid interaction between hSOD1 and hCCS. All subsequent experiments were therefore carried out in the SAY1 strain.

3.2.1 The effect of copper concentration on the interaction of hSOD1 with hCCS

To investigate the effect of copper concentration on the interaction of hCCS with hSOD1, the co-transformants were cultured in minimal yeast medium containing copper-depleted yeast nitrogen base with BCS or $CuSO_4$ added to it. As shown in Figure 60, the presence of excess copper in the growth medium does not have a significant effect on the hSOD1/hCCS interaction. However, a two-fold increase in interaction is observed in copper-deficient conditions compared to the co-transformants cultured in basal medium. Since copper concentration can have a significant effect on the hSOD1/hCCS interaction, it was proposed that the Cu(I)-binding residues in hCCS may also be required for the interaction of hSOD1 with hCCS, as discussed below.

3.2.2 The role of hCCSD1 and hCCSD3 in mediating the interaction of hCCS with hSOD1

A previous study investigating the role of each domain in Ccs1 suggested that D1 and D3 of Ccs1 can interact with each other (Schmidt *et al.*, 1999a). The authors studied the interactions in a *ccs1Δ* strain which is auxotrophic for Lys and Met during aerobic growth due to the lack of Sod1 activity (Culotta *et al.*, 1997). The expression of Ccs1 in the *ccs1Δ* strain was shown to recover Sod1 activity and complement for these auxotrophies (Culotta *et al.*, 1997). Schmidt *et al.* (1999a) found that CcsD1 when co-expressed with a construct containing CcsD2 and CcsD3 (CcsD2,D3) increased the complementation of the Lys auxotrophy of the *ccs1Δ* strain in comparison to when CcsD1 was not co-expressed with the CcsD2,D3 construct (Schmidt *et al.*, 1999a). In addition, the “pivot, insert, release” mechanism of the CCS-dependent SOD1 activation

pathway proposes that Cu(I) is transferred from CCSD1 to CCSD3, further suggesting that CCSD1 and CCSD3 can transiently interact with each other (Rae *et al.*, 2001). To investigate this hypothesis further p423lexAkan_hCCSD3 was co-transformed with either pJG4.5_hCCS or pJG4.5_hCCSD1. However, significant interactions were not detected between either full-length hCCS and hCCSD3 or between hCCSD1 and hCCSD3 (Figure 61).

Two studies reported the formation of a Cu(I)-cluster involving the Cys residues in the CXC-motif of hCCSD3 (Stasser *et al.*, 2005; Stasser *et al.*, 2007). Stasser *et al.* (2007) also proposed that in the absence of cluster formation hCCS dimerises via intersubunit interactions between D2 of each monomer. However, the formation of D3-mediated Cu(I)-cluster in hCCS when the concentration of Cu(I) was ~ 2-fold higher than the protein concentration, was suggested by the authors to induce dimerisation via the D3 Cys residues instead of D2 (Stasser *et al.*, 2007). This change in the dimeric arrangement of hCCS was proposed to increase the availability of D2 for interaction with hSOD1 (Stasser *et al.*, 2007). On the basis of these data it was hypothesised that the copper-binding Cys residues in D3 of hCCS may contribute to the complex formation with hSOD1. To test this hypothesis, hSOD1 was co-transformed with the hCCSD3 Cys mutation proteins. As shown in Figure 62, hCCS Cys244Ser and Cys244Ser,Cys246Ser mutations do not have a significant effect on the interaction of hCCS with hSOD1. Since Cys22 and Cys25 residues in hCCS can also bind Cu(I) (Eisses *et al.*, 2000; Stasser *et al.*, 2005), the role of these residues in mediating the interaction with hSOD1 was also explored. The Cys22Ser and Cys25Ser mutations in hCCS result in slightly increased interactions with hSOD1, although these differences were not found to be significant (Figure 62). Western blot and Ponceau S analyses indicate equivalent protein expression levels for hCCS WT and mutant proteins (Figure 63).

3.2.3 The role of hCCS Arg71 in mediating the interaction with hSOD1

As discussed in section 3.1.2, Cu(I)-binding in hCCSD1 has been proposed to induce the movement of Arg71 in hCCS towards the bound metal ion. To determine the role of Arg71 in the interaction with hSOD1 the effects of mutating it to Ala, Lys or Glu were also explored. As shown in Figure 64, the presence of either Ala or Lys at this position does not have a significant effect on the interaction of hCCS with hSOD1. However, the mutation of Arg71 to Glu results in a significant decrease in the interaction with hSOD1 suggesting that a negatively charged residue in this position is not favourable for interaction. Western blot and Ponceau S analyses indicate similar expression levels for hCCS WT and Arg71 mutant proteins (Figure 63c-d).

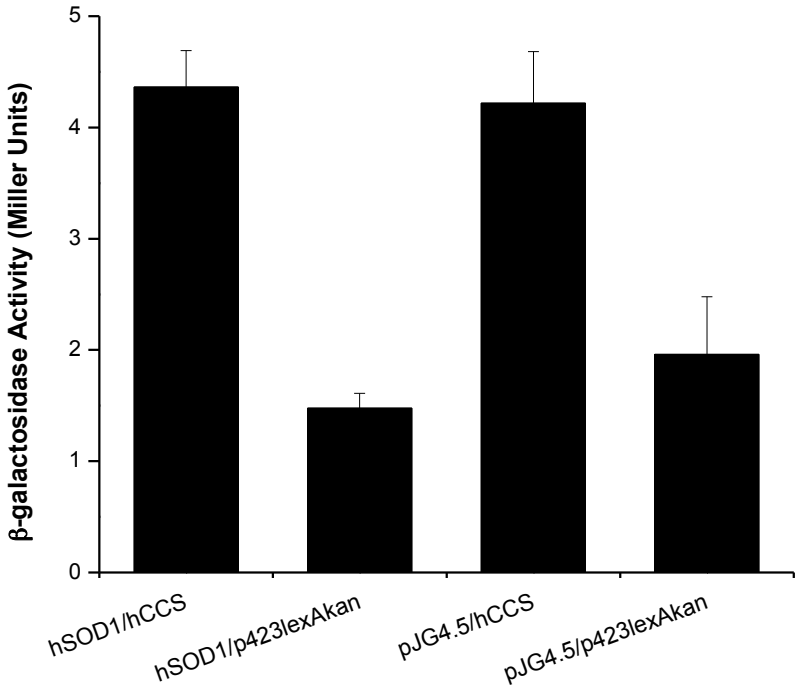

Figure 57: β-galactosidase activity assays of hSOD1 with hCCS using the yeast two-hybrid system. EGY48 cells were co-transformed with pJG4.5 and p423lexAkan with or without *hSOD1* and *hCCS* respectively, as the translational fusions. Each data bar represents the average of three co-transformants assayed in triplicate + SD.

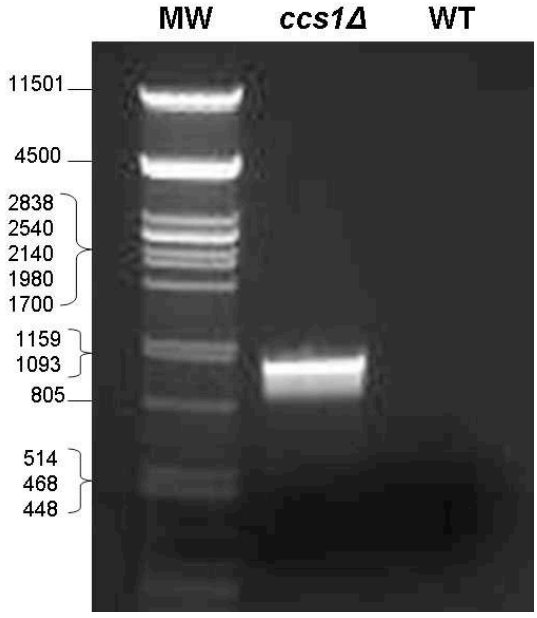

Figure 58: Agarose gel confirming the successful deletion of *CCS1* from the EGY48 strain. The SAY1 strain was created by replacing *ccs1* in EGY48 with the KAN^R gene by homologous recombination. A diagnostic PCR was performed where the genomic DNA from EGY48 and SAY1 strains were incubated with a DNA oligomer homologous to the *CCS1* promoter and a DNA oligomer homologous to KAN^R, as detailed in section 2. The presence of a DNA band at 887 bp in the lane containing genomic DNA from the SAY1 strain and the absence of a band in the lane containing genomic DNA from the EGY48 strain confirmed the successful deletion of *ccs1* from the genome. The sizes of the molecular weight markers (MW) in bp are shown above.

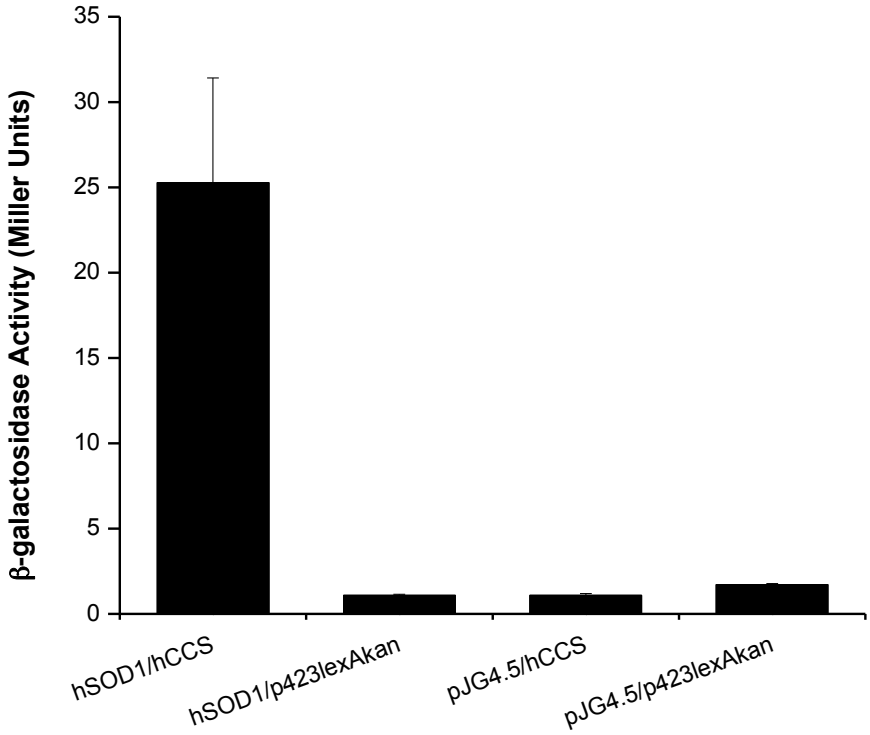

Figure 59: β-galactosidase activity assays of hSOD1 with hCCS using the yeast two-hybrid system. SAY1 cells were co-transformed with pJG4.5 and p423lexAkan with or without *hSOD1* and *hCCS* respectively, as the translational fusions. Each data bar represents the average of three co-transformants assayed in triplicate + SD.

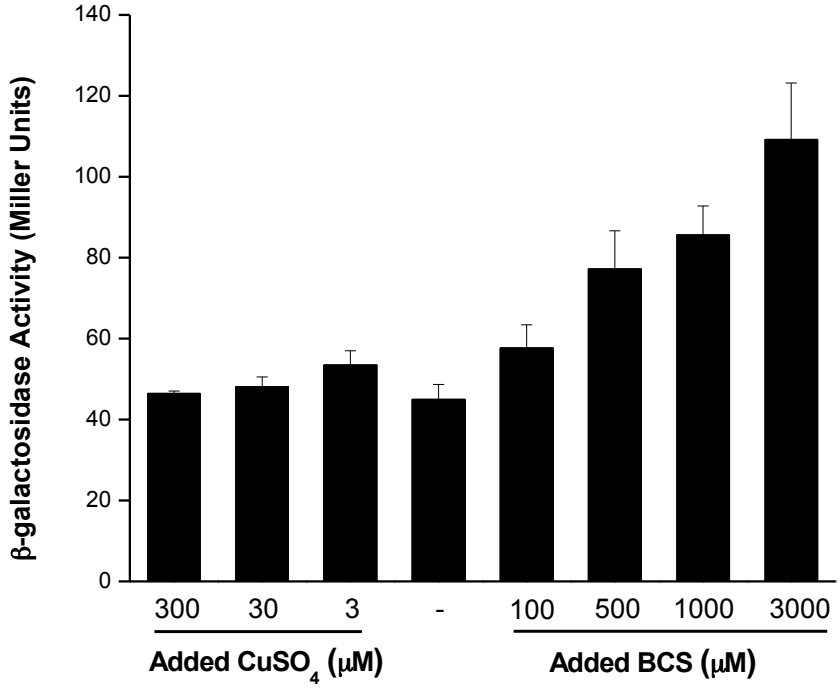

Figure 60: β-galactosidase activity assays using the yeast two-hybrid system for the co-transformants containing hSOD1 and hCCS cultured in basal medium or in medium containing $CuSO_4$ or BCS. SAY1 cells co-transformed with pJG4.5_hSOD1 and p423lexAkan_hCCS were grown with or without (-) added CuSO4 or BCS at the concentrations shown above and assayed for β-galactosidase activity. Each data bar represents the average of two co-transformants assayed in triplicate + SD.

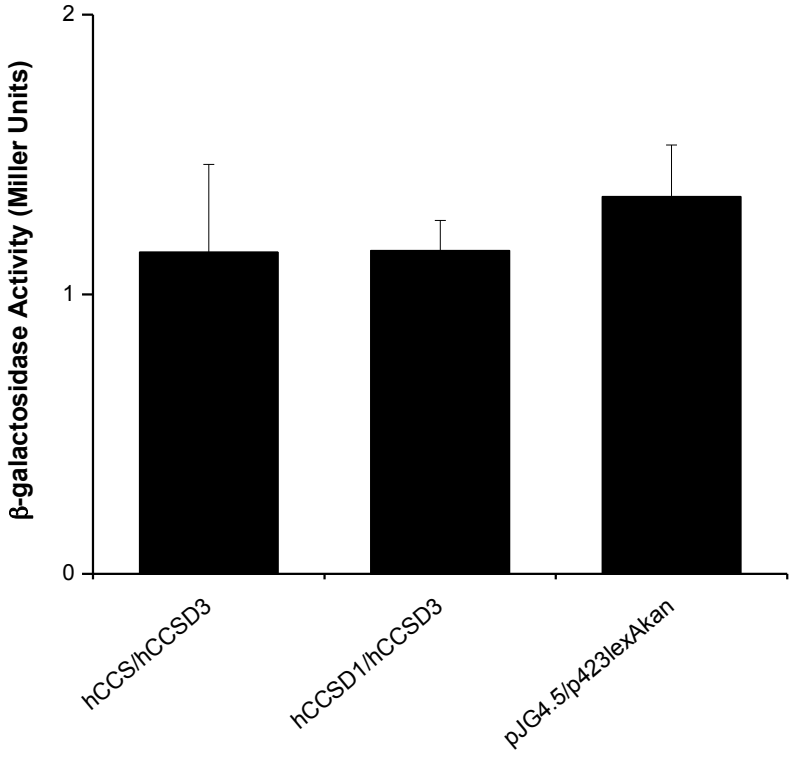

Figure 61: β-galactosidase activity assays of hCCS and hCCSD1 with hCCSD3 using the yeast two-hybrid system. EGY48 cells were co-transformed with pJG4.5 and p423lexAkan with or without the constructs mentioned above as the translational fusions. Each data bar represents the average of three co-transformants assayed in triplicate + SD cells.

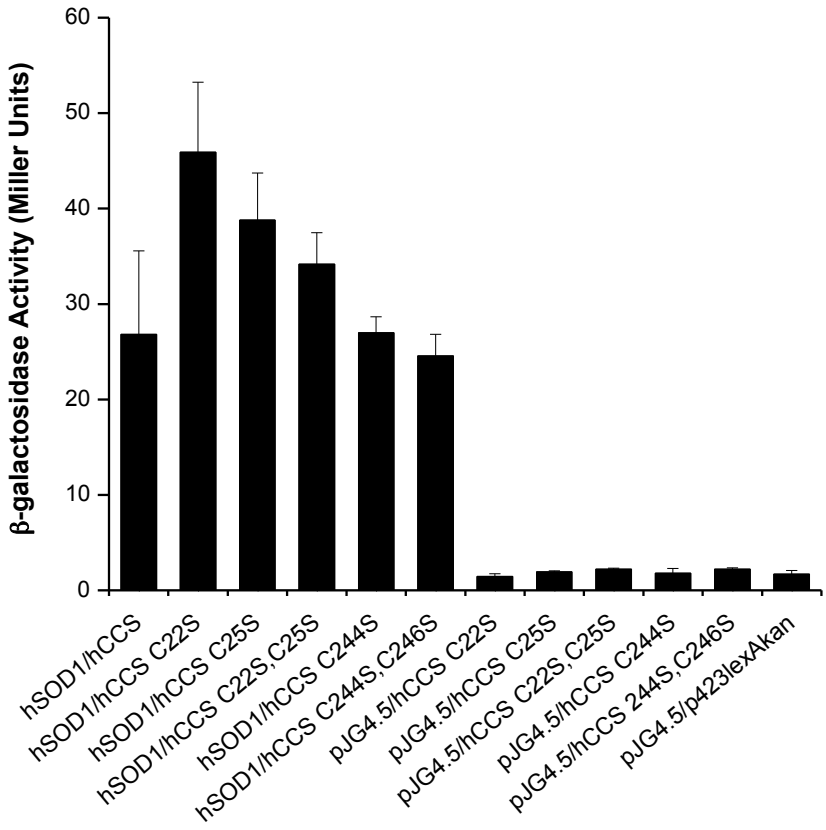

Figure 62: β-galactosidase activity assays showing the effect of hCCS Cys mutations on the interaction with hSOD1 using the yeast two-hybrid system. SAY1 cells were co-transformed with pJG4.5 and p423lexAkan with or without the constructs mentioned above as the translational fusions. Each data bar represents the average of three co-transformants assayed in triplicate + SD.

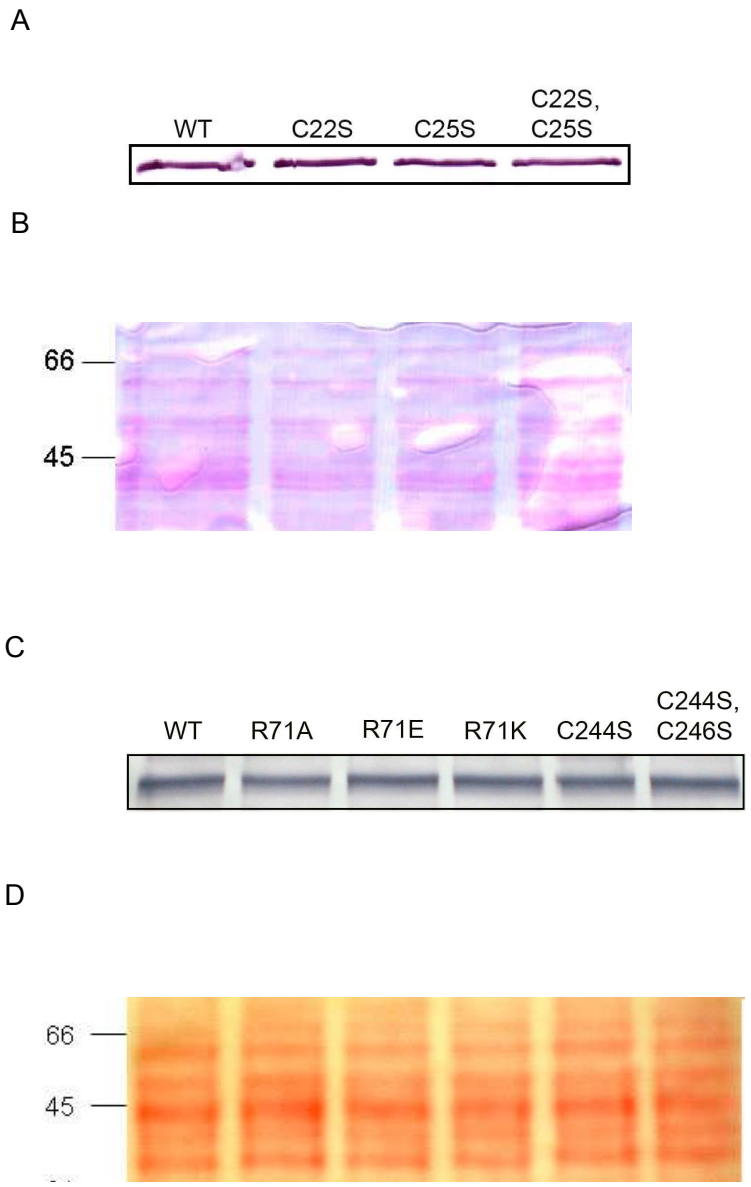

Figure 63: Western blot and Ponceau S analyses of hCCS WT, Cys22Ser, Cys25Ser, Arg71Ala, Arg71Glu, Arg71Lys, Cys244Ser and Cys244Ser,Cys246Ser proteins with the anti-LexA antibody. Whole cell extracts from SAY1 cells co-transformed with pJG4.5_hSOD1 and p423lexAkan with the hCCS constructs mentioned above as the translational fusions were analysed with the anti-LexA antibody by western blot analysis. (A) and (C) show intense bands at ~53 kDa for the hCCS translational fusions. The nitrocellulose membranes shown in (A) and (C) were stained with Ponceau S prior to immunoblotting to determine equivalent protein loading in each lane, as shown in (B) and (D) respectively. The position of the protein molecular weight markers in (B) and (D) are shown on the left in kDa.

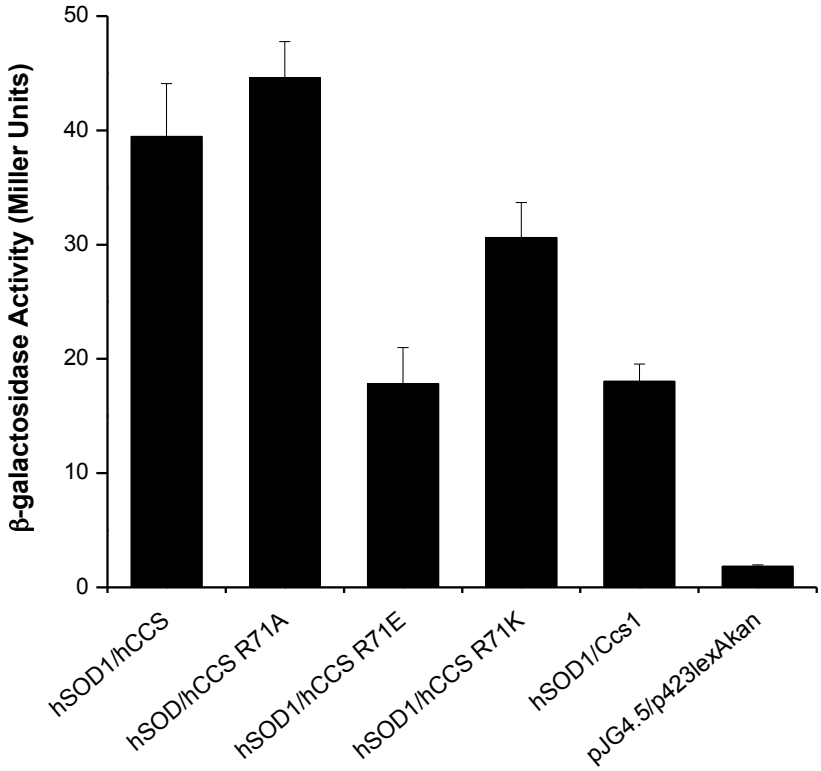

Figure 64: β-galactosidase activity assays showing the interaction of hSOD1 with hCCS WT, hCCS Arg71 mutation proteins and Ccs1 using the yeast two-hybrid system. SAY1 cells were co-transformed with pJG4.5 and p423lexAkan with or without the constructs mentioned above as the translational fusions. Each data bar represents the average of three co-transformants assayed in triplicate + SD.

In agreement with the study by Schmidt *et al.* (2000), a significant interaction was also detected between hSOD1 and Ccs1 although it is ~ 2-fold weaker than the interaction of hSOD1 with hCCS (Figure 64 and Figure 65). While the hCCS Arg71Lys mutation does not have a significant effect on the interaction with hSOD1 (Figure 64), the mutation of the analogous residue to Arg in Ccs1 (Lys66Arg) significantly increases its interaction with hSOD1 compared to the interaction of hSOD1 with Ccs1 WT protein (Figure 65). Western blot and Ponceau S analyses indicate equivalent protein expression levels for Ccs1 WT and Lys66Arg proteins (Figure 66). The results therefore suggest that the loop 5 residue in D1 of CCS may contribute in mediating the interactions with hSOD1.

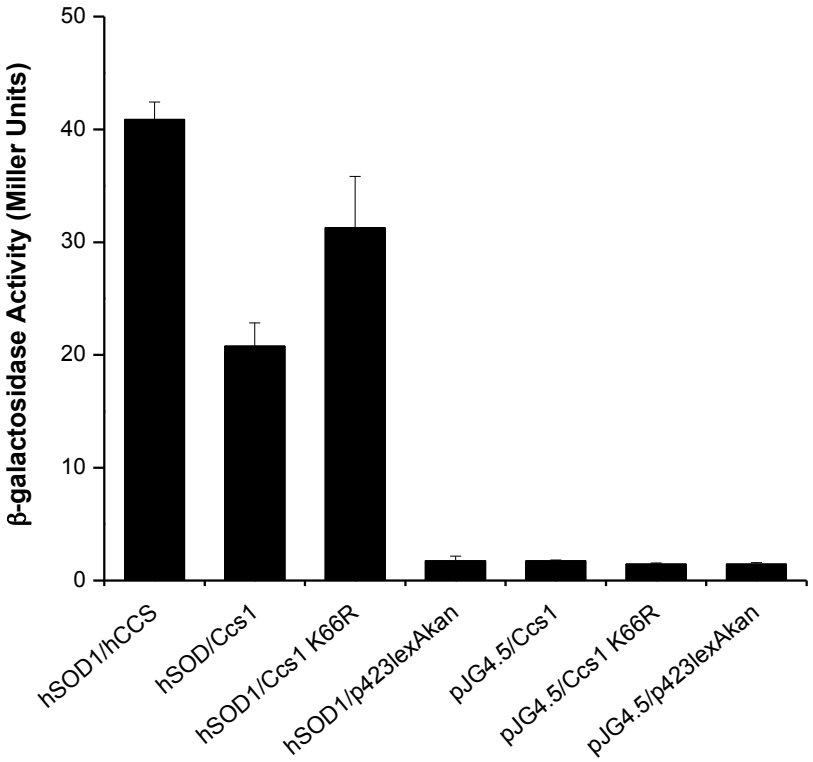

Figure 65: β-galactosidase activity assays showing the interaction of hSOD1 with hCCS, Ccs1 WT and Ccs1 Lys66Arg using the yeast two-hybrid system. SAY1 cells were co-transformed with pJG4.5 and p423lexAkan with or without the constructs mentioned above as the translational fusions. Each data bar represents the average of three co-transformants assayed in triplicate + SD.

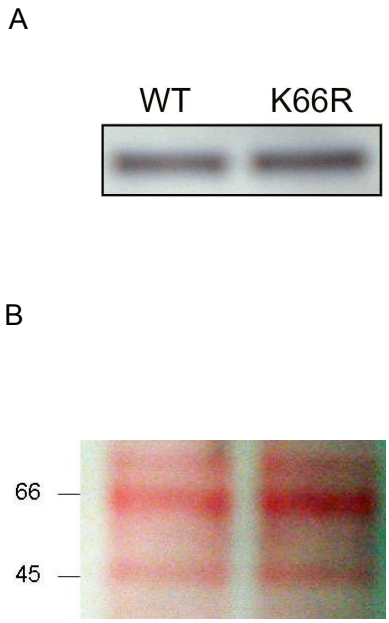

Figure 66: Western blot and Ponceau S analyses of Ccs1 WT and Lys66Arg proteins with the anti-LexA antibody. Whole cell extracts from SAY1 cells co-transformed with pJG4.5_hSOD1 and p423lexAkan with *CCS1* (WT) or *CCS1 lys66arg* as the translational fusions were analysed with the anti-LexA antibody by western blot analysis and show intense bands at ~ 52 kDa for the Ccs1 translational fusions (A). The nitrocellulose membrane was stained with Ponceau S to determine equivalent protein loading in each lane (B). The position of the protein molecular weight markers in (B) are shown on the left in kDa.

3.3 Studying the interaction of ScAtx1 with the metal-binding domains of PacS and CtaA

Since the BacterioMatch® bacterial two-hybrid system has successfully been used previously to study the interaction of ScAtx1 with the MBDs of PacS (PacS95) and CtaA (Borrelly *et al.*, 2004; Tottey *et al.*, 2002), the initial aim was to utilise the same system for studying these interactions further. While a significant interaction was detected between ScAtx1 and PacS95, the difference between the ScAtx1/PacS95 interaction and the negative controls was observed to be only ~ 2-fold (Figure 21). This difference was considered insufficient for effectively distinguishing between the effects of mutating a wide variety of amino acids in ScAtx1, PacS MBD and CtaA MBD on protein-protein interactions. Hence, the interactions of ScAtx1 with the MBDs of PacS and CtaA were explored using the yeast two-hybrid system instead. Precedents for studying the interactions between bacterial proteins using the yeast two-hybrid system are available (Lei *et al.*, 1999; Martinez-Argudo and Contreras, 2002; Pawlowski *et al.*, 2003).

3.3.1 Establishing the yeast two-hybrid system to study the interactions of ScAtx1 with the MBDs of PacS and CtaA

In order to establish the yeast two-hybrid system for studying the interaction of ScAtx1 with the PacS MBD, ScAtx1 was cloned in both pJG4.5 and p423lexAkan vectors. The structures of apo- (Banci *et al.*, 2006c) and Cu(I)-PacS MBD (Badarau *et al.*, 2010) show that the first 71 amino acids of PacS represent the ferredoxin-fold. Hence, only residues 1-71 of PacS, denoted here as $PacS_N$, were cloned into the yeast two-hybrid vectors. As shown in Figure 67, a significant interaction was detected between ScAtx1 and $PacS_N$ when ScAtx1 was cloned into the pJG4.5 vector and $PacS_N$ was cloned into the p423lexAkan vector, but not when cloned in the reverse order. Such “directionality” when studying protein-protein interactions using the yeast two-hybrid system has been reported previously. It is usually attributed to potential differences in protein folding due to the expression of the desired protein as a fusion complex with the two-hybrid DNA-binding and activation domain components (Estojak *et al.*, 1995; Kaufmann *et al.*, 2005). Subsequent experiments were performed by cloning all of the ScAtx1 constructs in pJG4.5 and $PacS_N$ constructs in p423lexAkan. To use ScAtx1 in the pJG4.5 vector, CtaA MBD was cloned into the p423lexAkan vector, as for $PacS_N$. Initially a CtaA MBD construct comprising residues 1-111 (CtaA111), similar to the construct used by Tottey *et al.* (2002) for bacterial two-hybrid studies, was cloned in the p423lexAkan vector. However, no significant interaction was detected between ScAtx1 and CtaA111 (Figure 68). The submission of the CtaA111 sequence into the Swiss PDB modelling software (http://swissmodel.expasy.org) revealed that only residues 25-91 are involved in forming the ferredoxin-fold. Therefore, a truncated construct containing CtaA residues 1-92 (CtaA92) was cloned in the p423lexAkan vector. As shown in Figure 68, a

significant interaction is observed between ScAtx1 and CtaA92. Hence, the CtaA92 construct, hereon denoted as $CtaA_N$, was used for all subsequent experiments in this study.

3.3.2 The effect of copper concentration on the interactions of ScAtx1 with $PacS_N$ and $CtaA_N$

Tottey *et al.* (2002) have previously shown that the bacterial two-hybrid interaction of ScAtx1 with PacS95 and CtaA111 is dependent upon the Cys residues in the CXXC motif of ScAtx1. In addition, Banci *et al.* (2006c) found that the addition of 1 mM BCS dissociated the ScAtx1-Cu(I)-PacS95 complex into apo-proteins. As mentioned previously (section 3.1), the interactions between homologous proteins have also been shown to be dependent on the presence of Cu(I). These data led to the hypothesis that the interactions of ScAtx1 with $PacS_N$ and $CtaA_N$ may also be dependent upon the intracellular Cu(I) concentration. To investigate the effect of copper concentration on the protein-protein interactions, the co-transformants containing ScAtx1 and $PacS_N$ or ScAtx1 and $CtaA_N$ were incubated in various concentrations of $CuSO_4$ or BCS and assayed for β-galactosidase activity. As shown in Figure 69, the addition of 30 μM or 300 μM $CuSO_4$ results in a small, albeit significant decrease in the interaction of ScAtx1 with $PacS_N$ compared to the co-transformants incubated in the basal medium. The interaction of ScAtx1 with $PacS_N$ also decreases significantly in the presence of 500 μM BCS compared to the co-transformants incubated in the basal medium. However, no significant change was evident in the β-galactosidase activity between the ScAtx1/$PacS_N$ co-transformants cultured in higher concentrations of BCS (1 mM or 3 mM) in comparison to the co-transformants incubated in the basal medium.

In contrast to ScAtx1/$PacS_N$ interaction, the addition of BCS results in increased interaction between ScAtx1 and $CtaA_N$ (Figure 70). The addition of 300 μM $CuSO_4$ to the growth medium also results in a significant decrease in the interaction between ScAtx1 and $CtaA_N$ compared to the co-transformants grown in the basal medium (Figure 70). The data therefore indicate that the interaction of ScAtx1 with both $PacS_N$ and $CtaA_N$ decreases in the presence of high concentration of added $CuSO_4$ (300 μM). While the addition of BCS significantly increases the interaction between ScAtx1 and $CtaA_N$, the effect of low copper concentration on the interaction of ScAtx1 and $PacS_N$ is inconclusive since this interaction was only disrupted in the presence of 500 μM BCS.

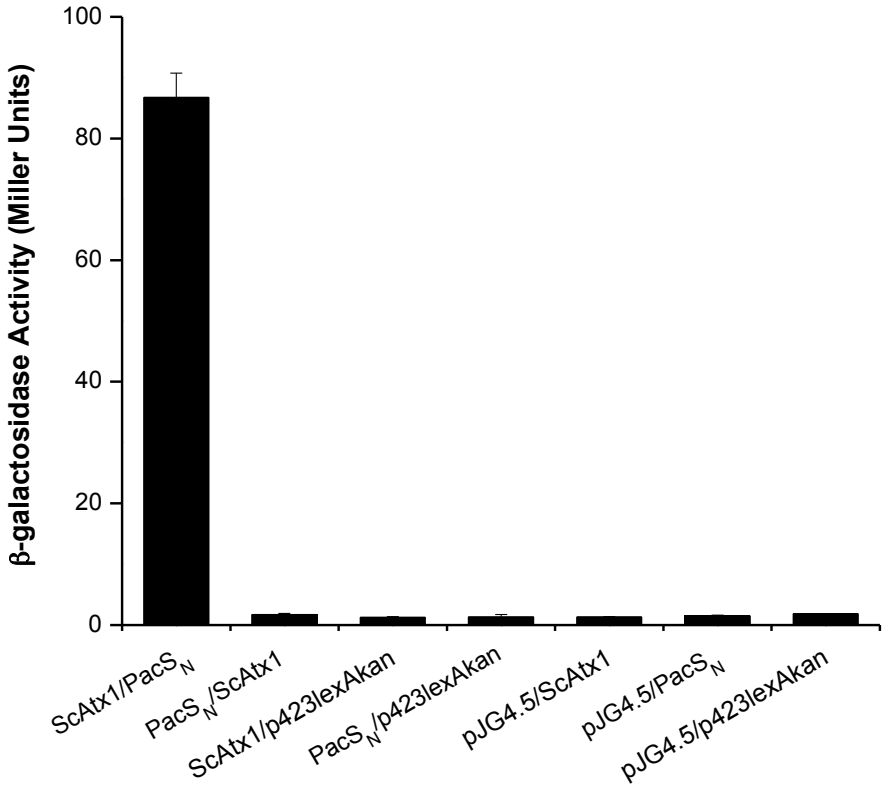

Figure 67: β-galactosidase activity assays of ScAtx1 with PacS$_N$ using the yeast two-hybrid system. EGY48 cells were co-transformed with pJG4.5 and p423lexAkan with or without the constructs mentioned above as the translational fusions. Each data bar represents the average of three co-transformants assayed in triplicate + SD.

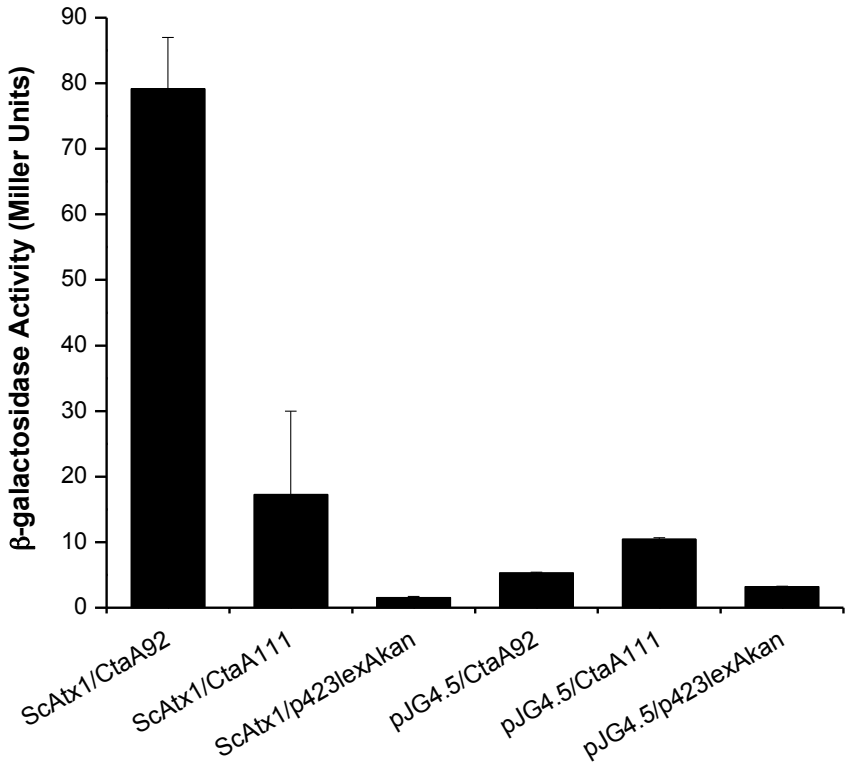

Figure 68: β-galactosidase activity assays of ScAtx1 with CtaA92 or CtaA111 using the yeast two-hybrid system. EGY48 cells were co-transformed with pJG4.5 and p423lexAkan with or without the constructs mentioned above as the translational fusions. Each data bar represents the average of three co-transformants assayed in triplicate + SD.

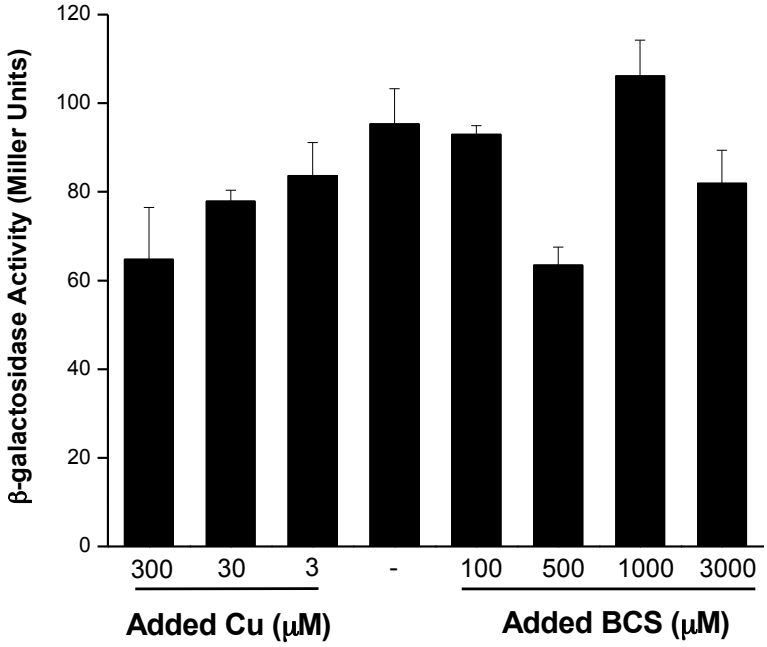

Figure 69: β-galactosidase activity assays using the yeast two-hybrid system for the co-transformants containing ScAtx1 and $PacS_N$ cultured in basal medium or in medium containing BCS or $CuSO_4$. EGY48 cells co-transformed with pJG4.5_ScAtx1 and p423lexAkan_$PacS_N$ were grown with or without (-) added CuSO4 or BCS at the concentrations shown above and assayed for β-galactosidase activity. Each data bar represents the average of two co-transformants assayed in triplicate + SD.

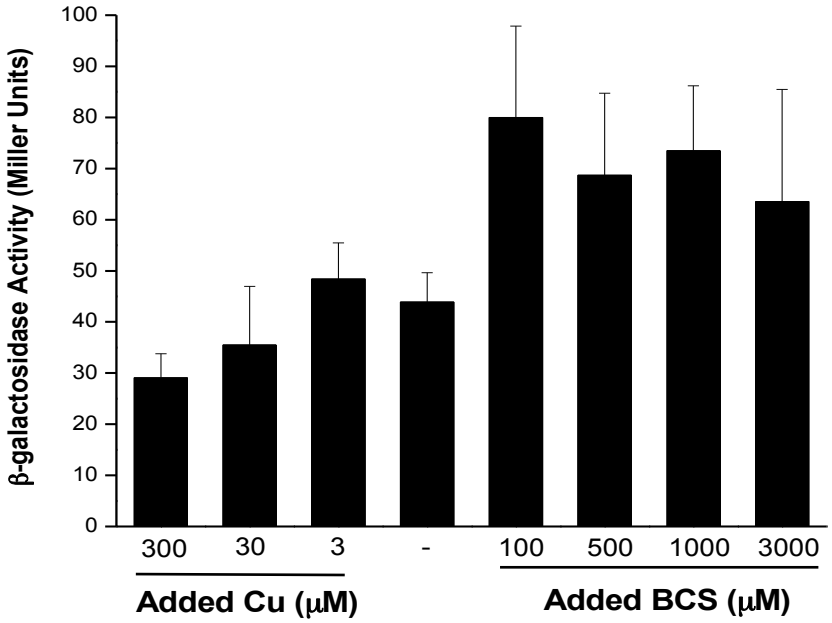

Figure 70: β-galactosidase activity assays using the yeast two-hybrid system for the co-transformants containing ScAtx1 and $CtaA_N$ cultured in basal medium or in medium containing BCS or $CuSO_4$. EGY48 cells co-transformed with pJG4.5_ScAtx1 and p423lexAkan_$CtaA_N$ were grown with or without (-) added CuSO4 or BCS at the concentrations shown above and assayed for β-galactosidase activity. Each data bar represents the average of two co-transformants assayed in triplicate + SD.

3.3.3 The role of residues surrounding the CXXC motif of ScAtx1, $PacS_N$ and $CtaA_N$ in mediating protein-protein interactions

Since the copper-binding Cys ligands in the CXXC motif of ScAtx1 have been shown to be essential for the interaction with $PacS_N$ and $CtaA_N$ (Tottey *et al.*, 2002), it was proposed that the residues located close to the CXXC motif in these proteins may also influence the interactions between these proteins. This hypothesis is further supported by the HADDOCK model of the ScAtx1-PacS95 complex which indicates that the residues around the metal-binding sites may be involved in complex formation (Banci *et al.*, 2006c). To investigate this hypothesis some of the residues adjacent to the CXXC motifs of ScAtx1, $PacS_N$ and $CtaA_N$ were mutated to determine their roles in protein-protein interactions. Arg13 in $PacS_N$ has been shown to be important for mediating the interaction with ScAtx1 (Banci *et al.*, 2010b). The Arg13Asp mutation in $PacS_N$ abolished the bacterial two-hybrid interaction with ScAtx1 (Banci *et al.*, 2010b). The corresponding residue is Ala in ScAtx1 (Ala11), as shown in Figure 71. To determine the effect of a positive charge in that position, $PacS_N$ Arg13 was mutated to Ala. The $PacS_N$ Arg13Ala mutation results in ~ 5-fold decrease in the interaction with ScAtx1 compared to the interaction of $PacS_N$ WT protein with ScAtx1 (Figure 72). The mutation of the analogous residue in $CtaA_N$, Lys34 to Ala abolishes the interaction with ScAtx1 (Figure 73). The mutation of ScAtx1 Ala11 to either Lys or Arg also results in significantly decreased interactions with $PacS_N$ and $CtaA_N$ (Figure 74).

The presence of an intermolecular hydrogen bond between the side chains of Glu13 in ScAtx1 and Cys14 in PacS95 was also reported in the modelled complex (Banci *et al.*, 2006c). The mutation of ScAtx1 Glu13 to either Ala or Gln was found to abolish the bacterial two-hybrid interaction with PacS95 (Banci *et al.*, 2006c). To determine if ScAtx1 Glu13 is also involved in mediating the interaction of ScAtx1 with $CtaA_N$, this residue was mutated to either Ala or Gln. For comparative purposes the effects of these mutations on the interaction with $PacS_N$ was also studied. In agreement with the previous findings, the mutation of Glu13 to either Ala or Gln results in significantly decreased interaction of ScAtx1 with $PacS_N$ (Figure 75a) confirming that the results obtained with the yeast two-hybrid system are comparable with the bacterial two-hybrid data. Unlike the previous study (Banci *et al.*, 2006c), significant differences are evident between the effects of the two mutations on the interaction with $PacS_N$. While the ScAtx1 Glu13Ala mutation results in ~ 4-fold decrease, the Glu13Gln mutation leads to only ~ 2-fold decrease in the interaction with $PacS_N$ compared to the interaction with ScAtx1 WT protein (Figure 75). Similarly, the ScAtx1 Glu13Gln mutation results in ~ 3-fold decrease in interaction, whereas the Glu13Ala mutation abolishes the interaction of ScAtx1 with $CtaA_N$ (Figure 76). Western blot and Ponceau S analyses indicate that the mutation of the above mentioned residues does not have an aberrant effect on the protein expression levels (Figure 77 and Figure 78).

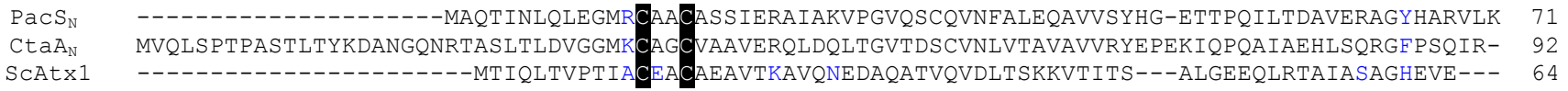

Figure 71: Sequence alignment of the PacS$_N$, CtaA$_N$ and ScAtx1 yeast two-hybrid constructs investigated in this study. Shown above is the amino acid sequence alignment for PacS$_N$, CtaA$_N$ and ScAtx1. Cys residues in the CXXC motif are highlighted in black while the other residues mutated in this study are shown in blue.

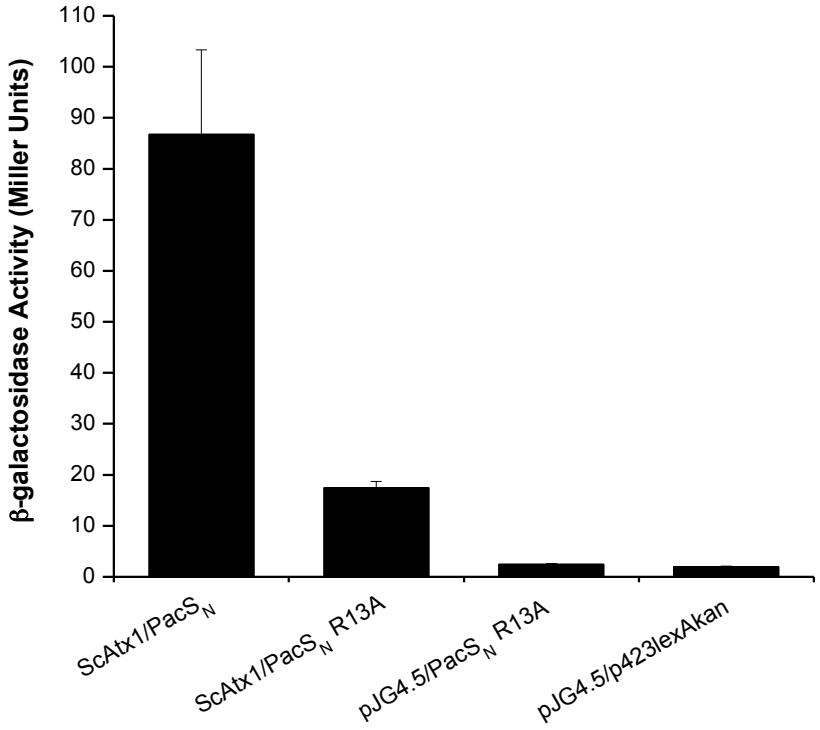

Figure 72: **β-galactosidase activity assays showing the effects of PacS$_N$ Arg13Ala mutation on the interaction with ScAtx1 using the yeast two-hybrid system.** EGY48 cells were co-transformed with pJG4.5 and p423lexAkan, with or without the constructs mentioned above, as the translational fusions. Each data bar represents the average of three co-transformants assayed in triplicate + SD.

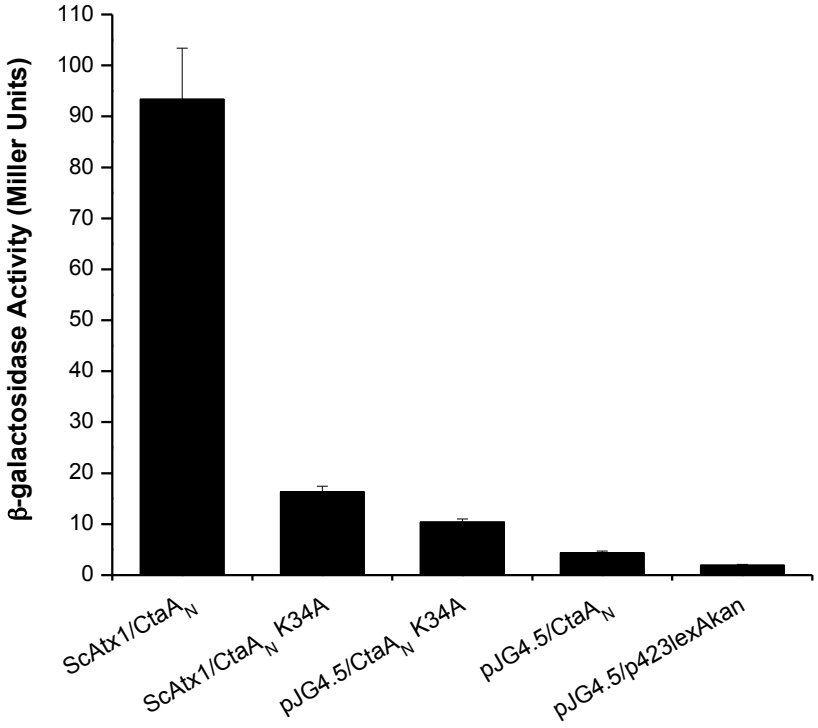

Figure 73: β-galactosidase activity assays showing the effects of CtaA$_N$ Lys34Ala mutation on the interaction with ScAtx1 using the yeast two-hybrid system. EGY48 cells were co-transformed with pJG4.5 and p423lexAkan with or without the constructs mentioned above as the translational fusions. Each data bar represents the average of three co-transformants assayed in triplicate + SD.

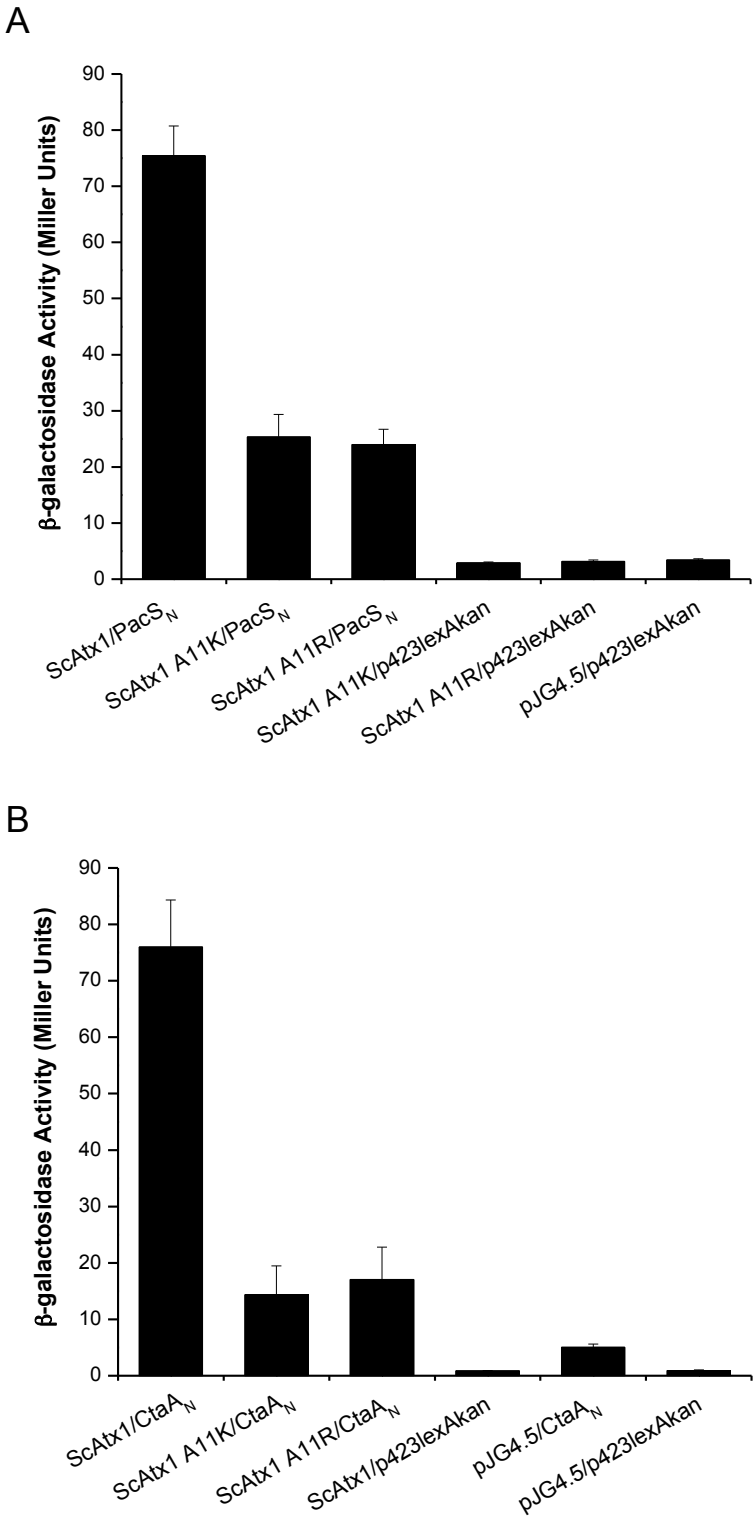

Figure 74: β-galactosidase activity assays showing the effects of ScAtx1 Ala11 mutations on the interactions with $PacS_N$ and $CtaA_N$ using the yeast two-hybrid system. EGY48 cells were co-transformed with pJG4.5 with or without the *scAtx1* constructs mentioned above and p423lexAkan with or without $pacS_N$ (A) or $ctaA_N$ (B) as the translational fusions. Each data bar represents the average of three co-transformants assayed in triplicate + SD.

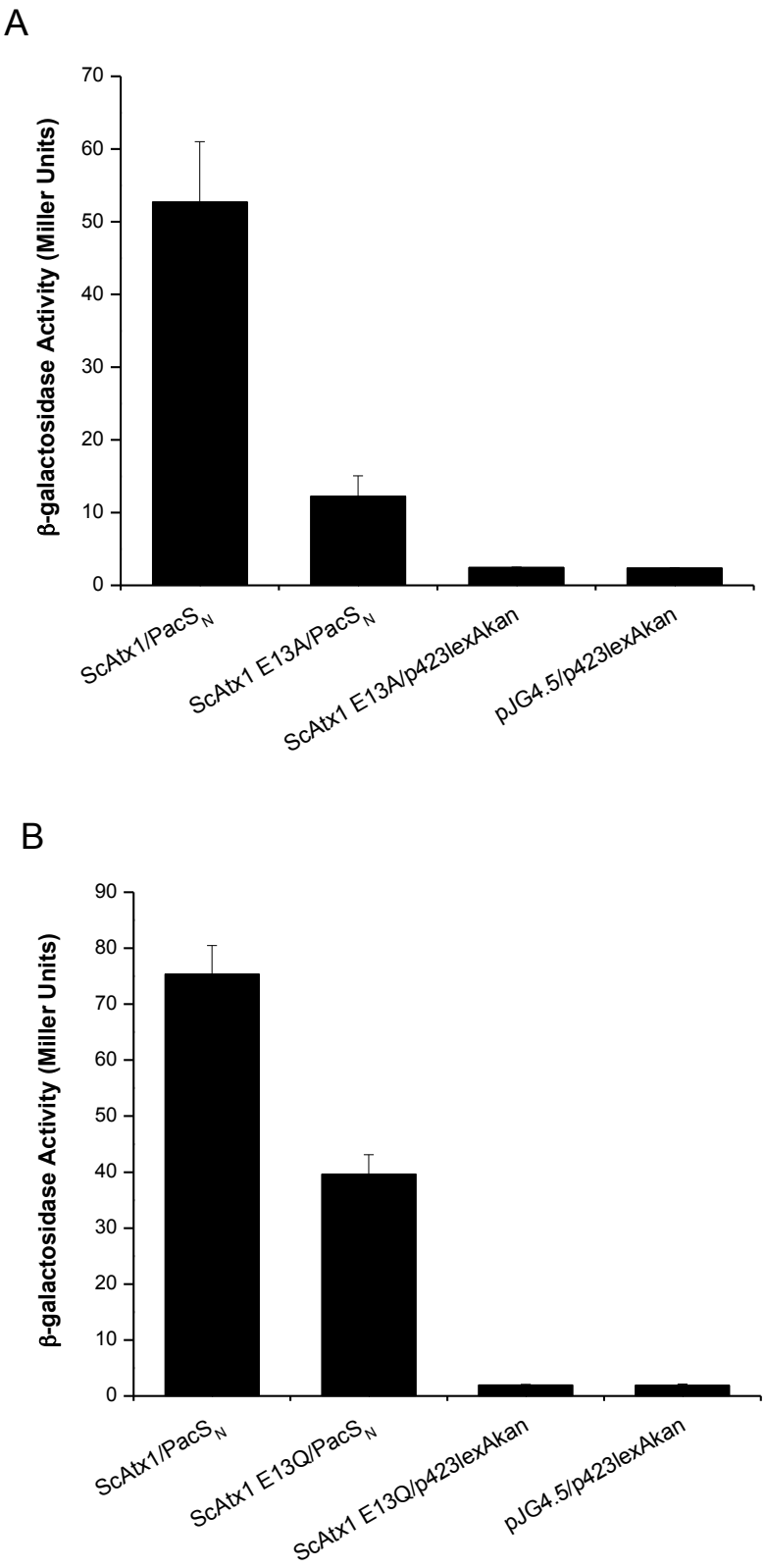

Figure 75: β-galactosidase activity assays showing the effects of ScAtx1 Glu13 mutations on the interactions with $PacS_N$ using the yeast two-hybrid system. EGY48 cells were co-transformed with p423lexAkan with or without *pacS$_N$* and pJG4.5 with or without *scAtx1*, *scAtx1 glu13ala* (A) or *scAtx1 glu13gln* (B) as the translational fusions. Each data bar represents the average of three co-transformants assayed in triplicate + SD.

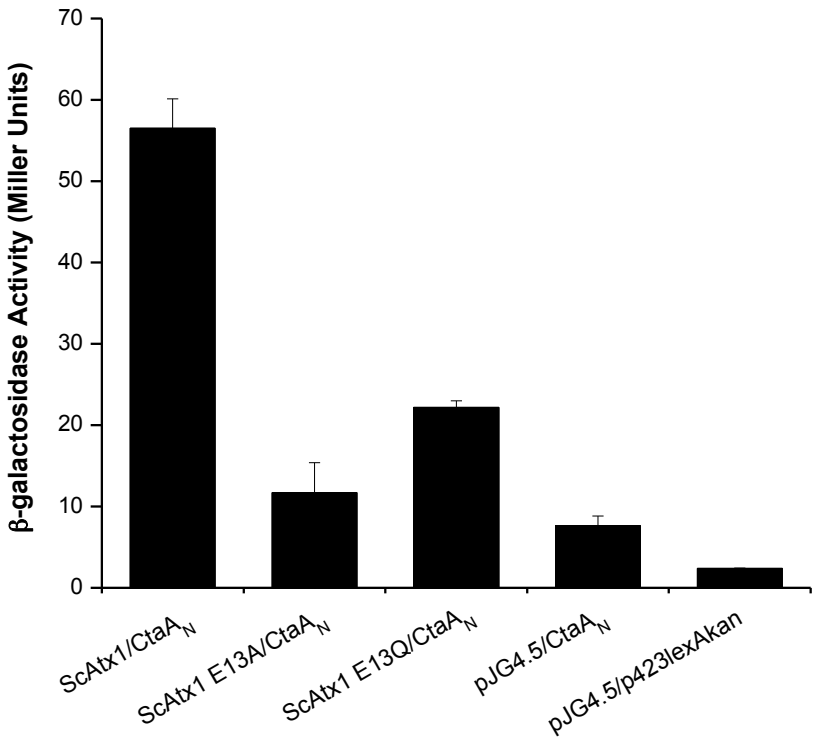

Figure 76: β-galactosidase activity assays showing the effect of ScAtx1 Glu13 mutation on the interaction with CtaA$_N$ using the yeast two-hybrid system. EGY48 cells were co-transformed with pJG4.5 and p423lexAkan with or without the constructs mentioned above as the translational fusions. Each data bar represents the average of three co-transformants assayed in triplicate + SD.

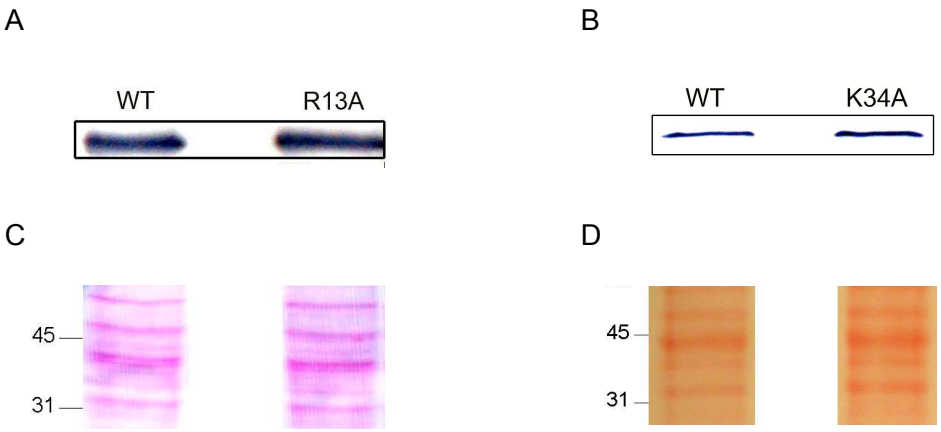

Figure 77: Western blot and Ponceau S analyses of $PacS_N$ WT and Arg13Ala, and $CtaA_N$ WT and Lys34Ala proteins with the anti-LexA antibody. Whole cell extracts from EGY48 cells co-transformed with pJG4.5_ScAtx1 and p423lexAkan with the *$pacS_N$* (A) or *$ctaA_N$* (B) constructs as the translational fusions were analysed with the anti-LexA antibody by western blot analysis. The intense bands in (A) at ~32 kDa represent the $PacS_N$ translational fusions, while the intense bands at ~ 34 kDa in (B) represent the $CtaA_N$ translational fusions. The nitrocellulose membranes from (A) and (B) were stained with Ponceau S prior to immunoblotting to determine equivalent protein loading in each lane, as shown in (C) and (D) respectively. The position of the protein molecular weight markers in (C) and (D) are shown on the left in kDa.

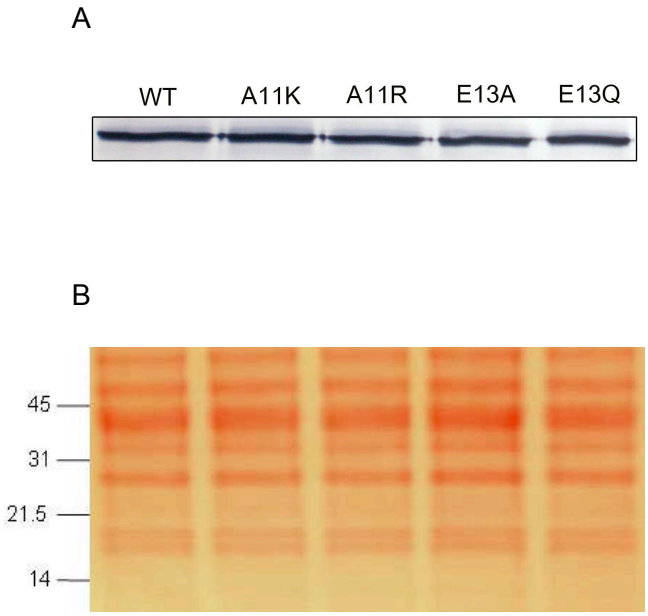

Figure 78: Western blot and Ponceau S analyses of ScAtx1 WT, Ala11Lys, Ala11Arg, Glu13Ala and Glu13Gln proteins with the anti-HA antibody. Whole cell extracts from EGY48 cells co-transformed with p423lexAkan_PacS_N and pJG4.5 with the *scAtx1* constructs shown above as the translational fusions were analysed with the anti-HA antibody by western blot analysis, and show intense bands at ~ 18 kDa for the ScAtx1 translational fusions in (A). The nitrocellulose membrane was stained with Ponceau S to determine equivalent protein loading in each lane (B). The position of the protein molecular weight markers in (B) are shown on the left in kDa.

3.3.4 Determining the role of the key loop 5 residues in ScAtx1 (His61), $PacS_N$ (Tyr65) and $CtaA_N$ (Phe87) in mediating protein-protein interactions

The ScAtx1 His61 residue, albeit distant in sequence from the CXXC motif, is located close to the metal-binding region in the structures of ScAtx1 (Badarau *et al.*, 2010; Banci *et al.*, 2004a). His61 has been proposed to act as a third Cu(I)-binding ligand in ScAtx1 in addition to Cys12 and Cys15 (Banci *et al.*, 2004a). However, in the crystal structures of the two Cu(I)-bound head-to-head ScAtx1 dimer and in the four Cu(I)-bound side-to-side ScAtx1 dimer, His61 was shown to be important for mediating hydrogen-bonding interactions rather than as a Cu(I)-binding ligand (Badarau *et al.*, 2010). Apart from its postulated role in metal-binding, this residue is of particular interest to this study with respect to its possible role in mediating the interactions with $PacS_N$ and $CtaA_N$. The analogous residue in Atx1 has been shown to be important for the yeast two-hybrid interaction with the MBDs of Ccc2 (Portnoy *et al.*, 1999). In addition, the mutation of the analogous residue in HAH1, Lys60 to either Ala or Tyr impaired the formation of a complex with ATP7B MBD4, as determined by gel filtration and circular dichroism experiments (Hussain *et al.*, 2009). Hence, ScAtx1 His61 and the analogous residues in the loop 5 of $PacS_N$ and $CtaA_N$ (Tyr65 and Phe87 respectively, as shown in Figure 71) were mutated, to determine the role of these residues on protein-protein interactions.

The mutation of ScAtx1 His61 to Ala significantly decreases the interaction with $PacS_N$ (Figure 79a), and abolishes the interaction with $CtaA_N$ (Figure 79b). To mimic the residues found in the MBDs of the target proteins, His61 was also mutated to Tyr or Phe. Both mutations abolish the interaction of ScAtx1 with $PacS_N$ (Figure 79a and Figure 80a). While the ScAtx1 His61Tyr mutation des not have a significant effect on the interaction with $CtaA_N$ (Figure 79b), the ScAtx1 His61Phe mutation significantly decreases the interaction with $CtaA_N$ (Figure 80b). The data therefore indicate that the presence of an aromatic residue in place of His61 abolishes the interaction of ScAtx1 with $PacS_N$ but does not have an equally drastic effect on the interaction of ScAtx1 with $CtaA_N$. The mutation of the residue in the analogous position in $PacS_N$, Tyr65 to His almost abolishes the interaction with ScAtx1 (Figure 81). However, ScAtx1 His61Ala shows a greater interaction with $PacS_N$ Tyr65His than the ScAtx1 WT protein (Figure 81). The level of interaction between ScAtx1 His61Ala and $PacS_N$ Tyr65His is similar to that between the WT proteins (Figure 81). The His61Tyr mutation does not have a similar effect as the His61Ala variant of ScAtx1 when co-transformed with $PacS_N$ Tyr65His construct. No significant interaction is observed between ScAtx1 His61Tyr and $PacS_N$ Tyr65His (Figure 81). The mutation of Phe87 in $CtaA_N$ (analogous position to His61 in ScAtx1) to His or Tyr also results in a significant decrease in the interaction with ScAtx1 compared to the interaction with $CtaA_N$ WT protein, albeit the interactions are not abolished completely (Figure 82).

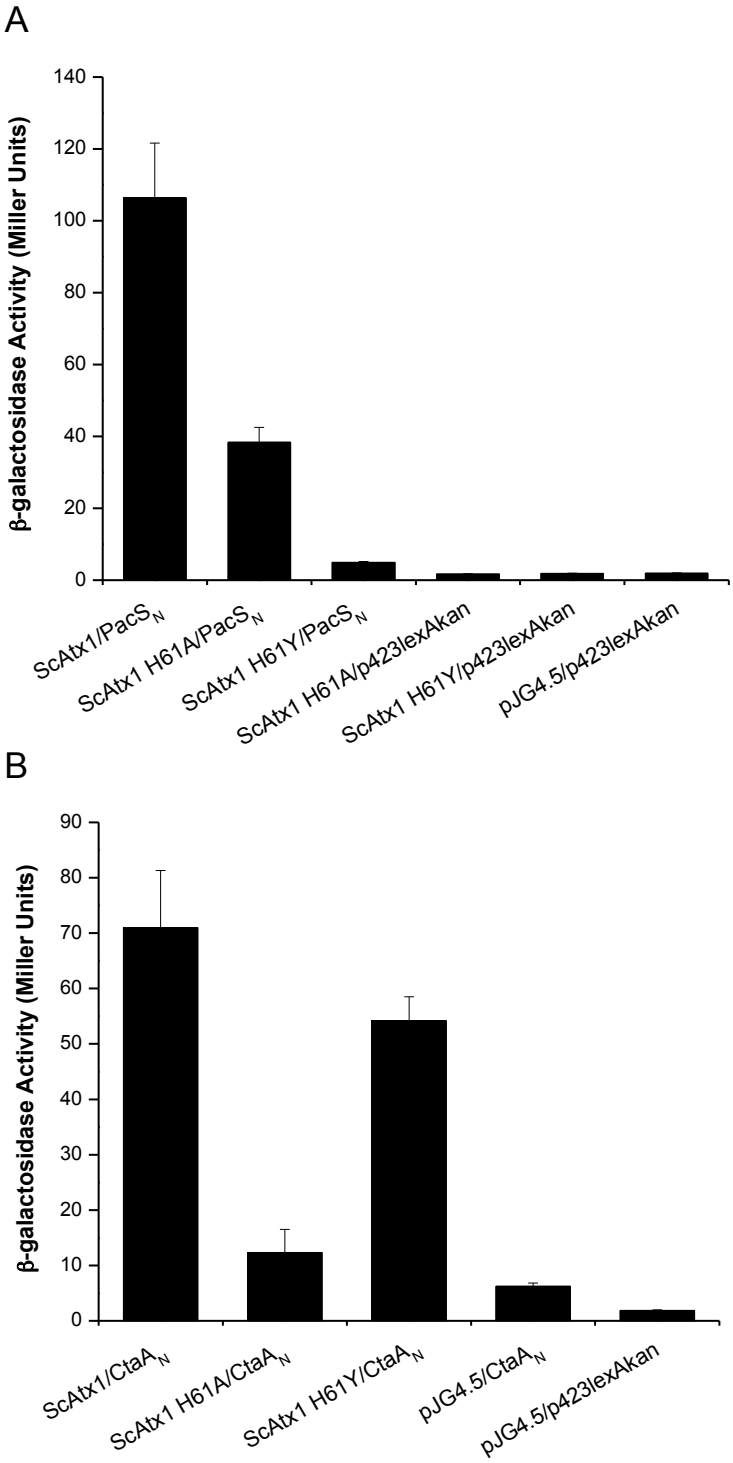

Figure 79: β-galactosidase activity assays showing the effects of ScAtx1 His61Ala and His61Tyr mutations on the interactions with $PacS_N$ and $CtaA_N$ using the yeast two-hybrid system. EGY48 cells were co-transformed with pJG4.5 with or without the *scAtx1* constructs mentioned above and p423lexAkan with or without $pacS_N$ (A) or $ctaA_N$ (B) as the translational fusions. Each data bar represents the average of three co-transformants assayed in triplicate + SD.

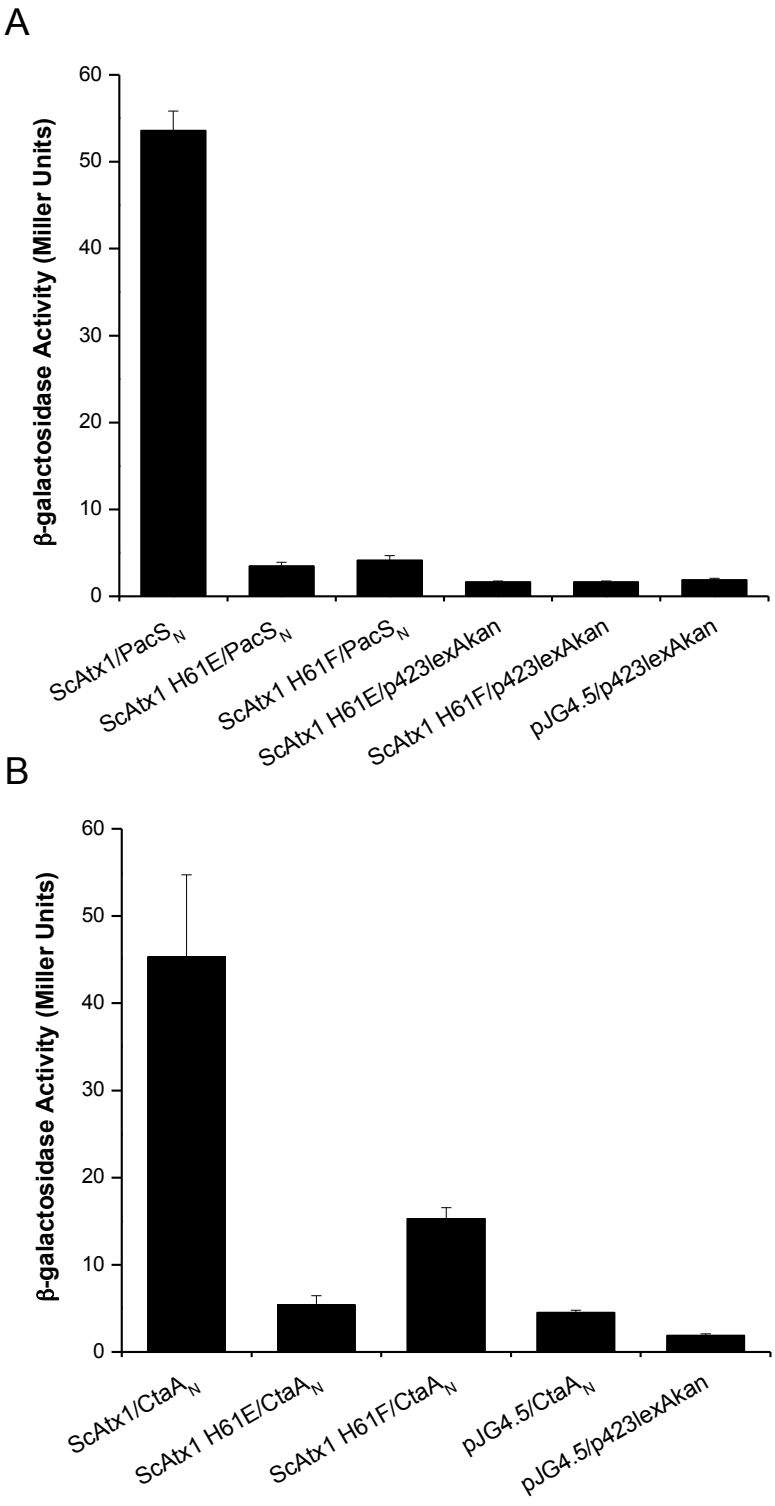

Figure 80: β-galactosidase activity assays showing the effects of ScAtx1 His61Glu and His61Phe mutations on the interactions with $PacS_N$ and $CtaA_N$ using the yeast two-hybrid system. EGY48 cells were co-transformed with pJG4.5 with or without the *scAtx1* constructs mentioned above and p423lexAkan with or without $pacS_N$ (A) or $ctaA_N$ (B) as the translational fusions. Each data bar represents the average of three co-transformants assayed in triplicate + SD.

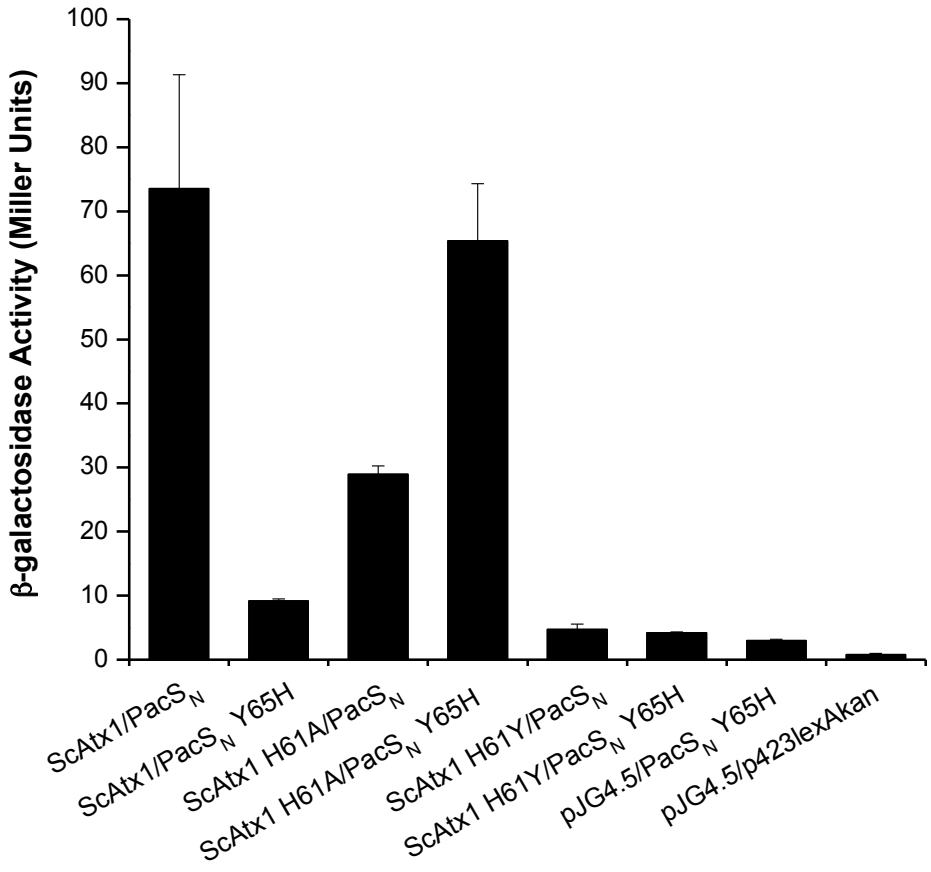

Figure 81: β-galactosidase activity assays showing the interaction of WT and His61Ala ScAtx1 with WT and Tyr65His PacS$_N$ using the yeast two-hybrid system. EGY48 cells were co-transformed with pJG4.5 and p423lexAkan with or without the constructs mentioned above as the translational fusions. Each data bar represents the average of three co-transformants assayed in triplicate + SD.

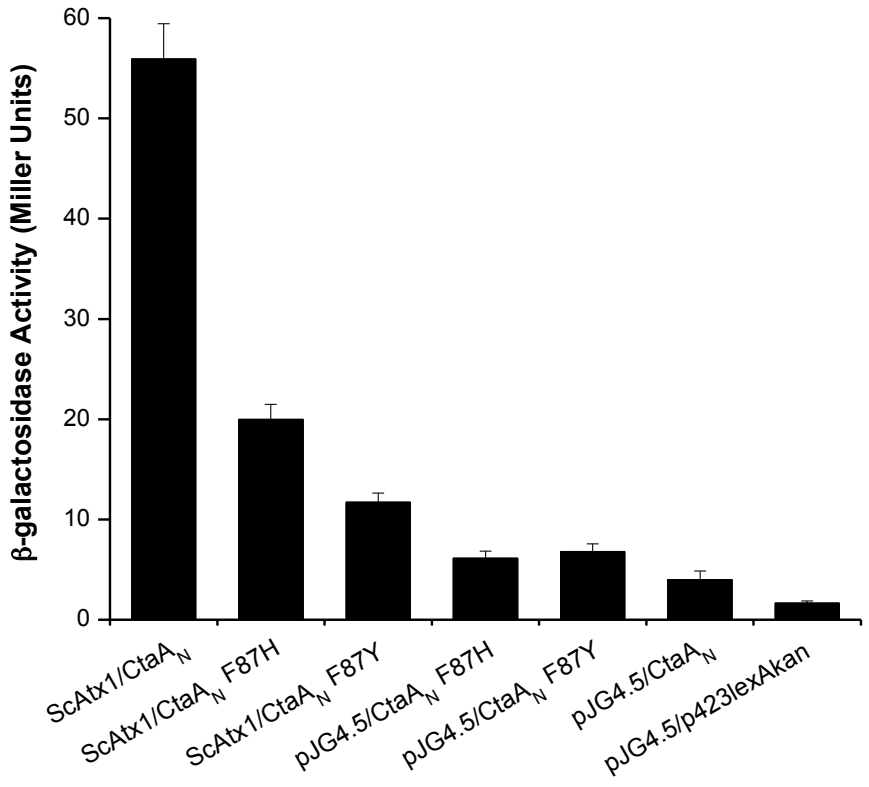

Figure 82: β-galactosidase activity assays showing the effect of CtaA$_N$ Phe87 mutations on the interaction with ScAtx1 using the yeast two-hybrid system. EGY48 cells were co-transformed with pJG4.5 and p423lexAkan with or without the constructs mentioned above as the translational fusions. Each data bar represents the average of three co-transformants assayed in triplicate + SD.

The results therefore indicate that the swapping around of the key loop 5 residues in ScAtx1, $PacS_N$ and $CtaA_N$ is not favourable for the interactions of ScAtx1 with $PacS_N$ or $CtaA_N$. The analogous residue in loop 5 of the ferredoxin-fold in eukaryotic homologues of ScAtx1 is found to be Lys (Arnesano *et al.*, 2002). To mimic the residue in eukaryotic copper metallochaperones, ScAtx1 His61 was mutated to Lys. In addition, His61 in ScAtx1 was also mutated to Glu to investigate the effect of a negative charge in this position on the interactions with $PacS_N$ and $CtaA_N$. While the ScAtx1 His61Glu mutation abolishes the interaction with both $PacS_N$ and $CtaA_N$ (Figure 80), the ScAtx1 His61Lys mutation yields different results with $PacS_N$ and $CtaA_N$ (Figure 83). The ScAtx1 His61Lys mutation results in ~ 2-fold decrease in the interaction with $PacS_N$ but almost abolishes the interaction with $CtaA_N$ (Figure 83). Western blot and Ponceau S analyses indicate that the mutations in ScAtx1 His61 and $CtaA_N$ Phe87 do not have an aberrant effect on protein expression (Figure 84 and Figure 85a). Slightly higher expression levels are observed for $PacS_N$ Tyr65His protein compared to the $PacS_N$ WT protein by visual inspection (Figure 85b). However, despite increased protein levels of $PacS_N$ Tyr65His protein, no significant interaction is evident with the ScAtx1 WT protein (Figure 81).

3.3.5 Determination of the structural arrangement of the complex formation of ScAtx1 with $PacS_N$ and $CtaA_N$

One of the aims of this study was to investigate if ScAtx1 can form structurally distinct complexes with $PacS_N$ and $CtaA_N$. This is based on the idea proposed by Badarau *et al.* (2010) that the two different structural arrangements obtained for the ScAtx1 dimers might be a reflection of the complex formation between ScAtx1 and its target MBDs. The models of the two different structural arrangements are the two Cu(I)-bound head-to-head dimer and the four Cu(I)-bound side-to-side dimer, shown in Figure 6. The four Cu(I)-bound side-to-side ScAtx1 dimer (Figure 6b) was observed to be very similar to the modelled complex of ScAtx1 and PacS95 (Banci *et al.*, 2006c). This structure is also very similar to the complexes reported for Atx1-Cu(I)-Ccc2a (Banci *et al.*, 2006b), HAH1-Cu(I)-ATP7A MBD1 (Banci *et al.*, 2009) and HAH1-Cu(I)-ATP7B MBD4 (Hussain *et al.*, 2009). In the absence of structural information regarding the complex between ScAtx1 and $CtaA_N$, it was suggested that while ScAtx1 and $PacS_N$ likely form a side-to-side complex, ScAtx1 and $CtaA_N$ may form a head-to-head complex. To investigate this further three residues in ScAtx1 were mutated in an attempt to solely disrupt the side-to-side complexes unlike the previously discussed mutations in ScAtx1 which may disrupt the formation of both side-to-side and head-to-head complexes. Based on the above mentioned crystal structures of the ScAtx1 dimers, the mutation of Lys21, Asn25 or Ser58 residues in ScAtx1 should not impair potential head-to-head complex

formation between ScAtx1 and its target MBDs, as shown in Appendix A. Western blot and Ponceau S analyses indicate that the mutation of these residues does not have an aberrant effect on protein expression (**Figure 86**).

ScAtx1 Lys21 was reported to be one of the key residues involved in mediating electrostatic interactions with PacS95 in the ScAtx1-PacS95 modelled complex (Banci *et al.*, 2006c). The superimposition of a Cu(I)-bound $PacS_N$ monomer against the four Cu(I)-bound side-to-side ScAtx1 dimer (Appendix B) indicates that the side chain of ScAtx1 Lys21 can potentially interact with the side chain of Glu61 in $PacS_N$. In an attempt to disrupt the formation of the ScAtx1-$PacS_N$ complex, Lys21 in ScAtx1 was mutated to Asp. As shown in Figure 87a, the ScAtx1 Lys21Asp mutation abolishes the interaction with $PacS_N$ consistent with the hypothesis that the Asp side chain can result in repulsion with the side chain of $PacS_N$ Glu61. In contrast to the ScAtx1 Lys21Asp mutation, the ScAtx1 Asn25Arg mutation does not have a significant effect on the interaction of ScAtx1 with $PacS_N$ (Figure 88a). Asn25 in ScAtx1 was mutated to Arg in an attempt to disrupt the formation of a side-to-side complex as a consequence of steric clashes due to the presence of the bulky side chain of Arg. However, the model presented in Appendix B shows that the side chain of Asn25 is also located close to the side chain of $PacS_N$ Glu61. The lack of significant effect of the Asn25Arg mutation on the interaction of ScAtx1 with $PacS_N$ is therefore consistent with the hypothesis that the Asn25Arg mutation can result in a favourable electrostatic interaction between the side chains of ScAtx1 Arg25 and PacS71 Glu61 if the proteins form a side-to-side complex. Ser58 in ScAtx1 was reported to interact with the side chains of Arg23 and Arg62 in PacS95 in the ScAtx1-PacS95 modelled complex (Banci *et al.*, 2006c). This residue was therefore mutated to Ala to disrupt the formation of hydrogen-bonding interactions with the residues in $PacS_N$. As shown in Figure 89a, the Ser58Ala mutation significantly decreases the interaction of ScAtx1 with $PacS_N$ but does not completely abolish it. These data are therefore consistent with the hypothesis that ScAtx1 and $PacS_N$ can form a side-to-side complexe which involve interactions between several residues in both of the proteins. Unlike the results obtained with $PacS_N$, all three ScAtx1 mutations (Lys21Asp, Asn25Arg and Ser58Ala) significantly decrease the interaction of ScAtx1 with $CtaA_N$ but do not completely abolish it (Figure 87b, Figure 88b and Figure 89b). These results are in contrast to the proposed hypothesis that ScAtx1 and $CtaA_N$ may form a head-to-head complex instead of a side-to-side complex and indicate that ScAtx1/$CtaA_N$ can also form a side-to-side complex similar to ScAtx1/$PacS_N$.

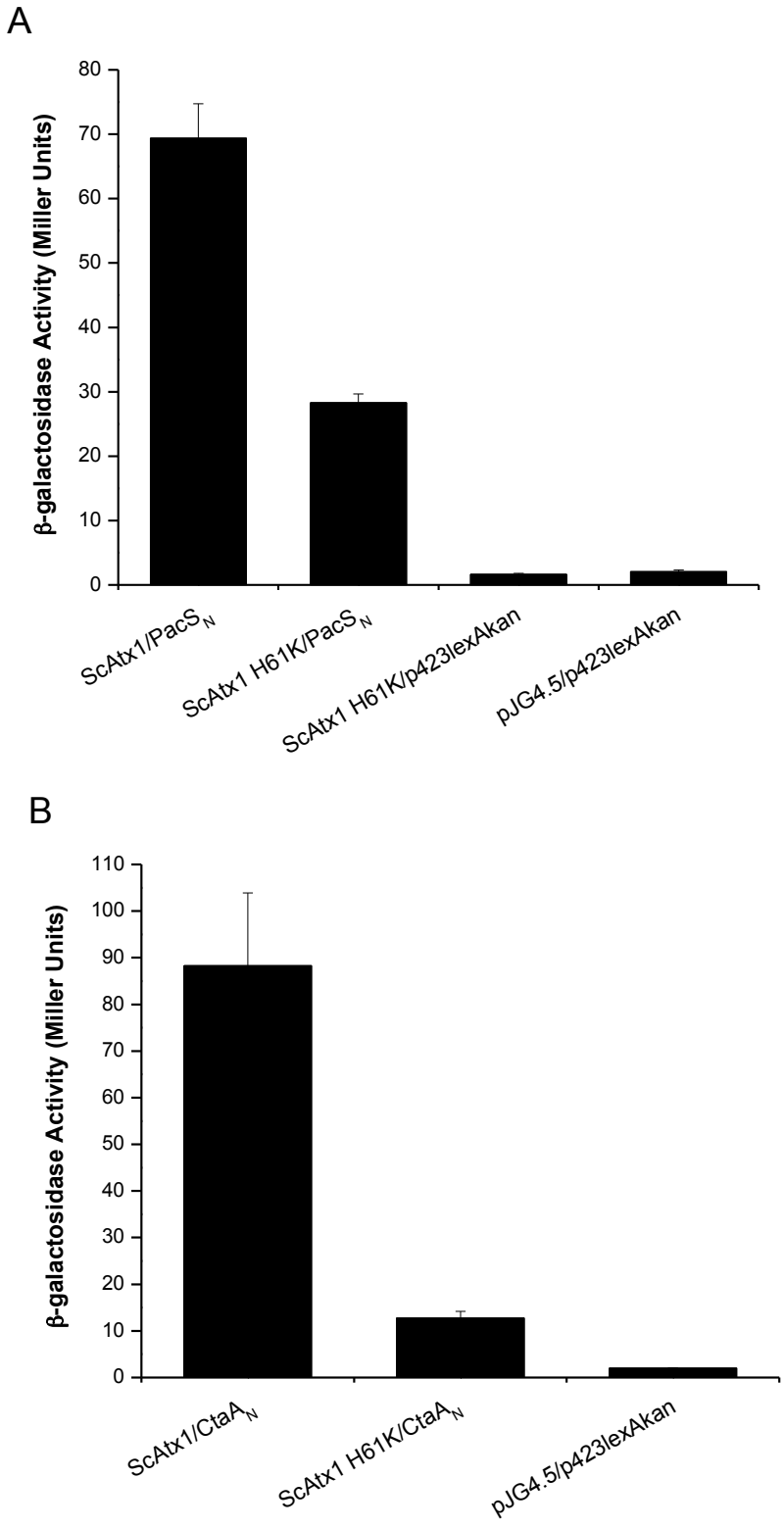

Figure 83: β-galactosidase activity assays showing the effects of ScAtx1 His61Lys mutation on the interactions with $PacS_N$ and $CtaA_N$ using the yeast two-hybrid system. EGY48 cells were co-transformed with pJG4.5 with or without the *scAtx1* constructs mentioned above and p423lexAkan with or without $pacS_N$ (A) or $ctaA_N$ (B) as the translational fusions. Each data bar represents the average of three co-transformants assayed in triplicate + SD.

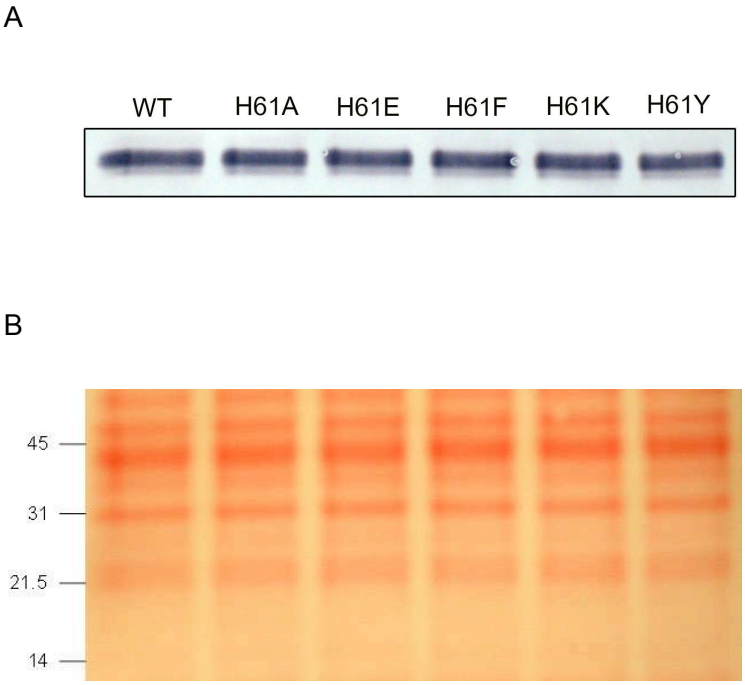

Figure 84: Western blot and Ponceau S analyses of ScAtx1 WT, His61Ala, His61Glu, His61Phe, His61Lys and His61Tyr proteins with the anti-HA antibody. Whole cell extracts from EGY48 cells co-transformed with p423lexAkan_PacS_N and pJG4.5 with the *scAtx1* constructs shown above as the translational fusions were analysed with the anti-HA antibody by western blot analysis and show intense bands at ~ 18 kDa for the ScAtx1 translational fusions in (A). The nitrocellulose membrane was stained with Ponceau S to determine equivalent protein loading in each lane (B). The position of the protein molecular weight markers in (B) are shown on the left in kDa.

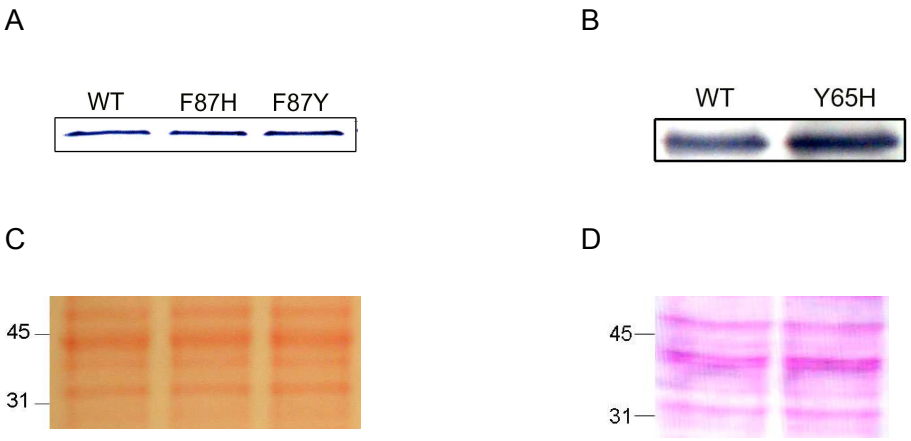

Figure 85: Western blot and Ponceau S analyses of $PacS_N$ WT and Tyr65His, and $CtaA_N$ WT, Phe87His and Phe87Tyr proteins with the anti-LexA antibody. Whole cell extracts from EGY48 cells co-transformed with pJG4.5_ScAtx1 and p423lexAkan with the *$ctaA_N$* (A) or *$pacS_N$* (B) constructs as the translational fusions were analysed with the anti-LexA antibody by western blot analysis. The intense bands in (A) at ~32 kDa represent the $PacS_N$ translational fusion, while the intense bands at ~ 34 kDa in (B) represent the $CtaA_N$ translational fusions. The nitrocellulose membranes from (A) and (B) were stained with Ponceau S prior to immunoblotting to determine equivalent protein loading in each lane, as shown in (C) and (D) respectively. The position of the protein molecular weight markers in (C) and (D) are shown on the left in kDa.

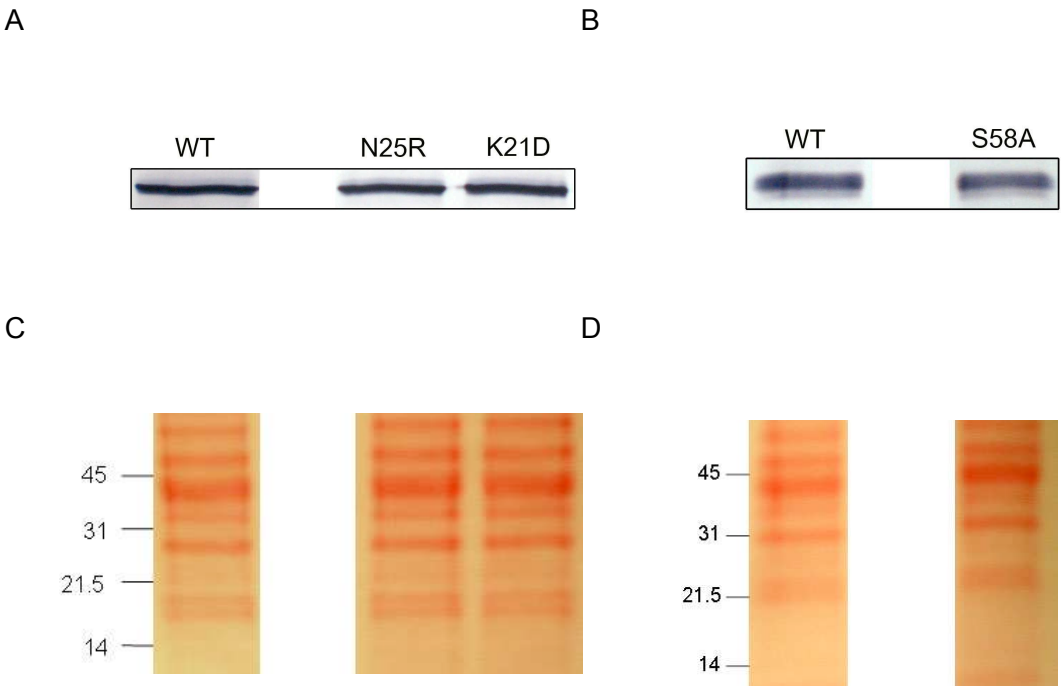

Figure 86: Western blot and Ponceau S analyses of ScAtx1 WT, Asn25Arg, Lys21Asp and Ser58Ala proteins with the anti-HA antibody. Whole cell extracts from EGY48 cells co-transformed with pJG4.5_ScAtx1 and p423lexAkan_PacS_N were analysed with the anti-HA antibody by western blot analysis. The intense bands in (A) and (B) at ~18 kDa represent the ScAtx1 translational fusion. The nitrocellulose membranes from (A) and (B) were stained with Ponceau S prior to immunoblotting to determine equivalent protein loading in each lane, as shown in (C) and (D) respectively. The position of the protein molecular weight markers in (C) and (D) are shown on the left in kDa.

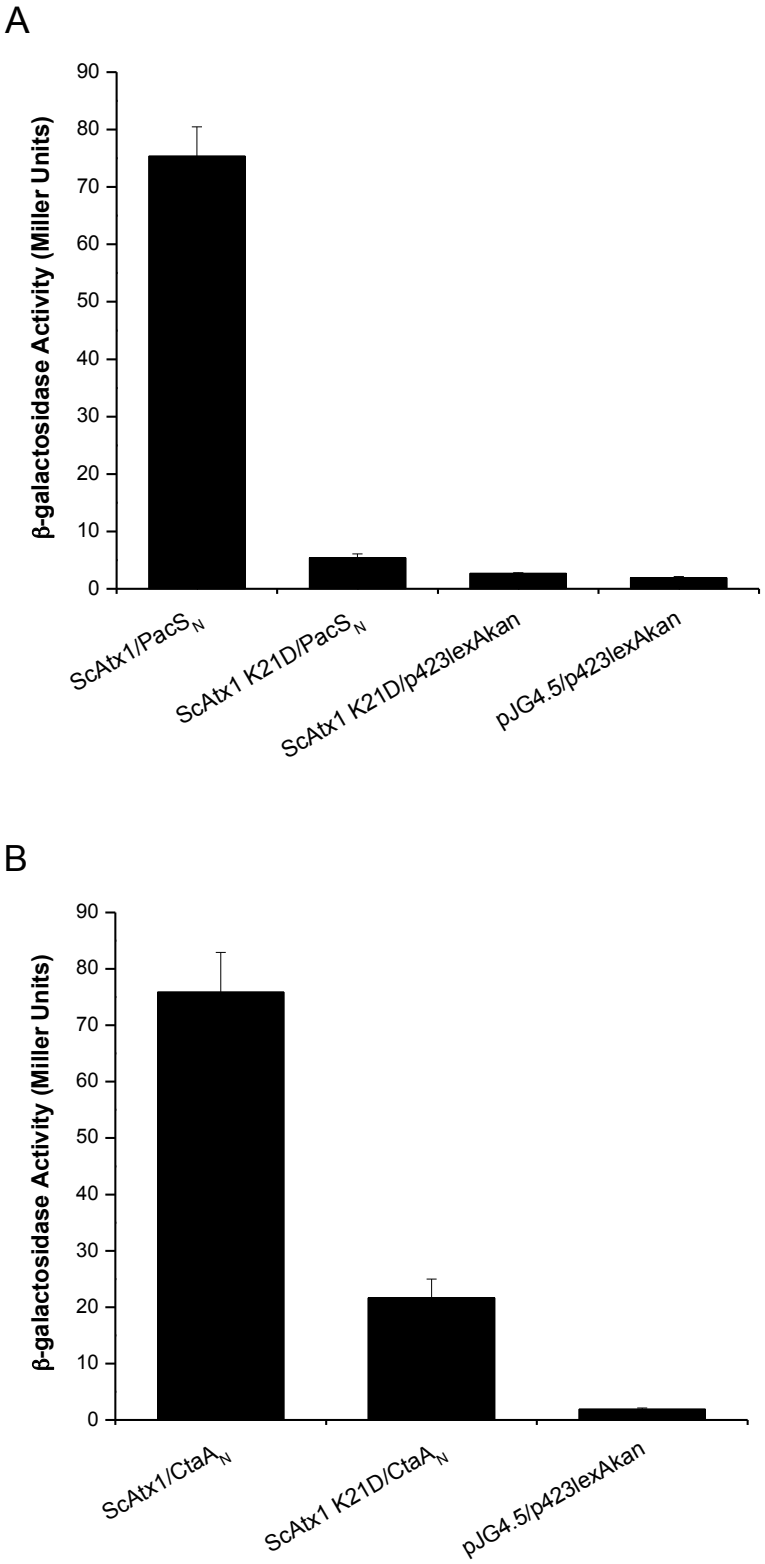

Figure 87: β-galactosidase activity assays showing the effect of ScAtx1 Lys21Asp mutation on the interactions with $PacS_N$ and $CtaA_N$ using the yeast two-hybrid system. EGY48 cells were co-transformed with pJG4.5 with or without the *scAtx1* constructs mentioned above and p423lexAkan with or without $pacS_N$ (A) or $ctaA_N$ (B) as the translational fusions. Each data bar represents the average of three co-transformants assayed in triplicate + SD.

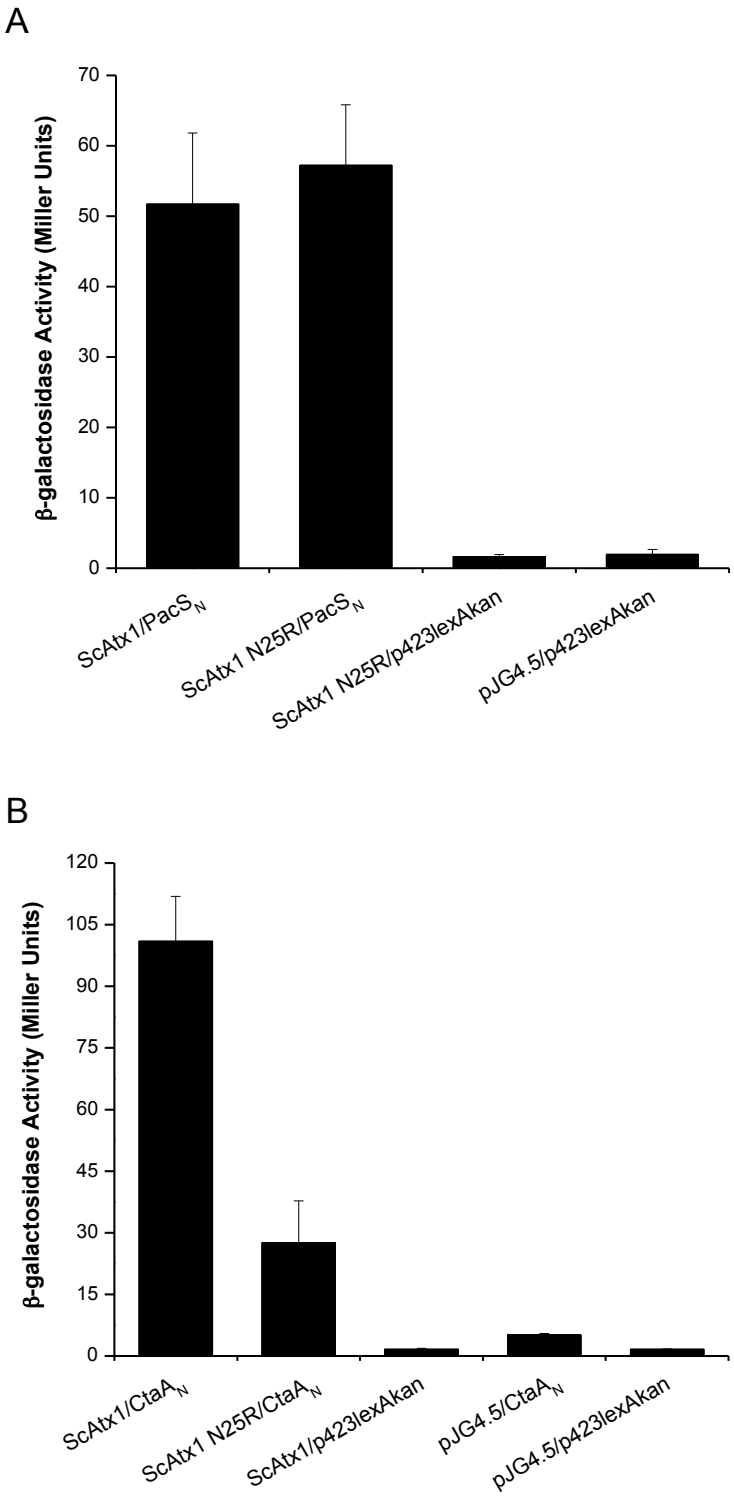

Figure 88: β-galactosidase activity assays showing the effect of ScAtx1 Asn25Arg mutation on the interaction with $PacS_N$ and $CtaA_N$ using the yeast two-hybrid system. EGY48 cells were co-transformed with pJG4.5 with or without the *scAtx1* constructs mentioned above and p423lexAkan with or without $pacS_N$ (A) or $ctaA_N$ (B) as the translational fusions. Each data bar represents the average of three co-transformants assayed in triplicate + SD.

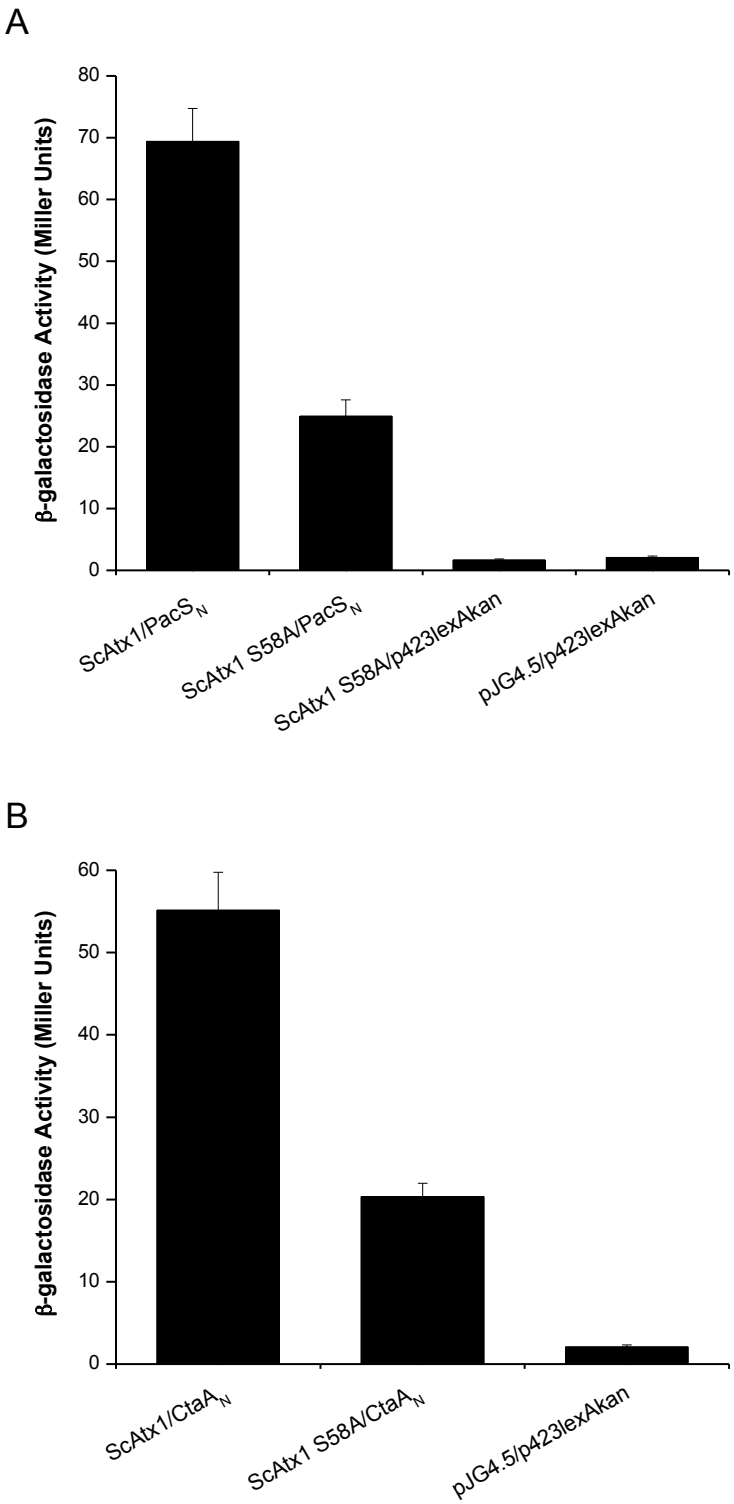

Figure 89: β-galactosidase activity assays showing the effect of ScAtx1 Ser58Ala mutation on the interaction with $PacS_N$ and $CtaA_N$ using the yeast two-hybrid system. EGY48 cells were co-transformed with pJG4.5 with or without the *scAtx1* constructs mentioned above and p423lexAkan with or without $pacS_N$ (A) or $ctaA_N$ (B) as the translational fusions. Each data bar represents the average of three co-transformants assayed in triplicate + SD.

4. Discussion

Copper metallochaperones play an important role in maintaining intracellular copper homeostasis by delivering Cu(I) to their specific target proteins which are important for a wide variety of functions including superoxide dismutation, photosynthesis and respiration. Interest in copper metallochaperones has increased as additional functions have been associated with them. For example, HAH1 can act as a transcription factor (Itoh *et al.*, 2008) and CCS deficiency can result in increased production of Aβ in neuronal cells (Gray *et al.*, 2010). These studies suggest that copper metallochaperones may serve as potential targets in therapies aiming to restore copper homeostasis in some of the diseases where copper mis-homeostasis is an integral part of the disease pathology including AD and PD.

Since some of the known copper metallochaperones can interact with multiple proteins (for example, HAH1, hCCS, EhCopZ and ScAtx1), a key challenge is to determine the factors that mediate the interaction of a copper metallochaperone with a specific protein. Favourable protein-protein interactions play a fundamental role in ensuring metal selectivity and its delivery to the correct target protein which prevents toxicity due to inappropriate metal-binding (Banci *et al.*, 2010c). The aim of this study was to further the understanding of the molecular basis of the interactions of copper metallochaperones with their partner proteins. This was investigated by studying two very different systems. In the first, the interactions of hCCS with hBACE1 CTD and hSOD1 were analysed. In the second system, the interaction of ScAtx1 with the MBDs of PacS and CtaA were studied. The strategy used to determine the molecular basis of these interactions involved the mutagenesis of metal-binding amino acids or surface residues potentially mediating interactions. The effects of mutations were studied using the yeast two-hybrid system. The role of copper concentration on protein-protein interactions was also investigated by analysing the effect of varying concentrations of $CuSO_4$ or BCS on β-galactosidase activity.

Yeast is one of the model organisms for studying protein-protein interactions especially of the human origin, since it contains homologues of most proteins and pathways, is much more convenient to manipulate but less complicated than human cells. As discussed in section 1.6, pathways of copper homeostasis are quite well preserved in yeast and humans. However, these advantages can also act as potential limiations of the yeast two-hybrid system in this study. One of the problems in studying hCCS-based interactions using the yeast two-hybrid system is the fact that a proportion both Ccs1 and Sod1 have been shown to be localised in the nucleus of *S. cerevisae* (Wood and Thiele, 2009), the site of yeast two-hybrid interactions. Consequently there is always a possibility that changes in interaction of hCCS with hBACE1 CTD or hSOD1 in this study (when testing the effect of a mutation or copper

concentration effect), is as a result of altered interactions with endogenous Ccs1 or Sod1. While Ccs1 and Sod1 have both been detected in the nucleus, the proportion of these proteins that resides in the nucleus is currently not known (Wood and Thiele, 2009). Considering that the fusion proteins are overexpressed in the yeast two-hybrid system, it is possible that intereference with endogenous proteins may not have a significant impact on the observed output. Due to time constraints, this issue could not be fully addressed in this study, but measures of how this could be investigated are discussed in chapter 5.

An added problem regarding the potential interactions of hCCS or hSOD1 with endogenous Ccs1 or Sod1 is the effect this may have on Mac1 activity. It has been shown that catalytically active Sod1 is required in the nucleus for Mac1 activity which induces the transcription of several proteins involved in copper and iron homeostasis including *CTR1* (Wood and Thiele, 2009). This is particularly relevant for the experiments investigating the interaction of hCCS with hSOD1, which were carried out in the SAY1 strain (which lacks Ccs1), as discussed further in section 4.2. However, these issues should not pose a problem for the study of the interaction of ScAtx1 with $PacS_N$ and $CtaA_N$ since there is no evidence to date to indicate the localisation of Atx1 in the yeast nucleus or that Ccs1 or Sod1 can interact with ScAtx1, $PacS_N$ or $CtaA_N$.

Additional limitations when studying the protein-protein interactions of copper-binding proteins by yeast two-hybrid involve the potential effects of altered copper concentration or copper availability on other copper-dependent pathways. For instance, copper is required by cytochrome *c* oxidase for respiration (section 1.3.2.4.3), superoxide dismutases for (primarily) anti-oxidant defense (section 1.3.2.3 and 1.3.2.4.2) and by Ccc2 for high-affinity iron uptake (section 1.3.3.1). Consequently, there is a possibility that the changes in protein-protein interactions observed in this study when testing the effects of protein mutations or altered copper conditions are due to an indirect effect on respiration, redox balance or iron homeostasis. Altered iron homeostastis in particular can cause a cascading effect by disrupting copper homeostasis, since the two pathways are closely linked and can overlap, as shown in Figure 17. Unfortunately, these potential problems could not be investigated in this study, however, given further time these issues can be investigated further by some of the measures discussed in Chapter 5. The results presented in this study are subsequently discussed under the presumption that the changes in protein-protein interactions observed in this study are primarily due to the mutations introduced in the proteins or due to altered copper conditions when studying the effects of added $CuSO_4$ or BCS on these interactions.

4.1 The molecular basis of the interaction of hCCS and HAH1 with hBACE1 CTD

The results obtained in this study demonstrate that the interaction of hCCS with hBACE1 CTD is mediated by Cu(I)-binding to the Cys residues in the CXXC motif of both molecules. Arg71 on loop 5 of hCCS may be important for mediating the hCCS/hBACE1 CTD interaction, although further evidence is required to confirm this. The Cu(I)-binding residues in hCCSD3 were not found to affect the hCCS/hBACE1 CTD interaction. Several amino acids located close to the CXXC motif in hBACE1 CTD influence the interaction with hCCS. In addition, this study demonstrates a significant interaction between HAH1 and hBACE1 CTD which is also mediated by the Cys residues in the CXXC motif of hBACE1 CTD and the surrounding amino acids. The results obtained are summarised in Table 7.

The hCCS/hBACE1 CTD interaction is mediated by the D1 of hCCS. These results are in agreement with the study by Angeletti *et al.* (2005) where a significant interaction between hBACE1 CTD and hCCSD2 or hCCSD3 was not observed. The fact that the hCCS/hBACE1 CTD interaction is ~ 5-fold stronger than the hCCSD1/hBACE1 CTD interaction indicates that although hCCSD2 and hCCSD3 do not interact with hBACE1 CTD directly, their presence does assist in interaction. Similar to the previous finding (Angeletti *et al.*, 2005), no significant interaction was observed between Ccs1 and hBACE1 CTD. A key difference between hCCS and Ccs1 is their quaternary structure. hCCS is a dimer irrespective of Cu(I) loading (Rae *et al.*, 2001), while apo-Ccs1 is a monomer with the Cu(I)-bound protein a mixture of monomeric and dimeric forms (Schmidt *et al.*, 1999a). This suggests that the dimerisation of CCS may be an important requirement for its interaction with hBACE1 CTD. That is, hBACE1 CTD may interact more strongly with the homo-dimer of hCCS than with the hCCS monomer. A significant interaction was consistently detected between HAH1 and hBACE1 CTD which was similar in strength to the hCCSD1/hBACE1 CTD interaction. Since hCCSD1 and HAH1 both have a ferredoxin-fold, and high amino acid homology (as discussed in 1.3.2.4.2), the similarity in their interactions with hBACE1 CTD is not surprising. However, Angeletti *et al.* (2005) did not detect a significant interaction between HAH1 and hBACE1 CTD. The reason underlying this discrepancy is not clear especially because the HAH1 construct and the yeast two-hybrid strain used in this study and by Angeletti *et al.* (2005) were obtained from the same source.

Table 7: Summary of the results obtained for the interaction of hBACE1 CTD with hCCS, hCCSD1 and HAH1. The effects of the mutations made in hCCS and hCCSD1 on the interaction with hBACE1 CTD are shown in (A) and (B). The effects of mutating the residues in hBACE1 CTD on the interaction with hCCS, hCCSD1 and HAH1 are shown in (C). A decreased interaction (compared to the interaction with WT protein) is represented by '↓', increased interaction by '↑' and the lack of significant protein-protein interaction by 'X'. Interactions that are similar to WT are represented by '~ WT'.

A

hCCS mutations	Effect on yeast two-hybrid interaction with hBACE1 CTD	Figure Reference
Cys22Ser	9-fold ↓	36
Cys25Ser	8-fold ↓	36
Cys22Ser,Cys25Ser	X	36
Arg71Ala	3-fold ↓	39
Arg71Glu	10-fold ↓	39
Arg71Lys	11-fold ↓	39
Cys244Ser	~ WT	44
Cys244Ser,Cys246Ser	~ WT	44

B

hCCSD1 mutations	Effect on yeast two-hybrid interaction with hBACE1 CTD	Figure Reference
Cys22Ser	2-fold ↓	37
Cys25Ser	2-fold ↓	37
Cys22Ser,Cys25Ser	X	37
Arg71Ala	3-fold ↓	40
Arg71Glu	3-fold ↓	40
Arg71Lys	3-fold ↓	40

C

hBACE1 CTD mutations	Effect on yeast two-hybrid interactions with copper metallochaperones			Figure Reference
	hCCS	hCCSD1	HAH1	
Cys478Ser	2-fold ↑	2-fold ↑	2-fold ↑	46
Trp480Met	2-fold ↓	4-fold ↓	X	50
Arg481Ala	2-fold ↓	X	2-fold ↓	51
Arg481Glu	7-fold ↓	X	2-fold ↓	52
Arg481Lys	2-fold ↑	3-fold ↑	X	51
Cys482Ser	X	X	X	47
Arg484Ala	2-fold ↑	3-fold ↑	3-fold ↑	53
Cys485Ser	X	X	X	48
Arg487Ala	2-fold ↑	~ WT	2-fold ↑	54
Asp491Ala,Asp492Ala	~ WT	~ WT	X	55

The experiments investigating the effect of copper concentration on the hCCS/hBACE1 CTD interaction indicate that this interaction may be mediated by the formation of a Cu(I)-bridged complex. While the hCCS/hBACE1 CTD interaction is not significantly affected in the presence of excess copper, the interaction significantly decreases in copper-deficient conditions (Figure 28e, Figure 32 and Figure 33). The addition of 500 µM BCS to the growth medium results in the induction of *CTR1* transcription as a consequence of decreased cellular copper content. In these conditions, the hCCS/hBACE1 CTD interaction was found to be ~ 2-fold lower compared to the interaction in basal medium (Figure 28e and Figure 32). The data also reveal an ~ 2-fold decrease in the amount of *CTR1* mRNA in co-transformants containing hCCS and hBACE1 CTD, compared to those containing empty vectors (Figure 28a, c). Since the copper content of the hCCS/hBACE1 CTD co-transformants in 500 µM BCS was similar to those containing empty vectors (Figure 28e, f), similar *CTR1* transcription levels were expected. This suggests that the presence of hCCS and hBACE1 CTD results in a decrease in *CTR1* transcription. There are two main factors that may account for this observation. Firstly, the binding of Cu(I) by hCCS and hBACE1 CTD in the nucleus can result in increased copper content in the yeast nucleus resulting in decreased Mac1 activation and subsequently reduced induction of *CTR1* transcription. Since the copper content determined is that for the whole cell, the nuclear copper concentration in the co-transformants is not known. Secondly, hCCS or hBACE1 CTD may directly interact with Mac1 or bind to another protein that regulates the activity of Mac1. The second hypothesis is supported by the results presented by Wood and Thiele (2009) who found that functional Sod1 was required for Mac1 activity. It has previously been shown that hCCS can interact with Sod1 in *S. cerevisiae* (Schmidt *et al.*, 2000). Based on these data it is very likely that hCCS can interact with endogenous Sod1 in the hCCS/hBACE1 CTD co-transformants. Whether this interaction can result in the activation of Sod1 too, considering hCCS is expressed as a fusion protein, is not known. If the interaction of the hCCS fusion protein with endogenous Sod1 can not activate Sod1 then this could result in decreased Sod1 activity in hCCS/hBACE1 CTD co-transformants accounting for the reduced *CTR1* transcription observed in this study. Alternatively, the activity of Sod1 in the yeast nucleus may also be reduced as a consequence of decreased availability of Ccs1 since hCCS has also been shown to dimerise with Ccs1 in *S. cerevisiae* (Schmidt *et al.*, 2000).

Irrespective of the reasons underlying decreased *CTR1* transcription in hCCS/hBACE1 CTD co-transformants, it can be concluded that the addition of 500 µM or higher concentrations of BCS results in decreased copper content and decreased interaction of hCCS with hBACE1 CTD (Figure 28e and Figure 32). Even though the addition of 1 mM and 3 mM BCS resulted in ~ 3-fold and > 100-fold reduction in the total-cell copper content respectively, compared to the hCCS/hBACE1 CTD co-

transformants incubated in medium containing 500 μM BCS, no significant differences were detected between the yeast two-hybrid interactions of these co-transformants. Therefore, while the hCCS/hBACE1 CTD interaction decreases in copper-deficient conditions it is not abolished even at high BCS concentrations. This may reflect the presence of sufficient Cu(I) ions in the nucleus to enable the formation of hCCS-Cu(I)-hBACE1 CTD complex even when incubated in the presence of up to 3 mM BCS. Unlike the hCCS/hBACE1 CTD interaction, the hCCSD1/hBACE1 CTD and the HAH1/hBACE1 CTD interactions did not decrease in copper-deficient conditions (Figure 34 and Figure 35). Therefore, the effect of copper concentration on the hCCS/hBACE1 CTD interaction requires the presence of domains 2 and 3 of hCCS in addition to D1. This leads to the possibility that the decrease in hCCS/hBACE1 CTD interaction in copper-deficient conditions may be influenced by decreased availability of hCCS for interaction with hBACE1 CTD as a consequence of its interactions with endogenous Ccs1 and Sod1. As shown in Figure 60, the presence of BCS results in ~ 2-fold increase in the hSOD1/hCCS interaction. However, these results have to be treated with caution since the hCCS/hSOD1 experiments were conducted in the SAY1 strain instead of the EGY48 strain. Based on the study by Wood and Thiele (2009) this can have an aberrant effect on the Mac1 activity, as discussed further in section 4.2.

The formation of a Cu(I)-bridged complex between hCCS and hBACE1 CTD is also supported by the data showing that the mutation of the Cys residues in the CXXC motifs of hCCS and hBACE1 CTD abolishes their interaction (Table 7). While the mutation of Cys482 or Cys485 in hBACE1 CTD completely impairs the interaction with hCCS (and hCCSD1), the mutation of both Cys22 and Cys25 in hCCS is required to abolish the interaction with hBACE1 CTD. Similar results have also been reported for the interaction of other copper metallochaperones with their target proteins. The mutation of the Cys residues in the CXXC motif of Atx1, HAH1 and ScAtx1 abolished the interactions with their respective target proteins (Larin *et al.*, 1999; Portnoy *et al.*, 1999; Tottey *et al.*, 2002). Cu(I) transfer between Cu(I) metallochaperones and their partner proteins is proposed to proceed via ligand exchange reactions involving three coordinate Cu(I)-thiol intermediates (Banci *et al.*, 2006b; Banci *et al.*, 2009; Rae *et al.*, 2001). The data presented in this study also indicate that the complex formation between hCCS and hBACE1 CTD involves Cu(I) coordination by three thiol ligands. hCCS-Cu(I)-hBACE1 CTD complex formation requires the presence of Cys482 and Cys485 of hBACE1 CTD and either one of the two Cys in the CXXC motif of hCCS, as shown in Figure 90a,b.

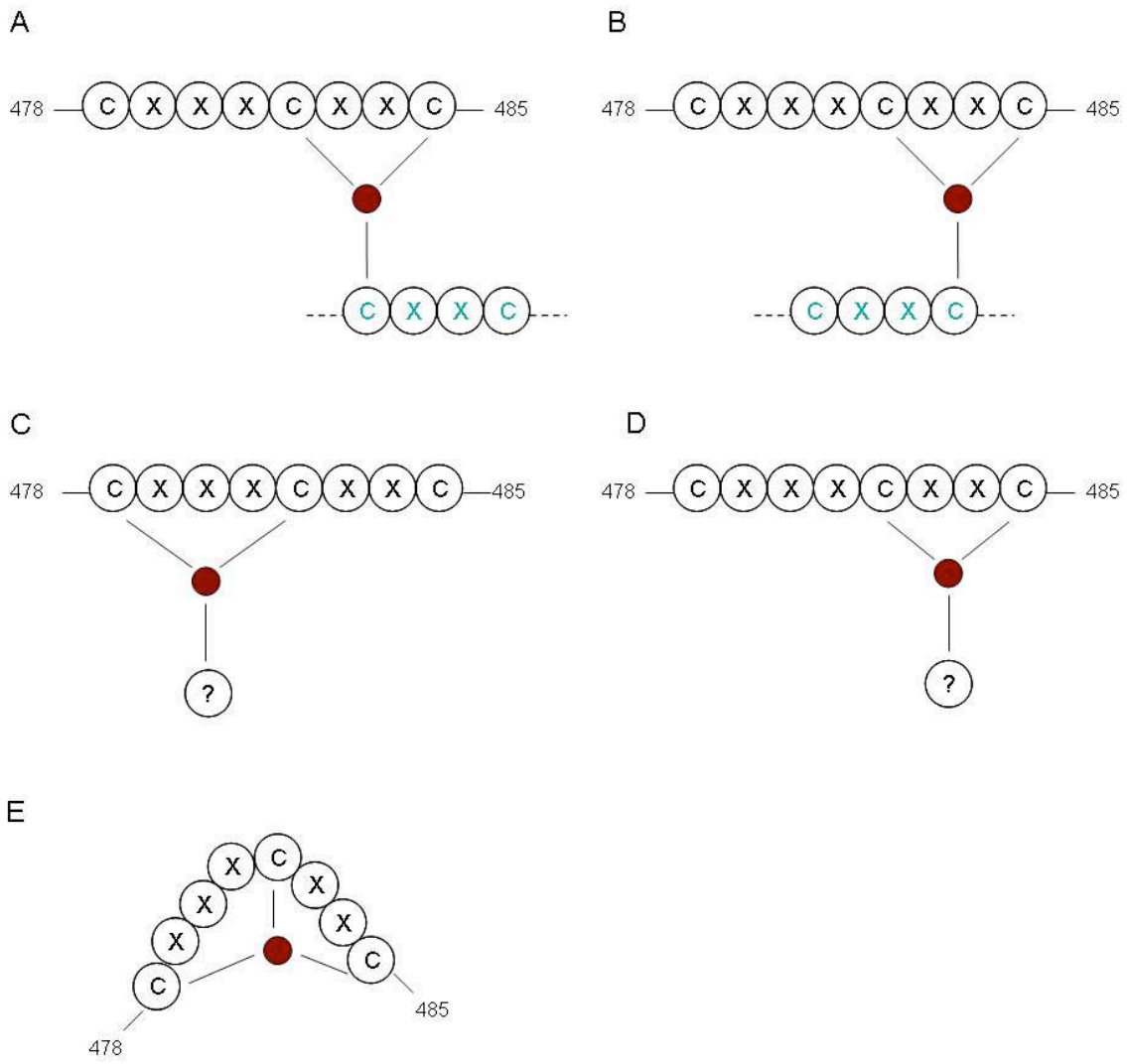

Figure 90: Possible copper-mediated coordinations sites involving the Cys residues in hBACE1 CTD and the CXXC motifs of hCCS and HAH1. Cu(I)-bridged complex formation between hBACE1 CTD and hCCS or HAH1 is shown in (A) and (B) where Cu(I) is bound by Cys482 and Cys485 of hBACE1 CTD and one of the Cys in the CXXC motif of the copper metallochaperone. The hBACE1 CTD Cys478-Cys485 amino acid sequence is represented by circles containing 'C' and 'X' in black (one letter amino acid code). Cu(I) is shown as a brown sphere. The CXXC motif from the copper metallochaperones is represented by circles containing 'C' and 'X' in green. Tri-coordinated Cu(I)-binding in hBACE1 CTD is shown in (C), (D) and (E). Cu(I) is bound by Cys478 and Cys482 or Cys482 and Cys485 of hBACE1 CTD in addition to an unidentified third ligand represented by the circle labelled '?' in (C) and (D) respectively (based on the study by Angeletti *et al.* (2005)). Cu(I) is bound by Cys478, Cys482 and Cys485 of hBACE1 CTD in (E).

Three coordinate Cu(I)-thiolate centres have also been reported for other copper metallochaperone-target protein complexes including Atx1-Cu(I)-Ccc2a (Banci *et al.*, 2006b) and HAH1-Cu(I)-ATP7A MBD1 (Banci *et al.*, 2009). In these studies, the N-terminal Cys residues in the CXXC motif of both proteins were essential for complex formation. In the NMR study investigating the complex formation between Atx1 and Ccc2a, the dominant complex involved both of the Cys residues of the CXXC motif of Ccc2a and the N-terminal Cys of the CXXC motif of Atx1 (Banci *et al.*, 2006b). It was further proposed that in the copper metallochaperone-Cu(I)-partner protein complexes, Cu(I) is localised comparatively closer towards the 'acceptor' protein (Banci *et al.*, 2010c). Based on the data obtained in this study, this may indicate that Cu(I) is transferred from hCCS to hBACE1 CTD since both of the Cys residues in the CXXC motif of hBACE1 CTD are essential for interaction whereas only one Cys residue in the CXXC motif of hCCS is required. A similar three coordinate Cu(I)-bridged complex may also form between HAH1 and hBACE1 CTD, since the mutation of either Cys482 or Cys485 in hBACE1 CTD also abolishes the interaction with HAH1 (Table 7c).

Interestingly, the hBACE1 CTD Cys478Ser mutation enhances the interaction of hBACE1 CTD with hCCS, hCCSD1 and HAH1 (Table 7c). Cu(I)-binding by hBACE1 CTD has been proposed to be a tri-coordinated site where Cys482 was found to be vital for Cu(I)-binding, in addition to either Cys478 or Cys485 and a third unidentified non-thiol ligand (Angeletti *et al.*, 2005) (Figure 90c,d). The hBACE1 CTD fusion protein may therefore exist in several different states in the presence of Cu(I) in the co-transformants containing hBACE1 CTD and hCCS (or HAH1), as shown in Figure 90. Based on the Cu(I)-coordination sites shown in Figure 90c,e; the hBACE1 CTD Cys478Ser mutation would remove one of the Cu(I)-ligands and disrupt the formation these coordination sites which could increase the complex formation with copper metallochaperones, accounting for the increase in interactions observed with the hBACE1 CTD Cys478Ser mutation. In contrast to this study, Angeletti *et al.* (2005) found that the mutation of all three Cys residues in hBACE1 CTD to Ala (triple mutant) did not impair the interaction of hBACE1 CTD with hCCS in a GST pull-down assay. All of the hBACE1 CTD mutant proteins in this study were studied *in vivo* to mimic the native environment. The different experimental conditions used in *in vitro* GST pull-down assays may account for the observed discrepancies.

In addition to the Cu(I)-binding Cys residues, the interaction of hBACE1 CTD with hCCS and HAH1 is also influenced by the residues surrounding the CXXC motif in hBACE1 CTD (Table 7c). The data show that the Trp480Met mutation in hBACE1 CTD decreases the interaction with hCCS and hCCSD1 and abolishes the interaction with HAH1. As discussed in section 3.1.4, Trp480 was mutated to Met to mimic the 'MXCXXC' motif commonly found in copper metallochaperones and other Cu(I)-binding proteins. The large hydrophobic side chain of Trp480 may play a

structural role in hBACE1 CTD by organising the arrangement of Cys482 and Cys485 in hBACE1 CTD for Cu(I) binding and for the interaction with copper metallochaperones. Since Trp has the largest side chain of all the amino acids, mutation of this residue to any other amino acid can potentially alter the peptide fold. However, to understand the role of this residue further Trp480 can be mutated to Phe or Tyr which also contain aromatic side chains and are more similar in size to Trp than Met. In addition, the effects of these (and other) mutations on the peptide fold can be studied by NMR or CD spectroscopy.

The hBACE1 CTD Arg481 residue was also found to be important for the interactions with hCCS and HAH1. The proximity of Arg481 to the CXXC motif in hBACE1 CTD suggests that the side chain of this residue may serve a two-fold purpose. It may be involved in the arrangement of the CXXC motif and also in assisting the neutralisation of the negative charge generated on the deprotonated Cys residues as a consequence of Cu(I)-binding to hBACE1 CTD. A similar role has been associated with the Lys65 residue in loop 5 of the ferredoxin-fold of Atx1 which is located close to the Atx1 MBS (Arnesano *et al.*, 2001b; Portnoy *et al.*, 1999). The data indicate that the presence of a positive charge in this position is important for the interaction of hBACE1 CTD with hCCS since the mutation of Arg481 to Lys not only preserves but in fact, increases the interaction whereas the mutation to Glu significantly decreases the interaction. The increase in interaction of hBACE1 CTD Arg481Lys with its partner proteins is likely because the positive charge in Lys is more localised compared to the side chain of Arg where the positive charge in the guanidinium group is more diffused (Creighton, 1993). The Arg481Ala mutation not only removes the positive charge associated with the Arg residue but also introduces a small hydrophobic residue in this position. Since the Arg481Ala mutation results in decreased interaction with hCCS and hCCSD1, this further suggests that both the size and property of Arg481 are important for interaction (Table 7c). In contrast to the interactions of hBACE1 CTD Arg481Lys with hCCS and hCCSD1, the hBACE1 CTD Arg481Lys mutation abolishes the interaction with HAH1. The substitution of hBACE1 CTD Arg481 with a neutral (Ala), acidic (Glu) or another basic (Lys) residue all had a detrimental effect on the interaction with HAH1. This suggests that hBACE1 CTD Arg481 is absolutely essential for the interaction with HAH1.

It was hypothesised that a similar function to hBACE1 CTD Arg481 may be performed by Arg71 in hCCS (analogous to Lys65 in Atx1). That is, Arg71 may also be involved in neutralisation of the net negative charge created in the metal-binding region upon Cu(I)-binding due to the deprotonation of the Cys residues. Based on this hypothesis it was expected that the mutation of Arg71 to Lys would not have a significant effect on the interaction with hBACE1 CTD, whereas the Arg71Ala and Arg71Glu mutations would result in decreased interactions. As expected, the mutation

of Arg71 to Ala or Glu in hCCS results in significantly decreased interaction with hBACE1 CTD (Table 7a-b). The presence of the negatively charged Glu residue in the place of Arg71 had a more drastic effect on protein-protein interaction than the presence of the neutral Ala residue. This is probably due to disrupted Cu(I)-binding in the hCCS Arg71Glu mutant protein as a result of the increase in negative charge in the metal-binding region. Contrary to expectations, the hCCS Arg71Lys mutation abolishes the interaction with hBACE1 CTD. This result is very surprising and difficult to rationalise based on the above hypothesis. It is possible that Arg71 plays a fundamental role in Cu(I)-binding in domain 1 of hCCS and Cu(I)-transfer, as proposed by Rae *et al.* (2001), which may be disrupted by the presence of Ala, Glu or Lys in this position. Perhaps Arg is the ideal residue in this position to allow both Cu(I)-binding and Cu(I)-transfer to take place in hCCSD1. This theory can be tested by studying the binding of Cu(I) in both WT and Arg71 mutants of hCCS using *in vitro* methods, as discussed in section 5.1. However, based on the results obtained in this study, the precise role of hCCS Arg71 in mediating the interaction with hBACE1 CTD can not be conclusively determined.

Unlike the Arg481Ala mutation in hBACE1 CTD, the Arg484Ala and Arg487Ala mutations increase the interaction of hBACE1 CTD with hCCS and HAH1 (Table 7c). Based on the structure of apo-hCCSD1 (Figure 91a), the only positively charged residue located close to the MBS is Arg71. However, the hCCS Arg71Ala and Arg71Lys mutations both decrease the interaction with hBACE1 CTD which indicates that the side chains of hBACE1 CTD Arg484 and Arg487 probably do not cause electrostatic repulsion in the complex with hCCS. The increase in interaction observed with the Arg484Ala and Arg487Ala mutations in hBACE1 CTD may therefore be due to altered arrangement of the CXXC motif in hBACE1 CTD which enhances its interaction with hCCS and HAH1. To clarify this hypothesis further, both Arg484 and Arg487 can be mutated to Lys as a positive control and to an acidic residue to further clarify the role (or the lack of importance) of charge in this position.

The interaction of hBACE1 CTD with HAH1 was also abolished by the Asp491Ala,Asp492Ala double mutation in hBACE1 CTD, whereas these changes did not have a significant effect on the interactions with hCCS and hCCSD1 (Table 7c). These mutations not only remove the negative charge in these positions but also introduce a small hydrophobic residue in place of them, which can potentially alter the peptide fold. Since these mutations did not have a significant effect on the interaction with hCCS, it suggests that these mutations likely have a specific effect on the interaction with HAH1 and not a global effect on peptide fold. The Asp491 and 492 residues may be important for mediating electrostatic interactions with one or more of the positively charged residues in HAH1. One of the differences between HAH1 and hCCSD1 is that HAH1 contains several Lys residues that generate a positively charged

surface on the molecule (Figure 91b). Some of these residues in HAH1 have been implicated in forming favourable electrostatic interactions with the negatively charged residues in the target protein which stabilise the formation of a complex between them (Banci *et al.*, 2009; Larin *et al.*, 1999). A similar interaction is also possible with hBACE1 CTD Asp491 and Asp492. Mutation of the Lys residues that are exposed on the surface of HAH1 and can potentially interact with Asp491 and Asp492 in hBACE1 CTD to either negatively charged residues or to a neutral residue will provide more evidence towards this theory. These positively charged residues in HAH1 are however, not conserved in the analogous locations in hCCSD1, which may account for the lack of significant effect observed with the hBACE1 CTD Asp491Ala, Asp492Ala mutations on the interactions with hCCS and hCCSD1.

4.1.1 Physiological relevance of the hCCS/hBACE1 CTD interaction

The results presented in this study provide important information regarding the molecular basis of the interaction of hCCS with hBACE1 CTD. Elucidating the physiological importance of this interaction is complicated by the fact that hCCS and hBACE1 CTD can both interact with several other proteins (Cole and Vassar, 2007; Dingwall, 2007). A multi-protein complex where hCCSD1 can bind hBACE1, hCCSD2 binds hSOD1 and hCCSD3 can interact with X11α which in turn can also associate with APP has been postulated (Dingwall, 2007). Although the existence of such a complex *in vivo* has not been shown, it nevertheless emphasises the difficulty in elucidating the molecular basis of the individual protein-protein interactions since other proteins can potentially influence them. There are only three studies to date that have addressed the hCCS/hBACE1 CTD interaction, but none of them have identified the amino acids involved in mediating this interaction (Angeletti *et al.*, 2005; Gray *et al.*, 2010; Rentmeister *et al.*, 2006). The most recent of these studies by Gray *et al.* (2010) reported increased BACE1 mediated cleavage of APP in cells lacking CCS, although whether this is due to factors including altered copper homeostasis or changes in the localisation of hBACE1 is currently not known. Investigating these factors is vital because hBACE1 CTD is known to be important for mediating the localisation and trafficking of hBACE1 (Benjannet *et al.*, 2001; Capell *et al.*, 2000; He *et al.*, 2002; Huse *et al.*, 2000; Walter *et al.*, 2001), as summarised in Figure 92.

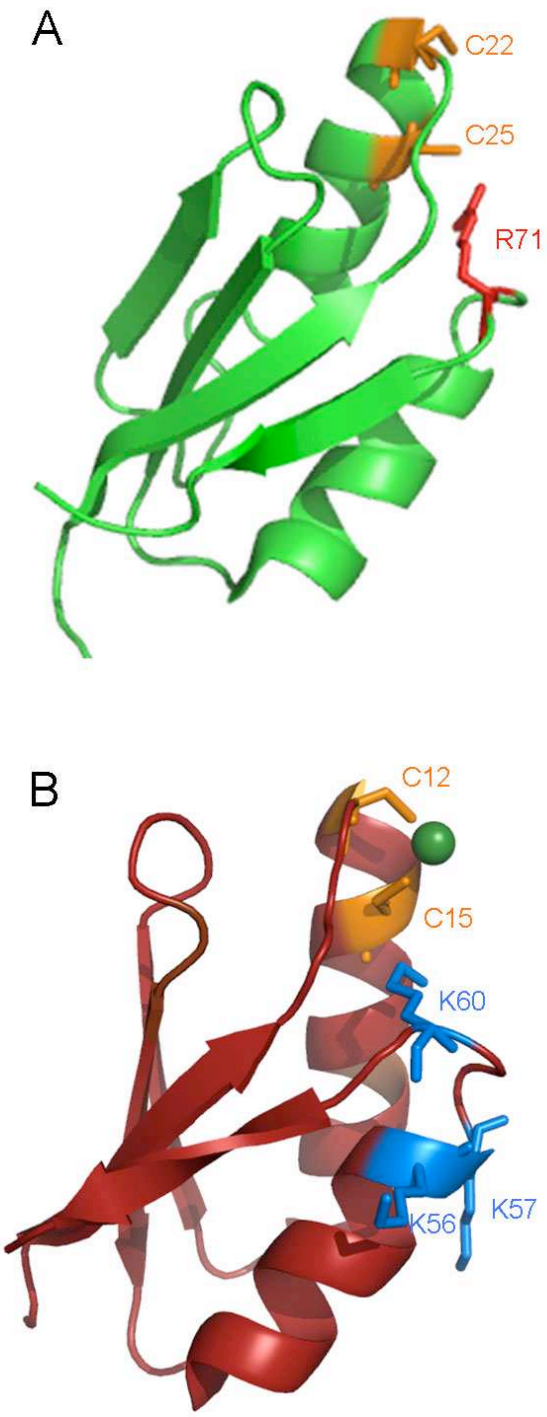

Figure 91: Structures of apo-hCCSD1 and Cu(I)-HAH1 monomers. The NMR structure of hCCSD1 (PDB accession code: 2crl) is shown in (A). The side chains of the Cys residues of the CXXC motif and Arg71 on loop 5 are shown. The crystal structure of Cu(I)-HAH1 is shown in (B) (PDB accession code: 1fee; only a monomer with the bound Cu(I) ion of the dimeric asymmetric unit is shown) (Wernimont *et al.*, 2000). The side chains of the Cys residues of the CXXC motif and some of the positively charges residues located close to the CXXC motif are shown, as labelled.

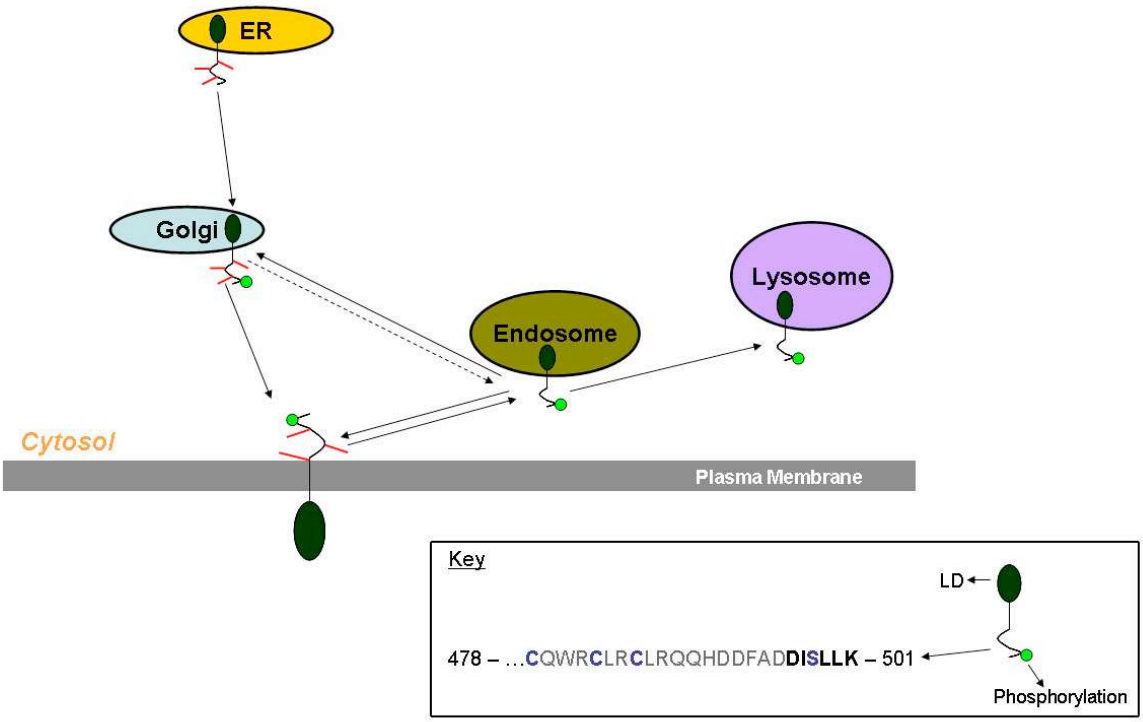

Figure 92: Model depicting the intracellular trafficking of hBACE1 and some of the post-translational modifications that hBACE1 CTD can undergo. hBACE1 is synthesised and glycosylated in the endoplasmic reticulum (ER) with its propeptide domain intact (Capell et al., 2000; Huse et al., 2000). The Cys residues in the CTD can undergo palmitoylation (represented by red lines) which has been suggested to facilitate its exit from the ER and may provide an additional anchor for plasma membrane (PM)-bound hBACE1 (Benjannet et al., 2001). The propeptide domain is cleaved in the Golgi apparatus where hBACE1 is further glycosylated (Capell et al., 2000; Huse et al., 2000) and can be phosphorylated (green sphere) at Ser498 (highlighted in blue in the amino acid sequence) in the CTD (Walter et al., 2001). The DISLL sequence (highlighted in the amino acid sequence) is required to mediate the intracellular localisation and trafficking of hBACE1 (Pastorino et al., 2002; Walter et al., 2001). It has been suggested that hBACE1 can traffic from the Golgi to the endosomal compartment (Huse et al., 2000) although this is yet to be confirmed experimentally. Leu499 and Leu500 are vital for the re-internalisation of hBACE1 from the PM, which is independent of the Ser498 phosphorylation status (Walter et al., 2001). In the endosome, phosphorylated hBACE1 CTD can interact with γ-ear-containing ADP-ribosylation factor-binding (GGA) proteins which can mediate its trafficking to the Golgi or the lysosome (He et al., 2002; He et al., 2005; Pastorino et al., 2002; Shiba et al., 2004; von Arnim et al., 2004). Non-phosphorylated hBACE1 can also recycle back to the PM (He et al., 2005). hBACE1 undergoes degradation in the lysosomal compartment (von Arnim et al., 2006).

hBACE1 CTD undergoes several post-translational modifications including phosphorylation (Walter *et al.*, 2001), palmitoylaton (Benjannet *et al.*, 2001) and farnesylation (Parsons and Austen, 2007). Particularly important for the hCCS/hBACE1 CTD interaction is the fact that the Cys478, Cys482 and Cys485 residues can all undergo palmitoylation (Benjannet *et al.*, 2001). However the precise role of palmitoylation of hBACE1 CTD is not clear. Benjannet *et al.* (2001) found that palmitoylation decreased the ectodomain shedding of hBACE1 and suggested that this could lead to decreased amyloidogenic processing of APP. In contrast, a study by Westmeyer *et al.* (2004) reported palmitoylation to be important for mediating the dimerisation of hBACE1 which significantly enhances the amyloidogenic processing of APP. The data obtained in this study indicate that only hBACE1 CTD that is not palmitoylated at Cys482 or Cys485, should be able to interact with hCCS. A previous study demonstrated that less than 10 % of hBACE1 locates to the plasma membrane, suggesting that ~ 90 % of hBACE1 is likely not palmitoylated (Hussain *et al.*, 2003). This implies that a large proportion of hBACE1 should be available for interaction with hCCS.

The data presented in this study also demonstrate that the hCCS/hBACE1 CTD interaction is impaired under copper-limiting conditions. Since decreased intracellular neuronal copper concentration has been implicated in AD (Filiz *et al.*, 2008), it suggests that in the diseased neurons hCCS may not be able to interact with hBACE1 CTD. Based on the findings by Gray *et al.* (2010) the decreased interaction of hCCS with hBACE1 CTD as a consequence of decreased intracellular copper concentration may subsequently result in increased amyloidogenic processing of APP and increased Aβ production, as summarised in Figure 93. The proposed role of hBACE1 in intracellular copper homeostasis also extends to the inactive form of hBACE1. Inactive hBACE1 is highly expressed in the pancreas although its function is currently not known (Vassar *et al.*, 1999). Since active and inactive hBACE1 differ in the luminal region of hBACE1 rather than its cytoplasmic domain (Bodendorf *et al.*, 2001; Ehehalt *et al.*, 2002), both forms of the protein should be able to bind copper and interact with hCCS. Further studies are however required to elucidate the role of this interaction *in vivo*. Some of the unanswered questions include – can hBACE1 bind Cu(I) via CTD in native conditions? Is Cu(I) transferred from hCCS to hBACE1 CTD or *vice versa*? Is the interaction between hCCS and hBACE1 CTD reduced in AD tissue as a consequence of decreased intracellular copper concentration?

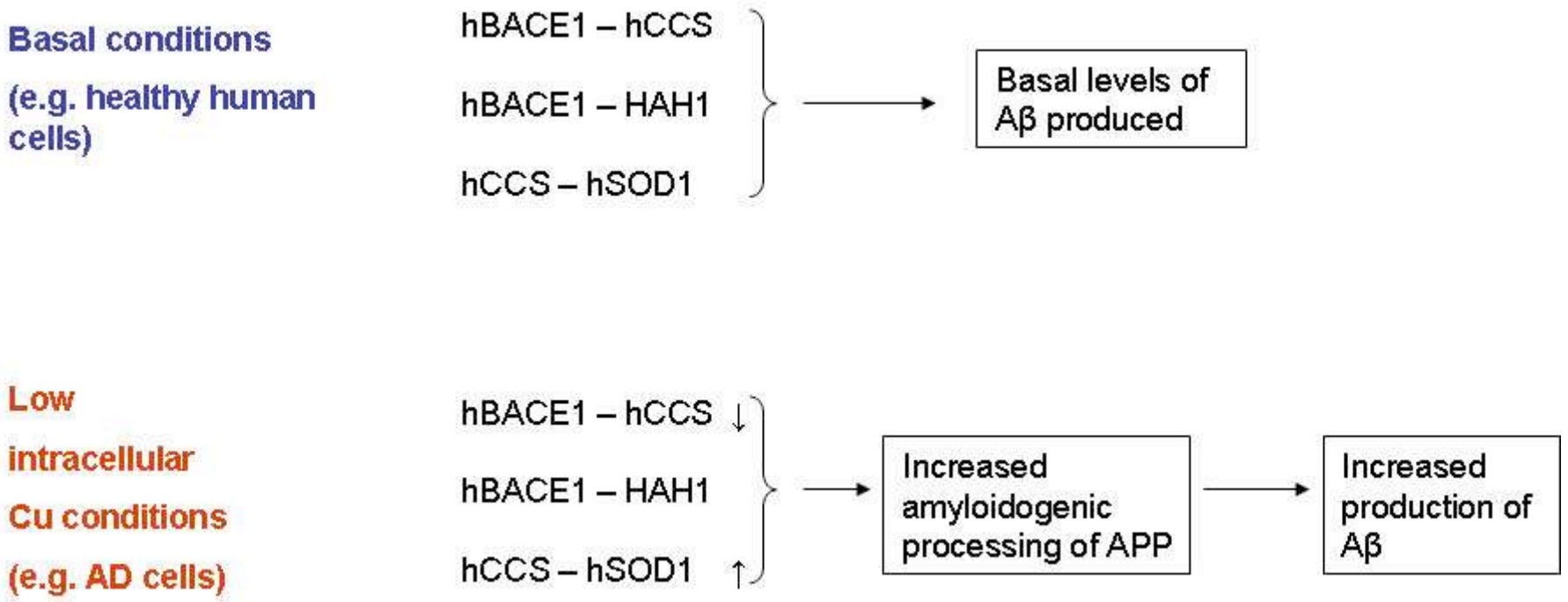

Figure 93: Model demonstrating the effect of copper concentration on the interactions of hBACE1 with hCCS and HAH1, and the interaction of hCCS with hSOD1 with respect to Aβ production. Under basal conditions, for example in healthy human cells, hBACE1 can interact with hCCS and HAH1 via its CTD and hCCS interacts with hSOD1 in the cytosol. In these cells basal levels of Aβ are produced. In conditions where the intracellular copper concentration is low, for example in AD, the interaction of hBACE1 with hCCS decreases whereas the interaction of hCCS with hSOD1 increases. This can lead to increased amyloidogenic processing of APP by hBACE1 resulting in increased production of Aβ (based on the study by Gray *et al.* 2010). The interaction of hBACE1 with HAH1 remains largely unaltered irrespective of the copper concentration.

4.2 Interaction of hSOD1 with hCCS

This study also aimed to further the understanding of the interaction of hCCS with hSOD1. The experiments investigating the effect of copper concentration on the hSOD1/hCCS interaction demonstrate that the interaction remains unaffected at high copper concentration (Figure 60). Similar results were also obtained for the interaction of hCCS with hSOD1 in the presence of 1 mM $CuSO_4$ in a GST-column binding assay (Casareno *et al.*, 1998). However, more than a two-fold increase was observed in the hSOD1/hCCS interaction in copper-deficient conditions (Figure 60). A study by Schmidt *et al.* (2000) found that the yeast two-hybrid interaction of Ccs1 with Sod1 also increased in the presence of BCS. Although no interactions were reported between hCCSD1 and hSOD1 (Casareno *et al.*, 1998) or between Ccs1D1 and Sod1 (Schmidt *et al.*, 2000), the presence of Ccs1D1 was shown to increase the interaction of Ccs1 with Sod1 (Schmidt *et al.*, 2000). In addition, it has been proposed that the CCS-dependent activation of SOD1 may involve the transfer of copper from D1 to D3 of CCS (Furukawa *et al.*, 2004; Rae *et al.*, 2001; Schmidt *et al.*, 1999a). However, no significant interaction was observed between full-length hCCS and hCCSD3 or between hCCSD1 and hCCSD3 in this study (Figure 61). While there is no information available regarding the structural conformation of hCCSD3, some knowledge can be gained from the Ccs1-Sod1 dimer where Ccs1D3 was partially folded into an α-helix (Lamb *et al.*, 2001). Submission of the hCCSD3 amino acid sequence into the Swiss PDB modelling software (http://swissmodel.expasy.org) did not yield any results, likely due to the relatively small size of this domain (comprising less than 40 amino acids). It is possible that hCCSD3 may only be able to obtain its native fold when expressed with hCCSD2 (and perhaps hCCSD1 too). Alternatively, the interaction of hCCSD3 with hCCS may be too weak to be detected by the yeast two-hybrid system.

To further investigate the role of hCCSD1 and hCCSD3 in the interaction with hSOD1, the Cu(I)-binding Cys residues in hCCSD1 and hCCSD3 were mutated. The data obtained in this study indicate that the mutation of Cys22 and Cys25 in hCCS do not have a significant effect on the interaction with hSOD1. The mutation of hCCS Cys244 and Cys246 also did not have a significant effect on the interaction with hSOD1 (Figure 62). Similar results were also observed for the yeast two-hybrid interaction of Sod1 with Ccs1 where the Cu(I)-binding residues in Ccs1D3 were mutated to Ser (Schmidt *et al.*, 2000). The role of Arg71 in hCCS in the interaction with hSOD1 is not clear since the mutation of Arg71 to Ala or Lys does not have a significant effect on the interaction with hSOD1, but the Arg71Glu mutation decreases the interaction (Figure 64). However, the mutation of Lys66Arg in Ccs1 increases its interaction with hSOD1 (Figure 65) suggesting that the residue in loop 5 of Ccs1 may be involved in mediating the interaction with hSOD1.

While the Cu(I)-binding Cys residues in hCCS do not have a significant effect on the interaction with hSOD1 in basal conditions, these residues may play a more important role in copper-deficient conditions. For instance, the absence of Ccs1D1 increased the interaction of Sod1 with a Ccs1 construct lacking D1 under copper-deficient conditions (Schmidt *et al.*, 2000). In addition, a Cu(I) cluster involving Cys244 and Cys246 of hCCS was reported to form when the concentration of Cu(I) was ~ 2-fold higher than the protein concentration (Stasser *et al.*, 2007). The authors further proposed that in excess copper conditions, hCCS may dimerise via the Cu(I) cluster in D3 which would subsequently increase the availability of hCCSD2 for interaction with hSOD1 (Stasser *et al.*, 2007). As mentioned above, the addition of up to 300 μM $CuSO_4$ did not have a significant effect on the hSOD1/hCCS interaction, whereas the interaction decreases in copper-deficient conditions. These data indicate that either a Cu(I)-cluster in hCCSD3 can not form in the yeast two-hybrid system used in this study or that the formation of a Cu(I)-cluster does not have a significant effect on the interaction of hCCS with hSOD1. However, it would be interesting to investigate the effects of mutating the Cu(I)-binding residues in hCCSD3 on the interaction with hSOD1 in copper-deficient and excess copper conditions. Before these experiments could be carried out, a study published by Wood and Thiele (2009) demonstrated that the deletion of *CCS1* or *SOD1* impaired the activation of Mac1 resulting in significantly decreased transcription of *CTR1* in the presence of 10 μM or 100 μM BCS. The authors further demonstrated that active SOD1 is required for Mac1 activity (Wood and Thiele, 2009). Since the hSOD1/hCCS two-hybrid experiments were carried out in the SAY1 strain which lacks *CCS1*, the nuclear copper homeostasis may have been severely compromised and severely altered the copper concentration in this strain compared to the EGY48 (WT) strain. However, it is possible that the presence of hCCS in the hSOD1/hCCS co-transformants may be able to activate endogenous Sod1 and restore Mac1 activity. In addition, the highest BCS concentration studied by Wood and Thiele (2009) was 100 μM whereas in this study up to 3 mM BCS was added to the growth medium. High concentrations of BCS (> 500 μM) may result in decreased nuclear copper concentration despite the absence of *CCS1* in SAY1 cells. Hence, prior to carrying out further experiments in this strain it is vital to perform S1 nuclease experiments on the above co-transformants to verify the induction of *CTR1* in the presence of BCS.

4.3 The interaction of ScAtx1 with $PacS_N$ and $CtaA_N$

Copper metallochaperones such as HAH1, Atx1, ScAtx1 and CopZ are known to interact with cognate MBDs of Cu(I)-ATPases (Banci *et al.*, 2003a; Larin *et al.*, 1999; Portnoy *et al.*, 1999; Pufahl *et al.*, 1997; Radford *et al.*, 2003; Tottey *et al.*, 2002). These protein-protein interactions tend to involve the formation of a Cu(I)-bridged complex where Cu(I) is coordinated by the Cys residues of the CXXC motif (Banci *et al.*,

2006b; Banci *et al.*, 2009; Pufahl *et al.*, 1997). However, the functional implications of the interactions of copper metallochaperones with the MBDs and the role of the MBDs have not been elucidated. Studies investigating the role of MBDs in *A. fulgidus* led to the proposal that apo-MBDs in AfCopA can interact with the N-domain of AfCopA and occlude ATP-binding, thereby preventing Cu(I) transport by AfCopA (Gonzalez-Guerrero *et al.*, 2009; Gonzalez-Guerro and Arguello, 2008; Wu *et al.*, 2008). The acquisition of Cu(I) from Cu(I)-AfCopZ by the MBDs of AfCopA leads to a conformational change which enables ATP binding and Cu(I) transport (Gonzalez-Guerrero *et al.*, 2009; Gonzalez-Guerro and Arguello, 2008; Wu *et al.*, 2008). Cu(I)-bound AfCopZ has also been shown to transport Cu(I) directly to the intramembranous Cu(I)-binding site in AfCopA *in vitro* (Gonzalez-Guerro and Arguello, 2008). A regulatory role has also been proposed for the eukaryotic MBDs in mediating the trafficking and localisation of the Cu(I)-ATPases (Lutsenko *et al.*, 2007a). Atx1 can deliver Cu(I) to both of the MBDs of Ccc2 (Morin *et al.*, 2009; Portnoy *et al.*, 1999; Pufahl *et al.*, 1997; van Dongen *et al.*, 2004). Deletion of both of the MBDs of Ccc2 prevents the transport of Cu(I) to the trans-golgi network (Morin *et al.*, 2009). Furthermore, it has been shown that each MBD of Ccc2 when expressed individually can transfer Cu(I) to a Ccc2 construct lacking both of the MBDs (Morin *et al.*, 2009). This led to the proposal that Cu(I) is transferred from Atx1 to the MBDs of Ccc2 which transport Cu(I) to the intramembranous Cu(I)-binding site in Ccc2 (Morin *et al.*, 2009). The mutation of the Cu(I)-binding Cys residues in the MBDs of ATP7A has been shown to disrupt its trafficking to the plasma membrane (Voskoboinik *et al.*, 1999). HAH1 has been reported to interact most strongly with MBDs 1 and 4 of ATP7A in a Cu(I)-dependent manner and may simultaneously transfer copper to MBDs 5 and 6 (Banci *et al.*, 2007). It has been proposed that in excess copper conditions the interaction of HAH1 with ATP7A MBDs 1 and 4 can result in the localisation of ATP7A at the plasma membrane resulting in Cu(I)-export from the cytosol (Banci *et al.*, 2007).

The interaction of copper metallochaperones with the MBDs are therefore of particular interest for furthering the understanding of their role in regulating Cu(I)-ATPases localisation, trafficking or activity. This study investigated the interactions of the cyanobacterial ScAtx1 with the proposed Cu(I) donor ($CtaA_N$) and acceptor ($PacS_N$). The residues located close to the Cu(I)-binding site and the key residues on the loop 5 of ScAtx1, $PacS_N$ and $CtaA_N$ were shown to be important for mediating protein-protein interactions, as summarised in Table 8. The idea that ScAtx1 can interact with $PacS_N$ and $CtaA_N$ by forming two structurally different complexes (head-to-head or side-to-side) was also investigated. The data indicate that both ScAtx1-$PacS_N$ and ScAtx1-$CtaA_N$ can likely form side-to-side complexes.

Table 8: Summary of the results obtained in this study demonstrating the effects of mutating the residues in ScAtx1 (A), $PacS_N$ (B) and $CtaA_N$ (C) on the yeast two-hybrid interactions with their respective partner proteins. Decreased interactions (compared to the interaction with WT protein) as a result of a mutation are represented by '↓', increased interactions are represented by '↑' and the lack of an interaction by 'X'. '-' indicates that the interaction was not studied. Interactions that are similar to WT are represented by '~ WT'.

A

ScAtx1 mutations	Effect on yeast two-hybrid interaction with $PacS_N$	Effect on yeast two-hybrid interaction with $CtaA_N$	Figure Reference
Ala11Lys	3-fold ↓	5-fold ↓	74
Ala11Arg	3-fold ↓	4-fold ↓	74
Glu13Ala	4-fold ↓	X	75a, 76
Glu13Gln	2-fold ↓	3-fold ↓	75b, 76
Lys21Asp	X	4-fold ↓	87
Asn25Arg	~ WT	4-fold ↓	88
Ser58Ala	3-fold ↓	3-fold ↓	89
His61Ala	3-fold ↓	X	79
His61Glu	X	X	80
His61Lys	2-fold ↓	7-fold ↓	83
His61Phe	X	3-fold ↓	80
His61Tyr	X	~ WT	79

B

$PacS_N$ mutations	Effect on yeast two-hybrid interaction with ScAtx1		
	ScAtx1 WT	ScAtx1 His61Ala	ScAtx1 His61Tyr
Arg13Ala	5-fold ↓ (Fig. 72)	-	-
Tyr65His	8-fold ↓ (Fig. 81)	~ WT (Fig. 81)	X (Fig. 81)

C

$CtaA_N$ mutations	Effect on yeast two-hybrid interaction with ScAtx1	Figure Reference
Lys34Ala	X	73
Phe87His	3-fold ↓	82
Phe87Tyr	5-fold ↓	82

A limited effect of copper concentration was observed on the interaction of ScAtx1 with $PacS_N$ and $CtaA_N$. A small decrease in the interaction of ScAtx1 with $PacS_N$ and $CtaA_N$ is evident in the presence of 300 µM $CuSO_4$ (Figure 69 and Figure 70). The yeast two-hybrid interactions of HAH1 or Atx1 with ATP7B MBD2 or ATP7B MBD4 have also been shown to decrease at high copper concentrations (van Dongen *et al.*, 2004). High copper concentrations may facilitate Cu(I)-bound homo-dimerisation of ScAtx1, which would reduce the amount of ScAtx1 available for interaction with $PacS_N$ or $CtaA_N$. It has previously been shown that apo-ScAtx1 is monomeric with Cu(I)-loading inducing dimerisation (Badarau *et al.*, 2010; Banci *et al.*, 2004a). It was further reported that in the presence of excess Cu(I), ScAtx1 can bind two Cu(I) ions per monomer which increases the stability of the ScAtx1 homo-dimer (Badarau *et al.*, 2010). The interaction of ScAtx1 with $CtaA_N$ increases in copper-deficient conditions. Since less homo-dimerisation of ScAtx1 would be expected at lower copper concentrations (Badarau *et al.*, 2010), this would increase the availability of ScAtx1 monomers for interaction with $CtaA_N$. However no significant effect of BCS addition was observed on the ScAtx1/$PacS_N$ interaction except in the presence of 500 µM BCS. The addition of 500 µM BCS, results in a small decrease in the ScAtx1/$PacS_N$ interaction compared to the co-tranformants incubated in basal medium. The reasons for the decrease in interaction in the presence of 500 µM BCS are not clear since higher concentrations of BCS did not have a significant effect on the ScAtx1/$PacS_N$ interaction. This may indicate the presence of sufficient Cu(I) ions in the yeast nucleus to enable the interactions despite the addition of up to 3 mM BCS to the growth medium.

The interactions of ScAtx1 with $PacS_N$ and $CtaA_N$ are influenced by the residues surrounding the CXXC motif in these proteins. The mutation of $PacS_N$ Arg13 and $CtaA_N$ Lys34 to Ala decreases the interaction with ScAtx1. These data are in agreement with the studies by Banci *et al.* (2010b) who found that the presence of Asp18 in the analogous location in the cyanobacterial Zn(II)-transporter ZiaA, hindered its interaction with ScAtx1. The authors demonstrated that the mutation of $PacS_N$ Arg13 to Asp abolished the interaction with ScAtx1, whereas the ZiaA Asp18Arg mutation enhanced its interaction with ScAtx1 in a bacterial two-hybrid system (Banci *et al.*, 2010b). The mutation of the analogous ScAtx1 Ala11 residue to either Lys or Arg also decreases the interaction with $PacS_N$ and $CtaA_N$. This indicates that while a positively charged residue is required at this position in $PacS_N$ and $CtaA_N$, the presence of two positively charged residues in the complex with ScAtx1 can lead to electrostatic repulsion.

Arg13 in $PacS_N$ and Lys34 in $CtaA_N$ have also been proposed to form favourable electrostatic interactions with Glu13 in ScAtx1 (Banci *et al.*, 2004a). In addition, the side chain of Glu13 in ScAtx1 can also form an inter-molecular hydrogen bond with the side chain of Cys14 in $PacS_N$ (the N-terminal Cys of the CXXC motif in

$PacS_N$) (Banci *et al.*, 2006c). The mutation of Glu13 in ScAtx1 to Ala or Gln decreases the interactions with $PacS_N$ and $CtaA_N$ (Table 8). Both of the mutations were expected to disrupt the formation of favourable electrostatic interactions with the MBDs (Arg13 in $PacS_N$ and Lys34 in $CtaA_N$). Future experiments can be designed to test this hypothesis further by comparing the interaction of wild-type proteins with various combinations of mutant proteins, as discussed in section 5.3. For example, reversing the charges in these positions, that is, replacing ScAtx1 Glu13 with Lys and $PacS_N$ Arg13 or $CtaA_N$ Lys34 with Glu, would be expected to yield wild-type like yeast two-hybrid interactions (in terms of magnitude) which would further demonstrate that these residues are involved in key electrostatic interactions which are important for complex formation between these proteins. The data indicate that the Glu13Ala mutation in ScAtx1 decreases the interactions with $PacS_N$ and $CtaA_N$ more than the Glu13Gln mutation. This is likely because the side chain of Ala can not form hydrogen-bonding interactions, whereas the side chain of Gln can. However, depending upon the acid dissociation constant (pK_a) of the Gln side chain, it may not be able to accept protons from Cys unlike ScAtx1 Glu13 (Banci *et al.*, 2006c). The data suggest that a hydrogen bond may also form between ScAtx1 Glu13 and $CtaA_N$ Cys35 as reported in the ScAtx1-$PacS_N$ complex which is disrupted by the mutation of Glu13 to Ala or Gln (Banci *et al.*, 2006c).

In addition to the above discussed residues, the role of the key loop 5 residues in mediating protein-protein interactions was also investigated. The key loop 5 residue in ScAtx1 is His61 which is not conserved in the ferredoxin-fold of the known copper chaperones. In most bacterial copper metallochaperones this residue is Tyr, whereas in the eukaryotic copper metallochaperones this residue is typically Lys (Arnesano *et al.*, 2002). The mutation of ScAtx1 His61 to Arg enhanced the bacterial two-hybrid interaction of ScAtx1 with PacS MBD but did not affect the interaction with CtaA MBD (Borrelly *et al.*, 2004). To understand the role of this residue further, ScAtx1 His61 was mutated to a variety of amino acids and the results obtained are summarised in Table 8a, b. In addition, the analogous residues in $PacS_N$ (Tyr65) and $CtaA_N$ (Phe87) were also mutated to gain a greater understanding of the role of the key loop 5 residue in mediating protein-protein interactions.

The data indicate that the substitution of ScAtx1 His61 or $PacS_N$ Tyr65 with another amino acid containing an aromatic side chain severely disrupts the interaction of ScAtx1 with $PacS_N$. In the ScAtx1/$PacS_N$ complex – the Tyr/Tyr, Phe/Tyr and Tyr/His combinations impair complex formation, whereas the His/Tyr (WT proteins), Ala/Tyr, Ala/His combinations are less disruptive. This suggests that the presence of two non-native aromatic side chains can result in steric clashes in the ScAtx1/$PacS_N$ complex. Unlike the ScAtx1/$PacS_N$ interaction, the mutation of ScAtx1 His61 to Tyr or Phe does not abolish the interaction with $CtaA_N$. In fact, the interaction of $CtaA_N$ with

ScAtx1 His61Tyr was similar to the interaction with ScAtx1 WT protein. The ScAtx1 His61Tyr mutation is particularly interesting as two crystal structures for this variant are available. These include a side-to-side homo-dimer containing 4 Cu(I) and one chloride ion, and a 4 Cu(I)-bound trimer (Badarau *et al.*, 2010). In addition, ScAtx1 His61Tyr was found to be a monomer in solution in the presence of 1 equivalent of Cu(I) (Badarau *et al.*, 2010). This further supports the data in this study demonstrating that the presence of two Tyr residues (in the ScAtx1 His61Tyr/$PacS_N$ complex) near the metal-binding region is more disruptive than the presence of a Tyr and a Phe residue (in ScAtx1 His61Tyr/CtaA92 complex). Alternatively, it is possible that the interaction with $PacS_N$ was not detected because the formation of this complex was less favourable compared to the homo-dimersation of ScAtx1 His61Tyr. Therefore, in the two-hybrid system there is likely an equilibrium between the formation of homo- and hetero-dimers where only the latter will be detected when assaying for β-galactosidase activity. The mutation of Phe87 in $CtaA_N$ to Tyr or His decreases the interaction with ScAtx1 but does not abolish it completely. The fact that swapping around of the loop 5 residues in $CtaA_N$ and $PacS_N$ can have such detrimental effects on the interactions with ScAtx1 confirms that these residues are not interchangeable but specific for each interaction.

Badarau *et al.* (2010) reported that His61 forms several inter- and intramolecular interactions in the ScAtx1 homo-dimers. In the head-to-head two Cu(I)-bound dimer, His61 forms an intra-subunit hydrogen bond with Cys15 and an inter-subunit hydrogen bond with Cys12. In the side-to-side dimer, His61 was found to hydrogen bond with one of the chloride ions. Since the ScAtx1 homo-dimer structures have been proposed to reflect the complexes of ScAtx1 with CtaA or $PacS_N$ (Badarau *et al.*, 2010), it is not surprising that the mutation of ScAtx1 His61 to Ala whose side chain can not form hydrogen bonds, decreases the interaction of ScAtx1 with both $PacS_N$ and $CtaA_N$. Similar results were also obtained for the interaction of HAH1 with ATP7B MBD4, where the authors demonstrated that the Lys60Ala mutation in HAH1 (analogous to position His61 of ScAtx1) significantly decreased complex formation (Hussain *et al.*, 2009). It has been proposed that Lys65 in Atx1 (analogous to position His61 in ScAtx1) is also important for the stabilisation of the complex formation with Ccc2 MBDs (Arnesano *et al.*, 2004; Portnoy *et al.*, 1999). The side chain of Atx1 Lys65 has been suggested to neutralise the net negative charge of the metal-binding region generated as a consequence of deprotonation of the Cys ligands upon binding Cu(I) (Portnoy *et al.*, 1999). The Lys65Glu mutation in Atx1 was shown to abolish the yeast two-hybrid interaction with Ccc2 MBDs, further demonstrating that the presence of a positively charged residue in this position is important for interaction (Portnoy *et al.*, 1999). Depending upon the pK_a of the His side chain, which is typically around 6 (Mallesha *et al.*, 2001), it can either be neutral or positively charged. If present in its

protonated form, ScAtx1 His61 may also play a role in the neutralization of the negative charge of the metal-binding region in the Cu(I)-bound complex with MBD, similar to Lys65 in Atx1. Therefore, the substitution of ScAtx1 His61 with a positively charged residue should be more favourable than the substitution with a negatively charged residue.

As expected, the ScAtx1 His61Glu mutation abolishes the interactions with both $PacS_N$ and $CtaA_N$. However, the ScAtx1 His61Lys mutation also abolishes the interaction with $CtaA_N$ and decreases the interaction with $PacS_N$. The lack of interaction between ScAtx1 His61Lys and $CtaA_N$ indicates that the presence of a positively charged residue in this position is not sufficient to stabillise the interaction of ScAtx1 with $CtaA_N$. A computational study investigating the mutation of Tyr65 in loop 5 of BsCopZ to Lys demonstrated that this mutation increases the flexibility of the Cu(I)-binding loop in holo-BsCopZ (Rodriguez-Granillo and Wittung-Stafshede, 2009b). If the ScAtx1 His61Lys mutation has a similar effect as the BsCopZ Tyr65Lys mutation, this could account for the decrease in interactions with the MBDs observed in this study. The substitution of Lys60 in HAH1 with Tyr was also reported to decrease complex formation with ATP7B MBD4 (Hussain *et al.*, 2009). Both of these studies found that the substitution of the loop 5 residue with a non-native residue that can donate hydrogen bonds (Tyr or Lys in these studies) had a less detrimental effect than the mutation to a non hydrogen-bond forming residue (such as Ala) (Hussain *et al.*, 2009; Rodriguez-Granillo and Wittung-Stafshede, 2009b). However, in this study the mutation of ScAtx1 His61 to Ala or Lys had an almost equally disruptive effect on the interaction with the target domains. This signifies that the presence of a hydrogen bond donor in this position is not sufficient for complex formation, but properties such as charge and size of the loop 5 residue are also important for interactions. The data therefore indicate that His61 has evolved to be the best choice of amino acid in this position to enable ScAtx1 to interact optimally with both $PacS_N$ and $CtaA_N$.

While mutations in loop 5 of these proteins can lead to disruption of hydrogen-bonding interactions or change the net charge of the metal-binding site all of which can impair complex formation, these mutations can also lead to changes in the structure of loop 5. It would therefore be beneficial to study the effects of the loop 5 residue mutations on the structure by alternative techniques such as molecular mechanics or computational analysis, X-ray crystallography, NMR or CD spectroscopy which can shed further light on the role of these residues. While Cu(I)-binding for the ScAtx1 His61Tyr mutant has been studied by Badarau *et al.* (2010) and was found to be similar to WT ScAtx1, similar experiments need to be carried out for the other loop 5 mutant proteins to deduce if the effects of these mutations seen on complex formation may be due to reduced Cu(I)-binding, as discussed further in section 5.3.

All of the above discussed mutations decrease the interaction of ScAtx1 with $CtaA_N$ more than the ScAtx1/$PacS_N$ interaction, suggesting that changes in the residues surrounding the CXXC motif are more important for ScAtx1/$CtaA_N$ complex formation than the ScAtx1/$PacS_N$ complex. This was initially thought to reflect potentially different structural arrangements of the ScAtx1/$PacS_N$ and ScAtx1/$CtaA_N$ complexes. A modelled complex of ScAtx1-$PacS_N$ demonstrates that these proteins may interact via a side-to-side arrangement (Banci *et al.*, 2006c). Since the crystal structures obtained for the ScAtx1 dimers demonstrate two different structural arrangements (head-to-head and side-to-side, see section 1.2.2.4), the authors suggested that the head-to-head dimer may reflect the arrangement of the ScAtx1-$CtaA_N$ complex (Badarau *et al.*, 2010). The inter-subunit contact area in the head-to-head arrangement of 2 Cu(I) per ScAtx1 dimer was found to be ~230 $Å^2$ per monomer (Badarau *et al.*, 2010) and is mainly localised to the metal-binding region of ScAtx1 (Figure 6a). Whereas, the 4 Cu(I) per ScAtx1 side-to-side dimer, the intersubunit contact area is much larger (~440 $Å^2$ per monomer) and includes not only the metal-binding region but also areas distal from the MBS (Badarau *et al.*, 2010), as evident from Figure 6c. Therefore, any mutations that can affect the MBS can disrupt the formation of both the side-to-side and head-to-head complexes; although mutations in the metal-binding region would be expected to disrupt the ScAtx1/$CtaA_N$ interaction more than the ScAtx1/$PacS_N$ interaction if the former interacts via the formation of a head-to-head complex. Therefore, in order to investigate if ScAtx1 forms structurally different complexes with its partner proteins, three surface residues were selected in ScAtx1 - Lys21, Asn25 and Ser58 which were estimated to be sufficiently distal from the MBS to not affect Cu(I)-binding in ScAtx1. Although Cu(I)-binding studies would be beneficial as a control to conclusively determine that the mutation of these three residues does not impair Cu(I)-binding.

ScAtx1 Lys21 residue was reported to be involved in mediating electrostatic interactions with PacS95 in the modelled complex with ScAtx1 (Banci *et al.*, 2006c). As discussed previously in sections 2.7 and 3.3.5, a ScAtx1/$PacS_N$ model was created by superimposing a monomer of $PacS_N$ on the ScAtx1 4 Cu(I)-bound side-to-side dimer. The ScAtx1/$PacS_N$ model shown in Appendix B is presented again in Figure 94a to assist in comparison with the ScAtx1/$CtaA_N$ model (Figure 94b). In the ScAtx1/$PacS_N$ model, the side chain of the ScAtx1 Lys21 residue is located close to the side chain of Glu61 in $PacS_N$. ScAtx1 Lys21 was therefore mutated to Asp in an attempt to cause electrostatic repulsion with $PacS_N$ Glu61 which would further indicate that ScAtx1 and $PacS_N$ form a side-to-side complex. In contrast, the ScAtx1 Lys21Asp mutant was expected to interact similar to WT ScAtx1 with $CtaA_N$ based on the hypothesis that ScAtx1/$CtaA_N$ may form a head-to-head complex. While the lack of an interaction between ScAtx1 Lys21Asp and $PacS_N$ supports the above-mentioned hypothesis, the decrease in interaction observed with $CtaA_N$ (Table 8a) suggests that it

may also form a side-to-side complex. The residue corresponding to $PacS_N$ Glu61 is Ser (Ser83) in $CtaA_N$. While Ser can not form an electrostatic interaction with Lys21, it may interact via hydrogen bonding. The presence of a potential hydrogen bond acceptor (Asp) in place of a potential hydrogen bond donor (Lys) in ScAtx1 Lys21Asp can disrupt hydrogen-bonding interactions with Ser83 of $CtaA_N$, accounting for the decrease in interaction with $CtaA_N$.

Another residue located close to the interaction surface in the ScAtx1/$PacS_N$ and ScAtx1/$CtaA_N$ complexes is Asn25 of ScAtx1. The side chain of ScAtx1 Asn25 can potentially interact with Glu61 and Ser83 of $PacS_N$ and $CtaA_N$. ScAtx1 Asn25 has also been implicated in mediating hydrogen-bonding interactions between the monomers in the ScAtx1-PacS95 modelled complex (Banci *et al.*, 2006c) and in the ScAtx1 4 Cu(I)-bound side-to-side dimer which may be important for the stabilisation of the complex (Badarau *et al.*, 2010). This residue was substituted with Arg with the aim to disrupt potential hydrogen-bonding interactions in the side-to-side complex due to the increase in bulk at this position. Surprisingly, the ScAtx1 Asn25Arg mutation decreases the interaction with $CtaA_N$, but does not have a significant effect on the interaction with $PacS_N$ (Table 8a). While the bulkiness of Arg in place of Asn25 in ScAtx1 disrupts the complex formation with both $PacS_N$ and $CtaA_N$, in the ScAtx1/$PacS_N$ complex this effect may be compensated by favourable electrostatic interactions between the basic side chain of Arg25 in ScAtx1 and the acidic side chain of $PacS_N$ Glu61. The residue analogous to Glu61 of $PacS_N$ is Ser83 in $CtaA_N$ (Figure 70) which will not form a favourable electrostatic interaction with the side chain of Arg25. In the ScAtx1/$CtaA_N$ complex, presence of the long side chain of Arg25 in ScAtx1 can instead interfere with the side chains of some of the residues in the second α-helix of $CtaA_N$, accounting for the decrease in interaction observed for ScAtx1 Asn25Arg with $CtaA_N$.

The third residue chosen to investigate the potentially different structural complexes of ScAtx1 with its binding partners was Ser58. Ser58 was implicated in forming key hydrogen-bonding interactions with the $PacS_N$ monomer in the model of this complex (Banci *et al.*, 2006c). In the ScAtx1-$PacS_N$ modelled complex, the side chain of Ser58 is proposed to form a hydrogen-bonding interaction with the side chain of Lys27 of $PacS_N$ (Banci *et al.*, 2006c). This is also represented by the models shown in Figure 95a. In addition, the backbone carbonyl of Ser58 was proposed to interact with the side chains of Arg23 and Arg62 of $PacS_N$ (Banci *et al.*, 2006c). In $CtaA_N$, the residues in the analogous position to Arg23, Lys27 and Arg62 of $PacS_N$ are Arg44, Gln48 and Gln84 respectively, as shown in Figure 95b. ScAtx1 Ser58 was therefore mutated to the non-hydrogen-bonding Ala residue in an attempt to destabilise complex formation. The ScAtx1 Ser58Ala mutation had an equally disruptive effect on the

interactions with both $PacS_N$ and $CtaA_N$ suggesting that both of these complexes form via a side-to-side arrangement.

In the absence of structural information regarding the ScAtx1/$CtaA_N$ complex, in particular, the results obtained in this study contribute vitally to furthering the understanding of the complex formation of ScAtx1 with the target MBDs. However, it must be emphasised that the data analyses in this study is based on theoretical models of the complexes created by superimposition of $PacS_N$ and $CtaA_N$ molecules on the ScAtx1 homodimer. In addition, these models do not include any bound Cu(I) ions and therefore present an incomplete picture of the complexes. Cu(I)-binding is known to cause changes in the loop regions of ScAtx1 in particular (Banci *et al.*, 2004a; Banci *et al.*, 2006c), which may alter protein-protein interactions at the interface. Structural evidence for the complex formation of ScAtx1 with its binding partners is therefore required to confirm the results obtained in this study, as discussed further in Section 5.3. The data obtained in this study indicate that both ScAtx1/$PacS_N$ and ScAtx1/$CtaA_N$ can form a side-to-side complex when they interact. However, the Lys21Asp mutation in ScAtx1 was the only change that completely abolished the interaction of ScAtx1 with either of the partner proteins, whereas all of the other mutations either had no effect or only decreased the interactions. Perhaps in order to abolish complex formation, the interacting residues have to be mutated in both of the proteins. For example, as discussed above, disruption in complex formation due to the Asn25Arg mutation in ScAtx1 has been proposed to be compensated for by an interaction with the Glu61 residue in $PacS_N$. To test this theory further, $PacS_N$ Glu61 can be mutated to Gln which is sterically similar to Glu and will remove the charge in this position and therefore disrupt potential electrostatic interactions, as discussed further in Section 5.3. There is also a possibility that both ScAtx1/$PacS_N$ and ScAtx1/$CtaA_N$ may form a mixture of side-to-side and head-to-head complexes. If this is the case, then the interactions with MBDs detected by yeast two-hybrid as a consequence of the mutations in Lys21, Asn25 and Ser58 in ScAtx1 may represent the formation of a head-to-head complex which may be weaker than the side-to-side complex. Therefore, the possibility that ScAtx1/$PacS_N$ and ScAtx1/$CtaA_N$ can form head-to-head complexes as well as side-to-side complexes can not be excluded.

A

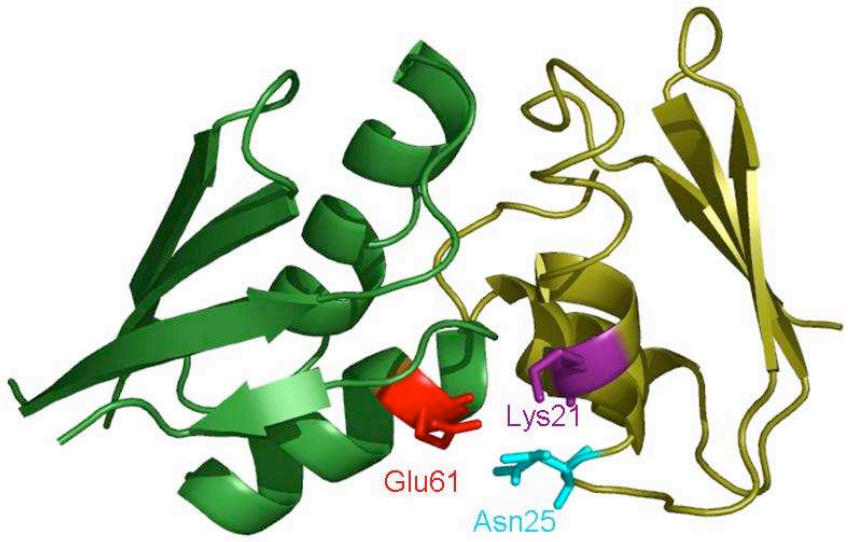

B

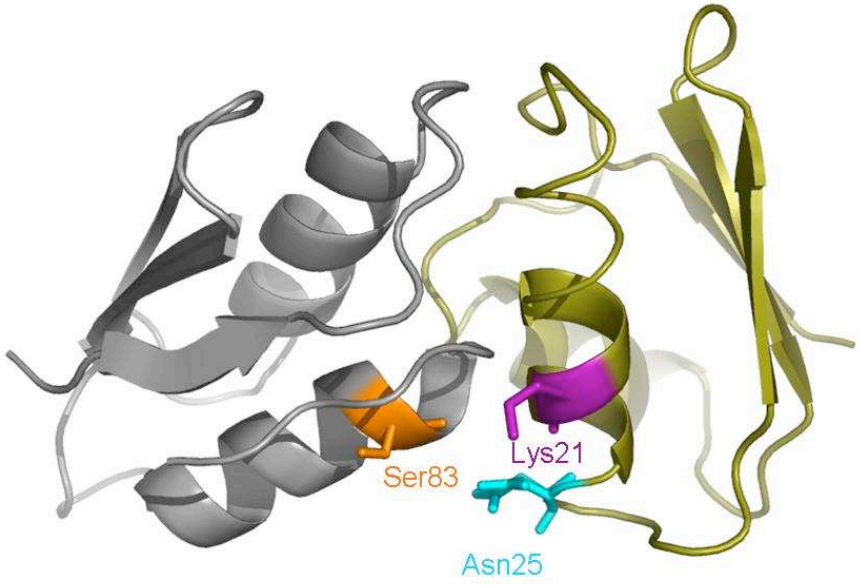

Figure 94: Models of possible complexes of ScAtx1 with $PacS_N$ and $CtaA_N$ showing the interactions of ScAtx1 Lys21 and Asn25. Models of complex formation of ScAtx1 (shown in yellow) (PDB accession code: 2xmk) with $PacS_N$ (PDB accession code: 2xmw) shown in green (A) or $CtaA_N$ shown in grey (B) (Badarau *et al.*, 2010). The side chains of $PacS_N$ Glu61 (red), ScAtx1 Lys21 (purple), ScAtx1 Asn25 (blue) and $CtaA_N$ Ser83 (orange) are shown as sticks. Neither Cu(I) nor the chloride ions bound in the original structures are shown.

A

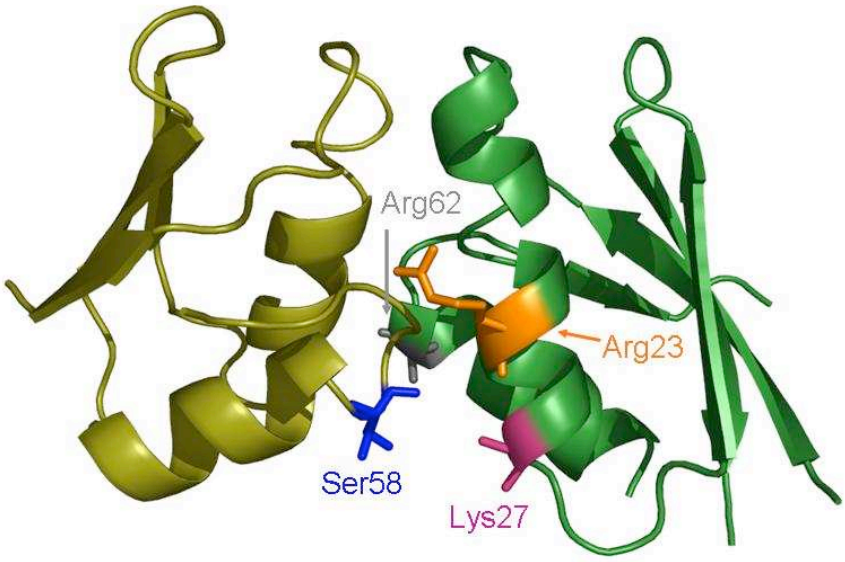

B

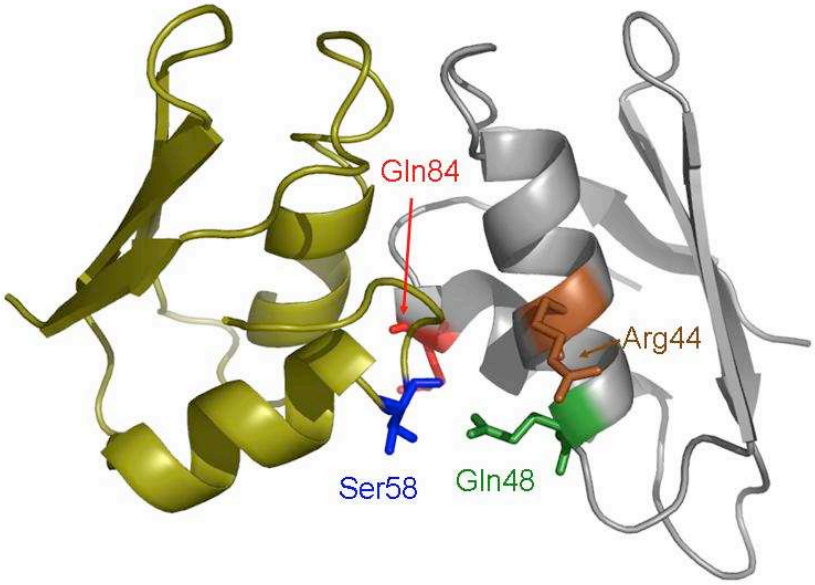

Figure 95: Models of possible complexes of ScAtx1 with $PacS_N$ and $CtaA_N$ showing the interactions of ScAtx1 Ser58. Models of complex formation of ScAtx1 (shown in yellow) (PDB accession code: 2xmk) with $PacS_N$ (PDB accession code: 2xmw) shown in green (A) or $CtaA_N$ shown in grey (B) (Badarau *et al.*, 2010). The side chains of $PacS_N$ Lys27 (purple), $PacS_N$ Arg23 (orange), $PacS_N$ Arg62 (grey), ScAtx1 Ser58 (blue), $CtaA_N$ Arg44 (brown), $CtaA_N$ Gln48 (green) and $CtaA_N$ Gln84 (red) are shown as sticks. Neither Cu(I) nor the chloride ions bound in the original structures are shown.

5. Future Work

As discussed in Chapter 4, the results obtained in this study are analysed based on the presumption that the changes in protein-protein interactions observed in this study are as a consequence of the introduced protein mutations or altered copper conditions (when analysed in the presence of $CuSO_4$ or BCS). However, it is possible that the observed changes may be due to an indirect effect of impaired respiration, redox imbalance or disrupted iron homeostasis. In order to confirm that these pathways were not significantly affected in the co-transformants analysed in this study, it is vital to perform some control experiments. For instance, cytochrome *c* oxidase activity assays can be carried out on all co-tranfsormants to investigate if the introduced mutations or altered copper conditions have a significant effect on respiration. Similarly Sod1 activity assays can be performed to ensure that the cotransformed proteins or the presence of $CuSO_4$ and BCS are not disrupting its activity. In order to determine the effects of protein mutations, $CuSO_4$ or BCS on iron homeostasis, S1 nuclease assays can be carried out to analyse the transcriptional levels of *FRE1* or *FET3*. However, the transcription of *FRE1* and *FET3* are affected by both copper and iron levels sensed by Mac1 and the iron-responsive transcription factor Aft1 (Georgatsou *et al.*, 1997; Labbe *et al.*, 1997; Yamaguchi-Iwai *et al.*, 1995; Yamaguchi-Iwai *et al.*, 1996). Hence, it is quite possible that the transcriptional levels of *FRE1* and *FET3* may be altered in the presence of $CuSO_4$ and BCS. It would therefore be useful to study protein-protein interactions in the presence of $FeCl_3$ or an iron chelator to investigate the effects of altered iron concentration on them.

5.1 Interaction of hCCS with hBACE1 CTD

This study demonstrates that hCCS and hBACE1 CTD may form a Cu(I)-bridged complex. The interaction of hCCS with hBACE1 CTD requires the Cys residues in the CXXC motifs of both molecules. To provide further support for the Cu(I)-dependent interaction between hCCS and hBACE1 CTD, the complex formation can be studied *in vitro* using NMR or CD spectroscopy. This study also suggests that hBACE1 CTD may accept Cu(I) from Cu(I)-loaded hCCS. *In vitro* experiments using Cu(I) chelators such as BCS can be performed in an anaerobic chamber to determine the precise Cu(I)-affinity of hBACE1 CTD and compare them to the Cu(I)-binding affinity of hCCSD1. These experiments can also be used to investigate if Cu(I) is transferred from hCCS to hBACE1 CTD of *vice versa*. Cu(I) transfer can also be studied *in vivo* in *S. cerevisae* similar to the method used previously for studying the transfer of Cu(I) from Cox17 to Sco1 (Horng *et al.*, 2004). Similar to Sco1 and Cox17, hBACE1 CTD and hCCS can also be cloned in a yeast episomal expression vector under an inducible promoter. The

proteins can be purified and the Cu(I) content can be analysed by ICP-MS allowing for comparisons between the Cu(I)-loaded state of each protein in single and double transformants. This experiment would also provide the added advantage of studying these proteins in the cytoplasm which is where they are typically located instead of the yeast nucleus (the site of yeast two-hybrid interaction).

The data presented in this study also highlight several residues in hBACE1 CTD that may be important for the arrangement of the CXXC motif in hBACE1 CTD. Additional mutations to some of these residues can however provide further evidence to demonstrate the role of these residues in complex formation with hCCS and HAH1. For example, hBACE1 CTD Trp480 residue can be mutated to Phe and Tyr which are both hydrophobic and most similar in size to Trp than any of the other naturally produced amino acids, and would therefore be expected to have a milder effect on protein-protein interactions compared to the Trp480Met mutant created in this study. Trp480 can also be mutated to Ala to create a drastic mutation where both residues are hydrophobic but very different in size, this mutation would be expected to abolish the interaction with hCCS and HAH1 if Trp480 plays a major role in the arrangement of the CXXC motif for Cu(I)-binding. The Arg484 and 487 residues in hBACE1 CTD can be mutated to Lys or the acidic residues Glu or Asp to determine if the presence of charge in this position can have any effect on complex formation. The above discussed *in vitro* and *in vivo* experiments can provide further information regarding the effects of these mutations on the Cu(I)-binding affinity of hBACE1 CTD. In addition, it would also be useful to investigate the folding or the structure of hBACE1 CTD in both its apo- and Cu(I)-loaded form, which can again be studied by either CD or NMR spectroscopy.

The role of hCCS Arg71 residue in mediating complex formation with hBACE1 CTD is not clear. To understand its role further, the mutants created in this study should be studied using UV-Vis spectroscopy by conducting competition assays between BCS and the purified mutant proteins in an anaerobic chamber to determine the Cu(I)-binding affinities of these mutant proteins and compare this with WT hCCS. This would indicate if the mutation of Arg71 can affect Cu(I)-binding in hCCS. These mutants can also be studied by CD spectroscopy to determine if the mutations have a significant effect on protein folding. This study also suggests that hBACE1 CTD may interact more strongly with the dimeric form of hCCS rather than an hCCS monomer in the yeast two-hybrid system. This hypothesis can be tested by mutating Phe133 and Gly134 to Glu in domain 2 of hCCS which has previously been shown to disrupt complex formation with Sod1 (Schmidt *et al.*, 2000).

CCS deficiency has been shown to result in increased amyloidogenic processing of APP by BACE1 leading to enhanced Aβ-production *in vivo* (Gray *et al.*, 2010), although the reasons underlying this are currently not known. This study

indicates that the interaction of hCCS with hBACE1 CTD decreases in copper-deficient conditions. On the basis of these results, it would be useful to investigate if the effects on the amyloidogenic processing of APP by BACE1 can be ameliorated by increasing the concentration of copper in these cells. In addition, the role of copper concentration on hBACE1 should be studied in the context of localisation and trafficking of hBACE1 *in vivo*.

5.2 Interaction of hSOD1 with hCCS

The data obtained in this study indicate that the yeast two-hybrid interaction of hSOD1 with hCCS increases in copper-deficient conditions. However, these experiments were carried out in the SAY1 strain which lacks *CCS1* to prevent interference by the interaction of hCCS with endogenous Ccs1. There is evidence to indicate that the transcription of *CTR1* may be compromised in the absence of *CCS1* (Wood and Thiele, 2009). The authors demonstrated that the activity of Mac1 (which regulates the transcription of *CTR1*) requires the presence of functional Sod1 in *S. cerevisiae*. Since hCCS can interact with Sod1 in *S. cerevisiae* (Schmidt *et al.*, 2000) it is possible that Sod1 activity and *CTR1* transcription may be rescued in the SAY1 strain used in this study. This hypothesis can be tested by assaying for the transcription of *CTR1* in the hSOD1/hCCS co-transformants (from the SAY1 strain) using the S1 nuclease experiments. This study also shows that the Cu(I)-binding Cys residues in hCCSD1 and hCCSD3 are not involved in the interaction of hSOD1 with hCCS. However, these residues may play a more important role under conditions of copper-deficiency. Provided the transcription of *CTR1* is not impaired in the SAY1 strain, yeast two-hybrid experiments can be designed to investigate this hypothesis.

If the expression of *CTR1* is compromised in the SAY1 strain then additional measures would have to be employed to study the interaction of hSOD1 with hCCS in yeast. By introducing mutations in the nuclear localisaton signal for *CCS1* and *SOD1*, the presence of Ccs1 and Sod1 in the nucleus can be prevented. However, this would likely result in disrupted Mac1 activity. One possible way to overcome this issue could be by replacing *SOD1* with the gene coding for *C. elegans* SOD1. It has been shown that *C. elegans* SOD1 can be activated by a CCS-independent pathway (Jensen and Culotta, 2005) and can also restore Mac1 activity in *S. cerevisiae* cells lacking *CCS1* and *SOD1* (Wood and Thiele, 2009). Whether hCCS or hSOD1 can form a complex with *C. elegans* SOD1 would also need to be tested prior to manipulating the strain used for yeast two-hybrid analysis.

5.3 Interaction of ScAtx1 with $PacS_N$ and $CtaA_N$

The key residues in the loop 5 of the ferredoxin-like fold of ScAtx1 (His61), $PacS_N$ (Tyr65) and $CtaA_N$ (Phe87) have been shown to be important for the interaction of ScAtx1 with $PacS_N$ and $CtaA_N$ in this study. However, the precise role of these residues in mediating the protein-protein interactions is not very clear. Additional experiments are therefore required to elucidate this further. Mutation of analogous residues has been studied in BsCopZ (Rodriguez-Granillo and Wittung-Stafshede, 2009b) and HAH1 (Rodriguez-Granillo and Wittung-Stafshede, 2009a) using computational analysis. Similar experiments can also be performed with the ScAtx1, $PacS_N$ and $CtaA_N$ loop 5 mutants to study their effects on protein folding. Additional information about these mutations on both the protein itself and the complex formation with its partner protein can be gained by studying these proteins by NMR or CD spectroscopy and X-ray crystallography. The effects of these mutations on the Cu(I)-binding affinity of these proteins should also be investigated. In addition, the role of these residues in Cu(I) transfer and the kinetics of Cu(I)-binding and transfer between ScAtx1 and $PacS_N$ or $CtaA_N$ should also be investigated.

The residues surrounding the metal-binding region in these proteins were also shown to be important for complex formation. Due to the proximity of these residues to the Cu(I)-binding site, it would be useful to determine if these amino acids can also affect the Cu(I)-binding or Cu(I)-transfer between ScAtx1 and its target MBDs. The role of some of these residues can be deciphered further by studying additional mutants. For example, studying the interaction of ScAtx1 Glu13Lys and ScAtx1 Glu13Ala with $PacS_N$ Arg13Glu or $CtaA_N$ Lys34Glu will indicate if the complex formation can tolerate the swapping of charges in these positions. This study also indicates that ScAtx1 can likely form a side-to-side complex with $CtaA_N$, similar to $PacS_N$. Due to time constraints, this study concentrated on mutating some of the residues on the interacting surface of ScAtx1 only to determine the effects on complex formation with its MBDs. To understand the role of Lys21, Asn25 and Ser58 in ScAtx1 further, complimentary mutations should also be made in $PacS_N$ and $CtaA_N$. These would include mutating the Glu61 residue in $PacS_N$ to Gln (to remove the charge in this position but retain hydrogen-bonding ability), Lys (to reverse the charge in this position) or Ala (to remove both the charge and the hydrogen-bonding ability at this position); mutating Ser83 in $CtaA_N$ to Ala to disrupt hydrogen-bonding interactions with ScAtx1. As discussed in section 4.3, Arg23 and Arg62 in $PacS_N$ have also been implicated in mediating hydrogen-bonding and electrostatic interactions with ScAtx1 residues, to investigate this further these residues can be mutated to either an acidic or a neutral residue and study their effects by yeast two-hybrid analysis. Analogous mutations can also be made in $CtaA_N$ to provide similar information. While a HADDOCK model is available for the ScAtx1-PacS95 complex (Banci *et al.*, 2006c), there is no structure available for the

ScAtx1-$CtaA_N$ complex. However, the modelled complex of ScAtx1-PacS95 is not available publically and since it is a model and not a crystal structure, it is essential to study the complex formation of ScAtx1 with $PacS_N$ and $CtaA_N$ using NMR spectroscopy or X-ray crystallography to provide detailed structural information regarding their interaction.

References

Achila, D., Banci, L., Bertini, I., Bunce, J., Ciofi-Baffoni, S., and Huffman, D. L. (2006) Structure of human Wilson protein domains 5 and 6 and their interplay with domain 4 and the copper chaperone HAH1 in copper uptake. *Proc Natl Acad Sci U S A* **103**, 5729-34.

Adlard, P. A., Cherny, R. A., Finkelstein, D. I., Gautier, E., Robb, E., Cortes, M., Volitakis, I., Liu, X., Smith, J. P., Perez, K., Laughton, K., Li, Q. X., Charman, S. A., Nicolazzo, J. A., Wilkins, S., Deleva, K., Lynch, T., Kok, G., Ritchie, C. W., Tanzi, R. E., Cappai, R., Masters, C. L., Barnham, K. J., and Bush, A. I. (2008) Rapid restoration of cognition in Alzheimer's transgenic mice with 8-hydroxy quinoline analogs is associated with decreased interstitial Abeta. *Neuron* **59**, 43-55.

Agarwal, S., Hong, D., Desai, N. K., Sazinsky, M. H., Arguello, J. M., and Rosenzweig, A. C. (2010) Structure and interactions of the C-terminal metal binding domain of *Archaeoglobus fulgidus* CopA. *Proteins* **78**, 2450-8.

Aller, S. G., and Unger, V. M. (2006) Projection structure of the human copper transporter CTR1 at 6-A resolution reveals a compact trimer with a novel channel-like architecture. *Proc Natl Acad Sci U S A* **103**, 3627-32.

Amaravadi, R., Glerum, D. M., and Tzagoloff, A. (1997) Isolation of a cDNA encoding the human homolog of COX17, a yeast gene essential for mitochondrial copper recruitment. *Hum Genet* **99**, 329-33.

Anastassopoulou, I., Banci, L., Bertini, I., Cantini, F., Katsari, E., and Rosato, A. (2004) Solution structure of the apo and copper(I)-loaded human metallochaperone HAH1. *Biochemistry* **43**, 13046-53.

Andreini, C., Banci, L., Bertini, I., and Rosato, A. (2008) Occurrence of copper proteins through the three domains of life: a bioinformatic approach. *J Proteome Res* **7**, 209-16.

Angeletti, B., Waldron, K. J., Freeman, K. B., Bawagan, H., Hussain, I., Miller, C. C., Lau, K. F., Tennant, M. E., Dennison, C., Robinson, N. J., and Dingwall, C. (2005) BACE1 cytoplasmic domain interacts with the copper chaperone for superoxide dismutase-1 and binds copper. *J Biol Chem* **280**, 17930-7.

Aoyama, K., Watabe, M., and Nakaki, T. (2008) Regulation of neuronal glutathione synthesis. *J Pharmacol Sci* **108**, 227-38.

Arguello, J. M., Eren, E., and Gonzalez-Guerrero, M. (2007) The structure and function of heavy metal transport P_{1B}-ATPases. *Biometals* **20**, 233-48.

Arnesano, F., Banci, L., Bertini, I., Cantini, F., Ciofi-Baffoni, S., Huffman, D. L., and O'Halloran, T. V. (2001a) Characterization of the binding interface between the copper chaperone Atx1 and the first cytosolic domain of Ccc2 ATPase. *J Biol Chem* **276**, 41365-76.

Arnesano, F., Banci, L., Bertini, I., Huffman, D. L., and O'Halloran, T. V. (2001b) Solution structure of the Cu(I) and apo forms of the yeast metallochaperone, Atx1. *Biochemistry* **40**, 1528-39.

Arnesano, F., Banci, L., Bertini, I., Ciofi-Baffoni, S., Molteni, E., Huffman, D. L., and O'Halloran, T. V. (2002) Metallochaperones and metal-transporting ATPases: a comparative analysis of sequences and structures. *Genome Res* **12**, 255-71.

Arnesano, F., Banci, L., Bertini, I., and Bonvin, A. M. (2004) A docking approach to the study of copper trafficking proteins; interaction between metallochaperones and soluble domains of copper ATPases. *Structure* **12**, 669-76.

Arnesano, F., Balatri, E., Banci, L., Bertini, I., and Winge, D. R. (2005) Folding studies of Cox17 reveal an important interplay of cysteine oxidation and copper binding. *Structure* **13**, 713-22.

Arredondo, M., Munoz, P., Mura, C. V., and Nunez, M. T. (2003) DMT1, a physiologically relevant apical Cu^{1+} transporter of intestinal cells. *Am J Physiol Cell Physiol* **284**, C1525-30.

Atwood, C. S., Scarpa, R. C., Huang, X., Moir, R. D., Jones, W. D., Fairlie, D. P., Tanzi, R. E., and Bush, A. I. (2000) Characterization of copper interactions with alzheimer amyloid beta peptides: identification of an attomolar-affinity copper binding site on amyloid beta1-42. *J Neurochem* **75**, 1219-33.

Atwood, C. S., Obrenovich, M. E., Liu, T., Chan, H., Perry, G., Smith, M. A., and Martins, R. N. (2003) Amyloid-beta: a chameleon walking in two worlds: a review of the trophic and toxic properties of amyloid-beta. *Brain Res Brain Res Rev* **43**, 1-16.

Atwood, C. S., Perry, G., Zeng, H., Kato, Y., Jones, W. D., Ling, K. Q., Huang, X., Moir, R. D., Wang, D., Sayre, L. M., Smith, M. A., Chen, S. G., and Bush, A. I. (2004) Copper mediates dityrosine cross-linking of Alzheimer's amyloid-beta. *Biochemistry* **43**, 560-8.

Ausubel, F. M., Brent, R., Kingston, R. E., Moore, D. D., Seidman, J. G., Smith, J. A., and Struhl, K. (2002) *Short Protocols in Molecular Biology*. John Wiley & Sons, Inc., USA.

Badarau, A., Firbank, S. J., McCarthy, A. A., Banfield, M. J., and Dennison, C. (2010) Visualizing the metal-binding versatility of copper trafficking sites. *Biochemistry* **49**, 7798-810.

Bagai, I., Rensing, C., Blackburn, N. J., and McEvoy, M. M. (2008) Direct metal transfer between periplasmic proteins identifies a bacterial copper chaperone. *Biochemistry* **47**, 11408-14.

Balamurugan, K., and Schaffner, W. (2006) Copper homeostasis in eukaryotes: teetering on a tightrope. *Biochim Biophys Acta* **1763**, 737-46.

Balasubramanian, R., and Rosenzweig, A. C. (2007) Structural and mechanistic insights into methane oxidation by particulate methane monooxygenase. *Acc Chem Res* **40**, 573-80.

Balasubramanian, R., and Rosenzweig, A. C. (2008) Copper methanobactin: a molecule whose time has come. *Curr Opin Chem Biol* **12**, 245-9.

Banci, L., Bertini, I., Ciofi-Baffoni, S., Huffman, D. L., and O'Halloran, T. V. (2001a) Solution structure of the yeast copper transporter domain Ccc2a in the apo and Cu(I)-loaded states. *J Biol Chem* **276**, 8415-26.

Banci, L., Bertini, I., Del Conte, R., Markey, J., and Ruiz-Duenas, F. J. (2001b) Copper trafficking: the solution structure of *Bacillus subtilis* CopZ. *Biochemistry* **40**, 15660-8.

Banci, L., Bertini, I., Ciofi-Baffoni, S., D'Onofrio, M., Gonnelli, L., Marhuenda-Egea, F. C., and Ruiz-Duenas, F. J. (2002) Solution structure of the N-terminal domain of a potential copper-translocating P-type ATPase from *Bacillus subtilis* in the apo and Cu(I) loaded states. *J Mol Biol* **317**, 415-29.

Banci, L., Bertini, I., Ciofi-Baffoni, S., Del Conte, R., and Gonnelli, L. (2003a) Understanding copper trafficking in bacteria: interactions between the copper transport protein CopZ and the N-terminal domain of the copper ATPase CopA from *Bacillus subtilis*. *Biochemistry* **42**, 1939-1949.

Banci, L., Bertini, I., and Del Conte, R. (2003b) Solution structure of apo CopZ from *Bacillus subtilis*: further analysis of the changes associated with the presence of copper. *Biochemistry* **42**, 13422-8.

Banci, L., Bertini, I., Del Conte, R., Mangani, S., and Meyer-Klaucke, W. (2003c) X-ray absorption and NMR spectroscopic studies of CopZ, a copper chaperone in *Bacillus subtilis*: the coordination properties of the copper ion. *Biochemistry* **42**, 2467-74.

Banci, L., Bertini, I., Ciofi-Baffoni, S., Su, X. C., Borrelly, G. P., and Robinson, N. J. (2004a) Solution structures of a cyanobacterial metallochaperone: insight into an atypical copper-binding motif. *J Biol Chem* **279**, 27502-10.

Banci, L., Bertini, I., Del Conte, R., D'Onofrio, M., and Rosato, A. (2004b) Solution structure and backbone dynamics of the Cu(I) and apo forms of the second metal-binding domain of the Menkes protein ATP7A. *Biochemistry* **43**, 3396-403.

Banci, L., Bertini, I., Cantini, F., Migliardi, M., Rosato, A., and Wang, S. (2005a) An atomic-level investigation of the disease-causing A629P mutant of the Menkes protein, ATP7A. *J Mol Biol* **352**, 409-17.

Banci, L., Bertini, I., Ciofi-Baffoni, S., Chasapis, C. T., Hadjiliadis, N., and Rosato, A. (2005b) An NMR study of the interaction between the human copper(I) chaperone and the second and fifth metal-binding domains of the Menkes protein. *Febs J* **272**, 865-71.

Banci, L., Bertini, I., Cantini, F., DellaMalva, N., Herrmann, T., Rosato, A., and Wuthrich, K. (2006a) Solution structure and intermolecular interactions of the third metal-binding domain of ATP7A, the Menkes disease protein. *J Biol Chem* **281**, 29141-7.

Banci, L., Bertini, I., Cantini, F., Felli, I. C., Gonnelli, L., Hadjiliadis, N., Pierattelli, R., Rosato, A., and Voulgaris, P. (2006b) The Atx1-Ccc2 complex is a metal-mediated protein-protein interaction. *Nat Chem Biol* **2**, 367-8.

Banci, L., Bertini, I., Ciofi-Baffoni, S., Kandias, N. G., Robinson, N. J., Spyroulias, G. A., Su, X. C., Tottey, S., and Vanarotti, M. (2006c) The delivery of copper for thylakoid import observed by NMR. *Proc. Natl Acad. Sci. USA* **103**, 8320-8325.

Banci, L., Bertini, I., Cantini, F., Della-Malva, N., Migliardi, M., and Rosato, A. (2007) The different intermolecular interactions of the soluble copper-binding domains of the menkes protein, ATP7A. *J Biol Chem* **282**, 23140-6.

Banci, L., Bertini, I., Cantini, F., Rosenzweig, A. C., and Yatsunyk, L. A. (2008a) Metal binding domains 3 and 4 of the Wilson disease protein: solution structure and interaction with the copper(I) chaperone HAH1. *Biochemistry* **47**, 7423-9.

Banci, L., Bertini, I., Ciofi-Baffoni, S., Janicka, A., Martinelli, M., Kozlowski, H., and Palumaa, P. (2008b) A structural-dynamical characterization of human Cox17. *J Biol Chem* **283**, 7912-20.

Banci, L., Bertini, I., Calderone, V., Della-Malva, N., Felli, I. C., Neri, S., Pavelkova, A., and Rosato, A. (2009) Copper(I)-mediated protein-protein interactions result from suboptimal interaction surfaces. *Biochem J* **422**, 37-42.

Banci, L., Bertini, I., Ciofi-Baffoni, S., Kozyreva, T., Zovo, K., and Palumaa, P. (2010a) Affinity gradients drive copper to cellular destinations. *Nature* **465**, 645-8.

Banci, L., Bertini, I., Ciofi-Baffoni, S., Poggi, L., Vanarotti, M., Tottey, S., Waldron, K. J., and Robinson, N. J. (2010b) NMR structural analysis of the soluble domain of ZiaA-ATPase and the basis of selective interactions with copper metallochaperone Atx1. *J Biol Inorg Chem* **15**, 87-98.

Banci, L., Bertini, I., McGreevy, K. S., and Rosato, A. (2010c) Molecular recognition in copper trafficking. *Nat Prod Rep* **27**, 695-710.

Barnham, K. J., McKinstry, W. J., Multhaup, G., Galatis, D., Morton, C. J., Curtain, C. C., Williamson, N. A., White, A. R., Hinds, M. G., Norton, R. S., Beyreuther, K., Masters, C. L., Parker, M. W., and Cappai, R. (2003) Structure of the Alzheimer's disease amyloid precursor protein copper binding domain. A regulator of neuronal copper homeostasis. *J Biol Chem* **278**, 17401-7.

Bauerly, K. A., Kelleher, S. L., and Lonnerdal, B. (2004) Functional and molecular responses of suckling rat pups and human intestinal Caco-2 cells to copper treatment. *J Nutr Biochem* **15**, 155-62.

Bayer, T. A., Schafer, S., Simons, A., Kemmling, A., Kamer, T., Tepest, R., Eckert, A., Schussel, K., Eikenberg, O., Sturchler-Pierrat, C., Abramowski, D., Staufenbiel, M., and Multhaup, G. (2003) Dietary Cu stabilizes brain superoxide dismutase 1 activity and reduces amyloid Abeta production in APP23 transgenic mice. *Proc Natl Acad Sci U S A* **100**, 14187-92.

Bellingham, S. A., Ciccotosto, G. D., Needham, B. E., Fodero, L. R., White, A. R., Masters, C. L., Cappai, R., and Camakaris, J. (2004) Gene knockout of amyloid precursor protein and amyloid precursor-like protein-2 increases cellular copper levels in primary mouse cortical neurons and embryonic fibroblasts. *J Neurochem* **91**, 423-8.

Benjannet, S., Elagoz, A., Wickham, L., Mamarbachi, M., Munzer, J. S., Basak, A., Lazure, C., Cromlish, J. A., Sisodia, S., Checler, F., Chretien, M., and Seidah, N. G. (2001) Post-translational processing of beta-secretase (beta-amyloid-converting enzyme) and its ectodomain shedding. The pro- and transmembrane/cytosolic domains affect its cellular activity and amyloid-beta production. *J Biol Chem* **276**, 10879-87.

Bento, I., Carrondo, M. A., and Lindley, P. F. (2006) Reduction of dioxygen by enzymes containing copper. *J Biol Inorg Chem* **11**, 539-47.

Bertini, I., Cavallaro, G., and McGreevy, K. S. (2010) Cellular copper management--a draft user's guide. *Coordination Chemistry Reviews* **254**, 506-524.

Bisaglia, M., Tessari, I., Mammi, S., and Bubacco, L. (2009) Interaction between alpha-synuclein and metal ions, still looking for a role in the pathogenesis of Parkinson's disease. *Neuromolecular Med* **11**, 239-51.

Blindauer, C. A., and Leszczyszyn, O. I. (2010) Metallothioneins: unparalleled diversity in structures and functions for metal ion homeostasis and more. *Nat Prod Rep* **27**, 720-41.

Boal, A. K., and Rosenzweig, A. C. (2009a) Structural biology of copper trafficking. *Chem Rev* **109**, 4760-79.

Boal, A. K., and Rosenzweig, A. C. (2009b) Crystal structures of cisplatin bound to a human copper chaperone. *J Am Chem Soc* **131**, 14196-7.

Bodendorf, U., Fischer, F., Bodian, D., Multhaup, G., and Paganetti, P. (2001) A splice variant of beta-secretase deficient in the amyloidogenic processing of the amyloid precursor protein. *J Biol Chem* **276**, 12019-23.

Borchardt, T., Camakaris, J., Cappai, R., Masters, C. L., Beyreuther, K., and Multhaup, G. (1999) Copper inhibits beta-amyloid production and stimulates the non-amyloidogenic pathway of amyloid-precursor-protein secretion. *Biochem J* **344 Pt 2**, 461-7.

Borrelly, G. P., Blindauer, C. A., Schmid, R., Butler, C. S., Cooper, C. E., Harvey, I., Sadler, P. J., and Robinson, N. J. (2004) A novel copper site in a cyanobacterial metallochaperone. *Biochem J* **378**, 293-7.

Bowness, P. W. (2004) Intracellular zinc and copper: sequestration and trafficking in *Anabaena Pcc 7120*. PhD Thesis, The University of Newcastle, UK.

Brown, D. R. (2009) Brain proteins that mind metals: a neurodegenerative perspective. *Dalton Trans*, 4069-76.

Brown, N. M., Torres, A. S., Doan, P. E., and O'Halloran, T. V. (2004) Oxygen and the copper chaperone CCS regulate posttranslational activation of Cu,Zn superoxide dismutase. *Proc Natl Acad Sci U S A* **101**, 5518-23.

Bunce, J., Achila, D., Hetrick, E., Lesley, L., and Huffman, D. L. (2006) Copper transfer studies between the N-terminal copper binding domains one and four of human Wilson protein. *Biochim Biophys Acta* **1760**, 907-12.

Bush, A. I. (2000) Metals and neuroscience. *Curr Opin Chem Biol* **4**, 184-91.

Bush, A. I. (2003) The metallobiology of Alzheimer's disease. *Trends Neurosci* **26**, 207-14.

Bush, A. I., and Tanzi, R. E. (2008) Therapeutics for Alzheimer's disease based on the metal hypothesis. *Neurotherapeutics* **5**, 421-32.

Butt, T. R., Sternberg, E. J., Gorman, J. A., Clark, P., Hamer, D., Rosenberg, M., and Crooke, S. T. (1984) Copper metallothionein of yeast, structure of the gene, and regulation of expression. *Proc Natl Acad Sci U S A* **81**, 3332-6.

Capaldi, R. A. (1990) Structure and function of cytochrome c oxidase. *Annu Rev Biochem* **59**, 569-96.

Capell, A., Steiner, H., Willem, M., Kaiser, H., Meyer, C., Walter, J., Lammich, S., Multhaup, G., and Haass, C. (2000) Maturation and pro-peptide cleavage of beta-secretase. *J Biol Chem* **275**, 30849-54.

Carr, H. S., George, G. N., and Winge, D. R. (2002) Yeast Cox11, a protein essential for cytochrome c oxidase assembly, is a Cu(I)-binding protein. *J Biol Chem* **277**, 31237-42.

Carroll, M. C., Girouard, J. B., Ulloa, J. L., Subramaniam, J. R., Wong, P. C., Valentine, J. S., and Culotta, V. C. (2004) Mechanisms for activating Cu- and Zn-containing superoxide dismutase in the absence of the CCS Cu chaperone. *Proc Natl Acad Sci U S A* **101**, 5964-9.

Caruano-Yzermans, A. L., Bartnikas, T. B., and Gitlin, J. D. (2006) Mechanisms of the copper-dependent turnover of the copper chaperone for superoxide dismutase. *J Biol Chem* **281**, 13581-7.

Casareno, R. L., Waggoner, D., and Gitlin, J. D. (1998) The copper chaperone CCS directly interacts with copper/zinc superoxide dismutase. *J Biol Chem* **273**, 23625-8.

Chance, B., Sies, H., and Boveris, A. (1979) Hydroperoxide metabolism in mammalian organs. *Physiol Rev* **59**, 527-605.

Chang, L. Y., Slot, J. W., Geuze, H. J., and Crapo, J. D. (1988) Molecular immunocytochemistry of the CuZn superoxide dismutase in rat hepatocytes. *J Cell Biol* **107**, 2169-79.

Chelly, J., Tumer, Z., Tonnesen, T., Petterson, A., Ishikawa-Brush, Y., Tommerup, N., Horn, N., and Monaco, A. P. (1993) Isolation of a candidate gene for Menkes disease that encodes a potential heavy metal binding protein. *Nat Genet* **3**, 14-9.

Cherny, R. A., Atwood, C. S., Xilinas, M. E., Gray, D. N., Jones, W. D., McLean, C. A., Barnham, K. J., Volitakis, I., Fraser, F. W., Kim, Y., Huang, X., Goldstein, L. E., Moir, R. D., Lim, J. T., Beyreuther, K., Zheng, H., Tanzi, R. E., Masters, C. L., and Bush, A. I. (2001) Treatment with a copper-zinc chelator markedly and rapidly inhibits beta-amyloid accumulation in Alzheimer's disease transgenic mice. *Neuron* **30**, 665-76.

Chung, C. T., Niemela, S. L., and Miller, R. H. (1989) One-step preparation of competent *Escherichia coli*: transformation and storage of bacterial cells in the same solution. *Proc Natl Acad Sci U S A* **86**, 2172-5.

Ciriolo, M. R., Desideri, A., Paci, M., and Rotilio, G. (1990) Reconstitution of Cu,Zn-superoxide dismutase by the Cu(I).glutathione complex. *J Biol Chem* **265**, 11030-4.

Cobine, P., Wickramasinghe, W. A., Harrison, M. D., Weber, T., Solioz, M., and Dameron, C. T. (1999) The *Enterococcus hirae* copper chaperone CopZ delivers copper(I) to the CopY repressor. *FEBS Lett* **445**, 27-30.

Cole, S. L., and Vassar, R. (2007) The Alzheimer's disease beta-secretase enzyme, BACE1. *Mol Neurodegener* **2**, 22.

Coulson, E. J., Paliga, K., Beyreuther, K., and Masters, C. L. (2000) What the evolution of the amyloid protein precursor supergene family tells us about its function. *Neurochem Int* **36**, 175-84.

Creighton, T. E. (1993) *Proteins*. W.H. Freeman and Company, New York, USA.

Crichton, R. R., and Pierre, J. L. (2001) Old iron, young copper: from Mars to Venus. *Biometals* **14**, 99-112.

Cuajungco, M. P., Faget, K. Y., Huang, X., Tanzi, R. E., and Bush, A. I. (2000) Metal chelation as a potential therapy for Alzheimer's disease. *Ann N Y Acad Sci* **920**, 292-304.

Culotta, V. C., Howard, W. R., and Liu, X. F. (1994) CRS5 encodes a metallothionein-like protein in *Saccharomyces cerevisiae*. *J Biol Chem* **269**, 25295-302.

Culotta, V. C., Klomp, L. W., Strain, J., Casareno, R. L., Krems, B., and Gitlin, J. D. (1997) The copper chaperone for superoxide dismutase. *J Biol Chem* **272**, 23469-72.

Culotta, V. C., Yang, M., and O'Halloran, T. V. (2006) Activation of superoxide dismutases: putting the metal to the pedal. *Biochim Biophys Acta* **1763**, 747-58.

Dainty, S. J., Patterson, C. J., Waldron, K. J., and Robinson, N. J. (2010) Interaction between cyanobacterial copper chaperone Atx1 and zinc homeostasis. *J Biol Inorg Chem* **15**, 77-85.

Dalle-Donne, I., Rossi, R., Colombo, G., Giustarini, D., and Milzani, A. (2009) Protein S-glutathionylation: a regulatory device from bacteria to humans. *Trends Biochem Sci* **34**, 85-96.

Dancis, A., Roman, D. G., Anderson, G. J., Hinnebusch, A. G., and Klausner, R. D. (1992) Ferric reductase of Saccharomyces cerevisiae: molecular characterization, role in iron uptake, and transcriptional control by iron. *Proc Natl Acad Sci U S A* **89**, 3869-73.

Das, S. K., and Ray, K. (2006) Wilson's disease: an update. *Nat Clin Pract Neurol* **2**, 482-93.

Davis, A. V., and O'Halloran, T. V. (2008) A place for thioether chemistry in cellular copper ion recognition and trafficking. *Nat Chem Biol* **4**, 148-51.

De Feo, C. J., Aller, S. G., Siluvai, G. S., Blackburn, N. J., and Unger, V. M. (2009) Three-dimensional structure of the human copper transporter hCTR1. *Proc Natl Acad Sci U S A* **106**, 4237-42.

De Freitas, J., Wintz, H., Kim, J. H., Poynton, H., Fox, T., and Vulpe, C. (2003) Yeast, a model organism for iron and copper metabolism studies. *Biometals* **16**, 185-97.

DeSilva, T. M., Veglia, G., and Opella, S. J. (2005) Solution structures of the reduced and Cu(I) bound forms of the first metal binding sequence of ATP7A associated with Menkes disease. *Proteins* **61**, 1038-49.

Dingwall, C. (2007) A copper-binding site in the cytoplasmic domain of BACE1 identifies a possible link to metal homoeostasis and oxidative stress in Alzheimer's disease. *Biochem Soc Trans* **35**, 571-3.

Duttaroy, A., Paul, A., Kundu, M., and Belton, A. (2003) A Sod2 null mutation confers severely reduced adult life span in Drosophila. *Genetics* **165**, 2295-9.

Egli, D., Yepiskoposyan, H., Selvaraj, A., Balamurugan, K., Rajaram, R., Simons, A., Multhaup, G., Mettler, S., Vardanyan, A., Georgiev, O., and Schaffner, W. (2006) A family knockout of all four Drosophila metallothioneins reveals a central role in copper homeostasis and detoxification. *Mol Cell Biol* **26**, 2286-96.

Ehehalt, R., Michel, B., De Pietri Tonelli, D., Zacchetti, D., Simons, K., and Keller, P. (2002) Splice variants of the beta-site APP-cleaving enzyme BACE1 in human brain and pancreas. *Biochem Biophys Res Commun* **293**, 30-7.

Eisses, J. F., Stasser, J. P., Ralle, M., Kaplan, J. H., and Blackburn, N. J. (2000) Domains I and III of the human copper chaperone for superoxide dismutase interact via a cysteine-bridged Dicopper(I) cluster. *Biochemistry* **39**, 7337-42.

Eisses, J. F., Chi, Y., and Kaplan, J. H. (2005) Stable plasma membrane levels of hCTR1 mediate cellular copper uptake. *J Biol Chem* **280**, 9635-9.

Eisses, J. F., and Kaplan, J. H. (2005) The mechanism of copper uptake mediated by human CTR1: a mutational analysis. *J Biol Chem* **280**, 37159-68.

Estojak, J., Brent, R., and Golemis, E. A. (1995) Correlation of two-hybrid affinity data with in vitro measurements. *Mol Cell Biol* **15**, 5820-9.

Faller, P. (2009) Copper and zinc binding to amyloid-beta: coordination, dynamics, aggregation, reactivity and metal-ion transfer. *Chembiochem* **10**, 2837-45.

Faller, P., and Hureau, C. (2009) Bioinorganic chemistry of copper and zinc ions coordinated to amyloid-beta peptide. *Dalton Trans*, 1080-94.

Fan, B., Grass, G., Rensing, C., and Rosen, B. P. (2001) *Escherichia coli* CopA N-terminal Cys(X)(2)Cys motifs are not required for copper resistance or transport. *Biochem Biophys Res Commun* **286**, 414-8.

Fan, B., and Rosen, B. P. (2002) Biochemical characterization of CopA, the *Escherichia coli* Cu(I)-translocating P-type ATPase. *J Biol Chem* **277**, 46987-92.

Farquhar, J., Bao, H., and Thiemens, M. (2000) Atmospheric influence of Earth's earliest sulfur cycle. *Science* **289**, 756-9.

Faux, N. G., Ritchie, C. W., Gunn, A., Rembach, A., Tsatsanis, A., Bedo, J., Harrison, J., Lannfelt, L., Blennow, K., Zetterberg, H., Ingelsson, M., Masters, C. L., Tanzi, R. E., Cummings, J. L., Herd, C. M., and Bush, A. I. (2010) PBT2 rapidly improves cognition in Alzheimer's Disease: additional phase II analyses. *J Alzheimers Dis* **20**, 509-16.

Ferreira, A. M., Ciriolo, M. R., Marcocci, L., and Rotilio, G. (1993) Copper(I) transfer into metallothionein mediated by glutathione. *Biochem J* **292 (Pt 3)**, 673-6.

Filiz, G., Price, K. A., Caragounis, A., Du, T., Crouch, P. J., and White, A. R. (2008) The role of metals in modulating metalloprotease activity in the AD brain. *Eur Biophys J* **37**, 315-21.

Fleming, R. E., and Gitlin, J. D. (1990) Primary structure of rat ceruloplasmin and analysis of tissue-specific gene expression during development. *J Biol Chem* **265**, 7701-7.

Fogel, S., and Welch, J. W. (1982) Tandem gene amplification mediates copper resistance in yeast. *Proc Natl Acad Sci U S A* **79**, 5342-6.

Forman, H. J., and Fridovich, I. (1973) On the stability of bovine superoxide dismutase. The effects of metals. *J Biol Chem* **248**, 2645-9.

Franke, S., Grass, G., Rensing, C., and Nies, D. H. (2003) Molecular analysis of the copper-transporting efflux system CusCFBA of *Escherichia coli*. *J Bacteriol* **185**, 3804-12.

Frausto da Silva, J. J. R., and Williams, R. J. P. (2001) *The Biological Chemistry of the Elements*. Oxford University Press. Oxford.

Fu, D., Beeler, T. J., and Dunn, T. M. (1995) Sequence, mapping and disruption of CCC2, a gene that cross-complements the Ca(2+)-sensitive phenotype of csg1 mutants and encodes a P-type ATPase belonging to the Cu(2+)-ATPase subfamily. *Yeast* **11**, 283-92.

Furukawa, Y., Torres, A. S., and O'Halloran, T. V. (2004) Oxygen-induced maturation of SOD1: a key role for disulfide formation by the copper chaperone CCS. *Embo J* **23**, 2872-81.

Furukawa, Y., and O'Halloran, T. V. (2006) Posttranslational modifications in Cu,Zn-superoxide dismutase and mutations associated with amyotrophic lateral sclerosis. *Antioxid Redox Signal* **8**, 847-67.

Gaballa, A., and Helmann, J. D. (2003) Bacillus subtilis CPx-type ATPases: characterization of Cd, Zn, Co and Cu efflux systems. *Biometals* **16**, 497-505.

Gambling, L., Andersen, H. S., and McArdle, H. J. (2008) Iron and copper, and their interactions during development. *Biochem Soc Trans* **36**, 1258-61.

Garrick, M. D., Dolan, K. G., Horbinski, C., Ghio, A. J., Higgins, D., Porubcin, M., Moore, E. G., Hainsworth, L. N., Umbreit, J. N., Conrad, M. E., Feng, L., Lis, A., Roth, J. A., Singleton, S., and Garrick, L. M. (2003) DMT1: a mammalian transporter for multiple metals. *Biometals* **16**, 41-54.

Gatti, D., Mitra, B., and Rosen, B. P. (2000) *Escherichia coli* soft metal ion-translocating ATPases. *J Biol Chem* **275**, 34009-12.

Georgatsou, E., Mavrogiannis, L. A., Fragiadakis, G. S., and Alexandraki, D. (1997) The yeast Fre1p/Fre2p cupric reductases facilitate copper uptake and are regulated by the copper-modulated Mac1p activator. *J Biol Chem* **272**, 13786-92.

Gitlin, J. D., Schroeder, J. J., Lee-Ambrose, L. M., and Cousins, R. J. (1992) Mechanisms of caeruloplasmin biosynthesis in normal and copper-deficient rats. *Biochem J* **282 (Pt 3)**, 835-9.

Gitschier, J., Moffat, B., Reilly, D., Wood, W. I., and Fairbrother, W. J. (1998) Solution structure of the fourth metal-binding domain from the Menkes copper-transporting ATPase. *Nat Struct Biol* **5**, 47-54.

Glenner, G. G., and Wong, C. W. (1984) Alzheimer's disease: initial report of the purification and characterization of a novel cerebrovascular amyloid protein. *Biochem Biophys Res Commun* **120**, 885-90.

Glerum, D. M., Shtanko, A., and Tzagoloff, A. (1996a) SCO1 and SCO2 act as high copy suppressors of a mitochondrial copper recruitment defect in *Saccharomyces cerevisiae*. *J Biol Chem* **271**, 20531-5.

Glerum, D. M., Shtanko, A., and Tzagoloff, A. (1996b) Characterization of COX17, a yeast gene involved in copper metabolism and assembly of cytochrome oxidase. *J Biol Chem* **271**, 14504-9.

Goate, A., Chartier-Harlin, M. C., Mullan, M., Brown, J., Crawford, F., Fidani, L., Giuffra, L., Haynes, A., Irving, N., James, L., and et al. (1991) Segregation of a missense mutation in the amyloid precursor protein gene with familial Alzheimer's disease. *Nature* **349**, 704-6.

Gonzalez-Guerrero, M., Hong, D., and Arguello, J. M. (2009) Chaperone-mediated Cu^{+} delivery to Cu^{+} transport ATPases: requirement of nucleotide binding. *J Biol Chem* **284**, 20804-11.

Gonzalez-Guerro, M., and Arguello, J. M. (2008) Mechanisms of Cu^{+}-transporting ATPases: soluble Cu^{+} chaperones directly transfer Cu^{+} to transmembrane transport sites. *Proc. Natl Acad. Sci. USA* **105**, 5992-5997.

Gouras, G. K., Xu, H., Jovanovic, J. N., Buxbaum, J. D., Wang, R., Greengard, P., Relkin, N. R., and Gandy, S. (1998) Generation and regulation of beta-amyloid peptide variants by neurons. *J Neurochem* **71**, 1920-5.

Graden, J. A., and Winge, D. R. (1997) Copper-mediated repression of the activation domain in the yeast Mac1p transcription factor. *Proc Natl Acad Sci U S A* **94**, 5550-5.

Gray, E. H., De Vos, K. J., Dingwall, C., Perkinton, M. S., and Miller, C. C. (2010) Deficiency of the copper chaperone for superoxide dismutase increases amyloid-beta production. *J Alzheimers Dis* **21**, 1101-5.

Greenough, M., Pase, L., Voskoboinik, I., Petris, M. J., O'Brien, A. W., and Camakaris, J. (2004) Signals regulating trafficking of Menkes (MNK; ATP7A) copper-translocating P-type ATPase in polarized MDCK cells. *Am J Physiol Cell Physiol* **287**, C1463-71.

Grundke-Iqbal, I., Iqbal, K., Tung, Y. C., Quinlan, M., Wisniewski, H. M., and Binder, L. I. (1986) Abnormal phosphorylation of the microtubule-associated protein tau (tau) in Alzheimer cytoskeletal pathology. *Proc Natl Acad Sci U S A* **83**, 4913-7.

Gunshin, H., Mackenzie, B., Berger, U. V., Gunshin, Y., Romero, M. F., Boron, W. F., Nussberger, S., Gollan, J. L., and Hediger, M. A. (1997) Cloning and characterization of a mammalian proton-coupled metal-ion transporter. *Nature* **388**, 482-8.

Guo, Y., Smith, K., Lee, J., Thiele, D. J., and Petris, M. J. (2004) Identification of methionine-rich clusters that regulate copper-stimulated endocytosis of the human Ctr1 copper transporter. *J Biol Chem* **279**, 17428-33.

Haass, C., Hung, A. Y., and Selkoe, D. J. (1991) Processing of beta-amyloid precursor protein in microglia and astrocytes favors an internal localization over constitutive secretion. *J Neurosci* **11**, 3783-93.

Haass, C., Schlossmacher, M. G., Hung, A. Y., Vigo-Pelfrey, C., Mellon, A., Ostaszewski, B. L., Lieberburg, I., Koo, E. H., Schenk, D., Teplow, D. B., and et al. (1992) Amyloid beta-peptide is produced by cultured cells during normal metabolism. *Nature* **359**, 322-5.

Hall, L. T., Sanchez, R. J., Holloway, S. P., Zhu, H., Stine, J. E., Lyons, T. J., Demeler, B., Schirf, V., Hansen, J. C., Nersissian, A. M., Valentine, J. S., and Hart, P. J. (2000) X-ray crystallographic and analytical ultracentrifugation analyses of truncated and full-length yeast copper chaperones for SOD (LYS7): a dimer-dimer model of LYS7-SOD association and copper delivery. *Biochemistry* **39**, 3611-23.

Hamza, I., Schaefer, M., Klomp, L. W., and Gitlin, J. D. (1999) Interaction of the copper chaperone HAH1 with the Wilson disease protein is essential for copper homeostasis. *Proc Natl Acad Sci U S A* **96**, 13363-8.

Hardy, J., and Selkoe, D. J. (2002) The amyloid hypothesis of Alzheimer's disease: progress and problems on the road to therapeutics. *Science* **297**, 353-6.

Hardy, J. A., and Higgins, G. A. (1992) Alzheimer's disease: the amyloid cascade hypothesis. *Science* **256**, 184-5.

Harris, Z. L., Durley, A. P., Man, T. K., and Gitlin, J. D. (1999) Targeted gene disruption reveals an essential role for ceruloplasmin in cellular iron efflux. *Proc Natl Acad Sci U S A* **96**, 10812-7.

Harrison, S. M., Harper, A. J., Hawkins, J., Duddy, G., Grau, E., Pugh, P. L., Winter, P. H., Shilliam, C. S., Hughes, Z. A., Dawson, L. A., Gonzalez, M. I., Upton, N., Pangalos, M. N., and Dingwall, C. (2003) BACE1 (beta-secretase) transgenic and knockout mice: identification of neurochemical deficits and behavioral changes. *Mol Cell Neurosci* **24**, 646-55.

Hassett, R., and Kosman, D. J. (1995) Evidence for Cu(II) reduction as a component of copper uptake by Saccharomyces cerevisiae. *J Biol Chem* **270**, 128-34.

Hassett, R., Dix, D. R., Eide, D. J., and Kosman, D. J. (2000) The Fe(II) permease Fet4p functions as a low affinity copper transporter and supports normal copper trafficking in Saccharomyces cerevisiae. *Biochem J* **351 Pt 2**, 477-84.

He, X., Chang, W. P., Koelsch, G., and Tang, J. (2002) Memapsin 2 (beta-secretase) cytosolic domain binds to the VHS domains of GGA1 and GGA2: implications on the endocytosis mechanism of memapsin 2. *FEBS Lett* **524**, 183-7.

He, X., Li, F., Chang, W. P., and Tang, J. (2005) GGA proteins mediate the recycling pathway of memapsin 2 (BACE). *J Biol Chem* **280**, 11696-703.

Hearnshaw, S., West, C., Singleton, C., Zhou, L., Kihlken, M. A., Strange, R. W., Le Brun, N. E., and Hemmings, A. M. (2009) A tetranuclear Cu(I) cluster in the metallochaperone protein CopZ. *Biochemistry* **48**, 9324-6.

Hellman, N. E., and Gitlin, J. D. (2002) Ceruloplasmin metabolism and function. *Annu Rev Nutr* **22**, 439-58.

Hesse, L., Beher, D., Masters, C. L., and Multhaup, G. (1994) The beta A4 amyloid precursor protein binding to copper. *FEBS Lett* **349**, 109-16.

Holtzman, N. A., and Gaumnitz, B. M. (1970) Studies on the rate of release and turnover of ceruloplasmin and apoceruloplasmin in rat plasma. *J Biol Chem* **245**, 2354-8.

Holzer, A. K., Samimi, G., Katano, K., Naerdemann, W., Lin, X., Safaei, R., and Howell, S. B. (2004) The copper influx transporter human copper transport protein 1 regulates the uptake of cisplatin in human ovarian carcinoma cells. *Mol Pharmacol* **66**, 817-23.

Holzer, A. K., Varki, N. M., Le, Q. T., Gibson, M. A., Naredi, P., and Howell, S. B. (2006) Expression of the human copper influx transporter 1 in normal and malignant human tissues. *J Histochem Cytochem* **54**, 1041-9.

Horng, Y. C., Cobine, P. A., Maxfield, A. B., Carr, H. S., and Winge, D. R. (2004) Specific copper transfer from the Cox17 metallochaperone to both Sco1 and Cox11 in the assembly of yeast cytochrome C oxidase. *J Biol Chem* **279**, 35334-40.

http://swissmodel.expasy.org

http://www.ebi.ac.uk/Tools/clustalw/

Huang, X., Atwood, C. S., Hartshorn, M. A., Multhaup, G., Goldstein, L. E., Scarpa, R. C., Cuajungco, M. P., Gray, D. N., Lim, J., Moir, R. D., Tanzi, R. E., and Bush, A. I. (1999) The A beta peptide of Alzheimer's disease directly produces hydrogen peroxide through metal ion reduction. *Biochemistry* **38**, 7609-16.

Huffman, D. L., and O'Halloran, T. V. (2000) Energetics of copper trafficking between the Atx1 metallochaperone and the intracellular copper transporter, Ccc2. *J Biol Chem* **275**, 18611-4.

Hung, I. H., Suzuki, M., Yamaguchi, Y., Yuan, D. S., Klausner, R. D., and Gitlin, J. D. (1997) Biochemical characterization of the Wilson disease protein and functional expression in the yeast *Saccharomyces cerevisiae*. *J Biol Chem* **272**, 21461-6.

Hung, I. H., Casareno, R. L., Labesse, G., Mathews, F. S., and Gitlin, J. D. (1998) HAH1 is a copper-binding protein with distinct amino acid residues mediating copper homeostasis and antioxidant defense. *J Biol Chem* **273**, 1749-54.

Huse, J. T., Pijak, D. S., Leslie, G. J., Lee, V. M., and Doms, R. W. (2000) Maturation and endosomal targeting of beta-site amyloid precursor protein-cleaving enzyme. The Alzheimer's disease beta-secretase. *J Biol Chem* **275**, 33729-37.

Hussain, F., Olson, J. S., and Wittung-Stafshede, P. (2008) Conserved residues modulate copper release in human copper chaperone Atox1. *Proc Natl Acad Sci U S A* **105**, 11158-63.

Hussain, F., Rodriguez-Granillo, A., and Wittung-Stafshede, P. (2009) Lysine-60 in copper chaperone Atox1 plays an essential role in adduct formation with a target Wilson disease domain. *J Am Chem Soc* **131**, 16371-3.

Hussain, I., Powell, D., Howlett, D. R., Tew, D. G., Meek, T. D., Chapman, C., Gloger, I. S., Murphy, K. E., Southan, C. D., Ryan, D. M., Smith, T. S., Simmons, D. L., Walsh, F. S., Dingwall, C., and Christie, G. (1999) Identification of a novel aspartic protease (Asp 2) as beta-secretase. *Mol Cell Neurosci* **14**, 419-27.

Hussain, I., Hawkins, J., Shikotra, A., Riddell, D. R., Faller, A., and Dingwall, C. (2003) Characterization of the ectodomain shedding of the beta-site amyloid precursor protein-cleaving enzyme 1 (BACE1). *J Biol Chem* **278**, 36264-8.

Irving, H., and Williams, R. J. P. (1948) Order of stability of metal complexes. *Nature* **162**, 746-747.

Islinger, M., Li, K. W., Seitz, J., Volkl, A., and Luers, G. H. (2009) Hitchhiking of Cu/Zn superoxide dismutase to peroxisomes--evidence for a natural piggyback import mechanism in mammals. *Traffic* **10**, 1711-21.

Itoh, S., Kim, H. W., Nakagawa, O., Ozumi, K., Lessner, S. M., Aoki, H., Akram, K., McKinney, R. D., Ushio-Fukai, M., and Fukai, T. (2008) Novel role of antioxidant-1 (Atox1) as a copper-dependent transcription factor involved in cell proliferation. *J Biol Chem* **283**, 9157-67.

Itoh, S., Ozumi, K., Kim, H. W., Nakagawa, O., McKinney, R. D., Folz, R. J., Zelko, I. N., Ushio-Fukai, M., and Fukai, T. (2009) Novel mechanism for regulation of extracellular SOD transcription and activity by copper: role of antioxidant-1. *Free Radic Biol Med* **46**, 95-104.

Jensen, L. T., Howard, W. R., Strain, J. J., Winge, D. R., and Culotta, V. C. (1996) Enhanced effectiveness of copper ion buffering by CUP1 metallothionein compared with CRS5 metallothionein in *Saccharomyces cerevisiae*. *J Biol Chem* **271**, 18514-9.

Jensen, L. T., Posewitz, M. C., Srinivasan, C., and Winge, D. R. (1998) Mapping of the DNA binding domain of the copper-responsive transcription factor Mac1 from Saccharomyces cerevisiae. *J Biol Chem* **273**, 23805-11.

Jensen, L. T., and Culotta, V. C. (2005) Activation of CuZn superoxide dismutases from *Caenorhabditis elegans* does not require the copper chaperone CCS. *J Biol Chem* **280**, 41373-9.

Jiang, J., Nadas, I. A., Kim, M. A., and Franz, K. J. (2005) A Mets motif peptide found in copper transport proteins selectively binds Cu(I) with methionine-only coordination. *Inorg Chem* **44**, 9787-94.

Jiao, Y., and Yang, P. (2007) Mechanism of copper(II) inhibiting Alzheimer's amyloid beta-peptide from aggregation: a molecular dynamics investigation. *J Phys Chem B* **111**, 7646-55.

Jin, L. W., Ninomiya, H., Roch, J. M., Schubert, D., Masliah, E., Otero, D. A., and Saitoh, T. (1994) Peptides containing the RERMS sequence of amyloid beta/A4 protein precursor bind cell surface and promote neurite extension. *J Neurosci* **14**, 5461-70.

Jones, C. E., Daly, N. L., Cobine, P. A., Craik, D. J., and Dameron, C. T. (2003) Structure and metal binding studies of the second copper binding domain of the Menkes ATPase. *J Struct Biol* **143**, 209-18.

Joshi, A., Serpe, M., and Kosman, D. J. (1999) Evidence for (Mac1p)2.DNA ternary complex formation in Mac1p-dependent transactivation at the CTR1 promoter. *J Biol Chem* **274**, 218-26.

Kanamaru, K., Kashiwagi, S., and Mizuno, T. (1993) The cyanobacterium, *Synechococcus* sp. PCC7942, possesses two distinct genes encoding cation-transporting P-type ATPases. *FEBS Lett* **330**, 99-104.

Kang, J., Lemaire, H. G., Unterbeck, A., Salbaum, J. M., Masters, C. L., Grzeschik, K. H., Multhaup, G., Beyreuther, K., and Muller-Hill, B. (1987) The precursor of Alzheimer's disease amyloid A4 protein resembles a cell-surface receptor. *Nature* **325**, 733-6.

Kaplan, J. H., and Lutsenko, S. (2009) Copper transport in mammalian cells: special care for a metal with special needs. *J Biol Chem* **284**, 25461-5.

Karr, J. W., Akintoye, H., Kaupp, L. J., and Szalai, V. A. (2005) N-Terminal deletions modify the Cu^{2+} binding site in amyloid-beta. *Biochemistry* **44**, 5478-87.

Kasting, J. F., and Siefert, J. L. (2002) Life and the evolution of Earth's atmosphere. *Science* **296**, 1066-8.

Kaufmann, K., Anfang, N., Saedler, H., and Theissen, G. (2005) Mutant analysis, protein-protein interactions and subcellular localization of the Arabidopsis B sister (ABS) protein. *Mol Genet Genomics* **274**, 103-18.

Keller, G. A., Warner, T. G., Steimer, K. S., and Hallewell, R. A. (1991) Cu,Zn superoxide dismutase is a peroxisomal enzyme in human fibroblasts and hepatoma cells. *Proc Natl Acad Sci U S A* **88**, 7381-5.

Kerfeld, C. A., and Krogmann, D. W. (1998) Photosynthetic cytochromes c in cyanobacteria, algae, and plants. *Annu Rev Plant Physiol Plant Mol Biol* **49**, 397-425.

Khalimonchuk, O., Bird, A., and Winge, D. R. (2007) Evidence for a pro-oxidant intermediate in the assembly of cytochrome oxidase. *J Biol Chem* **282**, 17442-9.

Kihlken, M. A., Leech, A. P., and Le Brun, N. E. (2002) Copper-mediated dimerization of CopZ, a predicted copper chaperone from *Bacillus subtilis*. *Biochem J* **368**, 729-39.

Kim, B. E., Nevitt, T., and Thiele, D. J. (2008) Mechanisms for copper acquisition, distribution and regulation. *Nat Chem Biol* **4**, 176-85.

Kim, H. J., Graham, D. W., DiSpirito, A. A., Alterman, M. A., Galeva, N., Larive, C. K., Asunskis, D., and Sherwood, P. M. (2004) Methanobactin, a copper-acquisition compound from methane-oxidizing bacteria. *Science* **305**, 1612-5.

Kirby, K., Hu, J., Hilliker, A. J., and Phillips, J. P. (2002) RNA interference-mediated silencing of Sod2 in Drosophila leads to early adult-onset mortality and elevated endogenous oxidative stress. *Proc Natl Acad Sci U S A* **99**, 16162-7.

Kirby, K., Jensen, L. T., Binnington, J., Hilliker, A. J., Ulloa, J., Culotta, V. C., and Phillips, J. P. (2008) Instability of superoxide dismutase 1 of Drosophila in mutants deficient for its cognate copper chaperone. *J Biol Chem* **283**, 35393-401.

Klomp, A. E., Tops, B. B., Van Denberg, I. E., Berger, R., and Klomp, L. W. (2002) Biochemical characterization and subcellular localization of human copper transporter 1 (hCTR1). *Biochem J* **364**, 497-505.

Klomp, A. E., Juijn, J. A., van der Gun, L. T., van den Berg, I. E., Berger, R., and Klomp, L. W. (2003) The N-terminus of the human copper transporter 1 (hCTR1) is localized extracellularly, and interacts with itself. *Biochem J* **370**, 881-9.

Klomp, L. W., and Gitlin, J. D. (1996) Expression of the ceruloplasmin gene in the human retina and brain: implications for a pathogenic model in aceruloplasminemia. *Hum Mol Genet* **5**, 1989-96.

Klomp, L. W., Lin, S. J., Yuan, D. S., Klausner, R. D., Culotta, V. C., and Gitlin, J. D. (1997) Identification and functional expression of HAH1, a novel human gene involved in copper homeostasis. *J Biol Chem* **272**, 9221-6.

Knobloch, M., Konietzko, U., Krebs, D. C., and Nitsch, R. M. (2007) Intracellular Abeta and cognitive deficits precede beta-amyloid deposition in transgenic arcAbeta mice. *Neurobiol Aging* **28**, 1297-306.

Knopfel, M., Schulthess, G., Funk, F., and Hauser, H. (2000) Characterization of an integral protein of the brush border membrane mediating the transport of divalent metal ions. *Biophys J* **79**, 874-84.

Knopfel, M., Smith, C., and Solioz, M. (2005) ATP-driven copper transport across the intestinal brush border membrane. *Biochem Biophys Res Commun* **330**, 645-52.

Kong, G. K., Adams, J. J., Cappai, R., and Parker, M. W. (2007a) Structure of Alzheimer's disease amyloid precursor protein copper-binding domain at atomic resolution. *Acta Crystallogr Sect F Struct Biol Cryst Commun* **63**, 819-24.

Kong, G. K., Adams, J. J., Harris, H. H., Boas, J. F., Curtain, C. C., Galatis, D., Masters, C. L., Barnham, K. J., McKinstry, W. J., Cappai, R., and Parker, M. W. (2007b) Structural studies of the Alzheimer's amyloid precursor protein copper-binding domain reveal how it binds copper ions. *J Mol Biol* **367**, 148-61.

Kong, G. K., Miles, L. A., Crespi, G. A., Morton, C. J., Ng, H. L., Barnham, K. J., McKinstry, W. J., Cappai, R., and Parker, M. W. (2008) Copper binding to the Alzheimer's disease amyloid precursor protein. *Eur Biophys J* **37**, 269-79.

Kontush, A., Berndt, C., Weber, W., Akopyan, V., Arlt, S., Schippling, S., and Beisiegel, U. (2001) Amyloid-beta is an antioxidant for lipoproteins in cerebrospinal fluid and plasma. *Free Radic Biol Med* **30**, 119-28.

Kosik, K. S., Joachim, C. L., and Selkoe, D. J. (1986) Microtubule-associated protein tau (tau) is a major antigenic component of paired helical filaments in Alzheimer disease. *Proc Natl Acad Sci U S A* **83**, 4044-8.

Kuo, M. T., Chen, H. H., Song, I. S., Savaraj, N., and Ishikawa, T. (2007) The roles of copper transporters in cisplatin resistance. *Cancer Metastasis Rev* **26**, 71-83.

Labbe, S., Zhu, Z., and Thiele, D. J. (1997) Copper-specific transcriptional repression of yeast genes encoding critical components in the copper transport pathway. *J Biol Chem* **272**, 15951-8.

LaFerla, F. M., Green, K. N., and Oddo, S. (2007) Intracellular amyloid-beta in Alzheimer's disease. *Nat Rev Neurosci* **8**, 499-509.

Laliberte, J., Whitson, L. J., Beaudoin, J., Holloway, S. P., Hart, P. J., and Labbe, S. (2004) The *Schizosaccharomyces pombe* Pccs protein functions in both copper trafficking and metal detoxification pathways. *J Biol Chem* **279**, 28744-55.

Lamb, A. L., Wernimont, A. K., Pufahl, R. A., Culotta, V. C., O'Halloran, T. V., and Rosenzweig, A. C. (1999) Crystal structure of the copper chaperone for superoxide dismutase. *Nat Struct Biol* **6**, 724-9.

Lamb, A. L., Wernimont, A. K., Pufahl, R. A., O'Halloran, T. V., and Rosenzweig, A. C. (2000) Crystal structure of the second domain of the human copper chaperone for superoxide dismutase. *Biochemistry* **39**, 1589-95.

Lamb, A. L., Torres, A. S., O'Halloran, T. V., and Rosenzweig, A. C. (2001) Heterodimeric structure of superoxide dismutase in complex with its metallochaperone. *Nat Struct Biol* **8**, 751-5.

Lannfelt, L., Blennow, K., Zetterberg, H., Batsman, S., Ames, D., Harrison, J., Masters, C. L., Targum, S., Bush, A. I., Murdoch, R., Wilson, J., and Ritchie, C. W. (2008) Safety, efficacy, and biomarker findings of PBT2 in targeting Abeta as a modifying therapy for Alzheimer's disease: a phase IIa, double-blind, randomised, placebo-controlled trial. *Lancet Neurol* **7**, 779-86.

Larin, D., Mekios, C., Das, K., Ross, B., Yang, A. S., and Gilliam, T. C. (1999) Characterization of the interaction between the Wilson and Menkes disease proteins and the cytoplasmic copper chaperone, HAH1p. *J Biol Chem* **274**, 28497-504.

Leary, S. C., Kaufman, B. A., Pellecchia, G., Guercin, G. H., Mattman, A., Jaksch, M., and Shoubridge, E. A. (2004) Human SCO1 and SCO2 have independent, cooperative functions in copper delivery to cytochrome c oxidase. *Hum Mol Genet* **13**, 1839-48.

Leary, S. C., Sasarman, F., Nishimura, T., and Shoubridge, E. A. (2009) Human SCO2 is required for the synthesis of CO II and as a thiol-disulphide oxidoreductase for SCO1. *Hum Mol Genet* **18**, 2230-40.

Lebovitz, R. M., Zhang, H., Vogel, H., Cartwright, J., Jr., Dionne, L., Lu, N., Huang, S., and Matzuk, M. M. (1996) Neurodegeneration, myocardial injury, and perinatal death in mitochondrial superoxide dismutase-deficient mice. *Proc Natl Acad Sci U S A* **93**, 9782-7.

Lee, J., Pena, M. M., Nose, Y., and Thiele, D. J. (2002a) Biochemical characterization of the human copper transporter Ctr1. *J Biol Chem* **277**, 4380-7.

Lee, J., Petris, M. J., and Thiele, D. J. (2002b) Characterization of mouse embryonic cells deficient in the ctr1 high affinity copper transporter. Identification of a Ctr1-independent copper transport system. *J Biol Chem* **277**, 40253-9.

Lee, P. L., Gelbart, T., West, C., Halloran, C., and Beutler, E. (1998) The human Nramp2 gene: characterization of the gene structure, alternative splicing, promoter region and polymorphisms. *Blood Cells Mol Dis* **24**, 199-215.

Lei, S., Pulakat, L., and Gavini, N. (1999) Genetic analysis of nif regulatory genes by utilizing the yeast two-hybrid system detected formation of a NifL-NifA complex that is implicated in regulated expression of nif genes. *J Bacteriol* **181**, 6535-9.

Leitch, J. M., Jensen, L. T., Bouldin, S. D., Outten, C. E., Hart, P. J., and Culotta, V. C. (2009a) Activation of Cu,Zn-superoxide dismutase in the absence of oxygen and the copper chaperone CCS. *J Biol Chem* **284**, 21863-71.

Leitch, J. M., Yick, P. J., and Culotta, V. C. (2009b) The right to choose: multiple pathways for activating copper,zinc superoxide dismutase. *J Biol Chem* **284**, 24679-83.

LeShane, E. S., Shinde, U., Walker, J. M., Barry, A. N., Blackburn, N. J., Ralle, M., and Lutsenko, S. (2010) Interactions between copper-binding sites determine the redox status and conformation of the regulatory N-terminal domain of ATP7B. *J Biol Chem* **285**, 6327-36.

Levy-Lahad, E., Wasco, W., Poorkaj, P., Romano, D. M., Oshima, J., Pettingell, W. H., Yu, C. E., Jondro, P. D., Schmidt, S. D., Wang, K., and et al. (1995) Candidate gene for the chromosome 1 familial Alzheimer's disease locus. *Science* **269**, 973-7.

Li, L., Vulpe, C. D., and Kaplan, J. (2003) Functional studies of hephaestin in yeast: evidence for multicopper oxidase activity in the endocytic pathway. *Biochem J* **375**, 793-8.

Li, Y., Huang, T. T., Carlson, E. J., Melov, S., Ursell, P. C., Olson, J. L., Noble, L. J., Yoshimura, M. P., Berger, C., Chan, P. H., Wallace, D. C., and Epstein, C. J. (1995) Dilated cardiomyopathy and neonatal lethality in mutant mice lacking manganese superoxide dismutase. *Nat Genet* **11**, 376-81.

Lim, C. M., Cater, M. A., Mercer, J. F., and La Fontaine, S. (2006a) Copper-dependent interaction of glutaredoxin with the N termini of the copper-ATPases (ATP7A and ATP7B) defective in Menkes and Wilson diseases. *Biochem Biophys Res Commun* **348**, 428-36.

Lim, C. M., Cater, M. A., Mercer, J. F., and La Fontaine, S. (2006b) Copper-dependent interaction of dynactin subunit p62 with the N terminus of ATP7B but not ATP7A. *J Biol Chem* **281**, 14006-14.

Lin, S. J., and Culotta, V. C. (1995) The ATX1 gene of *Saccharomyces cerevisiae* encodes a small metal homeostasis factor that protects cells against reactive oxygen toxicity. *Proc Natl Acad Sci U S A* **92**, 3784-8.

Lin, S. J., Pufahl, R. A., Dancis, A., O'Halloran, T. V., and Culotta, V. C. (1997) A role for the Saccharomyces cerevisiae ATX1 gene in copper trafficking and iron transport. *J Biol Chem* **272**, 9215-20.

Lin, X., Koelsch, G., Wu, S., Downs, D., Dashti, A., and Tang, J. (2000) Human aspartic protease memapsin 2 cleaves the beta-secretase site of beta-amyloid precursor protein. *Proc Natl Acad Sci U S A* **97**, 1456-60.

Lode, A., Kuschel, M., Paret, C., and Rodel, G. (2000) Mitochondrial copper metabolism in yeast: interaction between Sco1p and Cox2p. *FEBS Lett* **485**, 19-24.

Loftin, I. R., Franke, S., Roberts, S. A., Weichsel, A., Heroux, A., Montfort, W. R., Rensing, C., and McEvoy, M. M. (2005) A novel copper-binding fold for the periplasmic copper resistance protein CusF. *Biochemistry* **44**, 10533-40.

Loftin, I. R., Franke, S., Blackburn, N. J., and McEvoy, M. M. (2007) Unusual Cu(I)/Ag(I) coordination of *Escherichia coli* CusF as revealed by atomic resolution crystallography and X-ray absorption spectroscopy. *Protein Sci* **16**, 2287-93.

Lovell, M. A., Robertson, J. D., Teesdale, W. J., Campbell, J. L., and Markesbery, W. R. (1998) Copper, iron and zinc in Alzheimer's disease senile plaques. *J Neurol Sci* **158**, 47-52.

Lu, Z. H., and Solioz, M. (2001) Copper-induced proteolysis of the CopZ copper chaperone of *Enterococcus hirae*. *J Biol Chem* **276**, 47822-7.

Lutsenko, S., Petrukhin, K., Cooper, M. J., Gilliam, C. T., and Kaplan, J. H. (1997) N-terminal domains of human copper-transporting adenosine triphosphatases (the Wilson's and Menkes disease proteins) bind copper selectively in vivo and in vitro with stoichiometry of one copper per metal-binding repeat. *J Biol Chem* **272**, 18939-44.

Lutsenko, S., Barnes, N. L., Bartee, M. Y., and Dmitriev, O. Y. (2007a) Function and regulation of human copper-transporting ATPases. *Phys Rev* **87**, 1011-46.

Lutsenko, S., LeShane, E. S., and Shinde, U. (2007b) Biochemical basis of regulation of human copper-transporting ATPases. *Arch Biochem Biophys* **463**, 134-48.

Ma, Z., Jacobsen, F. E., and Giedroc, D. P. (2009) Coordination chemistry of bacterial metal transport and sensing. *Chem Rev* **109**, 4644-81.

Magnani, D., and Solioz, M. (2007): How Bacteria Handle Copper259-285. In D. H. Nies, and S. Silver (Eds): *Molecular microbiology of heavy metals*, Springer Berlin/Heiderlberg, Heidelberg.

Maher, P. (2005) The effects of stress and aging on glutathione metabolism. *Ageing Res Rev* **4**, 288-314.

Mallesha, H., Kumar, K. R. R., Kumar, B. K. V., Mantelingu, K., and Rangappa, K. S. (2001) Histidine as a catalyst in organic synthesis: A facile *in situ* synthesis of α, N-diarylnitrones. *Proc Indian Acad Sci (Chem Sci)* **113**, 291-6.

Mana-Capelli, S., Mandal, A. K., and Arguello, J. M. (2003) Archaeoglobus fulgidus CopB is a thermophilic Cu2+-ATPase: functional role of its histidine-rich-N-terminal metal binding domain. *J Biol Chem* **278**, 40534-41.

Mandal, A. K., Cheung, W. D., and Arguello, J. M. (2002) Characterization of a thermophilic P-type Ag+/Cu+-ATPase from the extremophile Archaeoglobus fulgidus. *J Biol Chem* **277**, 7201-8.

Maret, W., and Li, Y. (2009) Coordination dynamics of zinc in proteins. *Chem Rev* **109**, 4682-707.

Markossian, K. A., and Kurganov, B. I. (2003) Copper chaperones, intracellular copper trafficking proteins. Function, structure, and mechanism of action. *Biochemistry (Mosc)* **68**, 827-37.

Martinez-Argudo, I., and Contreras, A. (2002) PII T-loop mutations affecting signal transduction to NtrB also abolish yeast two-hybrid interactions. *J Bacteriol* **184**, 3746-8.

Maryon, E. B., Molloy, S. A., Zimnicka, A. M., and Kaplan, J. H. (2007) Copper entry into human cells: progress and unanswered questions. *Biometals* **20**, 355-64.

Masters, C. L., Simms, G., Weinman, N. A., Multhaup, G., McDonald, B. L., and Beyreuther, K. (1985) Amyloid plaque core protein in Alzheimer disease and Down syndrome. *Proc Natl Acad Sci U S A* **82**, 4245-9.

Maurer, I., Zierz, S., and Moller, H. J. (2000) A selective defect of cytochrome c oxidase is present in brain of Alzheimer disease patients. *Neurobiol Aging* **21**, 455-62.

Maynard, C. J., Cappai, R., Volitakis, I., Cherny, R. A., White, A. R., Beyreuther, K., Masters, C. L., Bush, A. I., and Li, Q. X. (2002) Overexpression of Alzheimer's disease amyloid-beta opposes the age-dependent elevations of brain copper and iron. *J Biol Chem* **277**, 44670-6.

Maynard, C. J., Bush, A. I., Masters, C. L., Cappai, R., and Li, Q. X. (2005) Metals and amyloid-beta in Alzheimer's disease. *Int J Exp Pathol* **86**, 147-59.

McCord, J. M., and Fridovich, I. (1969) Superoxide dismutase. An enzymic function for erythrocuprein (hemocuprein). *J Biol Chem* **244**, 6049-55.

McLoughlin, D. M., Standen, C. L., Lau, K. F., Ackerley, S., Bartnikas, T. P., Gitlin, J. D., and Miller, C. C. (2001) The neuronal adaptor protein X11alpha interacts with the copper chaperone for SOD1 and regulates SOD1 activity. *J Biol Chem* **276**, 9303-7.

Mercer, J. F., Livingston, J., Hall, B., Paynter, J. A., Begy, C., Chandrasekharappa, S., Lockhart, P., Grimes, A., Bhave, M., Siemieniak, D., and et al. (1993) Isolation of a partial candidate gene for Menkes disease by positional cloning. *Nat Genet* **3**, 20-5.

Mercer, J. F., Barnes, N., Stevenson, J., Strausak, D., and Llanos, R. M. (2003) Copper-induced trafficking of the Cu-ATPases: a key mechanism for copper homeostasis. *Biometals* **16**, 175-84.

Merchant, S., and Bogorad, L. (1986) Regulation by copper of the expression of plastocyanin and cytochrome c552 in Chlamydomonas reinhardi. *Mol Cell Biol* **6**, 462-9.

Messens, J., Collet, J. F., Van Belle, K., Brosens, E., Loris, R., and Wyns, L. (2007) The oxidase DsbA folds a protein with a nonconsecutive disulfide. *J Biol Chem* **282**, 31302-7.

Miller, C. C., McLoughlin, D. M., Lau, K. F., Tennant, M. E., and Rogelj, B. (2006) The X11 proteins, Abeta production and Alzheimer's disease. *Trends Neurosci* **29**, 280-5.

Miller, J. (1972) *Experiments in Molecular Genetics*. Cold Spring Harbor Laboratory Press, Cold Spring Harbor, NY, USA.

Miyayama, T., Suzuki, K. T., and Ogra, Y. (2009) Copper accumulation and compartmentalization in mouse fibroblast lacking metallothionein and copper chaperone, Atox1. *Toxicol Appl Pharmacol* **237**, 205-13.

Molina-Holgado, F., Hider, R. C., Gaeta, A., Williams, R., and Francis, P. (2007) Metals ions and neurodegeneration. *Biometals* **20**, 639-54.

Molloy, S. A., and Kaplan, J. H. (2009) Copper-dependent recycling of hCTR1, the human high affinity copper transporter. *J Biol Chem* **284**, 29704-13.

Morin, I., Gudin, S., Mintz, E., and Cuillel, M. (2009) Dissecting the role of the N-terminal metal-binding domains in activating the yeast copper ATPase in vivo. *Febs J* **276**, 4483-95.

Morita, H., Ikeda, S., Yamamoto, K., Morita, S., Yoshida, K., Nomoto, S., Kato, M., and Yanagisawa, N. (1995) Hereditary ceruloplasmin deficiency with hemosiderosis: a clinicopathological study of a Japanese family. *Ann Neurol* **37**, 646-56.

Morrissette, D. A., Parachikova, A., Green, K. N., and LaFerla, F. M. (2009) Relevance of transgenic mouse models to human Alzheimer disease. *J Biol Chem* **284**, 6033-7.

Mufti, A. R., Burstein, E., Csomos, R. A., Graf, P. C., Wilkinson, J. C., Dick, R. D., Challa, M., Son, J. K., Bratton, S. B., Su, G. L., Brewer, G. J., Jakob, U., and Duckett, C. S. (2006) XIAP Is a copper binding protein deregulated in Wilson's disease and other copper toxicosis disorders. *Mol Cell* **21**, 775-85.

Multhaup, G., Strausak, D., Bissig, K. D., and Solioz, M. (2001) Interaction of the CopZ copper chaperone with the CopA copper ATPase of *Enterococcus hirae* assessed by surface plasmon resonance. *Biochem Biophys Res Commun* **288**, 172-7.

Munoz, M., Villar, I., and Garcia-Erce, J. A. (2009) An update on iron physiology. *World J Gastroenterol* **15**, 4617-26.

Musci, G., Di Marco, S., Bellenchi, G. C., and Calabrese, L. (1996) Reconstitution of ceruloplasmin by the Cu(I)-glutathione complex. Evidence for a role of Mg2+ and ATP. *J Biol Chem* **271**, 1972-8.

Naslund, J., Haroutunian, V., Mohs, R., Davis, K. L., Davies, P., Greengard, P., and Buxbaum, J. D. (2000) Correlation between elevated levels of amyloid beta-peptide in the brain and cognitive decline. *Jama* **283**, 1571-7.

Nies, D. H. (2007): Molecular Microbiology of Heavy Metals117-142. In A. Steinbuchel (Ed.), Springer.

Nikaido, H., and Vaara, M. (1985) Molecular basis of bacterial outer membrane permeability. *Microbiol. Rev.* **49**, 1-32.

Oddo, S., Caccamo, A., Shepherd, J. D., Murphy, M. P., Golde, T. E., Kayed, R., Metherate, R., Mattson, M. P., Akbari, Y., and LaFerla, F. M. (2003) Triple-transgenic model of Alzheimer's disease with plaques and tangles: intracellular Abeta and synaptic dysfunction. *Neuron* **39**, 409-21.

Odermatt, A., Suter, H., Krapf, R., and Solioz, M. (1992) An ATPase operon involved in copper resistance by *Enterococcus hirae*. *Ann N Y Acad Sci* **671**, 484-6.

Odermatt, A., Suter, H., Krapf, R., and Solioz, M. (1993) Primary structure of two P-type ATPases involved in copper homeostasis in *Enterococcus hirae*. *J Biol Chem* **268**, 12775-9.

Odermatt, A., Krapf, R., and Solioz, M. (1994) Induction of the putative copper ATPases, CopA and CopB, of *Enterococcus hirae* by Ag^{+} and Cu^{2+}, and Ag^{+} extrusion by CopB. *Biochem Biophys Res Commun* **202**, 44-8.

Odermatt, A., and Solioz, M. (1995) Two trans-acting metalloregulatory proteins controlling expression of the copper-ATPases of *Enterococcus hirae*. *J. Biol. Chem.* **270**, 4349-4354.

Opazo, C., Luza, S., Villemagne, V. L., Volitakis, I., Rowe, C., Barnham, K. J., Strozyk, D., Masters, C. L., Cherny, R. A., and Bush, A. I. (2006) Radioiodinated clioquinol as a biomarker for beta-amyloid: Zn complexes in Alzheimer's disease. *Aging Cell* **5**, 69-79.

Ostergaard, H., Tachibana, C., and Winther, J. R. (2004) Monitoring disulfide bond formation in the eukaryotic cytosol. *J Cell Biol* **166**, 337-45.

Parge, H. E., Hallewell, R. A., and Tainer, J. A. (1992) Atomic structures of wild-type and thermostable mutant recombinant human Cu,Zn superoxide dismutase. *Proc Natl Acad Sci U S A* **89**, 6109-13.

Parsons, R. B., and Austen, B. M. (2007) Protein-protein interactions in the assembly and subcellular trafficking of the BACE (beta-site amyloid precursor protein-cleaving enzyme) complex of Alzheimer's disease. *Biochem Soc Trans* **35**, 974-9.

Pastorino, L., Ikin, A. F., Nairn, A. C., Pursnani, A., and Buxbaum, J. D. (2002) The carboxyl-terminus of BACE contains a sorting signal that regulates BACE trafficking but not the formation of total A(beta). *Mol Cell Neurosci* **19**, 175-85.

Pawlowski, A., Riedel, K. U., Klipp, W., Dreiskemper, P., Gross, S., Bierhoff, H., Drepper, T., and Masepohl, B. (2003) Yeast two-hybrid studies on interaction of proteins involved in regulation of nitrogen fixation in the phototrophic bacterium *Rhodobacter capsulatus*. *J Bacteriol* **185**, 5240-7.

Pena, M. M., Koch, K. A., and Thiele, D. J. (1998) Dynamic regulation of copper uptake and detoxification genes in *Saccharomyces cerevisiae*. *Mol Cell Biol* **18**, 2514-23.

Penninckx, M. J. (2002) An overview on glutathione in Saccharomyces versus non-conventional yeasts. *FEMS Yeast Res* **2**, 295-305.

Petris, M. J., Mercer, J. F., Culvenor, J. G., Lockhart, P., Gleeson, P. A., and Camakaris, J. (1996) Ligand-regulated transport of the Menkes copper P-type ATPase efflux pump from the Golgi apparatus to the plasma membrane: a novel mechanism of regulated trafficking. *Embo J* **15**, 6084-95.

Petris, M. J., Smith, K., Lee, J., and Thiele, D. J. (2003) Copper-stimulated endocytosis and degradation of the human copper transporter, hCtr1. *J Biol Chem* **278**, 9639-46.

Petruzzella, V., Tiranti, V., Fernandez, P., Ianna, P., Carrozzo, R., and Zeviani, M. (1998) Identification and characterization of human cDNAs specific to BCS1, PET112, SCO1, COX15, and COX11, five genes involved in the formation and function of the mitochondrial respiratory chain. *Genomics* **54**, 494-504.

Phung, L. T., Ajlani, G., and Haselkorn, R. (1994) P-type ATPase from the cyanobacterium *Synechococcus* 7942 related to the human Menkes and Wilson disease gene products. *Proc Natl Acad Sci U S A* **91**, 9651-4.

Piccini, A., Russo, C., Gliozzi, A., Relini, A., Vitali, A., Borghi, R., Giliberto, L., Armirotti, A., D'Arrigo, C., Bachi, A., Cattaneo, A., Canale, C., Torrassa, S., Saido, T. C., Markesbery, W., Gambetti, P., and Tabaton, M. (2005) beta-amyloid is different in normal aging and in Alzheimer disease. *J Biol Chem* **280**, 34186-92.

Poger, D., Fuchs, J. F., Nedev, H., Ferrand, M., and Crouzy, S. (2005) Molecular dynamics study of the metallochaperone Hah1 in its apo and Cu(I)-loaded states: role of the conserved residue M10. *FEBS Lett* **579**, 5287-92.

Portnoy, M. E., Rosenzweig, A. C., Rae, T., Huffman, D. L., O'Halloran, T. V., and Culotta, V. C. (1999) Structure-function analyses of the ATX1 metallochaperone. *J Biol Chem* **274**, 15041-5.

Portnoy, M. E., Schmidt, P. J., Rogers, R. S., and Culotta, V. C. (2001) Metal transporters that contribute copper to metallochaperones in Saccharomyces cerevisiae. *Mol Genet Genomics* **265**, 873-82.

Prohaska, J. R., and Gybina, A. A. (2004) Intracellular copper transport in mammals. *J Nutr* **134**, 1003-6.

Prohaska, J. R. (2008) Role of copper transporters in copper homeostasis. *Am J Clin Nutr* **88**, 826S-9S.

Pufahl, R. A., Singer, C. P., Peariso, K. L., Lin, S. J., Schmidt, P. J., Fahrni, C. J., Culotta, V. C., Penner-Hahn, J. E., and O'Halloran, T. V. (1997) Metal ion chaperone function of the soluble Cu(I) receptor Atx1. *Science* **278**, 853-6.

Puig, S., Lee, J., Lau, M., and Thiele, D. J. (2002) Biochemical and genetic analyses of yeast and human high affinity copper transporters suggest a conserved mechanism for copper uptake. *J Biol Chem* **277**, 26021-30.

PyMol. PyMol molecular graphics system, Version 1.3, Schrodinger, LLC.

Radford, D. S., Kihlken, M. A., Borrelly, G. P., Harwood, C. R., Le Brun, N. E., and Cavet, J. S. (2003) CopZ from *Bacillus subtilis* interacts in vivo with a copper exporting CPx-type ATPase CopA. *FEMS Microbiol Lett* **220**, 105-12.

Rae, T. D., Schmidt, P. J., Pufahl, R. A., Culotta, V. C., and O'Halloran, T. V. (1999) Undetectable intracellular free copper: the requirement of a copper chaperone for superoxide dismutase. *Science* **284**, 805-8.

Rae, T. D., Torres, A. S., Pufahl, R. A., and O'Halloran, T. V. (2001) Mechanism of Cu,Zn-superoxide dismutase activation by the human metallochaperone hCCS. *J Biol Chem* **276**, 5166-76.

Redinbo, M. R., Yeates, T. O., and Merchant, S. (1994) Plastocyanin: structural and functional analysis. *J Bioenerg Biomembr* **26**, 49-66.

Rees, E. M., Lee, J., and Thiele, D. J. (2004) Mobilization of intracellular copper stores by the ctr2 vacuolar copper transporter. *J Biol Chem* **279**, 54221-9.

Rensing, C., Fan, B., Sharma, R., Mitra, B., and Rosen, B. P. (2000) CopA: An *Escherichia coli* Cu(I)-translocating P-type ATPase. *Proc Natl Acad Sci U S A* **97**, 652-6.

Rentmeister, A., Bill, A., Wahle, T., Walter, J., and Famulok, M. (2006) RNA aptamers selectively modulate protein recruitment to the cytoplasmic domain of beta-secretase BACE1 in vitro. *Rna* **12**, 1650-60.

Robinson, N. J., and Winge, D. R. (2010) Copper Metallochaperones. *Annu Rev Biochem* **79**, 537-62.

Rodriguez-Granillo, A., and Wittung-Stafshede, P. (2009a) Differential roles of Met10, Thr11, and Lys60 in structural dynamics of human copper chaperone Atox1. *Biochemistry* **48**, 960-72.

Rodriguez-Granillo, A., and Wittung-Stafshede, P. (2009b) Tuning of copper-loop flexibility in *Bacillus subtilis* CopZ copper chaperone: role of conserved residues. *J Phys Chem B* **113**, 1919-32.

Rodriguez-Granillo, A., Crespo, A., Estrin, D. A., and Wittung-Stafshede, P. (2010) Copper-transfer mechanism from the human chaperone Atox1 to a metal-binding domain of Wilson disease protein. *J Phys Chem B* **114**, 3698-706.

Rosenzweig, A. C., Huffman, D. L., Hou, M. Y., Wernimont, A. K., Pufahl, R. A., and O'Halloran, T. V. (1999) Crystal structure of the Atx1 metallochaperone protein at 1.02 A resolution. *Structure* **7**, 605-17.

Ruiz, F. H., Gonzalez, M., Bodini, M., Opazo, C., and Inestrosa, N. C. (1999) Cysteine 144 is a key residue in the copper reduction by the beta-amyloid precursor protein. *J Neurochem* **73**, 1288-92.

Sacher, A., Cohen, A., and Nelson, N. (2001) Properties of the mammalian and yeast metal-ion transporters DCT1 and Smf1p expressed in Xenopus laevis oocytes. *J Exp Biol* **204**, 1053-61.

Safaei, R., Maktabi, M. H., Blair, B. G., Larson, C. A., and Howell, S. B. (2009) Effects of the loss of Atox1 on the cellular pharmacology of cisplatin. *J Inorg Biochem* **103**, 333-41.

Sambrook, J., and Russell, D. (2001) *Molecular Cloning: A Laboratory Manual.*Cold Spring Harbor Laboratory Press, NY, USA.

Sazinsky, M. H., LeMoine, B., Orofino, M., Davydov, R., Bencze, K. Z., Stemmler, T. L., Hoffman, B. M., Arguello, J. M., and Rosenzweig, A. C. (2007) Characterization and structure of a Zn^{2+} and [2Fe-2S]-containing copper chaperone from *Archaeoglobus fulgidus*. *J Biol Chem* **282**, 25950-9.

Schaefer, M., Hopkins, R. G., Failla, M. L., and Gitlin, J. D. (1999) Hepatocyte-specific localization and copper-dependent trafficking of the Wilson's disease protein in the liver. *Am J Physiol* **276**, G639-46.

Scheinberg, I. H., and Gitlin, D. (1952) Deficiency of ceruloplasmin in patients with hepatolenticular degeneration (Wilson's disease). *Science* **116**, 484-5.

Schmidt, P. J., Rae, T. D., Pufahl, R. A., Hamma, T., Strain, J., O'Halloran, T. V., and Culotta, V. C. (1999a) Multiple protein domains contribute to the action of the copper chaperone for superoxide dismutase. *J Biol Chem* **274**, 23719-25.

Schmidt, P. J., Ramos-Gomez, M., and Culotta, V. C. (1999b) A gain of superoxide dismutase (SOD) activity obtained with CCS, the copper metallochaperone for SOD1. *J Biol Chem* **274**, 36952-6.

Schmidt, P. J., Kunst, C., and Culotta, V. C. (2000) Copper activation of superoxide dismutase 1 (SOD1) *in vivo*. Role for protein-protein interactions with the copper chaperone for SOD1. *J Biol Chem* **275**, 33771-6.

Schubert, W., Prior, R., Weidemann, A., Dircksen, H., Multhaup, G., Masters, C. L., and Beyreuther, K. (1991) Localization of Alzheimer beta A4 amyloid precursor protein at central and peripheral synaptic sites. *Brain Res* **563**, 184-94.

SGD project. "Saccharomyces Genome Database" http://www.yeastgenome.org (26th March, 2008)

Sherrington, R., Rogaev, E. I., Liang, Y., Rogaeva, E. A., Levesque, G., Ikeda, M., Chi, H., Lin, C., Li, G., Holman, K., and et al. (1995) Cloning of a gene bearing missense mutations in early-onset familial Alzheimer's disease. *Nature* **375**, 754-60.

Shiba, T., Kametaka, S., Kawasaki, M., Shibata, M., Waguri, S., Uchiyama, Y., and Wakatsuki, S. (2004) Insights into the phosphoregulation of beta-secretase sorting signal by the VHS domain of GGA1. *Traffic* **5**, 437-48.

Singleton, C., Banci, L., Ciofi-Baffoni, S., Tenori, L., Kihlken, M. A., Boetzel, R., and Le Brun, N. E. (2008) Structure and Cu(I)-binding properties of the N-terminal soluble domains of *Bacillus subtilis* CopA. *Biochem J* **411**, 571-9.

Singleton, C., Hearnshaw, S., Zhou, L., Le Brun, N. E., and Hemmings, A. M. (2009) Mechanistic insights into Cu(I) cluster transfer between the chaperone CopZ and its cognate Cu(I)-transporting P-type ATPase, CopA. *Biochem J* **424**, 347-56.

Singleton, C., and Le Brun, N. E. (2009) The N-terminal soluble domains of *Bacillus subtilis* CopA exhibit a high affinity and capacity for Cu(I) ions. *Dalton Trans* **28**, 688-96.

Sinha, S., Anderson, J. P., Barbour, R., Basi, G. S., Caccavello, R., Davis, D., Doan, M., Dovey, H. F., Frigon, N., Hong, J., Jacobson-Croak, K., Jewett, N., Keim, P., Knops, J., Lieberburg, I., Power, M., Tan, H., Tatsuno, G., Tung, J., Schenk, D., Seubert, P., Suomensaari, S. M., Wang, S., Walker, D., Zhao, J., McConlogue, L., and John, V. (1999) Purification and cloning of amyloid precursor protein beta-secretase from human brain. *Nature* **402**, 537-40.

Sinha, S., and Lieberburg, I. (1999) Cellular mechanisms of beta-amyloid production and secretion. *Proc Natl Acad Sci U S A* **96**, 11049-53.

Solioz, M., and Stoyanov, J. V. (2003) Copper homeostasis in *Enterococcus hirae*. *FEMS Microbiol Rev* **27**, 183-95.

Solioz, M., Abicht, H. K., Mermod, M., and Mancini, S. (2010) Response of gram-positive bacteria to copper stress. *J Biol Inorg Chem* **15**, 3-14.

Song, I. S., Chen, H. H., Aiba, I., Hossain, A., Liang, Z. D., Klomp, L. W., and Kuo, M. T. (2008) Transcription factor Sp1 plays an important role in the regulation of copper homeostasis in mammalian cells. *Mol Pharmacol* **74**, 705-13.

Speisky, H., Gomez, M., Carrasco-Pozo, C., Pastene, E., Lopez-Alarcon, C., and Olea-Azar, C. (2008) Cu(I)-glutathione complex: a potential source of superoxide radicals generation. *Bioorg Med Chem* **16**, 6568-74.

Speisky, H., Gomez, M., Burgos-Bravo, F., Lopez-Alarcon, C., Jullian, C., Olea-Azar, C., and Aliaga, M. E. (2009) Generation of superoxide radicals by copper-glutathione complexes: redox-consequences associated with their interaction with reduced glutathione. *Bioorg Med Chem* **17**, 1803-10.

Stasser, J. P., Eisses, J. F., Barry, A. N., Kaplan, J. H., and Blackburn, N. J. (2005) Cysteine-to-serine mutants of the human copper chaperone for superoxide dismutase reveal a copper cluster at a domain III dimer interface. *Biochemistry* **44**, 3143-52.

Stasser, J. P., Siluvai, G. S., Barry, A. N., and Blackburn, N. J. (2007) A multinuclear copper(I) cluster forms the dimerization interface in copper-loaded human copper chaperone for superoxide dismutase. *Biochemistry* **46**, 11845-56.

Stearman, R., Yuan, D. S., Yamaguchi-Iwai, Y., Klausner, R. D., and Dancis, A. (1996) A permease-oxidase complex involved in high-affinity iron uptake in yeast. *Science* **271**, 1552-7.

Stoyanov, J. V., Mancini, S., Lu, Z. H., Mourlane, F., Poulsen, K. R., Wimmer, R., and Solioz, M. (2010) The stress response protein Gls24 is induced by copper and interacts with the CopZ copper chaperone of *Enterococcus hirae*. *FEMS Microbiol Lett* **302**, 69-75.

Strain, J., and Culotta, V. C. (1996) Copper ions and the regulation of Saccharomyces cerevisiae metallothionein genes under aerobic and anaerobic conditions. *Mol Gen Genet* **251**, 139-45.

Stralin, P., Karlsson, K., Johansson, B. O., and Marklund, S. L. (1995) The interstitium of the human arterial wall contains very large amounts of extracellular superoxide dismutase. *Arterioscler Thromb Vasc Biol* **15**, 2032-6.

Strange, R. W., Antonyuk, S., Hough, M. A., Doucette, P. A., Rodriguez, J. A., Hart, P. J., Hayward, L. J., Valentine, J. S., and Hasnain, S. S. (2003) The structure of holo and metal-deficient wild-type human Cu, Zn superoxide dismutase and its relevance to familial amyotrophic lateral sclerosis. *J Mol Biol* **328**, 877-91.

Strausak, D., La Fontaine, S., Hill, J., Firth, S. D., Lockhart, P. J., and Mercer, J. F. (1999) The role of GMXCXXC metal binding sites in the copper-induced redistribution of the Menkes protein. *J Biol Chem* **274**, 11170-7.

Strausak, D., Howie, M. K., Firth, S. D., Schlicksupp, A., Pipkorn, R., Multhaup, G., and Mercer, J. F. (2003) Kinetic analysis of the interaction of the copper chaperone Atox1 with the metal binding sites of the Menkes protein. *J Biol Chem* **278**, 20821-7.

Suazo, M., Hodar, C., Morgan, C., Cerpa, W., Cambiazo, V., Inestrosa, N. C., and Gonzalez, M. (2009) Overexpression of amyloid precursor protein increases copper content in HEK293 cells. *Biochem Biophys Res Commun* **382**, 740-4.

Suzuki, K. T., Someya, A., Komada, Y., and Ogra, Y. (2002) Roles of metallothionein in copper homeostasis: responses to Cu-deficient diets in mice. *J Inorg Biochem* **88**, 173-82.

Syme, C. D., Nadal, R. C., Rigby, S. E., and Viles, J. H. (2004) Copper binding to the amyloid-beta (Abeta) peptide associated with Alzheimer's disease: folding, coordination geometry, pH dependence, stoichiometry, and affinity of Abeta-(1-28): insights from a range of complementary spectroscopic techniques. *J Biol Chem* **279**, 18169-77.

Tainer, J. A., Getzoff, E. D., Beem, K. M., Richardson, J. S., and Richardson, D. C. (1982) Determination and analysis of the 2 A-structure of copper, zinc superoxide dismutase. *J Mol Biol* **160**, 181-217.

Takahashi, N., Ortel, T. L., and Putnam, F. W. (1984) Single-chain structure of human ceruloplasmin: the complete amino acid sequence of the whole molecule. *Proc Natl Acad Sci U S A* **81**, 390-4.

Takeda, A., and Tamano, H. (2009) Insight into zinc signaling from dietary zinc deficiency. *Brain Res Rev* **62**, 33-44.

Tanchou, V., Gas, F., Urvoas, A., Cougouluegne, F., Ruat, S., Averseng, O., and Quemeneur, E. (2004) Copper-mediated homo-dimerisation for the HAH1 metallochaperone. *Biochem Biophys Res Commun* **325**, 388-94.

Tao, T. Y., Liu, F., Klomp, L., Wijmenga, C., and Gitlin, J. D. (2003) The copper toxicosis gene product Murr1 directly interacts with the Wilson disease protein. *J Biol Chem* **278**, 41593-6.

Terada, K., Nakako, T., Yang, X. L., Iida, M., Aiba, N., Minamiya, Y., Nakai, M., Sakaki, T., Miura, N., and Sugiyama, T. (1998) Restoration of holoceruloplasmin synthesis in LEC rat after infusion of recombinant adenovirus bearing WND cDNA. *J Biol Chem* **273**, 1815-20.

Terry, R. D., Masliah, E., Salmon, D. P., Butters, N., DeTeresa, R., Hill, R., Hansen, L. A., and Katzman, R. (1991) Physical basis of cognitive alterations in Alzheimer's disease: synapse loss is the major correlate of cognitive impairment. *Ann Neurol* **30**, 572-80.

Thiele, D. J. (1988) ACE1 regulates expression of the Saccharomyces cerevisiae metallothionein gene. *Mol Cell Biol* **8**, 2745-52.

Tottey, S., Rich, P. R., Rondet, S. A., and Robinson, N. J. (2001) Two Menkes-type atpases supply copper for photosynthesis in *Synechocystis* PCC 6803. *J Biol Chem* **276**, 19999-20004.

Tottey, S., Rondet, S. A., Borrelly, G. P., Robinson, P. J., Rich, P. R., and Robinson, N. J. (2002) A copper metallochaperone for photosynthesis and respiration reveals metal-specific targets, interaction with an importer, and alternative sites for copper acquisition. *J Biol Chem* **277**, 5490-7.

Tottey, S., Harvie, D. R., and Robinson, N. J. (2005) Understanding how cells allocate metals using metal sensors and metallochaperones. *Acc. Chem. Res.* **38**, 775-783.

Tottey, S., Waldron, K. J., Firbank, S. J., Reale, B., Bessant, C., Sato, K., Cheek, T. R., Gray, J., Banfield, M. J., Dennison, C., and Robinson, N. J. (2008) Protein-folding location can regulate manganese-binding versus copper- or zinc-binding. *Nature* **455**, 1138-42.

Treco, D. A., and Lundblad, V. (1993),Vol. 2, unit 13.1 pp. 2: *Current protocols in molecular biology*, John Wiley & Son, Inc., New York, NY.

Treiber, C., Simons, A., Strauss, M., Hafner, M., Cappai, R., Bayer, T. A., and Multhaup, G. (2004) Clioquinol mediates copper uptake and counteracts copper efflux activities of the amyloid precursor protein of Alzheimer's disease. *J Biol Chem* **279**, 51958-64.

Tumer, Z., and Moller, L. B. (2010) Menkes disease. *Eur J Hum Genet* **18**, 511-8.

Uversky, V. N., Lee, H. J., Li, J., Fink, A. L., and Lee, S. J. (2001a) Stabilization of partially folded conformation during alpha-synuclein oligomerization in both purified and cytosolic preparations. *J Biol Chem* **276**, 43495-8.

Uversky, V. N., Li, J., and Fink, A. L. (2001b) Metal-triggered structural transformations, aggregation, and fibrillation of human alpha-synuclein. A possible molecular NK between Parkinson's disease and heavy metal exposure. *J Biol Chem* **276**, 44284-96.

Valentine, J. S., Doucette, P. A., and Zittin Potter, S. (2005) Copper-zinc superoxide dismutase and amyotrophic lateral sclerosis. *Annu Rev Biochem* **74**, 563-93.

van den Berghe, P. V., Folmer, D. E., Malingre, H. E., van Beurden, E., Klomp, A. E., van de Sluis, B., Merkx, M., Berger, R., and Klomp, L. W. (2007) Human copper transporter 2 is localized in late endosomes and lysosomes and facilitates cellular copper uptake. *Biochem J* **407**, 49-59.

van den Berghe, P. V., and Klomp, L. W. (2010) Posttranslational regulation of copper transporters. *J Biol Inorg Chem* **15**, 37-46.

van Dongen, E. M., Klomp, L. W., and Merkx, M. (2004) Copper-dependent protein-protein interactions studied by yeast two-hybrid analysis. *Biochem Biophys Res Commun* **323**, 789-95.

van Es, M. A., and van den Berg, L. H. (2009) Alzheimer's disease beyond APOE. *Nat Genet* **41**, 1047-8.

Vassar, R., Bennett, B. D., Babu-Khan, S., Kahn, S., Mendiaz, E. A., Denis, P., Teplow, D. B., Ross, S., Amarante, P., Loeloff, R., Luo, Y., Fisher, S., Fuller, J., Edenson, S., Lile, J., Jarosinski, M. A., Biere, A. L., Curran, E., Burgess, T., Louis, J. C., Collins, F., Treanor, J., Rogers, G., and Citron, M. (1999) Beta-secretase cleavage of Alzheimer's amyloid precursor protein by the transmembrane aspartic protease BACE. *Science* **286**, 735-41.

Venugopal, C., Demos, C. M., Rao, K. S., Pappolla, M. A., and Sambamurti, K. (2008) Beta-secretase: structure, function, and evolution. *CNS Neurol Disord Drug Targets* **7**, 278-94.

von Arnim, C. A., Tangredi, M. M., Peltan, I. D., Lee, B. M., Irizarry, M. C., Kinoshita, A., and Hyman, B. T. (2004) Demonstration of BACE (beta-secretase) phosphorylation and its interaction with GGA1 in cells by fluorescence-lifetime imaging microscopy. *J Cell Sci* **117**, 5437-45.

von Arnim, C. A., Spoelgen, R., Peltan, I. D., Deng, M., Courchesne, S., Koker, M., Matsui, T., Kowa, H., Lichtenthaler, S. F., Irizarry, M. C., and Hyman, B. T. (2006) GGA1 acts as a spatial switch altering amyloid precursor protein trafficking and processing. *J Neurosci* **26**, 9913-22.

Voskoboinik, I., Strausak, D., Greenough, M., Brooks, H., Petris, M., Smith, S., Mercer, J. F., and Camakaris, J. (1999) Functional analysis of the N-terminal CXXC metal-binding motifs in the human Menkes copper-transporting P-type ATPase expressed in cultured mammalian cells. *J Biol Chem* **274**, 22008-12.

Vulpe, C., Levinson, B., Whitney, S., Packman, S., and Gitschier, J. (1993) Isolation of a candidate gene for Menkes disease and evidence that it encodes a copper-transporting ATPase. *Nat Genet* **3**, 7-13.

Vulpe, C. D., Kuo, Y. M., Murphy, T. L., Cowley, L., Askwith, C., Libina, N., Gitschier, J., and Anderson, G. J. (1999) Hephaestin, a ceruloplasmin homologue implicated in intestinal iron transport, is defective in the sla mouse. *Nat Genet* **21**, 195-9.

Waldron, K. J., Rutherford, J. C., Ford, D., and Robinson, N. J. (2009) Metalloproteins and metal sensing. *Nature* **460**, 823-30.

Waldron, K. J., Firbank, S. J., Dainty, S. J., Perez-Rama, M., Tottey, S., and Robinson, N. J. (2010) Structure and metal-loading of a soluble periplasm cupro-protein. *J Biol Chem* **285**, 32504-11.

Walker, J. M., Huster, D., Ralle, M., Morgan, C. T., Blackburn, N. J., and Lutsenko, S. (2004) The N-terminal metal-binding site 2 of the Wilson's Disease Protein plays a key role in the transfer of copper from Atox1. *J Biol Chem* **279**, 15376-84.

Walter, J., Schindzielorz, A., Hartung, B., and Haass, C. (2000) Phosphorylation of the beta-amyloid precursor protein at the cell surface by ectocasein kinases 1 and 2. *J Biol Chem* **275**, 23523-9.

Walter, J., Fluhrer, R., Hartung, B., Willem, M., Kaether, C., Capell, A., Lammich, S., Multhaup, G., and Haass, C. (2001) Phosphorylation regulates intracellular trafficking of beta-secretase. *J Biol Chem* **276**, 14634-41.

Wernimont, A. K., Huffman, D. L., Lamb, A. L., O'Halloran, T. V., and Rosenzweig, A. C. (2000) Structural basis for copper transfer by the metallochaperone for the Menkes/Wilson disease proteins. *Nat Struct Biol* **7**, 766-71.

Wernimont, A. K., Yatsunyk, L. A., and Rosenzweig, A. C. (2004) Binding of copper(I) by the Wilson disease protein and its copper chaperone. *J. Biol. Chem.* **279**, 12269-12276.

White, A. R., Reyes, R., Mercer, J. F., Camakaris, J., Zheng, H., Bush, A. I., Multhaup, G., Beyreuther, K., Masters, C. L., and Cappai, R. (1999) Copper levels are increased in the cerebral cortex and liver of APP and APLP2 knockout mice. *Brain Res* **842**, 439-44.

White, A. R., Du, T., Laughton, K. M., Volitakis, I., Sharples, R. A., Xilinas, M. E., Hoke, D. E., Holsinger, R. M., Evin, G., Cherny, R. A., Hill, A. F., Barnham, K. J., Li, Q. X., Bush, A. I., and Masters, C. L. (2006) Degradation of the Alzheimer disease amyloid beta-peptide by metal-dependent up-regulation of metalloprotease activity. *J Biol Chem* **281**, 17670-80.

Willem, M., Garratt, A. N., Novak, B., Citron, M., Kaufmann, S., Rittger, A., DeStrooper, B., Saftig, P., Birchmeier, C., and Haass, C. (2006) Control of peripheral nerve myelination by the beta-secretase BACE1. *Science* **314**, 664-6.

Wimmer, R., Herrmann, T., Solioz, M., and Wuthrich, K. (1999) NMR structure and metal interactions of the CopZ copper chaperone. *J Biol Chem* **274**, 22597-603.

Woese, C. R., and Fox, G. E. (1977) Phylogenetic structure of the prokaryotic domain: the primary kingdoms. *Proc Natl Acad Sci U S A* **74**, 5088-90.

Wood, L. K., and Thiele, D. J. (2009) Transcriptional activation in yeast in response to copper deficiency involves copper-zinc superoxide dismutase. *J Biol Chem* **284**, 404-13.

Wood, P. M. (1978) Interchangeable copper and iron proteins in algal photosynthesis. Studies on plastocyanin and cytochrome c-552 in Chlamydomonas. *Eur J Biochem* **87**, 9-19.

Wu, C. C., Rice, W. J., and Stokes, D. L. (2008) Structure of a copper pump suggests a regulatory role for its metal-binding domain. *Structure* **16**, 976-85.

Xiao, Z., and Wedd, A. G. (2002) A C-terminal domain of the membrane copper pump Ctr1 exchanges copper(I) with the copper chaperone Atx1. *Chem Commun (Camb)*, 588-9.

Xiao, Z., Loughlin, F., George, G. N., Howlettt, G. J., and Wedd, A. G. (2004) C-terminal domain of the membrane copper transporter Ctr1 from *Saccharomyces cerevisiae* binds four Cu(I) atoms as a cuprous-thiolate polynuclear cluster: sub-femtomolar Cu(I) affinity of three proteins involved in copper trafficking. *J. Am. Chem. Soc.* **126**, 3081-3090.

Xu, H. M., Jiang, H., Wang, J., Luo, B., and Xie, J. X. (2008) Over-expressed human divalent metal transporter 1 is involved in iron accumulation in MES23.5 cells. *Neurochem Int* **52**, 1044-51.

Xue, Y., Davis, A. V., Balakrishnan, G., Stasser, J. P., Staehlin, B. M., Focia, P., Spiro, T. G., Penner-Hahn, J. E., and O'Halloran, T. V. (2008) Cu(I) recognition via cation-pi and methionine interactions in CusF. *Nat Chem Biol* **4**, 107-9.

Yamaguchi-Iwai, Y., Dancis, A., and Klausner, R. D. (1995) AFT1: a mediator of iron regulated transcriptional control in Saccharomyces cerevisiae. *Embo J* **14**, 1231-9.

Yamaguchi-Iwai, Y., Stearman, R., Dancis, A., and Klausner, R. D. (1996) Iron-regulated DNA binding by the AFT1 protein controls the iron regulon in yeast. *Embo J* **15**, 3377-84.

Yamaguchi-Iwai, Y., Serpe, M., Haile, D., Yang, W., Kosman, D. J., Klausner, R. D., and Dancis, A. (1997) Homeostatic regulation of copper uptake in yeast via direct binding of MAC1 protein to upstream regulatory sequences of FRE1 and CTR1. *J Biol Chem* **272**, 17711-8.

Yan, R., Bienkowski, M. J., Shuck, M. E., Miao, H., Tory, M. C., Pauley, A. M., Brashier, J. R., Stratman, N. C., Mathews, W. R., Buhl, A. E., Carter, D. B., Tomasselli, A. G., Parodi, L. A., Heinrikson, R. L., and Gurney, M. E. (1999) Membrane-anchored aspartyl protease with Alzheimer's disease beta-secretase activity. *Nature* **402**, 533-7.

Yatsunyk, L. A., and Rosenzweig, A. C. (2007) Cu(I) binding and transfer by the N terminus of the Wilson disease protein. *J Biol Chem* **282**, 8622-31.

Ye, H., and Rouault, T. A. (2010) Human iron-sulfur cluster assembly, cellular iron homeostasis, and disease. *Biochemistry* **49**, 4945-56.

Younkin, S. G. (1998) The role of A beta 42 in Alzheimer's disease. *J Physiol Paris* **92**, 289-92.

Yuan, D. S., Stearman, R., Dancis, A., Dunn, T., Beeler, T., and Klausner, R. D. (1995) The Menkes/Wilson disease gene homologue in yeast provides copper to a ceruloplasmin-like oxidase required for iron uptake. *Proc Natl Acad Sci U S A* **92**, 2632-6.

Yuan, D. S., Dancis, A., and Klausner, R. D. (1997) Restriction of copper export in *Saccharomyces cerevisiae* to a late Golgi or post-Golgi compartment in the secretory pathway. *J Biol Chem* **272**, 25787-93.

Zhang, L., McSpadden, B., Pakrasi, H. B., and Whitmarsh, J. (1992) Copper-mediated regulation of cytochrome c553 and plastocyanin in the cyanobacterium *Synechocystis* 6803. *J Biol Chem* **267**, 19054-9.

Zhang, S., Wang, J., Song, N., Xie, J., and Jiang, H. (2009) Up-regulation of divalent metal transporter 1 is involved in 1-methyl-4-phenylpyridinium (MPP(+))-induced apoptosis in MES23.5 cells. *Neurobiol Aging* **30**, 1466-76.

Zheng, W., Xin, N., Chi, Z. H., Zhao, B. L., Zhang, J., Li, J. Y., and Wang, Z. Y. (2009) Divalent metal transporter 1 is involved in amyloid precursor protein processing and Abeta generation. *Faseb J* **23**, 4207-17.

Zhou, B., and Gitschier, J. (1997) hCTR1: a human gene for copper uptake identified by complementation in yeast. *Proc Natl Acad Sci U S A* **94**, 7481-6.

Zhu, Z., Labbe, S., Pena, M. M., and Thiele, D. J. (1998) Copper differentially regulates the activity and degradation of yeast Mac1 transcription factor. *J Biol Chem* **273**, 1277-80.

Zou, K., Gong, J. S., Yanagisawa, K., and Michikawa, M. (2002) A novel function of monomeric amyloid beta-protein serving as an antioxidant molecule against metal-induced oxidative damage. *J Neurosci* **22**, 4833-41.

Appendix A

A

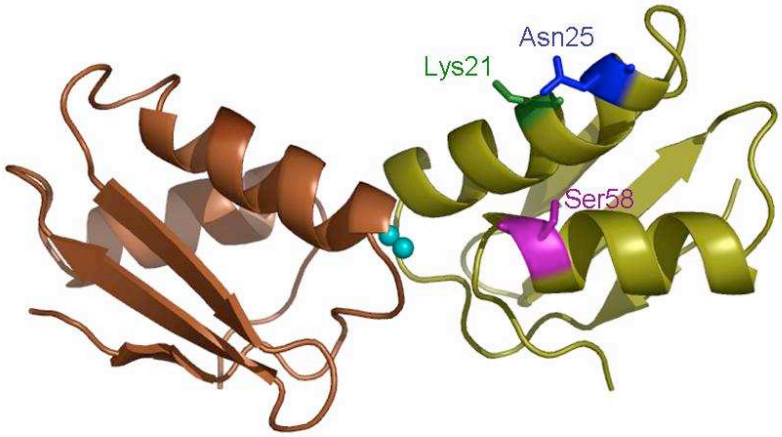

B

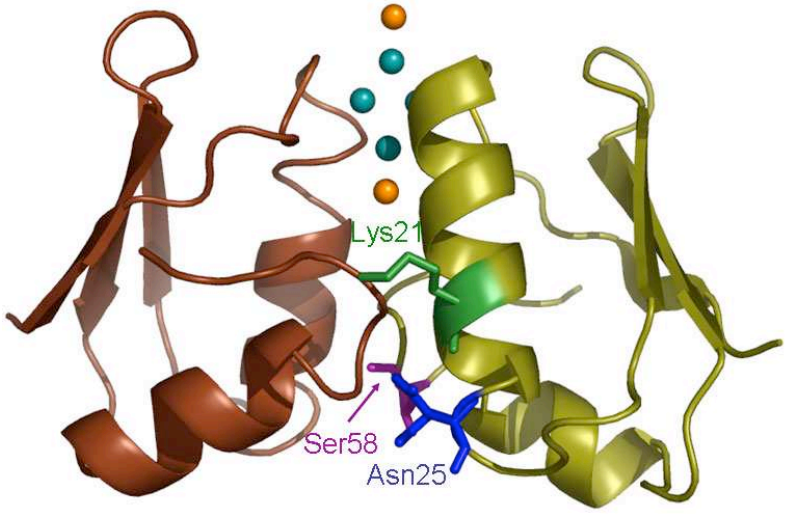

Figure 96: Crystal structures of the ScAtx1 dimers depicting the position of Lys21, Asn25 and Ser58. The crystal structures of the ScAtx1 head-to-head (PDB accession code: 2xmt) and side-to-side (PDB accession code: 2xmk) dimers are shown in (A) and (B) respectively (Badarau *et al.*, 2010). Each subunit in the dimer is represented in brown or yellow. The Cu(I) ions are shown as blue spheres while the chloride ions in (B) are shown as orange spheres. The side-chains of Lys21 (green), Asn25 (blue) and Ser58 (purple) are shown as sticks in the right-hand side subunit of the dimers.

Appendix B

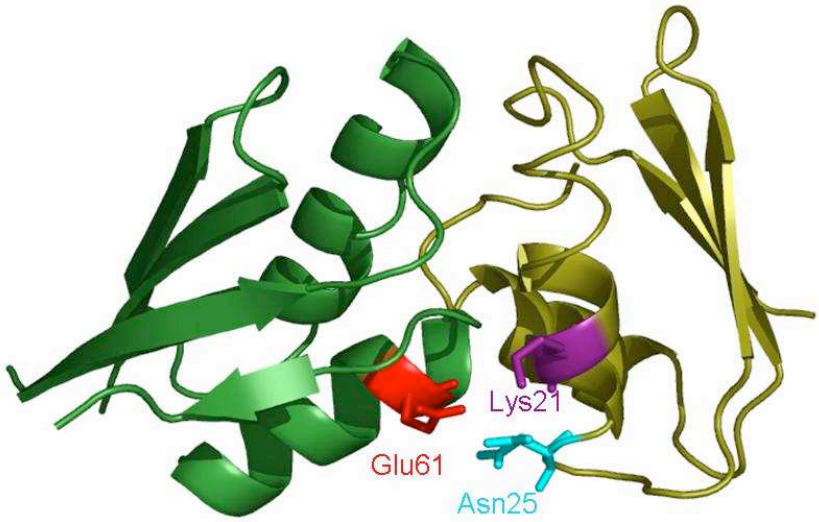

Figure 97: Model of the ScAtx1 and $PacS_N$ complex. In the above model, the ScAtx1 subunit (PDB accession code: 2xmk) is shown in yellow and the $PacS_N$ subunit (PDB accession code: 2xmw) is shown in green (Badarau *et al.*, 2010). The side-chains of $PacS_N$ Glu61 (red), ScAtx1 Lys21 (purple), and ScAtx1 Asn25 (blue) are shown as sticks. Neither the bound Cu(I) ions nor the chloride ions present in the original ScAtx1 homodimer are shown.